A Model for the Vacuum Pyrolysis of Biomass

By

Richardt Coenraad Rabe

Thesis submitted in partial fulfilment of the requirements for the degree of Master of Science in Engineering (Chemical Engineering) in the Department of Process Engineering at the University of Stellenbosch

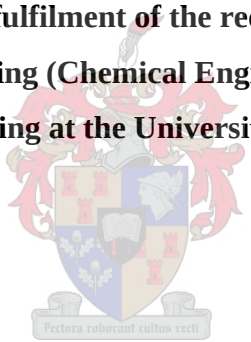

Supervisor: Prof. J.H. Knoetze

Stellenbosch

December 2005

Declaration

I, the undersigned, hereby declare that the work contained in this thesis is my own original work, except where specifically acknowledged in the text. Neither the present thesis nor any part thereof has been submitted previously at any other university.

Richardt Coenraad Rabe 26 May 2005

Synopsis

Biomass is a significant renewable energy source and much research is currently being done to enable the production of biofuels and chemicals from biomass. This study looks at vacuum pyrolysis, a technology which has the potential to turn biomass, amongst other waste materials, into commercially valuable commodities.

Vacuum pyrolysis is the thermal degradation of a feedstock in the absence of oxygen and under low pressure, to produce a bio-oil and char as main products, together with water and non-condensable gases. Both the oil and char have a high energy content and may be used as fuels. An incredible number of chemical compounds are also found in the oil and these compounds can be extracted and sold as high value chemicals.

Vacuum pyrolysis has been the subject of studies for a number of years now. In 1999 and 2000 **De Jongh (2001)** studied the possible applications of vacuum pyrolysis for the processing of waste materials at the University of Stellenbosch. His findings indicated that vacuum pyrolysis could be used in many industries to reduce waste and to produce char and oil with high energy values. The next step in the research of vacuum pyrolysis in South Africa is to build a pilot scale reactor. This study looked at developing a reactor model for vacuum pyrolysis in a pilot scale rotary oven. Kinetic experiments in a TGA (Thermogravimateric analyser) were also done on two alien plant species, Rooikrans and Swarthaak wood, to investigate the kinetics of vacuum pyrolysis and to provide a kinetic model to be used in conjunction with the reactor thermal model to predict conversions in the reactor. Batch experiments were also done in a tube furnace to provide data that could be compared with the results obtained by **De Jongh (2001)** and for comparison with the results obtained by the kinetic experiments.

The reactor model was developed for an indirect-heated rotary oven, and is a simple, one dimensional, steady state model that can be used to predict the temperature profiles of the gas, wall and bed along the length of the reactor. This thermal model was combined with the kinetic model to predict the conversion in the reactor.

A high nitrogen gas flow rate was used during the kinetic experiments in the TGA, to prevent sample oxidation. This high purge gas flow rate reduced the effect of the vacuum and virtually no difference was seen between the atmospheric and vacuum runs for fine sawdust. For bigger particles, diffusion and heat transfer limitations came into effect and thermal lag was observed, together with a lower final conversion. Increasing the heating rate also produced thermal lag and higher temperatures were needed to achieve the same conversion as for finer or smaller particles. Lower final conversions were achieved with swarthaak wood and this was attributed to the higher ash content of this plant.

The activation energy was determined for every level of conversion according to the modified Coats-Redfern isoconversional method developed by **Burnham and Braun (1999)**. A trend not too dissimilar from the one observed by **Reina et al (1998)** was seen with an almost constant activation energy during the early part of the pyrolysis reactions, followed by an increase in the activation energy for conversions above 60 %. It was found that a first order kinetic model adequately predicted the conversion as a function of temperature.

A first order kinetic equation for the thermal degradation of wood, together with the activation energies determined, was incorporated into the reactor thermal model. For the base case, with a fixed reactor diameter of 0.5 m, a reactor length of 3.4 m was predicted. The reactor model responded correctly to parameter changes, predicting longer or shorter reactor lengths depending on the change made.

The results obtained from the tube furnace were very similar to those obtained by **De Jongh (2001)** and also compared well with the results from the kinetic experiments in the TGA. Unfortunately the energy values of the oil samples could not be determined, but char energy values of around 30 MJ/kg were determined. In contrast to the results found by **De Jongh (2001),** the BET surface area for the charcoal samples was determined to be much higher (194 and 312 m^2/g), indicating the potential to upgrade these charcoals to activated carbon.

The model results produced in this study provides a good first estimate for the complete temperature and conversion profiles in the reactor. The major simplifying

assumption made was that the bed was perfectly mixed and that the bed temperature was uniform in the radial direction. Future work on the model should account for radial temperature profiles in the bed as well as the individual particles.

Opsomming

Biomassa is ‘n groot bron van hernubare energie en daar is tans heelwat navorsing aan die gang op die gebied van brandstof- en chemikalieproduksie uit biomassa. Hierdie studie fokus op ‘n spesifieke tegnologie, vakuum pirolise, wat gebruik kan word vir die omsetting van biomassa, asook ander afvalstowwe, na brandstof en chemikalieë.

Vakuum pirolise is ‘n termiese verwerkingstegnologie. Dit behels die afbreking van komplekse polimeriese materiale soos biomassa, onder lae druk, om ‘n olie, ryk in suurstof, en houtskool as hoofprodukte te lewer. Water en nie-kondenseerbare gasse word ook as neweprodukte geproduseer. Beide die olie en die houtskool het ‘n hoë energiewaarde en kan opgegradeer word na ‘n brandstof. Die olie kan ook gefraksioneer word om die chemikalieë wat daarin voorkom, te isoleer. Van die chemikalieë het ‘n hoë kommersiële waarde, wat hierdie opsie baie aantreklik maak.

Vakuum pirolise word al vir ‘n hele aantal jare bestudeer. In 1999 en 2000 het **De Jongh (2001)** die moontlike gebruik van vakuum pirolise vir die prosessering van afvalmateriale ondersoek. Sy bevindinge dui daarop dat vakuum pirolise in heelparty industrieë gebruik kan word om die afval te verminder en goeie kwaliteit houtskool en olie te produseer. Die volgende stap in die ontwikkeling van dié tegnologie in Suid-Afrika sal wees om ‘n loodsaanleg te bou. Hierdie studie was daarop gemik om ‘n reaktormodel vir vakuum pirolise in ‘n roterende oond te ontwikkel. Kinetiese eksperimente is gedoen op twee indringer plantspesies, Rooikrans en Swarthaak, in ‘n TGA (Thermogravimetric Analyser). Die doel hiermee was om ‘n kinetiese model te ontwikkel en te integreer met die reaktormodel om sodoende ook die omsetting in die reaktor te kan voorspel. ‘n Paar eksperimente is ook in ‘n buisoond uitgevoer om data te verskaf wat vergelyk kon word met dié van **De Jongh (2001)** en ook met die resultate verkry uit die kinetiese eksperimente.

Soos reeds genoem, is die reaktormodel ontwikkel vir vakuum pirolise in ‘n roterende oond. Die model is ‘n eenvoudige, eendimensionele model vir gestadigde toestande, en kan gebruik word om die gas, wand en bed temperature in die lengte van die reaktor te voorspel. Dié termiese model is geïntegreer met die kinetiese model om die omsetting in die reaktor te voorspel.

‘n Hoë stikstof vloeitempo is gedurende die TGA eksperimente gebruik om oksidering van die monster te verhoed. Hierdie hoë vloeitempo het die effek van die lae druk verminder en feitlik geen verskil is tussen die vakuum en atmosferiese lopies vir fyn saagsels opgemerk nie. Vir groter partikels het warmte-oordrags- en diffusie beperkinge ‘n rol begin speel. ‘n Verhoging in die verhittingstempo het termiese vertraging veroorsaak en effens hoër temperature is benodig om dieselfde omsettings te verkry. Laer finale omsettings is verkry vir die Swarthaak hout en die rede hiervoor was die hoër as-inhoud van hierdie plant.

Die “skynbare” aktiverings energie van die hout is vir elke vlak van omsetting bepaal deur middel van die gewysigde Coats-Redfern metode, ontwikkel deur **Burnham en Braun (1999)**. ‘n Soortgelyke neiging as die deur **Reine et al (1998)** waargeneem, is ook hier gesien: die skynbare aktiveringsenergie het ‘n konstante waarde gehad tot en met ‘n omsetting van ongeveer 60 %, waarna dit skielik begin styg het. Daar is gevind dat ‘n eerste-orde kinetiese model die omsetting redelik akkuraat as funksie van temperatuur kon voorspel.

Dié eerste-orde kinetiese model is met die termiese reaktormodel geïntegreer en ‘n reaktorlengte van 3.4 m is vir ‘n reaktor met ‘n deursnee van 0.5 m in die basislopie voorspel. Die reaktor model het korrek gereageer op veranderings in die beheer parameters en het langer of korter reaktorlengtes voorspel na gelang van die verandering.

Die resultate verkry met die buisoond was baie soortgelyk aan dié van **De Jongh (2001)** en het ook goed vergelyk met die resultate van die kinetiese eksperimente. Ongelukkig kon die energiewaardes van die olie nie bepaal word nie, maar ‘n gemiddelde energiewaarde van 30 MJ/kg is vir die houtskool bepaal. In teenstelling met **De Jongh (2001)** se resultate was die BET oppervlakarea vir die houtskool monsters baie hoër (194 en 312 m^2/g), wat die moontlikheid daar stel om die houtskool op te gradeer na geaktiveerde koolstof.

‘n Redelike goeie eerste skatting van die temperatuur- en omsettingsprofiel in die reaktor is deur die model gemaak. Die hoofaanname was dat daar geen temperatuur

veranderings in die radiale rigting van die bed is nie. Hierdie tekortkoming sal in toekomstige werk aangespreek moet word.

Acknowledgements

There are a number of people who helped to make this project possible and who deserve special thanks.

First of all I would like to thank my supervisor, Professor Knoetze, for his guidance, support and patience over the last three years.

I owe a great deal of gratitude to oom Freddy Greef, who spent countless hours fixing the TGA and who helped me to finally get some decent results.

I would like to thank Gordon Jemwa and J.P. Harper for sacrificing many hours to help me with the Matlab programming. Without their help I would never have finished.

I would also like to thank Hanlie Botha and Vincent for their help and technical support. Thank you also to James, Charles and June for all the support, chats and laughs.

I would like to thank my friends and office mates for their support: Lafras, Pierre, Grant and Robbie.

Lastly I would like to thank the most important person in my life, Meryl, who has supported me and persevered with me throughout all my years of study.

Table of Contents

Pectora roborant cultus recti

List of Tables

List of Figures

Nomenclature

A	Area or effective heat transfer area per unit oven length	$[m^2]$ or [m]
	or	
	Pre-exponential factor	$[s^{-1}]$
B	Biomass fraction	
C_p	Specific heat capacity at constant pressure	[J/kgK]
C_1, C_2	Mass fraction of charcoal	
E_a	Apparent activation energy	[J/mol]
h	Heat transfer coefficient	$[W/m^2K]$
ΔH_{rxn}	Heat of reaction	[J/kg]
k, K	Arrhenius kinetic constant	$[s^{-1}]$
	or	
	Thermal conductivity	$[W/m^2K]$
L	Length	[m]
$\dot{m}$	Mass flow rate	[kg/s]
n	Reaction order	
Q	Volumetric flow rate of the reactor bed	$[m^3/s]$
r	Radius	[m]
R	Universal gas constant	[J/kgK]
t	time	[min] or [s]
T	Temperature	[K] or [˚C]
ΔU_p	Approximation of exponential integral	
V_s	Bed velocity	[m/s]
W	Residual mass fraction or mass fraction	
z, Z	Axial distance	[m]

Pectora roborant cultus recti

Greek symbols

α	Conversion	
β	Heating rate	[˚C/min]
δ	Deposition coefficient	

ε	Emissivity	
λ	Rate of species production	[kg/m^{3}s]
ρ	Density	[kg/m^3]
τ	Residence time	[s]

Subscripts

b	bed or surface of bed
g	gas
0	initial
p	remaining
w	wall
z	axial position

1 Introduction

1.1 The production of commercially valuable products from biomass and waste materials

Biomass is a significant renewable energy resource and there is currently much research in the area of biofuels and chemicals production, using biomass as a feedstock. A number of technologies exist, including pyrolysis and gasification, which can be used for this purpose. The advantage of these technologies is that waste materials can be used to produce these commercially valuable commodities. This reduces the pressure on the environment and thus enables sustainable development. This study focuses on one such technology, vacuum pyrolysis, for the conversion of biomass to oil and char for use as fuels.

1.2 Pyrolysis of biomass

Pyrolysis of biomass is not a new technology. In pyrolysis, biomass is thermally degraded in the absence of oxygen to prevent complete gasification from taking place. Gas, pyrolysis oil and charcoal are produced. The oil and charcoal can be used as high energy-content fuels and in some instances the oil can be upgraded to create high value chemicals. Fast or flash pyrolysis is a variant of pyrolysis and can be used to maximise the gas or liquid product yield according to the temperature employed.

1.3 Vacuum pyrolysis versus atmospheric pyrolysis

Vacuum pyrolysis is a relatively new variant of pyrolysis with many recycling applications. It can be used to convert biomass as well as other wastes like rubber, plastics and dry sewage sludge into usable products. During vacuum pyrolysis of biomass, the feedstock is thermally decomposed under reduced pressure. The complex polymeric structures that make up the organic matter decompose into primary fragments when heated up in the reactor. These macromolecules are quickly removed from the reactor by a vacuum pump and are then recovered after condensation in the form of pyrolytic oils. The quick removal of the vapours reduces

the residence times of these macromolecules and hence minimises secondary decomposition reactions such as cracking, repolymerisation and recondensation, which occur during atmospheric pyrolysis. Charcoal, non-condensable gases and a large amount of water are also produced. The products obtained in this manner are of superior quality because "their chemical characteristics are often closely related to those of the complex molecules which make up the original organic matter" **(Darmstadt, 2002)**. The operating conditions for vacuum pyrolysis are milder than those used in atmospheric pyrolysis and incineration. Temperatures between 400˚C and 500˚C and pressures of about 0.15 atmospheres are typically used. This enables the recovery of large quantities of pyrolytic oils and charcoal. The low pressure used in the reactor is the main factor that controls the composition and quality of the products.

1.4 The history of vacuum pyrolysis

The study of vacuum pyrolysis in the laboratory has been underway for many years, but it is not yet used extensively in industry as a method of waste processing. Most of the research for industrial application in this field has been done by Professor Roy and co-workers at Laval University in Québec in Canada. Several waste materials have been studied and many new applications have been found. Many experiments were done in a multiple-hearth furnace and finally a new horizontal moving bed reactor for vacuum pyrolysis was designed, patented and succesfully demonstrated on an industrial scale. The plant was built in Jonquière, Québec in 1998-1999 and the process, developed jointly with Groupe Pyrovac inc. from Canada and Ecosun bv from the Netherlands, is called the Pyrocycling^{TM} process.

In a recent study **De Jongh (2001)** investigated the use of vacuum pyrolysis for the treatment of intruder plants, tannery wastes, sewage sludge and PVC. He concluded that plant clearing projects would benefit from vacuum pyrolysis to produce charcoal and oil from the cleared plants. Vacuum pyrolysis could also be used to handle leather wastes, turn waste sludge into compost and reduce the hazardous furan and dioxins produced during the thermal decomposition of PVC and other wastes by incineration and atmospheric pyrolysis.

1.5 The aims and scope of this study

The vacuum pyrolysis process is not yet widely proven in operation on a large scale. A number of different reactor types, like multiple-hearth furnaces, rotary kilns and screw-type conveyors, exist which may also be used for this process on an industrial scale. There is thus scope for the investigation of alternative reactor configurations. Kinetic data for vacuum pyrolysis is also not available and needs to be determined experimentally. For this study it was decided to use two intruder plant species for the kinetic experiments: Rooikrans and Swarthaak wood. Rooikrans, together with Port Jackson, covers great areas along the coast of South Africa. Both are extremely weedy species and difficult to remove. Swarthaak is found in the drier areas of South Africa, Botswana and Namibia. Because of the abundance of these alien plant species in South Africa, they have great potential as a feedstock source for a process such as vacuum pyrolysis.

The specific aims of this study were:

- To choose a reactor for vacuum pyrolysis on an industrial scale and develop a simple model for the process in this reactor.

- To investigate the kinetics and kinetic modelling of vacuum pyrolysis with the aim of providing a better understanding of the kinetics, and also to provide a kinetic model that can be used in conjunction with the reactor model.

- To do a number of runs in a batch tube furnace to provide data for the pyrolysis of Rooikrans wood that can be compared with the results obtained by **De Jongh (2001)**; to have data available for comparison with the TGA results of Rooikrans wood.

Experiments for kinetic analysis were done under vacuum using a TGA (thermogravimetric analyser) and different heating rates and isothermal temperatures were investigated. A couple of runs were also done under normal atmospheric conditions for comparative purposes. The tube furnace designed and built by **De**

Jongh (2001) was used to pyrolyse larger Rooikrans wood chips. Three different isothermal temperatures were used for the tube furnace experiments.

Figure 1.1 below is a mindmap of the thesis to show the development of the thesis and how the different chapters fit together.

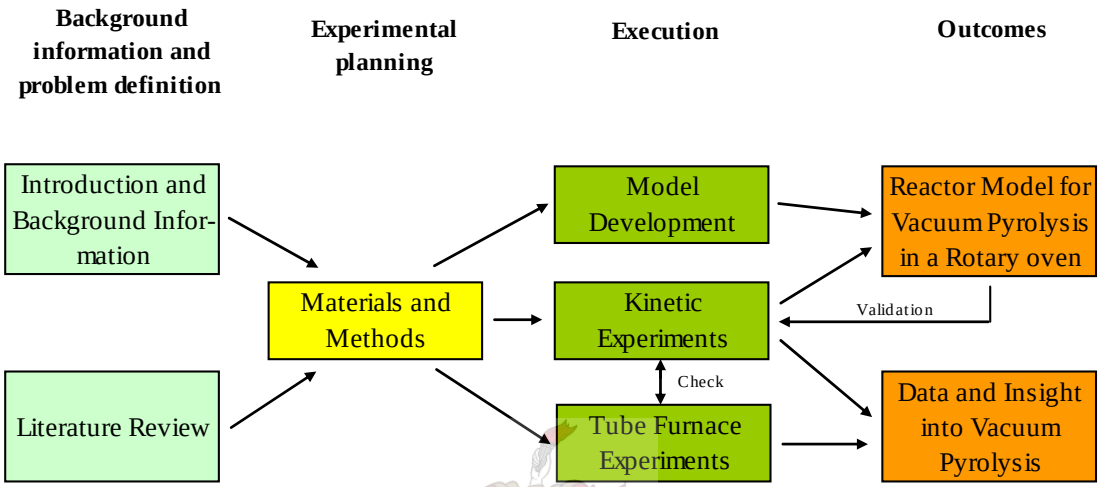

Figure 1.1 Thesis mindmap

2 Literature Review

Rooikrans wood was used throughout this project for the study of vacuum pyrolysis of biomass. A number of experiments were also done with Swarthaak wood for comparative purposes. This section gives an overview of the structure and chemical composition of wood, the pyrolysis and vacuum pyrolysis of lignocellulosic materials. Vacuum pyrolysis is compared with atmospheric pyrolysis and the progress made in the field of vacuum pyrolysis up to the present time is discussed. An overview of potential reactor technologies is given and the section is concluded with a discussion of the kinetics of biomass pyrolysis.

2.1 The structure and chemical composition of wood

Wood is not a solid homogeneous substance, but a porous solid, consisting of different cells with different functions **(Jane, 1970)**. The more central part of the wood is termed the heartwood and consists mainly of dead cells. The outer part of the wood is younger, contains the living cells, and is termed the sapwood. Histologically heartwood and sapwood is identical. As the tree grows, the sapwood is converted to heartwood, but the only real change that takes place is that the vessels become blocked with tyloses, an intrusive growth of the cell walls, or gummy material. Heartwood is often darker in colour than the sapwood and this is because of the deposition of extraneous materials like tannins, resins and colouring matters. As a result, the heartwood of a tree is usually heavier than the sapwood. The relative amounts of heartwood and sapwood is usually fairly constant in any species, but varies between species.

Trees may be divided into two major groups: Softwoods (gymnosperms) and hardwoods (angiosperms). The terms ‘hardwood’ and ‘softwood’ is not a measure of the hardness of the wood. Softwoods are evergreen, but hardwoods shed their leaves. The main difference with respect to wood anatomy between hardwoods and softwoods is the presence of vessels in hardwoods **(Thomas, 1976)**. Vessels are cells with the exclusive function of conducting water through the tree. Softwoods have cells termed longitudinal tracheids with a dual purpose of support and conduction.

Softwoods contain two main types of cells: longitudinal tracheids, for conduction and support, and transverse parenchyma for food storage. Hardwoods are more complex and contain four main types of cells: vessel segments for conduction, longitudinal fibres for support and transverse and axial parenchyma for food storage.

The internal cell wall structure of most woody plant cells consists of a primary cell wall (outside), a middle lamella and a secondary cell wall that consists of three layers, S_1, S_2, S_3. The S_2 layer of the secondary cell wall is the thickest layer of all the layers.

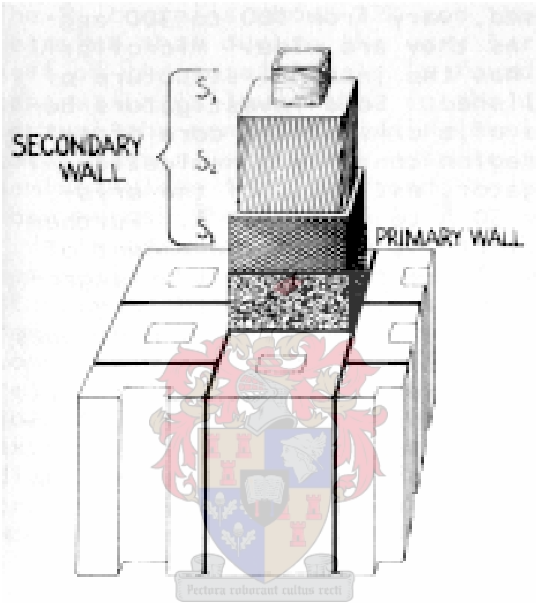

Figure 2.1 Drawing of cell wall **(Thomas, 1976)**.

Cell walls consist primarily of three polymeric materials namely, cellulose, hemicellulose and lignin. These three materials usually constitute about 95% to 98% of the cell wall with the remainder consisting of lower molecular weight compounds called extractives. Another important component in lignocellulosic materials is ash. The chemical composition of the cells of wood is influenced by a number of factors including species, location of cells within the tree and the growth environment. The relative amounts of the different components vary significantly between hardwood and softwood species. An average chemical composition of the cell wall is given by **Thomas (1976)**:

Table 2.1 Average Percentage Chemical Composition of Softwoods and Hardwoods **(Thomas, 1976)**.

	Softwoods	Hardwoods
Cellulose	42 ± 2	45 ± 2
Hemicellulose	27 ± 2	30 ± 5
Lignin	28 ± 3	20 ± 4
Extractives	3 ± 2	5 ± 3

Cellulose is a linear polymer of anhydro – D – glucopyranose units linked by ß – (1 – 4) glycosidic bonds. Cellulose molecules are linked laterally by hydrogen bonds into linear bundles and this results in a strong lateral association **(Thomas, 1976)**. The strong association and near perfect alignment gives rise to crystallinity.

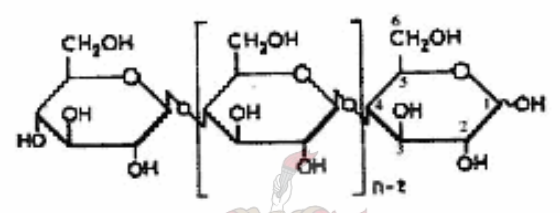

Figure 2.2 Cellulose Structure (http://www.fibersource.com/f-tutor/cellulose.htm)

Hemicelluloses are also polymers of anhydrosugar units, but unlike cellulose, hemicellulose may contain a number of different sugar units, usually of the order of 150 to 200 units. Hemicelluloses and lignin surround the crystalline cellulose.

Lignins, unlike cellulose and hemi-cellulose, are not carbohydrates, but complex, cross linked three-dimensional polymers that are formed from phenolic compounds. Lignin acts as the glue that holds the wood fibres together. Due to the aromatic nature of lignins, they are hydrophobic. The three-dimensional structure provides rigidity and makes lignins difficult to break. Hardwood and softwood lignins differ in structure because the building blocks are different. Syringyl serves as the basic building block for hardwood lignins whereas guaiacyl serves as the basic building block for softwood lignins. Hardwood lignins are more easily degraded than those of softwoods. The distribution of the constituents across the cell wall is not uniform.

The extractives present in the heartwood constitute about 2 – 5 % of the cell wall and consist of many different chemical compounds. The major types are terpenes, fatty

acids, aromatic compounds and volatile oils **(Thomas, 1976)**. The type and amount of extractives present differ considerably from species to species.

2.2 Thermal decomposition of lignocellulosic materials

Lignocellulosic materials are chemically complex materials. The thermal decomposition, or pyrolysis, of such materials is therefore also a very complex process with a number of different reactions taking place. These include cracking, depolymerisation, devolatilisation and recondensation reactions. The main pyrolysis products are gas, pyrolysis oil, water and charcoal. Because of the complexity of this process, an exact model or mechanism does not exist. Many researchers however, have studied the decomposition reactions of the main constituents of wood, namely cellulose, hemicellulose and lignin. **Shafizadeh and Chin (1976)** stated that the thermal analysis of cottonwood showed that the thermal behaviour of wood reflected the thermal responses of its three major components. **Koufopanos (1989)** also stated that the major biomass components react in the same way when they are isolated or form part of the biomass. This is the route a number of researchers have followed in an attempt to model pyrolysis behaviour, especially the kinetics of decomposition **(Ward and Braslow, 1985; Varhegyi et al, 1997; Di Blasi, 1998)**. Before discussing the proposed mechanisms for the pyrolysis of biomass, a brief review of the pyrolysis reactions of the individual components will be given.

2.2.1 Cellulose pyrolysis chemistry

Cellulose decomposes between 325 and 375˚C. It is accepted today that there are two major competitive pathways during the pyrolysis of cellulose **(Antal and Varhegyi, 1995)**. The first pathway leads to the formation of levoglucosan, which is a relatively stable product, and a second pathway which leads to the formation of glycolaldehyde. Essig et al. **(Antal and Varhegyi, 1995)** showed that higher temperatures and heating rates favour the second pathway.

Richards and co-workers **(Antal and Varhegyi, 1995)** have postulated that levoglucosan is formed by a midchain, heterolytic scission of the glucosidic linkage. This leads to a shortened chain, terminated by a resonance-stabilised glucosyl cation. This cation stabilises itself as the 1,6-anhydride (levoglucosan). Subsequent scission

of the glucosidic bond adjacent to the levoglucosan end group produces levoglucosan. Richards postulated that glycolaldehyde is formed via dehydration and a retro-Diels-Alder reaction from C_5 and C_6 of a glucose unit in cellulose. Conditions which favour the formation of levoglucosan result in low yields for glycolaldehyde and vice versa. The effect of temperature on the productivity of the two pathways is minimal but salts and metal ions, however, have a significant effect on the course of the pyrolysis reactions. For instance, decreasing the metal ion content from 450 to 60 ppm increased the levoglucosan yield from 28% to 52% and decreased the glycolaldehyde yield by a factor of three **(Antal and Varhegyi, 1995)**. Other tarry pyrolysis products include glucofuranose, 3-deoxyhexitols, D-glucitol and oligosaccharide derivatives **(Shafizadeh and Chin, 1976)**. Water and char are also formed during cellulose pyrolysis.

2.2.2 Hemicellulose pyrolysis chemistry

The pyrolysis reactions of hemicellulose (xylan) are similar to those involved in cellulose pyrolysis. **Shafizadeh and Chin (1976)** report a tar yield of 16% on the pyrolysis of xylan at 300˚C. The tar contained 17% of a mixture of oligosaccharides and acid-hydrolysis of this mixture produced a 54% yield of D-xylose. Structural analysis of the polymers showed that they were branched chain polymers. This indicated that they were derived from the random condensation of xylosyl units which formed by the cleavage of the glycosidic groups, similar to that occurring in cellulose pyrolysis. Hemicellulose is the least stable compound of the three main biomass components and decomposes between 225 and 325˚C.

2.2.3 Lignin pyrolysis chemistry

The thermal decomposition of lignin occurs over the temperature range 250 to 500˚C, but the decomposition is most rapid between 310 and 420˚C. The most abundant product is char, but monomeric and oligomeric products are also formed, as well as low molecular mass volatiles **(Varhegyi et al., 1997)**. The thermal decomposition mechanism for lignin is not well understood. According to **Varhegyi et al. (1997)** the low molecular mass products are formed by the cleavage of functional groups. These oxygen functionalities, which are abundant in lignin, have different thermal stabilities and therefore the scission of these groups takes place at different temperatures. Complex char forming reactions occur at higher temperatures and involves the

complete rearrangement of the carbon skeleton. As with cellulose pyrolysis, the presence of cations significantly affects the course of decomposition.

2.2.4 Biomass pyrolysis

Attempts have been made to describe and model the pyrolysis of biomass as the sum of its parts. However, in a review of semi-global mechanisms for the primary pyrolysis of lignocellulosic fuels, **Di Blasi (1998)** stated that the extrapolation of the thermal behaviour of the main components to describe kinetics of complex fuels, such as wood, is only a rough approximation because it has not been possible to establish exact correlations. The reason for this is most probably the presence of inorganic matter in the biomass which acts as a catalyst or inhibitor for the degradation of cellulose, as was stated earlier. **Varhegyi et al. (1997)** found that inorganic salts shifted the cellulose decomposition to lower temperatures. **Roy et al. (1990)** also investigated the role of extractives during the vacuum pyrolysis of lignocellulosic materials. It was found that the extractives, lignin and the orientation of the cellulosic fibres all significantly influenced the production of pyrolysis oils and formic acid. Lignin and extractives also inhibited the production of acetic acid and levoglucosan respectively. Further factors which affect the degradation process are the purity and physical properties of the cellulose.

Pectora roborant cultus recti

In his study of the co-pyrolysis of PVC and wood to try and model the pyrolysis of municipal solid waste, **De Jongh (2001)** also found that significant interaction took place between the materials pyrolysed together. The oil and charcoal yields obtained for the pyrolysis of aged Kraalbos and PVC differed greatly from those predicted for a non-interactive system. It was concluded that further research was necessary.

Reina, et al. (1998) did a number of pyrolysis experiments with waste wood and their results confirm, together with a number of other researchers, the theory that lignocellulosic materials thermally decompose in two stages. They proposed a mechanistic model for the pyrolysis of wood by merging the theory of two stages with the decomposition mechanism proposed by Shafizadeh **(Reina et al. 1998)**. The first

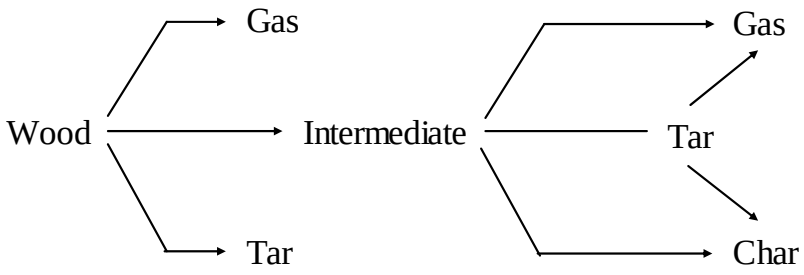

Figure 2.3 Pyrolysis mechanism proposed by **Reina et al. (1998)**

stage of pyrolysis involves the depolymerisation or decomposition of cellulose and lignin to form an intermediate organic compound of low molecular weight. Gases and tars are also produced by the pyrolysis of these two components to give volatile compounds that are released during this first stage. Lignin is more resistant to decomposition than cellulose and decomposes at higher temperatures. This causes an overlap of these two components during the first stage and also an increase in the activation energy during the last part of this stage. The second stage is the decomposition of the intermediate product from the first stage to give more tars, gases and char. At the high temperatures used during pyrolysis these tars are further decomposed to form gases and more char.

2.2.5 Pyrolysis liquid

The liquid product from pyrolysis is formed by condensing the vapours formed during pyrolysis after removal from the reactor or reaction vessel. This liquid is often referred to as tar or bio-oil.

A description of the composition and characteristics of pyrolysis liquid is found on the Biomass Pyrolysis Network (PyNe) website (www.pyne.co.uk). PyNe is sponsored by IEA Bioenergy which is an organisation established by the International Energy Agency (IEA). A short summary is given here.

Crude pyrolysis liquid has a dark brown colour with a distinctive smoky smell. It is composed of a complex mixture of oxygenated hydrocarbons and a significant amount of water (15 to 30 %). It contains several hundred different chemical species in varying proportions, ranging from formaldehyde and acetic acid to high molecular

weight phenols, anhydrosugars and other oligosaccharides. The distinctive smell is caused by low molecular weight aldehydes and acids. The water is both from the original moisture content of the feedstock and the reaction. Pyrolysis liquid can be considered a micro-emulsion in which the continuous phase is an aqueous solution of holocellulose decomposition products, that stabilises the discontinuous phase of pyrolytic lignin macro-molecules through mechanisms such as hydrogen bonding. Aging and instability is believed to result from the breakdown of this emulsion. Pyrolysis liquid is not miscible with any hydrocarbon liquids.

The liquid has a typical density of 1.2 kg/litre (water included), compared to light fuel oil with a density of around 0.85 kg/litre. As a result, pyrolysis liquid has an energy content of about 42 % of the energy content of fuel oil on a weight basis, but 61% on a volume basis. The viscosity of pyrolysis liquid varies from 25 cSt to 1000 cSt. This depends, however, on the feedstock, the water content of the oil, the amount of light ends collected and the age of the oil.

In his Master's study **De Jongh (2001)** pyrolysed three different plant species: Asbos, Kraalbos and Scholtzbos. All three of these species are intruder plants in South Africa. He identified a large number of species in the pyrolysis liquid, the most predominant of which were Acetic acid, Phenol, 1,2-Benzenediol, 6 Methoxyeugenol and 2-Propanol.

2.3 Vacuum pyrolysis of lignocellulosic materials

Vacuum pyrolysis is a relatively new variant of pyrolysis. A vacuum pump is used to remove the vapours from the reactor. This reduces the residence time of the vapours in the reactor and thus minimises the secondary decomposition reactions which occur during atmospheric pyrolysis and result in lower oil yields. Some compounds do undergo fractionation and this, together with the compounds that are liberated from the main lignocellulosic structure, causes a large number of chemicals to be formed. The main products of vacuum pyrolysis are vapours, which are condensed after removal to form complex primary oil, and wood charcoal. Non-condensable gases and water are also produced as by-products **(Pakdel et al, 1994)**

De Jongh (2001), in his Master's thesis postulated that the formation of vapours (longer chain compounds) and gases (shorter chain compounds) and the degree to which recondensation reactions occur are affected by two main factors: The resistances to the free movement of the gases and vapours inside the particle and inside the sample bed. The vapour pressure inside the particle and the particle structure affects the movement inside the particle, but the bed density and reactor pressure affects the vapour movement through the bed. A longer residence time of the vapours inside the reactor will cause more side reactions to occur and this will lead to lower oil yields and higher charcoal yields. **De Jongh** proposed the following mechanism for the vacuum pyrolysis of wood based on the mechanism first proposed by **Reina et al. (1998)**:

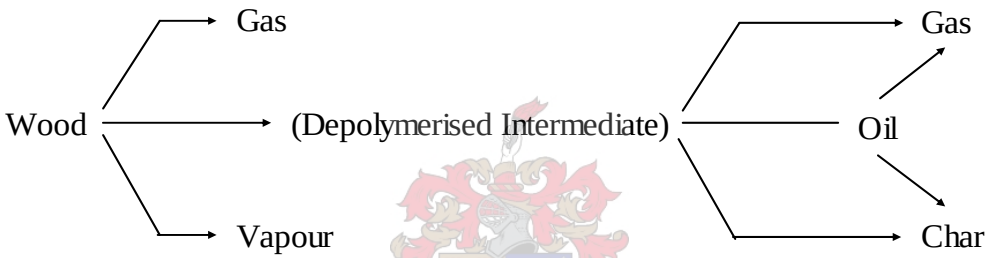

Figure 2.4 Proposed mechanism for the vacuum pyrolysis of wood **(De Jongh, 2001)**

A high degree of conversion is reached in the first stage due to the cracking of macromolecules (cellulose and lignin). This produces a decrease in the degree of polymerisation. Most of the volatile compounds are also released during this stage. The intermediate represents an organic compound of relatively low molecular weight. An increase in the apparent activation energy during the last part of stage one is caused by lignin, which is more resistant to thermal decomposition than cellulose. The second stage is effected at higher temperatures and represents a much smaller weight loss, attributed to the cracking of residual organic components that decompose to produce gases and chars.

2.4 Vacuum pyrolysis versus atmospheric pyrolysis

Vacuum Pyrolysis takes place under reduced pressures of typically 0.15 to 0.2 atmospheres and moderate temperatures of 350 to 520˚C. Under these conditions

organic materials crack and release fragments that evaporate quickly because of the low pressure. The vapours released are quickly removed from the reaction zone by the vacuum pump. This significantly reduces the residence time of vapours inside the reactor, and as a result, secondary decomposition reactions which result in lower oil yields are minimised. According to **Darmstadt (2002)** the products obtained in this manner are of superior quality because 'their chemical characteristics are often closely related to those of the complex molecules which make up the original organic matter.' Vacuum pyrolysis produces more oil, less charcoal and gas than atmospheric pyrolysis processes **(Roy and Chaala, 2003)**.

2.5 Previous progress in the field of vacuum pyrolysis

Vacuum pyrolysis of wood was first performed by Klason in 1914 with the objectives of finding the cause of the exothermic reaction and to identify the primary and secondary pyrolysis products **(De Jongh, 2001)**.

The majority of research on the vacuum pyrolysis process has been done by Professor Roy and others at Laval University in Quebec, Canada. In the early eighties they constructed a Process Development Unit (P.D.U.), which used a multiple-hearth furnace reactor, for the study of the vacuum pyrolysis process. The two main objectives of the P.D.U. were to obtain engineering data such as the thermal efficiency of the system and the heat requirements of the reactions, and to test the configuration and mechanical operation of the reactor with the aim of scaling up the reactor **(Roy et al. 1988)**. Separation of the water from the organic liquid phase was also achieved using a series of shell and tube heat exchangers. This is necessary because the further processing of pyrolytic oils mixed with water is difficult and expensive. The optimum temperature range for the maximum oil yield was found to be 425 to 450˚C.

In 1990 a 'Performance study of a 30 kg/h vacuum pyrolysis process development unit' was published **(Roy et al, 1990)**. The P.D.U was operated at a pressure of 9.3 kPa with a throughput of 28 kg/h for several hours. It was found that, under the conditions used, the conversion of biomass in oil and charcoal was at a maximum, but that the throughput capacity could be increased. A preliminary economic analysis

showed that a biomass vacuum pyrolysis plant becomes profitable if commodity and high-value chemicals are recovered and sold as by-products.

The next step in the development of the vacuum pyrolysis process came with the 'Conceptual design and evaluation of a biomass vacuum pyrolysis plant' **(Roy et al. 1992)**. A smaller and less expensive vacuum pyrolysis reactor was used to provide background data for the thermal decomposition of a bed of wood particles under vacuum. A process flow sheet was drawn up for a 7875 kg/h of wet biomass (50% moisture content) vacuum pyrolysis plant with a (continuous) tunnel reactor. Heat transfer calculations showed that radiation is the main mode of heat transfer between the reactor and the particle bed and also in the particle bed. It was shown that agitation of the moving bed of particles can significantly enhance the heat transfer and so decrease the reactor surface area and cost. The optimum reactor pressure was determined to be 15 kPa. It was found that reactor pressure did not significantly influence the capital investment required and a manufacturing cost of $115/t of pyrolysis oil was determined.

Further research led to the development of a horizontal moving and stirred bed reactor with improved heat transfer potential **(Roy et al. 1997)**. This reactor, US patent number 6,042,696, was developed to address the heat transfer limitations of conventional pyrolysis reactors such as multiple hearth furnaces, rotary kilns and screw type reactors. Novelties include the feedstock transport and agitation system as well as the heating system, which make use of commercial molten salts. A new heat transfer model, based on Schlünder's heat transfer model, was developed and takes into account the mechanical movement of the particles as a result of the agitation. The model is used to predict overall heat transfer coefficients for different feedstocks in the reactor, and coefficients ranging from 70 – 250 W/m^2K were obtained with this new system.

In 1998 the construction of the first industrial scale vacuum pyrolysis plant, using the technology developed by Professor Roy, was started in Jonquière, Canada. The process is known as the Pyrocycling^{TM} process (Figure 2.5) and is the result of a joint effort between Pyrovac Group Inc. and the Dutch company, Ecosun b.v. The plant has a throughput capacity of 3500 kg/h of air-dry feedstock and was built to

demonstrate and further improve the technology and produce pyrolysis oils and wood charcoal. A more detailed discussion of the reactor and process will follow in section 2.8.

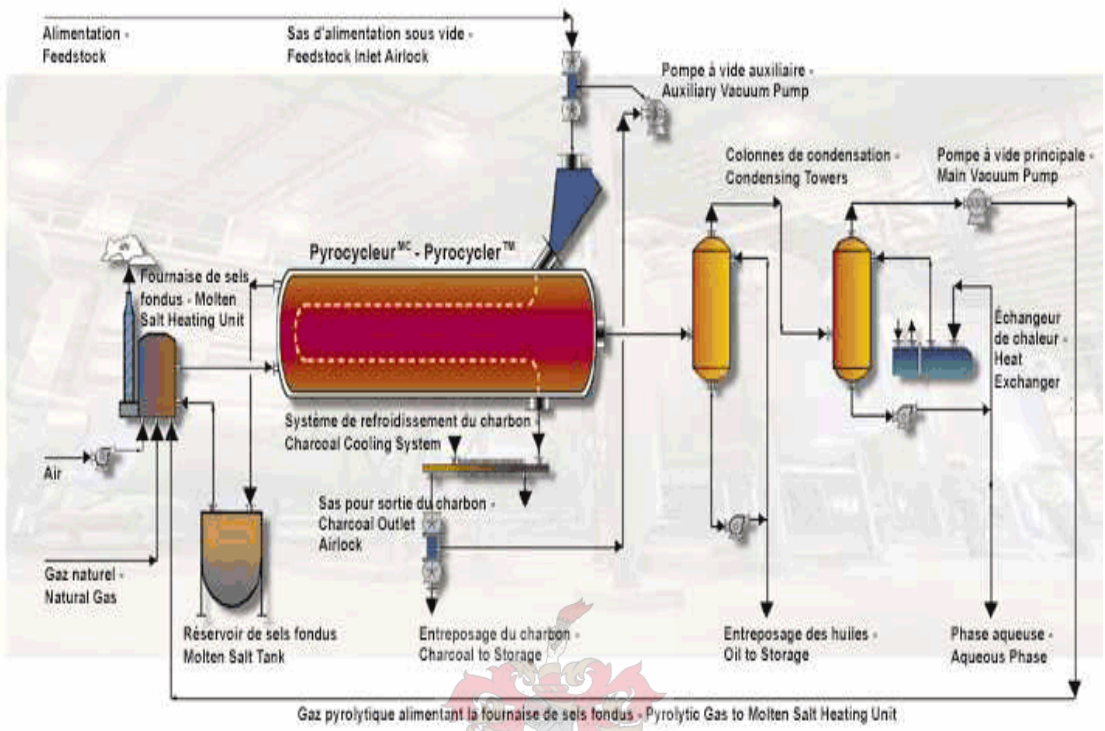

Figure 2.5 The Pyrocycling™ plant

2.6 Other fast pyrolysis technologies

Much research has been done on fast pyrolysis technologies. Fast pyrolysis is different from traditional pyrolysis technologies in that it uses a very high heating rate and a carefully controlled pyrolysis temperature of around 500 ˚C. Vapour residence times are kept low, typically less than 2 seconds, and the products are rapidly cooled to give the bio-oil product. Strictly speaking, vacuum pyrolysis is not a fast pyrolysis technology because of its relatively low heating rate. Similar results, in terms of the liquid product yields and quality, are achieved with vacuum pyrolysis because vapour residence times are minimized under vacuum **(**www.pyne.co.uk, **1999)**.

Meier and Faix (1999) give a review of the most relevant fast pyrolysis technologies and include the vacuum pyrolysis process developed by Professor Roy and Pyrovac Group Inc. Five other technologies are reviewed: A fluidized bed reactor, a

circulating fluidized bed reactor, ablative pyrolysis, a rotating cone reactor and a vortex reactor.

The most common reactor, which works successfully in various laboratories in the world, is the fluidised bed reactor. This reactor was developed at the University of Waterloo, Canada and the largest plant in Europe using this technology, at the time of the review, was the one in Meirama, Spain, of the company Union Fenosa. It has a capacity of 250 kg/h.

The ENSYN Rapid Thermal Process (RTP) is a circulating fluidised bed. It is installed in Bastardo (Umbria) Italy and has a throughput of 650 kg/h.

Ablative pyrolysis is a relatively new development, researched at Aston University, Birmingham, UK. Wood chips are pressed to a heated surface of the reactor by rotating blades. A liquid film is formed on the hot wood chip surface and scraped away by the friction. In this way new layers of wood are exposed for pyrolysis. The pyrolysis of the thin liquid layer which remains on the surface is then easily completed.

A rotating cone reactor was developed at Twente University in the Netherlands. This technology is based on the rapid heat transfer from the solid surface of a rotating cone to small wood particles which are mixed for better heat transfer with sand or catalytically active material. A 50 kg/h unit was succesfully tested. However, a disadvantage of this technology is the need for very small particles (around 200 μm).

Vortex reactors have been developed over the last decade by the National Renewable Energy Laboratory (NREL), Golden, CO, USA. A high speed steam current forces particles to rotate on the heated inner wall of a cylindrical reactor. The largest version evaluated was 20 kg/h unit.

It is clear from literature that there is not yet a preferred or “best” technology. All of the above-mentioned technologies have advantages and disadvantages. Many of these technologies are still very expensive compared to fossil based energy

(www.pyne.co.uk, **1999)** and more research is needed before these technologies become an established part of the liquid fuel production industry.

2.7 Evaluation of possible technologies for vacuum pyrolysis

One of aims of this study is to develop a simple model for a potential vacuum pyrolysis pilot plant reactor, using biomass as feedstock. Before such a model may be developed, it is necessary to first establish which reactor configuration will be used. For this reason an overview of potential reactor configurations are given below.

2.7.1 Rotary ovens

For vacuum pyrolysis of biomass a rotary oven similar to an indirect-heat calciner may be used. A description of a rotary calciner can be found in **Perry's Chemical Engineering Handbook, Chapter 12 (1997)**. A calciner consists of a cylindrical retort that rotates within a stationary, insulation lined furnace. Fuel combustion occurs within the annulus between the cylinder and the furnace. The cylinder extends beyond the furnace at both ends and this allows the tires, trunnions and running gear to be located away from the heat of the furnace. Screw feeders or other positive feeders are usually used for feeding material to and from the reactor. These feeders prevent leakage of gases into or out of the calciner. It is often required to cool the reactor product before discharge and in these cases an extension, the exterior of which is cooled by water sprays, is provided on the discharge side of the cylinder. To prevent the condensation of gases on the cooled-shell surfaces in this section, an exit tube is provided that extends through the cooled section and through which the hot gases are withdrawn.

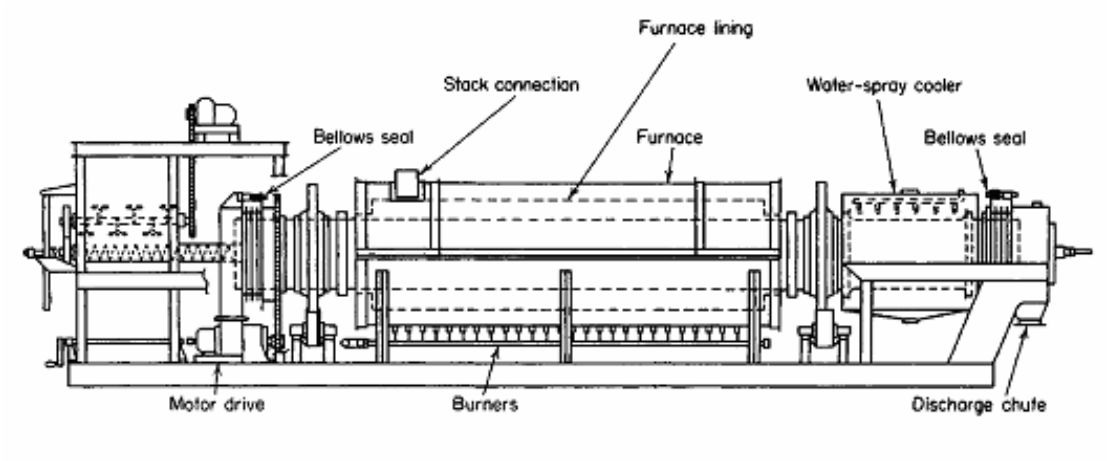

Figure. 2.6 Gas-fired indirect-heat rotary calciner with water-spray extended cooler and feeder assembly. **(Perry 7th ed, 1997)**

A simple flighting arrangement is used to prevent the solids from sliding over the smooth interior surface of the shell. Unlike a direct-heat rotary oven, the solids are not showered through an air stream and lifting flights are not needed. Instead, lifting bars running longitudinally are welded to the inside wall and these ensure that the product is constantly turned over to expose new surface for heat transfer. A scraper chain is sometimes used to prevent scaling of the shell interior by sticky solids.

It is common practice to support all parts on a self-contained frame because of the need for close-fitting gas seals. Positive rotary gas seals with one or more pressurised and purged annular chambers are used when a special gas atmosphere is required. A bellows seal can be used for low pressures.

The metal used will depend on the operating temperatures – normally carbon steel if the temperature is about 425˚C and stainless steel if the operating temperature is about 650˚C. The creep-stress abilities of cast alloys make them desirable when very high temperatures are needed. Electric heating elements or gas or oil burners may be used as heat source. The process is controlled by measuring the shell temperature and thermocouples or radiation pyrometers are employed for this purpose.

Meticulous alignment of the dryer is essential, first cold and then hot, when new and after removal of supporting runners. General maintenance includes renewal of

bearings and runners, rappers and lifters; also refractories (or whatever insulation) in combustion chambers.

Typical heat transfer coefficients achieved in indirect calciners range from 17 – 85 $W/m^{2\circ}C$. **(Perry, 1997)**.

Rotary dryers in general are simple, versatile and suitable for drying a wide range of materials rapidly at a low unit cost when quantities are large (**Nonhebel, 1971)**. Wet and sticky products however, may cause clogging. Accurate temperature control may also be difficult if there is variation in the feed characteristics **(Traub, 2003)**. Expansion and contraction due to heating and cooling makes sealing for vacuum difficult.

2.7.2 Conveyor belt reactors (Continuous band dryers)

An example of an indirect-heated conveyor is the conduction solid-band conveyor. These dryers are discussed in detail in **Nonhebel (1971).** Information on conveyor dryers can also be found in **Mujumdar (1995)** and **Perry's Chemical Engineering Handbook**. In this conveyor the solid band which conveys the material to be dried is pressed over a hot surface, usually a steam chest, so that it is heated by conduction through the band. It is normally operated under vacuum because the more conventional convection solid band dryer is more efficient under atmospheric conditions. Individual particles remain in fixed position with respect to one another and as a result of this, the particles all have essentially the same residence time and a uniform product is obtained.

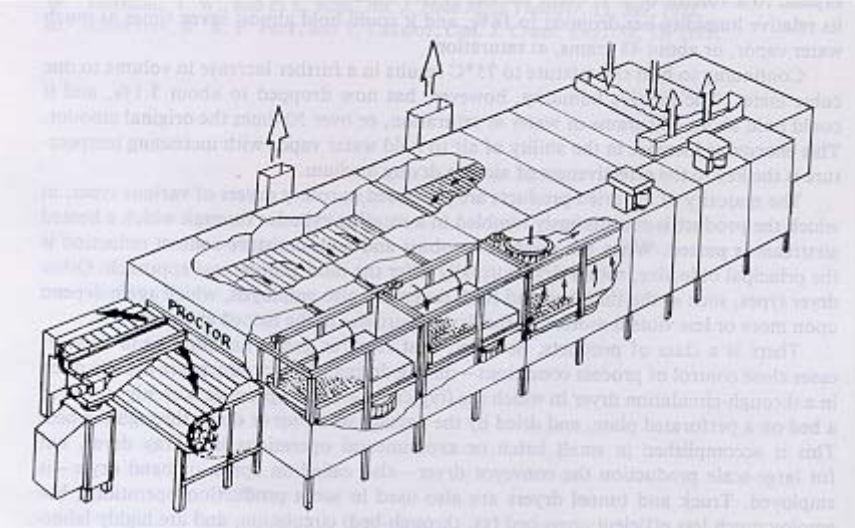

Figure. 2.7 Cutaway of a single-conveyor dryer **(Mujumdar, 1995)**.

The conveyer consists of a number of narrow bands in a cylindrical pressure chamber, operated under vacuum. The bands may be in series or stacked horizontally on top of each other. This reduces the dimensions of the expensive pressure chamber and minimises the floor space required. A fine mesh wire is usually used for the construction of the bands to allow them to be bent around a sharp radius. This helps to minimise the dimensions of the chamber. Material is fed to the bands via a manifold and extending orifices. The upper part of each band is supported on the steam chests which provide the source of heat. A number of independently connected steam chests are provided along the length of each band to allow the different sections to be operated at different temperatures. A final cooling section can also be added.

Material is discharged into a bin or bins which are held under vacuum and discharged periodically. Continuous discharging can be achieved by making use of a scroll or rotary valve. The continuous sealing system is however more susceptible to air leakage. A vacuum pump is used to withdraw the vapours generated in the chamber.

Any metal construction that will be able to stand the pressure conditions may be used for the construction of the shell. Corrosion-resistant materials can be used to line the shell where needed. The metal bands and steam chests are usually made of metal.

Conveyor systems are used when gentle material handling is needed. Accurate and close control of the process conditions such as residence time and temperatures are

possible. However, according to **Nonhebel (1971)** these dryers are intrinsically expensive. Heat transfer is poor and auxiliary plow-like mixing devices are necessary to achieve good results **(Perry, 1997)**.

2.7.3 Vibratory conveyors

An overview of vibratory conveyors may be found in chapter 14 of **Nonhebel (1971)**. Vibratory conveyors as heat transfer equipment for solids are discussed in **Perry (1997)**. Vibratory conveyors are primarily conveyors and only secondarily, dryers. Most vibratory conveyors are directional-throw units and consist of a spring-supported horizontal pan which can be excited in a number of different ways. Usually a direct-connected eccentric arm, rotating eccentric weights, an electromagnet, or a pneumatic or hydraulic cylinder is used to throw the material upwards and forwards so that it travels along the conveyor path in a series of short hops. The capacity of these conveyors varies from thousands of tons to grams, but capacity changes are not always easy. Mechanical vibrating conveyors are designed to operate at specific frequencies and do not perform well at other frequencies. Varying the depth of the bed on the trough may be the only realistic way to vary the capacity. Capacity variation is possible with electrical and hydraulic vibratory conveyors. This is done by controlling the electric current magnitude via rheostats and manually or automatically by pressure-control valves.

Heat is usually transferred by conduction through the bottom of the conveyor. The latent heat from condensing steam or other suitable vapours can be used to supply the heat. Sensible heat transfer is not preferred because of the low gas-film coefficient and low heat capacity of the gas. Sensible heat transfer from liquids is also not used because of the additional weight added to the vibratory deck. Other methods of heat transfer include a gas flame which impinges directly on the bottom of the pan. Infra-red heaters are sometimes mounted above the moving bed as a supplement to the other methods of heat transfer. Typical heat transfer coefficients achieved with this type of conveyor are 10 to 100 $W/m^{2\circ}C$. This heat transfer coefficient is usually somewhat higher than the heat transfer coefficients achieved in conventional as well as screw-type conveyors.

Vibrating conveyors are reasonably flexible because the troughs are easily modified to handle different materials. Granular or free flowing materials handle better than pulverized and sticky materials and finely divided solids tend to agglomerate even at fairly low moisture contents. A high friction factor on steel as well as an internal friction factor is necessary so that the conveying action is transmitted through the entire bed. The conveying action is usually gentle enough to prevent particle degradation. This also helps to eliminate dust problems. For slow drying materials, the equipment used is often excessively large with high power requirements which may preclude its use. If however, the conveyor is operated at its natural frequency, the power consumption may not be a problem. Vibratory conveyors can handle high temperatures.

Maintenance on vibratory conveyors is usually low, but suspension springs do need to be replaced regularly as they are susceptible to fatigue. Some unbalanced exciters also have a particularly destructive effect on bearings. Depending on the design, reasonably solid foundations are needed. Feed, discharge and sometimes distribution auxiliaries are required.

2.7.4 Screw conveyors

Information on screw conveyors are found in **Nonhebel (1971)** and **Perry (1997)**. Screw conveyors are used for simultaneous conveying and drying. It consists of a helicoid auger or screw inside a jacketed trough which can be open to the atmosphere, but is more often closed with a carrier gas to sweep out the evaporated moisture. It can also be designed to operate under vacuum. Capacities are limited to around 4.70 m^3/min. Very good mixing can be achieved in screw conveyors with the flights cut, cut and folded or replaced by a series of paddles. Ribbon flights allow sticky materials to be handled. When precise control of the transport rate is required, variable-pitch, tapered-flight, or stepped-flight units can be used.

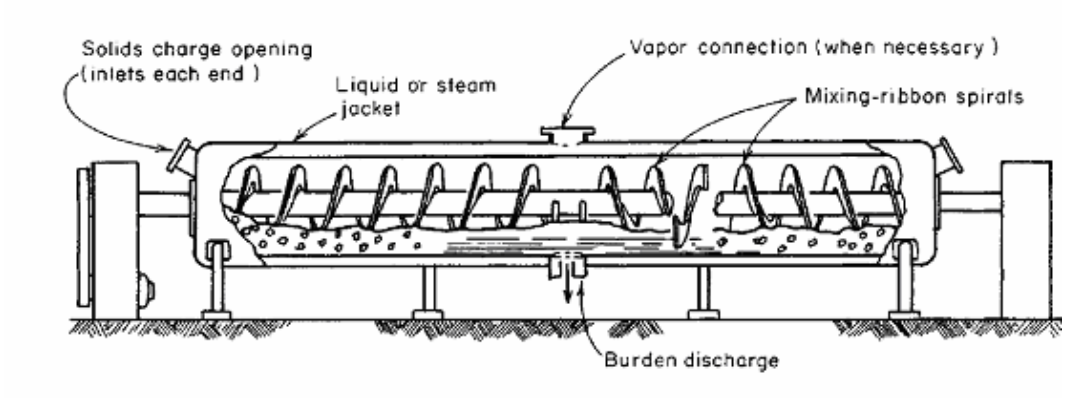

Figure 2.8 Screw conveyor **(Perry 7th ed., 1997)**

Screw conveyors can be made from mild steel, cast iron or stainless steel. Usually these conveyors are made up of standard sections coupled together and special attention should be given to bending stresses on the couplings. The hanger bearings which support the flights can sometimes obstruct the flow and care should be taken not to overload the trough. An advantage of screw conveyors is that the casing can be designed with a drop-bottom for easy cleaning. Ancillary equipment usually consists of feeding and discharge mechanisms. Special arrangements are needed for vacuum operation.

Heating is achieved using hot water, steam or high temperature heat transfer mediums such as pot oil, fused salts or Dowtherm. Electrical heating elements embedded in the casing have also been used. It is of course also possible to use gas fired burners as a heat source. Often hollow screws and pipes are also used for circulating the heat transfer medium to increase the heat transfer area. Heat transfer coefficients achieved in screw conveyors vary from 7 to 70 $W/m^{2\circ}C$ and can be as high as 85 $W/m^{2\circ}C$.

According to **Nonhebel (1971)**, screw conveyors are not widely used because of their limited efficiency as dryers. It is however useful for granular free-flowing materials which become friable at some stage during the drying process. For vacuum pyrolysis of wood chips such a reactor should therefore work well. Screw conveyors are generally not used for materials with a tendency to foul the heat transfer surface although recycling dried material often minimises this problem. Thrust bearings should also be located at the discharge end of the conveyor, if possible, so that the shaft is in tension. When handling non-abrasive, non-corrosive materials, few

problems arise in the operation of the screw conveyor. Depending on the feedstock used, particle size degradation may be a problem. If the temperature inside the reactor is kept high enough and the vapour extraction is good, condensation of gases and subsequent fouling of the heat transfer surface should not provide a serious problem during vacuum pyrolysis. Particle size degradation may however be a problem.

Two patents exist for the use of a screw conveyor for vacuum pyrolysis. The first patent, patent number US5720232, is used for the recovery of constituents from discarded tyres. In this particular invention, the rubber tyre pieces are transferred from a hopper to the pyrolysis chamber by a pan feeder system. This system prevents air and oxygen to enter the pyrolysis chamber. An auger is used to transfer the material through the pyrolysis chamber. The vapours are withdrawn through a heat exchanger and into a liquid-gas separator where the condensed liquids are removed and the gas is recycled for fuel. The solid residue from the pyrolysis chamber is transferred by a closed auger to a closed bin. A pressure sensitive switch is used to open the bin for discharge.

The second patent, patent number US2002072641, is a low energy method for the pyrolysis of rubber and other hydrocarbon material under vacuum. A clay catalyst is added to increase the rate of reaction. The rubber or hydrocarbon material is transported through the reactor by means of a helicoid auger. The input fuel is adjusted over time to maintain the desired reaction temperature and three phases are thus created sequentially in time or spatially inside the reactor. The first phase is the "activation phase", the second the "decomposition phase" and the third the "completion phase". Tandem batch feed hoppers and tandem batch feed collection bins, patent number US2002070104, are operated in sequence and under vacuum for the feed to and collection of material from the reactor.

2.7.5 Multiple hearth furnaces

A discussion of multiple hearth furnaces is given in **Nonhebel (1971)** and **Perry, (1997)**. Multiple hearth furnaces are also known under the following names: Herreshoff, McDougal, Wedge and Pacific. These furnaces consist of annular shaped hearths mounted above the other. Rabble arms, driven from a common centre shaft are provided on each hearth. The feed enters the furnace at the centre on the top

hearth and the rabble arms move the feed outwards to the edge of the hearth, where it falls down to the next hearth. Here it is moved to the centre where it falls down to the next hearth and this continues down the length of the reactor. The centre shaft is usually hollow and cooled internally by forced air. Burners may be mounted at any of the hearths. These furnaces handle granular materials and are used for roasting ores, drying and calcining. Industrial sizes are built from 2 to 7 metres in diameter with 4 to 16 hearths. Total hearth areas range from 6.5 to 335 m^2.

Vacuum pyrolysis in a multiple hearth furnace has been successfully demonstrated on a pilot scale by Professor C. Roy at Laval University in Quebec, Canada. It was, however, decided to design a different reactor with better heat transfer when the process was scaled up.

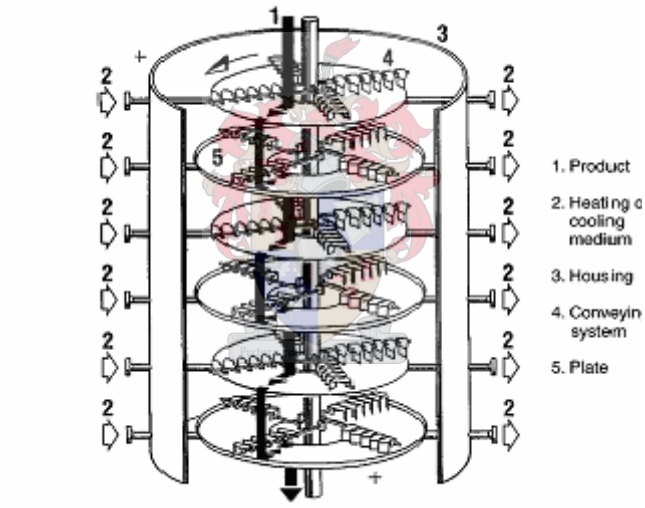

Figure 2.9 Indirect-heated continuous plate dryer for atmospheric, gastight, or full-vacuum operation. **(Perry, 7th ed, 1997)**.

2.7.6 Horizontal moving and stirred bed reactor

The horizontal moving and stirred bed reactor is a reactor that was developed and patented specifically for vacuum pyrolysis of bark particles by professor C. Roy and others from the University Laval in conjunction with the Institut Pyrovac Inc., in Quebec, Canada. The reactor (patent number US6042696) was developed with the aim of improving the heat transfer in the reactor compared to conventional pyrolysis reactors such as rotary kilns, screw-type reactors and multiple hearth furnaces. The feedstock transportation and agitation system as well as the indirect heating system

are all novelties of this reactor. As stated in section 2.5, a vacuum pyrolysis plant, the Pyrocyling^{TM} plant, was built in Jonquière, Canada in 1998/1999, to demonstrate the technology on an industrial scale. The plant has a biomass throughput capacity of 3.5 tonnes/hour.

The pyrolysis reactor consists of a cylindrical housing, 13m in length and 2.2m in diameter, with two heating plates, 10m long, 1.2m wide, one above the other inside the housing. A raking system moves the feedstock along the heating plates. The plates are made up of tubes through which molten salts are circulated as heating medium. Electric tracers were also installed in the shell as an additional source of heat. Screw conveyors are used for the feed and discharge of the material from the reactor and rotary valves were installed in line to prevent the escape of gases from the reactor. A vacuum pump withdraws the vapours and gases from the reactor via a two stage, packed column, condensation system and a pressure of 20 kPa is maintained inside the reactor.

The non-condensable fraction of the pyrolytic gases, withdrawn from the second packed tower, is fired together with natural gas in the molten salt heater to provide the energy required for the pyrolysis reactions. Typical products from this process are pyrolysis oils, water, wood charcoal and pyrolysis gas. The Pyrocycling^{TM} unit has a thermal efficiency of approximately 88% and does, therefore, not consume much energy. For a pilot-scale version of this reactor an overall heat transfer coefficient for wood was predicted between 81 and 107 W/m^{2}K. The prediction did, however, not take into account the phase changes and pyrolytic reactions which will occur during pyrolysis.

2.8 The kinetics of biomass pyrolysis

The literature on chemical kinetics is vast. The literature on the chemical kinetics of biomass pyrolysis is controversial **(Di Blasi, 1998)**. Many different methods exist and at this point there is still much discussion as to which ones to use and which ones not to use. This makes the modelling of biomass pyrolysis a difficult task.

Biomass, as stated before, is a complex material and the decomposition thereof involves many different reactions taking place at different temperatures. It is not possible to characterise these reactions at any significant level of detail, but the kinetic analysis must capture the essence of the exceedingly complex reaction set in a tractable mathematical way **(Burnham and Braun, 1999)**.

Kinetic studies of thermal decomposition reactions in solids, such as the pyrolysis of biomass, are usually performed by thermal analysis methods. As stated by **Vyazovkin (1996)**, these methods measure a difference in an extensive property, such as mass in a TGA. The change in measured property cannot be separated into the contributions from single reactions and as a result, the kinetics of single reactions occurring during the decomposition cannot be determined by thermal analysis methods. The complexity of the process can however not be ignored and the kinetic analysis should allow for a possible change of the rate-limiting step and the associated Arrhenius parameters. According to **Vyazovkin (1996)** the kinetics of thermal transformations are nevertheless commonly described by the equation of a single-step reaction

$$\frac{d\alpha}{dt} = k(T) f(\alpha) \qquad (2.1)$$

where f(α) is the reaction model, α is the extent of reaction, k(T) is the Arrhenius rate constant, described by the Arrhenius equation, T is the temperature and t is the time. This equation can be rewritten for non-isothermal conditions and a constant heating rate β:

$$\frac{d\alpha}{dT} = \left(\frac{A}{\beta}\right) \exp\left(\frac{-E}{RT}\right) f(\alpha) \qquad (2.2)$$

where A is the pre-exponential or frequency factor, E is the apparent activation energy and R is the universal gas constant. This equation and the numerous approximations of its integral form, form the basis of most of the methods of kinetic analysis. From these methods a single kinetic triplet (A, E and the reaction model) may be determined for the overall transformation process. This method does not allow for a

change in the rate limiting step. According to **Vyazovkin (1996)**, the problem with these simpler methods is that ambiguous values of the Arrhenius parameters may be obtained, because the method consists of fitting alternative reaction models to the data to evaluate the parameters. As a result the values thus obtained are dependent on the chosen reaction model and the problem is that different reaction models often fit the data equally well from a statistical point of view, whereas the numerical values of the Arrhenius parameters differ appreciably. This approach is called the "discriminating approach" because it discriminates between reaction models with the aim of choosing the "best" one. The problems inherent in this approach may be overcome by using an alternative approach. Isoconversional methods represent such an approach because it allows the determination of the kinetic parameters independent of the reaction model. According to the isoconversional principle, the reaction rate at a constant conversion depends only on the temperature **(Vyazovkin, 1997)**. One example of such a method is Friedman's method **(Brown et al, 2000)**. It is based on the following equation:

$$\ln \frac{d\alpha}{dt} = \ln\left(\beta \frac{d\alpha}{dT}\right) = \ln A + \ln[f(\alpha)] - \frac{E_a}{RT} \qquad (2.3)$$

E_a can be obtained from the slope of a plot of $\ln(d\alpha/dt)_i$ versus $1/T_i$ for a given value of α. The pre-exponential factor, A, can be determined from the extrapolation of a plot of the intercept against α_i. This equation holds, according to the literature, for an arbitrary reaction model, $(f(\alpha) = (1-\alpha)^n$. This assumption is, however, controversial. The above equation will only hold for a reaction order of 1, because otherwise the starting concentration needs to be accounted for.

The results of a project initiated by the International Confederation for Thermal Analysis and Calorimetry (ICTAC), which focussed on the computational aspects of kinetic analysis, were published in a series of papers in 2000 **(Brown et al, 2000)**. For this project, sets of kinetic data were prepared and distributed to volunteer participants for analysis. The participants were allowed to use any, or several, methods they wished. The data sets sent out consisted of sets of α, t data at several different constant temperatures, sets of α, T data at several constant heating rates, β, and sets of T, t data obtained at several different constant reaction rates, $d\alpha/dt$. Part A

of this series of papers presented the results and some discussion and conclusions. Parts B and C presented detailed individual discussions by two of the organisers while Parts D and E presented individual points-of-view from two of the participants.

Multi-heating rate and isoconversional methods were found to be the most effective methods of kinetic analysis. It was also concluded that 'goodness-of-fit' is a necessary but not sufficient condition for the identified reaction model to be sound. It was felt that a shift of emphasis from the computational aspects of kinetic analysis to better experimental planning was necessary with the purpose of revealing details of important bond redistribution processes that lead to the formation of new compounds and structures. The reaction mechanisms of multi-step solid-state processes need further investigation and studies need to be done to probe particular factors which may control solid state reactions. Physical processes such as melting, sublimation, diffusion, adsorption, sintering and crystallisation may also control the overall kinetics and need to be addressed.

Some important conclusions were made by **Maciejewski (2000)**. From the results of the project it was clear that the same process cannot be characterised by the same kinetic triplet under different experimental conditions. This means that kinetic triplets are not intrinsic properties of the solid. Single-heating rate data for the determination of kinetic parameters should be avoided because many different kinetic triplets can accurately describe a single α-T relationship. Computational methods which employ multi-heating rate data and at least three different heating rates should be used instead. Experimental conditions also affect the course of isothermal and non-isothermal α-t and α-T dependencies differently. This makes it difficult to compare kinetic parameters obtained from isothermal and non-isothermal experiments. There are two reasons why inconsistencies can occur between isothermal and non-isothermal kinetic triplets. The first is that the temperature ranges of isothermal and non-isothermal experiments are not the same, and the second is that truly isothermal conditions cannot be achieved for very low and very high ranges of the extent of the reaction. Isothermal experiments cannot be carried out at temperatures where the reaction rate is too fast, because significant decomposition may occur during the settling of the experimental temperature. This period of temperature settling is dependent on

experimental conditions (applied temperature ramp, sample mass and kind of carrier gas) and reactant properties (C_p, thermal conductivity, the mechanism of decomposition) and as a result of this, it is impossible to achieve strictly isothermal conditions over the full range of conversion. Determining the α - T dependence at the beginning of decomposition is also difficult. Self-heating and –cooling is another factor which affects the reliability of the kinetic data for very low and very high conversions. These effects increase with sample size and cause a deviation of the actual temperature from the preset temperature, which may invalidate the evaluation of the kinetic triplet (Activation Energy, Pre-exponential Factor and Reactor Model). The solution to the problem of achieving reliable kinetic data is to use non-isothermal experiments, carried out over a wider temperature range, to determine the kinetic parameters.

According to **Vyazovkin (2000)** the most important feature of a reliable method of kinetic analysis is its ability to handle multi-step processes that are typical for reactions of solids. Model-free and model-fitting methods that use sets of isothermal and/or non-isothermal data obtained at different temperatures and heating rates were found to be most effective in detecting this feature in the data provided in this project.

To avoid confusion it is necessary to make a point about the relationship between the term “mechanism” as used in section 2.2.4 and section 2.3 and the “kinetic scheme” derived from kinetic analysis. **Vyazovkin (1996)** states that the term “mechanism” is often used to designate a sequence of elementary steps involved in the process. This information cannot be obtained from thermal analysis data, as explained above. “Kinetic scheme” on the other hand is a more confined term that refers to the sequence of those steps which affect a change in the physical property measured by the thermal analysis technique. The combination of thermal analysis with other techniques is, however, capable of identifying a kinetic scheme close to the actual mechanism.

2.9 An alternative approach to the kinetic analysis of biomass pyrolysis

From the above literature it seems clear that isoconversional methods are the best way to determine the kinetic parameters of a complex material. Nevertheless, different methods do exist and one such method, used in this study for comparative purposes, is the one used by **Koufopanos et al. (1991)**. A brief description of this method is given below.

The chemical reactions of pyrolysis are simulated by a parallel and serial reaction kinetic scheme, given in Figure 2.10. This kinetic scheme is similar to the one proposed by **Reina et al (1998)** and **De Jongh (2001)** and indicates that biomass decomposes to volatiles, gases and char. These volatiles and gases may further react with the char to produce more volatiles, gases and char of a different composition. The primary pyrolysis products thus participate in secondary interactions (reaction 3) to yield a modified final product distribution.

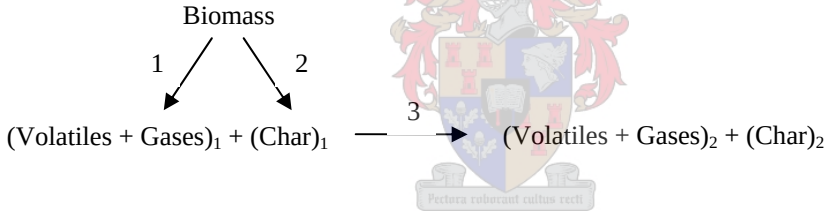

Figure 2.10 Kinetic scheme for the pyrolysis of biomass proposed by **Koufopanos et al. (1991)**.

The differential equations which describe the kinetic scheme outlined above are as follows:

$$\frac{dB}{dt} = -(K_1 + K_2)B^n \tag{2.4}$$

$$\frac{dC_1}{dt} = K_2 B^n - K_3 C_1 \tag{2.5}$$

$$\frac{dC_2}{dt} = \delta K_3 C_1 \tag{2.6}$$

$$W = B + C_1 + C_2 \tag{2.7}$$

These equations can be solved using the method of Runge-Kutta. The kinetic constants, K_1, K_2 and K_3 are described by the Arrhenius equation and A_1, E_1, A_2, E_2, A_3, E_3 and δ , where δ represents the fraction of volatiles and gases deposited on the char sites by the secondary reaction (3), are determined by fitting the scheme to the experimental mass-loss data. The best values of these parameters are chosen according to the least squares criterion with the following objective function:

$$F(K_1, K_2) = \sum_{j=1}^{m} (W_{theoretical} - W_{experimental})^2 \qquad (2.8)$$

This procedure can be applied for various pyrolysis temperatures and reaction orders. However, despite this not being stated explicitly, it appears as if it was assumed that reaction 3 is first order in the charcoal. For fine particles, the secondary reaction (3) and heat transfer effects can be neglected.

3 Materials and Methods

Thermogravimetric Analysis was used to determine the kinetics of vacuum pyrolysis of wood. Seven experiments were also done in a batch, tube-furnace, where wood chips were pyrolysed to produce oil and charcoal. The results from both sets of experiments were compared.

3.1 Thermogravimetric Analyser (TGA) experiments

A Du Pont 951 Thermogravimetric Analyser with a horizontal balance was used for all the TGA experiments. This TGA was preferred over the more modern Shimadzu TGA-50 because of its ability to handle low pressures. A schematic diagram of the TGA set-up is shown in Figure 3.1. The set-up consisted of a needle valve and a gas-flow meter, the TGA, a manometer, a cold-trap, an air leak, a three-way valve and a Pfeiffer vacuum pump. High purity Nitrogen gas was used as a purge.

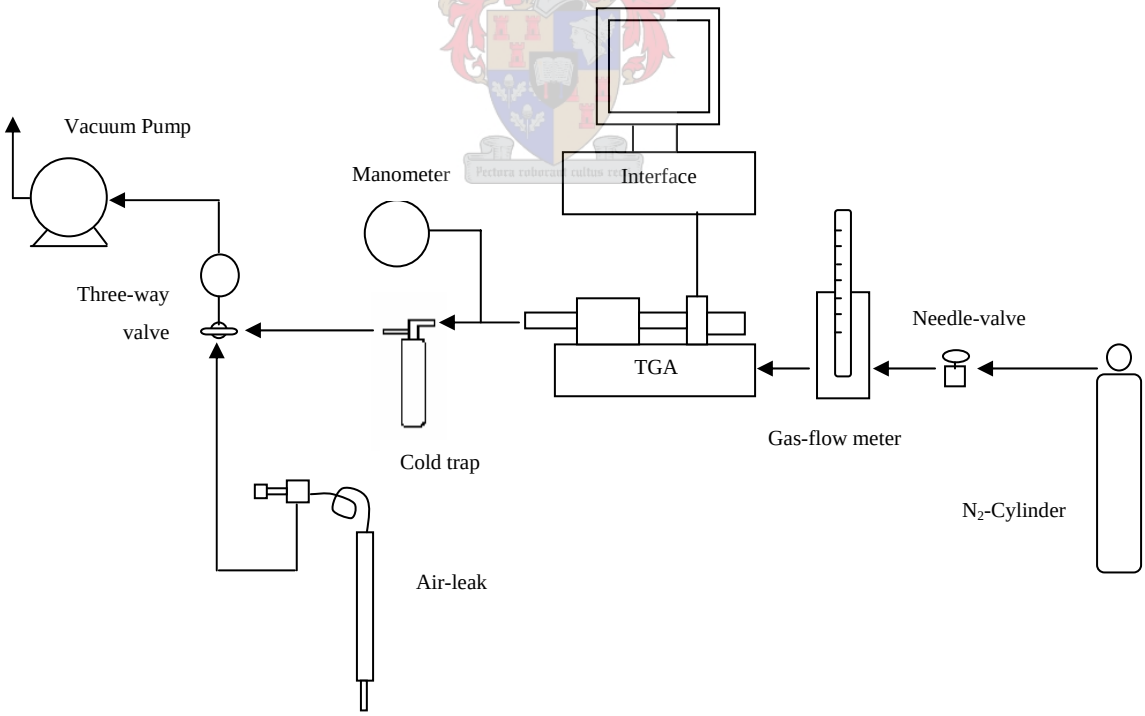

Figure 3.1 A schematic of the TGA set-up.

It was found that oxidation of the sample occurred at low Nitrogen flow rates (~ 100ml/min). This problem was eliminated by using a high Nitrogen flow rate, of the

order of 1400 – 1500 ml/min. The air leak was used to adjust the pressure in the reactor, measured by the manometer, to 140 mm Hg absolute (~18.67 kPa). In order to prevent air leaking in before the reactor, the pressure on the regulator was set to 50 kPa gauge pressure. The needle valve on the gas-flow meter did not seal properly and this necessitated installing another needle valve before the rotameter. This resulted in a lower pressure drop across the gas-flow meter. The reactor was connected to a cold trap. This cold trap was left at room temperature and allowed some condensation of the pyrolysis vapours before removal through the pump. This was necessary to prevent sticky build-up of oil in the vacuum pump.

Rooikrans wood (*Acacia cyclops*) and Swarthaak wood (*Acacia mellifera*) were used for all the TGA experiments. In order to investigate the effect of particle size on the extent of reaction, fine sawdust samples as well as larger block samples were prepared. The sawdust was generated using a belt sander and the size of the sawdust particles was determined using a high resolution laser particle size analyser, the Saturn DigiSizer 5200 V1.10. For Rooikrans wood the mean particle size was determined at 76 μm, and for Swarthaak, the mean particle size was 90 μm. Larger wood particles were prepared for the Rooikrans wood only. This was done using a handsaw and a utility knife. Blocks of roughly 1 mm by 1 mm by 1 mm and blocks of roughly 2-4 mm by 2-4 mm by 2-4 mm were prepared. Except for the larger blocks, the sample weight loaded onto the crucible for each run in the TGA was about 10 mg. The larger blocks weighed between 20 and 40 mg each. Only one of these was used for each experiment.

Isothermal experiments have traditionally been used for kinetic analysis, but the advances in computational power have made the analysis of non-isothermal data and more specifically, the estimation of the temperature integral, possible. Precise numerical integration techniques eliminate the source of difference between the kinetic parameters obtained from isothermal and non-isothermal experiments **(Maciejeski, 2000)**. Nevertheless, the kinetic values determined from isothermal and non-isothermal experiments often differ for a number of reasons, as explained in the literature study. Both non-isothermal and isothermal experiments were carried out for comparison. Heating rates of 2, 10, 20, 35, 50 and 100 ˚C/min were used for the

dynamic experiments and the isothermal experiments were carried out in the range 250 to 520 ˚C where the majority of the pyrolysis reactions take place.

Each run was started by loading the sample of approximately 10 mg onto the crucible and sealing the TGA. The vacuum pump was then switched on and the three-way valve opened slowly to evacuate the TGA. The nitrogen purge was then introduced and the air-leak adjusted until the pressure in the reactor was 140 mm Hg. The experimental conditions were then set in the TGA and the experiment started. At the end of the run, the TGA was left to cool down under vacuum. The procedure for calibrating the TGA can be found in appendix B.

3.2 Tube furnace experiments

Seven runs were done in a batch operated tube-furnace. The results were compared with the results obtained from the TGA analysis.

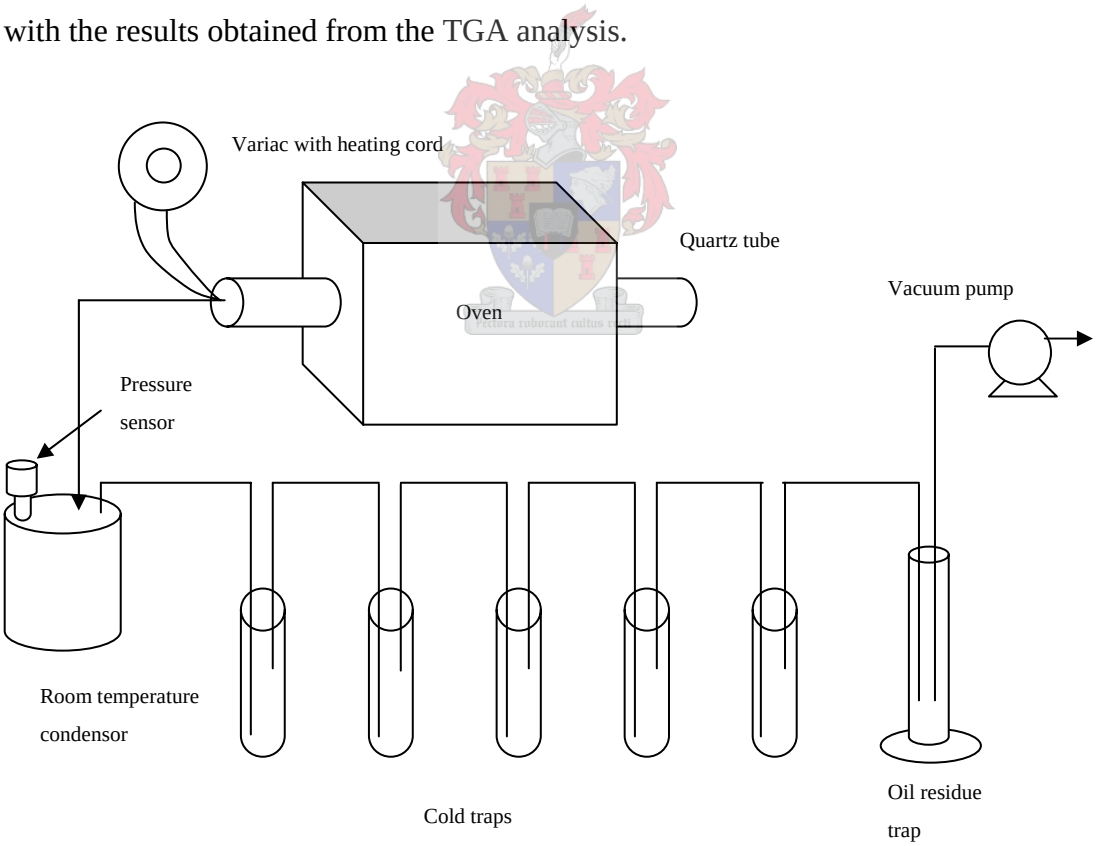

Figure 3.2 A schematic of the tube-furnace reactor set-up.

The tube reactor consists of a 1m long, 60mm OD quartz tube that is heated by six insulated, computer controlled heating elements. Temperature and pressure readings

are made possible by thermocouples and a Schaevitz type P2014-0002 differential pressure sensor with a range of 0 to 2 bar. Connected to the reactor is a series of cold traps, an oil residue trap and a vacuum pump. The exit pipe from the reactor to the first cold trap was maintained at a temperature of 100 to 120 ˚C to limit condensation before the traps. The vacuum pump removed the vapours from the reactor through the cold traps where the condensable vapours were condensed and recovered as liquid. Six cold traps were used. The first cold trap was left at room temperature and the following two cold traps were maintained at roughly 0 ˚C, using ice. The last three cold traps were kept at -78 ˚C using dry ice. The pressure in the reactor was maintained at less than 5 kPa absolute.

Wood samples of 100 g were loaded into the reactor for each run. Care was taken to ensure that the whole sample was within the hot-zone. After loading the reactor was sealed and evacuated. A heating rate of 10 ˚C/min was used to heat the sample to a set temperature where it was kept for 60 minutes. In his study, **De Jongh (2001)** found that a pyrolysis time of 60 minutes gave the best results in terms of oil yield per unit of energy input. After 60 minutes, the reactor was allowed to cool under vacuum for approximately 2 hours after which the char and condensed vapours were weighed. Only three isothermal temperatures were used in this study: 350, 450 and 520 ˚C.

3.3 Analytical methods

The char residue and oil from the tube-furnace experiments were weighed after each run and analysed. A more detailed description of the methods outlined below can be found in **De Jongh (2001)**.

3.3.1 Feedstock moisture content

Two different methods were used to determine the moisture content of the wood. The first method involved drying the samples for a week in a vacuum oven at a temperature of about 70 ˚C and calculating the water loss as a percentage of the feedstock mass. Larger wood chips and sawdust were used. A second method, the Karl Fischer method, was also used to determine the moisture content of the sawdust.

3.3.2 Charcoal ash analysis

The charcoal samples were heated in air to 600 ˚C and the residue weighed. The ash content was then calculated as a percentage of the original sample mass.

3.3.3 Charcoal Inorganic composition

The metal content of the char samples were determined using a Liberty Series II radial emission inductively coupled plasma (ICP) spectrometer. First, the carbon was burned off in air at 600 ˚C for 4 hours. The ash was then dissolved in Aqua Regia and diluted with water. From the known ash mass and dilution factor, the metal content of the charcoal can then be determined quantitatively.

3.3.4 Oil and Charcoal calorific value

A CP 500 Bomb Calorimeter with a Ni/Cr wire, 0.5 g of sample and Benzoic acid as primary standard was used to determine the calorific values of the oil and charcoal. The calorific, or energy values of the oil samples could unfortunately not be determined in this way because the oil could not be ignited. The reason for this was the high water content of the oil. It was however not an important part of this study and the calorific value of the oil was not determined.

3.3.5 Charcoal BET surface area

Samples were first degassed at 300 ˚C to remove all the volatiles from the sample. The multipoint Brunauer, Emmett and Teller (BET) method, using a Micrometrics ASAP 2010, was used to determine the specific area of the samples. A high surface area will indicate that the charcoal has the potential to be upgraded to activated carbon through steam activation.

3.3.6 Chemical compounds in oil

GC/MS analysis was performed on the oil samples from the first three experiments to identify some of the major components present in the oil. A summary of the method used is given below. A more detailed discussion can be found in **De Jongh (2001)**. First, the oil was pre-absorbed onto one gram of Taylor Mesh 80 silica gel before it was transferred to a 10 mm ID glass column filled with 15 grams of silica gel. 150 ml of eight increasingly polar eluants were then used to sequentially elute the column. The eluants used were petroleum ether, 75 % petroleum ether and 25 %

dicloromethane, 50 % petroleum ether and 50 % dicloromethane, 25 % petroleum ether and 75 % dicloromethane, dichloromethane, ethyl acetate, methanol and lastly 10 % formic acid and 90 % methanol. The eluted samples were concentrated in a rotary evaporator under reduced pressure until dry. After weighing, the samples were dissolved in 2 ml of the eluate and analysed on a Hewlett Packard G2800A GCD system using a BP1-PONA column (100 % dimethyl polysiloxane, 0.15 mm (ID), 0.5 μm (film), 50 m (length)) column.

3.3.7 Oil Water content

The Karl Fischer method was used to determine the water content of the oil samples. A metrohm KF Titrino was used to do the analysis, using the standardised Karl-Fischer reagent. A sample of the oil was injected into the reagent and the water content was determined as a percentage of the injected sample.

4 Model Development and Kinetics

In the literature study an overview of potential reactor technologies for vacuum pyrolysis of biomass was given. This overview is a necessary starting point in order to be able to choose the best possible reactor for vacuum pyrolysis in a South African context. A final decision can, however, only be made after an in-depth study of each individual reactor configuration. To quote **Nonhebel (1971)** slightly out of context, "The technically and economically correct choice may involve a major investigation and a knowledge of the answers to many complex questions." Such an investigation was not the primary focus of this study and a reactor had to be chosen in order to develop a model. Rotary ovens are robust, reasonably flexible and simple and for this reason it was decided to develop a simple model for the vacuum pyrolysis of biomass in a rotary oven. The purpose of this model is to provide an easy-to-solve first approximation for the design of such a reactor.

4.1 Reactor model development

For vacuum pyrolysis an indirect-heat rotary oven, similar to an indirect-heat calciner, will have to be used. Gas or oil burners, which will provide the heat, may be situated at either end of the reactor for co-current or counter-current flow with the bed. Alternatively the gas or oil burners can also be situated along the length of the reactor. A simplified drawing of such a reactor is given in Figure 4.1.

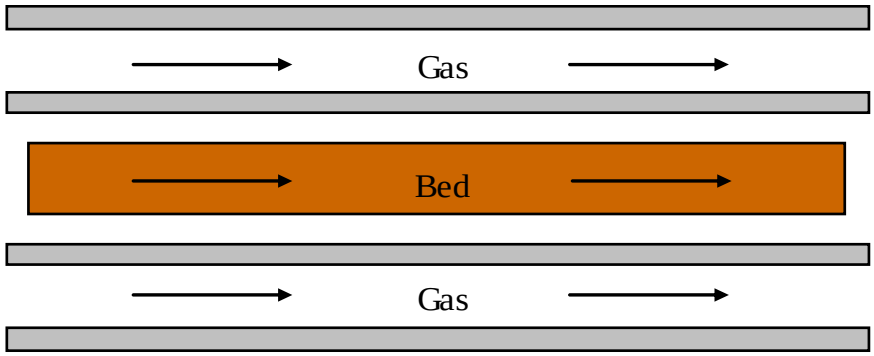

Figure 4.1 Schematic drawing of a co-current indirect-heat rotary oven for vacuum pyrolysis

A model for a conventional cement kiln would be a good starting point for the development of a model for vacuum pyrolysis in a rotary oven. The main difference, however, lies in the fact that in a traditional cement kiln, heat is transferred directly from the gas to the feedstock. During vacuum pyrolysis, the feedstock is heated indirectly. For this study a conventional one-dimensional, plug-flow model for rotary kilns **(Boateng and Barr, 1996)** was used as the basis for the thermal model. This model is used to predict the "average" conditions within the reactor as a function of axial position. The heat transfer equations can be derived by considering a transverse slice through the reactor and doing energy balances over the gas and bed. For simplification it was assumed that the wall offers negligible resistance to heat transfer and thus, the heat transferred from the gas to the wall equals the heat transferred from the wall to the bed. Heat is transferred from the burner gas to the wall by convection and radiation and from the wall to the bed by radiation and conduction. Since the reactor is operated under vacuum and no carrier gas is used, convection plays no major role in the heat transfer from the wall to the bed. For simplification of the model, convection was assumed to be the major mode of heat transfer from the gas to the reactor wall. Heat transfer by radiation becomes significant when the temperature of the heat source exceeds 300 ˚C **(Roy et al., 1992)**. In a rotary oven the inlet gas temperature may be as high as 1000 ˚C which would make radiation the dominant mode of heat transfer from the wall to the bed. **Roy et al. (1992)** investigated the heat transfer limitations during the vacuum pyrolysis process and found that heat transfer from the heat source (reactor wall) to the bed as well as the heat transfer within the bed of particles is governed by radiation. For heat transfer to a bed of wood particles, the effective surface contact between the wall and the particles are small in comparison with the size of the particles and, the quality of this contact is poor. For this reason the conduction term for heat transfer from the wall to the bed, was neglected in the model. This can be shown by using Schlünder's model **(Roy et al., 1997)** to calculate the surface-to-particle contact heat transfer coefficient. An example of this calculation is shown in Appendix E. A further assumption made is that the bed has perfect radial mixing and that there are therefore no radial temperature profiles within the bed. This is not entirely correct, because the rotation speed of the oven is not very high. Mixing will therefore not be perfect. This assumption was used nevertheless, because it simplified calculations significantly. Figure 4.2 below shows

the differential volume elements (DVE) used for the energy balances over the bed and the gas.

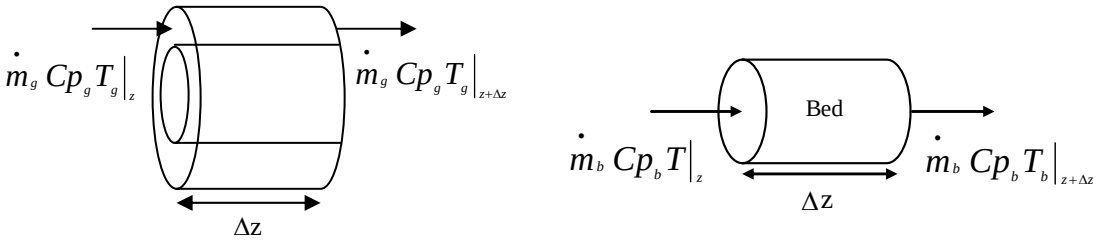

a) b)

Figure 4.2 DVE for axial transport through a) gas, and b) bed

Under steady state conditions an energy balance over a differential volume element (DVE) of the gas yields

$$\sum \dot{m}_g C_{p\,g} \frac{dT_g}{dz} = h_w A_w (T_g - T_w) \tag{4.1}$$

where A is the effective heat transfer area per unit oven length (m). An energy balance over a DVE of the bed yields

$$\sum \dot{m}_b C_{p\,b} \frac{dT_b}{dz} = \frac{\sigma A_w (T_w^4 - T_b^4)}{\frac{1}{\varepsilon_1} - \frac{1-\varepsilon_2}{\varepsilon_2}\left(\frac{r_{reactor}}{r_{bed}}\right)} - \lambda A_{bed} \Delta H_{rxn} \tag{4.2}$$

The first term on the right-hand side of equation 4.2, is the "source" term, which represents the radiation heat transfer rate between the wall and the bed. This form of the term assumes the two surfaces as infinite concentric cylinders **(Incropera and DeWitt, 1996)**. The second term on the right-hand side of equation 4.2 is the reactive term, with λ the rate of species production in the reactor and A the bed area (m^2). Since the resistance to heat transfer by the wall is neglected and the heat transferred from the gas to the wall equals the heat transferred from the wall to the bed, a third,

balance equation, is needed:

$$h_w A_w (T_g - T_w) = \frac{\sigma A_w (T_w^4 - T_b^4)}{\frac{1}{\varepsilon_1} - \frac{1-\varepsilon_2}{\varepsilon_2}\left(\frac{r_{reactor}}{r_{bed}}\right)} \qquad (4.3)$$

As is, the above three equations can be used to model the axial temperature profiles in the reactor. However, as mentioned earlier, these three equations assume a uniform temperature distribution across a transverse slice of the bed and this will only hold if mixing in the bed is very good. The temperature calculated from the above three equations may be seen as only the surface temperature of the particles in the bed and not the average bed temperature. Even though the reactor will reach steady state at some time, each individual particle, as it travels along the length of the reactor, remains in an unsteady state until it reaches a uniform temperature. If perfect mixing is assumed, the surface temperature of all the particles in the bed will be the same. The average temperature of an individual particle will then also be the average temperature of the whole bed. In order to account for this, a fourth equation can be used to calculate the average temperature of an individual, spherical particle, and thus the average temperature of the bed:

$$\frac{\partial T_{b(average)}}{\partial t} = \frac{\alpha}{r^2}\frac{\partial}{\partial r}\left(r^2 \frac{\partial T_{b(average)}}{\partial r}\right) \qquad (4.4)$$

Equation 4.4 is an unsteady-state equation with which the temperature profile inside the particle can be calculated. This can be done at successive axial positions. The initial and boundary equations for this equation are:

$$\text{at t} = 0,\ T_{b(average)} = T_{b(surface)0}$$

$$\text{at r} = 0,\ \frac{\partial T_{b(average)}}{\partial r} = 0$$

$$\text{at r} = R,\ -k\frac{\partial T_{b(avergage)}}{\partial r} = h_r (T_{b(surface)} - T_{b(average)})$$

where h_r is the radiative heat transfer coefficient, defined as

$$h_r = \frac{\sigma(T_{b(average)}^4 - T_{b(surface)}^4)}{T_{b(average)} - T_{b(surface)}} \qquad \textbf{(Roy et al, 1992)} \qquad (4.5)$$

The average bed temperature is then taken as the average particle temperature. The above 4 equations can be solved for successive axial positions.

4.2 The kinetics of biomass pyrolysis

The kinetics of biomass pyrolysis is incorporated into the reactor model through the term for the rate of species production in the reactor, λ, as seen in equation 4.2. λ may be defined as follows:

$$\lambda = \rho_{bed} \frac{d\alpha}{dt} \qquad (4.6)$$

with dα/dt predicted from the kinetic model. For the sake of simplicity, the commonly used equation for a single-step reaction, combined with an n^{th} order reaction model, was used to describe the kinetics of biomass pyrolysis:

$$\frac{d\alpha}{dt} = k(1-\alpha)^n \qquad (4.7)$$

where α is the extent of reaction, k is the rate constant and n is the reaction order. If n < 1 in a condensed phase reaction, it is usually considered a shrinking core reaction. A shrinking sphere has n = 2/3, a shrinking cylinder has n = 1/2 and a receding plane has n = 0. If is n > 1, the reaction can be interpreted as a γ distribution of reactivity **(Burnham and Braun, 1999)**. The rate constant, k, is described by the Arrhenius equation:

$$k = A\exp\left(\frac{-E_a}{RT}\right) \qquad (4.8)$$

where A is the pre-exponential or frequency factor and E_a is the activation energy. Biomass is a complex material, and E_a and A were not expected to be the same for every level of conversion. To avoid the pitfalls of conventional kinetic analysis, as outlined in the literature study, the modified Coats-Redfern method **(Burnham and Braun, 1999),** a model-free, multi-heating rate, isoconversional method, was used in this study for the determination of the activation energies and pre-exponential factors. Its derivation is given in Appendix C. It is similar to the method of Friedman and the method of Flynn, Wall and Ozawa **(Brown et al. 2000)**. Using

$$\ln\left[\frac{\beta}{T^2(1-2RT/E_a)}\right] = -\frac{E_a}{RT} + \ln\left(-\frac{AR}{E_a \ln(1-\alpha)}\right) \qquad (4.9)$$

at fixed conversions for each of the heating rates employed, the left-hand side is plotted versus 1/T. This yields a family of straight lines of slope $-E_a/R$. A is obtained from the intercept. Since the left-hand side is a weak function of E_a, the process is done iteratively by first assuming a value of E_a, then recalculating the left-hand side until convergence occurs. This is more accurate than moving $(1\text{-}2RT/E_a)$ into the intercept and assuming it is constant.

Once E_a and A is determined it is possible to predict the conversion of biomass as a function of temperature and time by integrating equation 4.7 **(Burnham and Braun, 1999)**. The general integrated solutions for 1st and nth order reactions, respectively, are

$$(1-\alpha) = \exp\left[-\int_0^t k(T)dt\right] \qquad (4.10)$$

and

$$(1-\alpha) = \left[1-(1-n)\int_0^t k(T)dt\right]^{1/(1-n)} \qquad (4.11)$$

Since it is unlikely that biomass pyrolysis reactions will take place under isothermal or constant heating rate conditions, numerical integration techniques have to be used

to take into account the complex thermal history. Equations 4.10 and 4.11 can be rewritten in a generalised form with the thermal history approximated as a series of constant heating-rate segments:

$$(1-\alpha) = \exp\left[-\sum_{0-p} \Delta U_p\right] \tag{4.12}$$

and

$$(1-\alpha) = \left[1-(1-n)\sum_{0-p} \Delta U_p\right]^{1/(1-n)} \tag{4.13}$$

where

$$\Delta U_p = \int_{tp}^{tp+1} k(T)dt \tag{4.14}$$

The non-zero lower limit of integration prevents the use of the usual constant heating rate solution and a three-term rational approximation for the integral is used instead **(Burnham and Braun, 1999)** and **(Gautschi and Cahill, 1964)**:

$$\Delta U_p = \frac{1}{\beta}\left\{\begin{array}{l} T_p k_p\left[1-\dfrac{(E_a/RT_p)^2 + a_1(E_a/RT_p) + a_2}{(E_a/RT_p)^2 + b_1(E_a/RT_p) + b_2}\right] - \\ T_{p-1} k_{p-1}\left[1-\dfrac{(E_a/RT_{p-1})^2 + a_1(E_a/RT_{p-1}) + a_2}{(E_a/RT_{p-1})^2 + b_1(E_a/RT_{p-1}) + b_2}\right] \end{array}\right\} \tag{4.15}$$

Once α has been determined, $d\alpha/dt$ and the rate of species production in the reactor, λ, can then be determined from equations 4.5 and 4.6.

For this model to be used to simulate the pyrolysis of biomass in a rotary oven, the activation energies and pre-exponential factors for every level of conversion need to be determined experimentally for the material to be used in the reactor. It is important to note that this model is not dependent on the reactor pressure, but, since the kinetic

parameters are determined experimentally under vacuum conditions, the model may be used to predict the pyrolysis of biomass under vacuum.

4.3 Computational procedure

As a first approximation, and due to time constraints, the temperature profile in the particles was neglected and only equations 4.1 to 4.3, together with the kinetic equations, were solved. A brief discussion of the procedure followed is given below before a flow diagram of the solution procedure is given.

Three temperatures and a reaction conversion are solved for as a function of reactor length in order to give the complete temperature profile along the reactor together with the conversion at every point. The three temperatures are the gas, wall and bed temperatures. Initially only the gas and bed temperatures are known. Newton's method is used to solve for the initial wall temperature from equation 4.3. Once all the initial conditions are known, the gas and bed temperatures for the first interval are solved for simultaneously from equations 4.1 and 4.2 using the method of Runge-Kutta. Newton's method is then used once again to solve for the wall temperature from equation 4.3, the "balance" equation. This procedure is repeated along the reactor length until the conversion in the reactor reaches about 80 %. Above 80 % the kinetic model failed to predict the conversion accurately. This does not necessarily present a practical problem, because conversions higher than about 80 % are unlikely in an industrial scale reactor. The summation of Δz gives the reactor length needed. A program was written in Matlab version 6.5 to solve equations 4.1 through to 4.15. The program code can be viewed in appendix F.

Outlined below is the procedure followed in the program to solve the above equations to obtain a complete solution for vacuum pyrolysis in a rotary oven.

4.3.1 Flow diagram of computational procedure

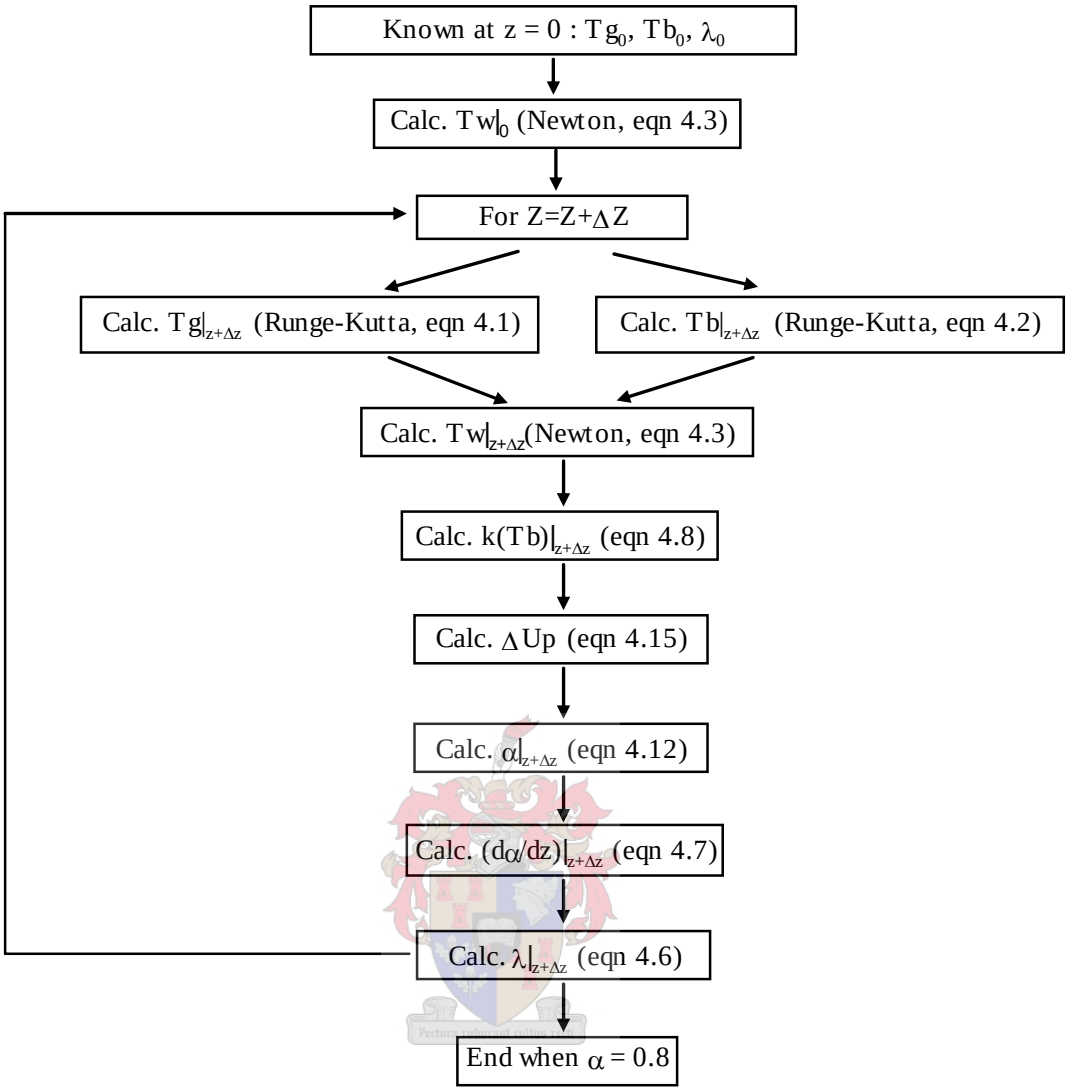

Figure 4.3 Flow diagram of computational procedure.

The results for the combined reactor and kinetic model will be given in chapter 6.

5. Thermogravimetric Analysis Results

Rooikrans (*Acacia cyclops*), a softwood, is a tree species commonly found in the Cape coastal areas. It is also an intruder plant, originally from southwestern Australia, and it was introduced in South Africa for the stabilization of sand dunes. It is an extremely weedy species and is difficult to remove once established **(Duke, 1983)**. Swarthaak (*Acacia* mellifera) is another alien plant species covering large areas in the dryer regions of South Africa. Because of their relative abundance, these species provide a good feedstock source for a pyrolysis process in this country and thus they were chosen for the experiments performed in this study. Experiments were also done with both Rooikrans and Swarthaak in the tube furnace (chapter 7) and this allowed comparison with the results obtained in a previous study by **De Jongh (2001)**.

In this section the results from the thermogravimetric experiments are presented and discussed. As stated previously, two types of experiments were conducted, namely, dynamic and isothermal experiments. Experiments were carried out at a total reactor pressure of 140 mm Hg absolute and under a nitrogen flow of about 1500ml/min. The reason for the high nitrogen flow rate has been explained in the materials and methods section. A run under normal atmospheric conditions, but with the same nitrogen flow rate, was also done. This allowed the comparison of vacuum pyrolysis in a TGA with normal atmospheric pyrolysis. It is also well known that heat and mass transfer limitations affect the pyrolysis reactions in larger particles. For this purpose, three different sample sizes were also pyrolysed in the TGA and the results analysed and discussed.

5.1 Dynamic (non-isothermal) results

All the experimental results are expressed as a function of the degree of conversion α, which is defined as follows:

$$\alpha = \frac{W_0 - W}{W_0} \qquad (5.1)$$

where W_0 is the sample weight at time t = 0, and W is the sample weight at time t = t. It should be noted that the term "conversion", as used in this study, is somewhat different to the traditional meaning of the word. Traditionally, a conversion of 80 % implies that 20 % of the original sample remains unreacted. In the case of pyrolysis in a TGA, a 100 % conversion to products is achieved, because what remains after the completion of the process, is char and not unreacted wood. "Conversion", as used in this study therefore refers to the percentage of mass loss achieved.

5.1.1 The pyrolysis of Rooikrans wood sawdust and the effect of heating rate

Figure 5.1 is a plot of the conversion of Rooikrans sawdust as a function of temperature. It can be observed from the graph that conversion starts to increase sharply above a temperature of 200 ˚C. This increase in conversion continues until a conversion of about 80 % is reached at a temperature of between 400 ˚C and 420 ˚C. Thereafter the increase in conversion decreases and tends asymptotically towards the maximum degree of conversion, which ranges between 85 % and 90 %. The same trend is observed for all the heating rates. It has to be noted at this point that an experimental error occurred with the 35˚C/min run. Instead of it being 35˚C/min, it was 100˚C/min. Unfortunately this was discovered too late. The graph for 35 ˚C/min is therefore left out of all Figures for the fine sawdust particles.

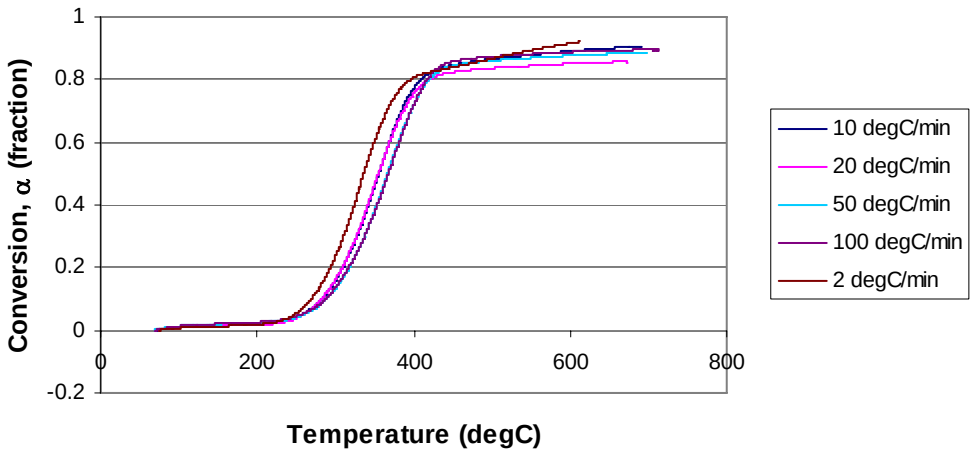

Figure 5.1 The effect of different heating rates and temperature on the conversion of Rooikrans wood sawdust.

The temperature difference between the oven and the sample is smallest for a heating rate of 2 ˚C/min. (It can be seen that this graph does not level off like the others. The reason for this is slight oxidation that occured and for this reason the run was stopped a little earlier.) As the heating rate increases, thermal lag becomes more significant, and the shift to the right observed in the graph for the higher heating rates relative to the lower ones, may be ascribed to this phenomenon. As the heating rate increases, the time taken to reach a certain temperature decreases and the conversion achieved at that temperature is decreased; or, to put it differently, the time the sample spends at a specific temperature decreases with an increase in heating rate, and hence the conversion achieved at that temperature also decreases. For a higher heating rate, the difference between the actual sample temperature and the measured temperature is larger. The difference in maximum conversion is most probably traceable to differences in the samples used. It may be noticed that the conversion of the sample heated at a rate of 2 ˚C/min reached the highest conversion. Also, the curve for this sample did not flatten in the same way as the other curves but continued to increase in a more linear fashion. The most probable reason for this is that air leaked into the TGA, resulting in partial oxidation of the sample.

To quantify the thermal lag in the oven, the measured thermocouple temperature was plotted against the theoretical temperature, defined as the temperature that the thermocouple should read at a specified time for the specific heating rate. Figure 5.2 is thus a plot of the actual or measured temperature versus the theoretical temperature. It can be seen from the graph that the oven used suffered from severe thermal lag. A temperature lag of roughly 200 ˚C is experienced almost throughout the temperature range and for all the heating rates. As heating rate increase, the initial thermal lag increases, because more time is required to achieve the set heating rate. However, as the temperature increases, the initial lag is decreased. For temperatures of about 300 ˚C and higher, the lag for all the heating rates are more or less the same. The oven lag is probably also mirrored in the sample. The effect of thermal lag caused by higher heating rates on the pyrolysis reactions is therefore less at higher temperatures.

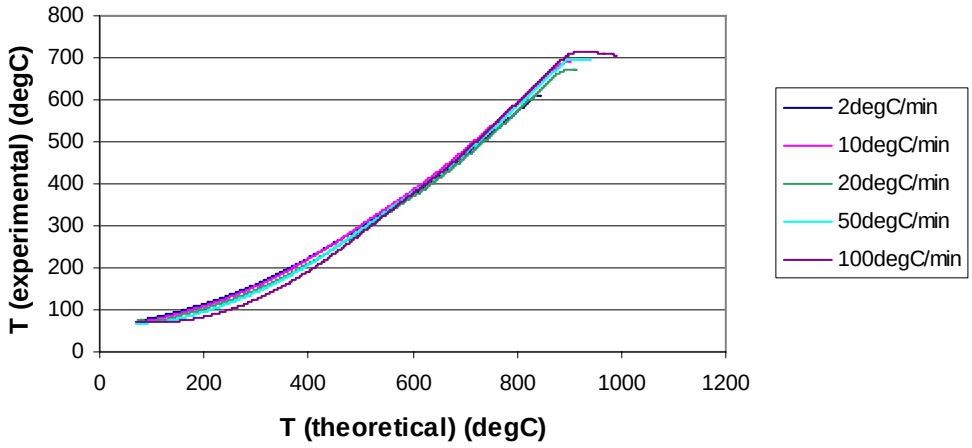

Figure 5.2 Measured temperature versus predicted temperature to quantify thermal lag in the oven.

Reina et al. (1998), who achieved similar results for the pyrolysis of different kinds of waste wood under atmospheric conditions, concluded that the results confirmed the existence of two stages for the pyrolysis process in the temperature range studied. **De Jongh (2001)** accepted this theory and modified it slightly for vacuum pyrolysis.

The Figure below provides further insight into the decomposition process:

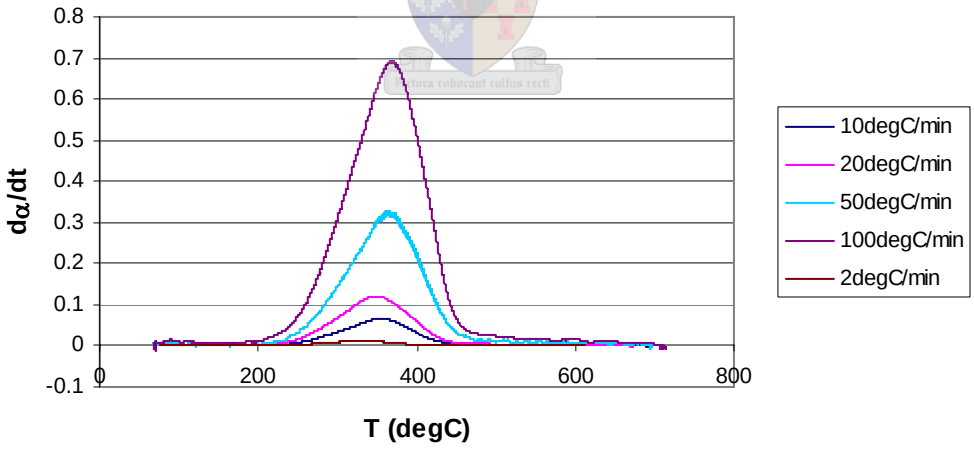

Figure 5.3 The effect of different heating rates and temperature on the instantaneous reaction rate during the pyrolysis of Rooikrans wood sawdust.

Figure 5.3 shows the instantaneous reaction rate of Rooikrans wood sawdust as a function of temperature. Higher heating rates produce higher reaction rates. This is because the same level of conversion is reached in a much shorter time. The maximum rate of reaction is reached between a temperature of roughly 360 ˚C and

370 ˚C. Above these temperatures the reaction rate drops to zero as the reactions reach completion.

According to **De Jongh (2001)**, the first stage, where a high degree of conversion is reached, is the result of the cracking of macromolecules (cellulose and lignin). A decrease in the degree of polymerisation is produced while most of the volatiles are also released during this stage. The second stage, beginning above 400 ˚C, is attributed to the cracking of residual compounds that decompose to produce gases and chars. It is also probable that lignin decomposition will continue above 400 ˚C.

To shed some more light on the effect of the heating rate on the pyrolysis process, dα/dT was plotted against temperature.

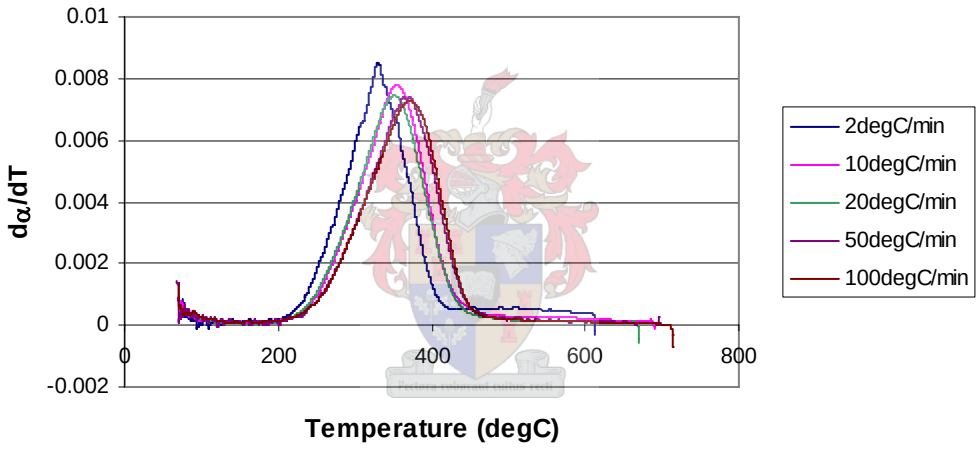

Figure 5.4 The change in conversion corresponding to a change in temperature as a function of temperature.

The above graph is really a plot of the slope of the graphs in Figure 5.1 as a function of temperature. As temperature increases, the increase in conversion caused by, say, a 5 ˚C increase in temperature, increases. This makes sense because from Figure 5.3 it can be seen that the rate of conversion increases with temperature. What is evident from this graph, however, is that the increase in conversion effected by an increase in temperature, at some temperature, cannot be increased by an increase in the heating rate. From Figure 5.1 it can be seen that the slopes of the graphs are the same for all the heating rates. Practically, this means that a temperature of, say, 450 ˚C is needed for the pyrolysis reactions to be completed. Increasing the heating rate, will increase

the rate ($d\alpha/dt$) at which the maximum conversion is reached, but it will not decrease the temperature necessary to achieve this conversion. The thermal lag caused by higher heating rates actually increases the temperature necessary to achieve a set conversion and decreasing the heating rate may therefore decrease the maximum temperature necessary to achieve maximum conversion. The same slope or $d\alpha/dT$ is thus achieved at a higher temperature for a higher heating rate, hence the right-shift of the graphs. It is, however, evident that the maximum slope, or $d\alpha/dT$, for a heating rate of 2 ˚C/min , is slightly higher than those for higher heating rates. This is because at a heating rate of 2 ˚C/min the thermal lag, and hence the temperature gradient in the sample, will be less than for the higher heating rates. Thus, at any given temperature, the average sample temperature is higher for the lower heating rates and the maximum increase in conversion for a set increase in temperature is higher because more of the sample is reacting at a higher temperature. This should be more evident for larger particles where temperature gradients will be more severe. The use of multiple heating rates for the calculation of the activation energies is thus justified because $d\alpha/dT$ is not much affected by the different heating rates. It should however be noted that increasing the heating rate may still affect the composition of the compounds released, and thus the oil yield **(De Jongh, 2001)**. Increasing the heating rate decreases the time spent at lower temperatures and may decrease the short chain compound yield. Less non-condensable gas may thus be produced and a higher oil yield will result.

Comparing atmospheric pyrolysis to vacuum pyrolysis, one could expect to see a higher mass loss at a lower temperature, because of the quick removal of vapour fragments from the wood particles and because boiling and sublimation temperatures are lowered. This was however not seen in the results from this study. Figure 5.5 is a plot of conversion versus temperature for a run at 20 ˚C/min under vacuum, and atmospheric pressure.

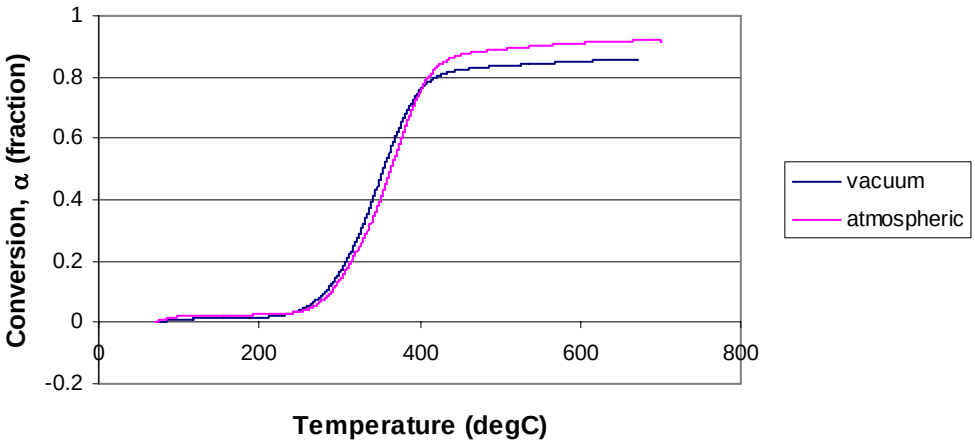

Figure 5.5 Conversion versus temperature for vacuum and atmospheric pressure at a heating rate of 20 ˚C/min for fine sawdust.

It is evident from the above graph that the reactions start at roughly the same temperature and that higher conversions are not reached at the same temperature for the run under vacuum conditions. It appears therefore that pyrolysis kinetics are not much affected by the lower pressures. For both cases however, diffusion limitations were minimal because of the fine particles used, and vapour removal was quick because of the high flow rate of nitrogen used. The effect of vacuum should be greater on an industrial scale though as bigger particles will be used and a high nitrogen flow rate will be unpractical. The use of vacuum should then serve to decrease the overall resistance experienced by molecules diffusing out of the wood particles.

5.1.2 The effect of particle size on the pyrolysis of Rooikrans wood

The effect of particle size was investigated by pyrolizing small Rooikrans wood blocks. Two different sizes were used: 1 – 2 mm blocks and 2 – 4 mm blocks. Because the heartwood and sapwood in Rooikrans is very distinct and because it would have been difficult to load the crucible in the TGA with a representative sample every time, it was decided to have separate blocks for heartwood and sapwood. The heartwood blocks had a brown colour while the sapwood blocks had a light brown to “cream” colour.

Figures 5.6 and 5.7 below show the effect of particle size on the conversion of heartwood and sapwood Rooikrans blocks.

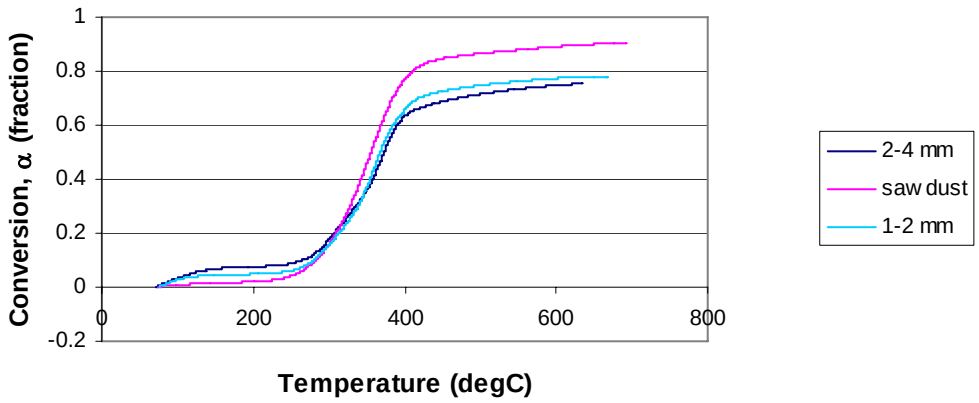

Figure 5.6 The effect of particle size on the conversion of the heartwood blocks of Rooikrans wood at a heating rate of 10 ˚C/min.

It is clear that the highest conversion is achieved for the fine sawdust. This was entirely expected. Heat transfer effects, which were virtually negligible for the fine sawdust particles, start affecting pyrolysis rate and conversion as the particle size increases. This is because of the lower average temperature of the larger particles. Diffusion limitations also come into effect in larger particles. The higher residence time of the volatiles in the solid results in secondary interactions with the char which will lead to higher char yields and a lower overall conversion **(Koufopanos et al, 1991)**. The initial increase in conversion, before the onset of the main reactions above 200 ˚C, may be attributed to the evaporation of water. It is noticeable however, that this increase in conversion is highest for the 2 – 4 mm blocks. As explained in the materials and methods section, the reactor is evacuated and the nitrogen flow rate set before heating and data logging starts. It is therefore possible that more evaporation takes place from the smaller particles before the onset of the experiment because diffusion of the water vapours from the smaller particles is easier. This mass loss is therefore not seen in the graph. It is also interesting to note the inflection point for the two larger particle sizes at around 350 ˚C. This is more clearly seen in the graph of the instantaneous reaction rate versus temperature, in Figure 5.8 below.

Exactly the same trend is observed for the sapwood blocks, as can be seen in the Figure below:

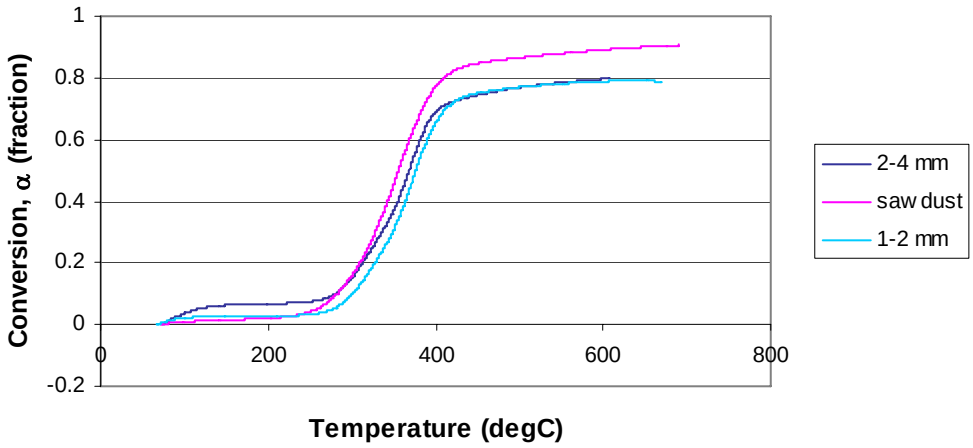

Figure 5.7 The effect of particle size on the conversion of the sapwood blocks of Rooikrans wood at a heating rate of 10 ˚C/min.

When comparing the graphs of instantaneous reaction rate versus temperature for the different size particles of the Rooikrans heartwood (Figure 5.8), the change in reaction rate is clearly seen at temperatures of around 320 ˚C.

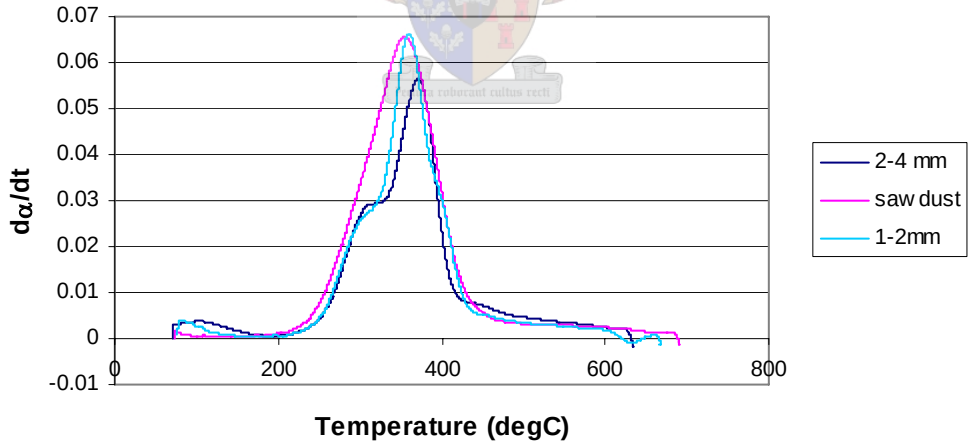

Figure 5.8 The effect of different particle sizes on the instantaneous reaction rate during the pyrolysis of heartwood blocks at a heating rate of 10 ˚C/min.

The sudden decrease and increase in reaction rate observed at a temperature of around 320 – 330 ˚C, may possibly be explained by diffusion limitations. The initial increase in reaction rate is the result of volatile components breaking down and diffusing out of the sample. As the temperature increases, the larger molecules in the wood start to

decompose and at this point the resistance to diffusion may be high because of the size of the molecules. Because the molecules cannot at this point diffuse out from the wood quickly enough, the rate of reaction, or mass loss, cannot increase at the same rate, hence the "kink" observed in the curve. However, as the temperature continues to increase, these larger molecules break down into smaller molecules which diffuse out more easily, resulting in an increase in the reaction rate again. Also, the further the reactions progress, the bigger the pores in the wood particles become, thus lowering the resistance to diffusion.

According to **Antal and Varhegyi (1995)** two distinct peaks are usually observed on the derivative TGA curves (dx/dt versus T, as in Figure 5.8) for the pyrolysis of small samples of whole biomass at low to moderate heating rates. The lower peak is associated with hemicellulose decomposition, which takes place between 225 and 325 ˚C, and the taller peak with cellulose decompostion, taking place between 325 to 375 ˚C. Lignin has a very flat peak associated with it because it decomposes over a very wide range of temperatures, namely 250 to 500 ˚C. However, the presence of mineral salts in the biomass causes the peaks to merge, by catalyzing pyrolytic decomposition reactions in unpredictable ways. The peaks observed in Figure 5.8 and also Figure 5.9 below are reasonably sharp though, suggesting a lower mineral content in the Rooikrans wood. The question that arises however is why this phenomenon is not observed for the sawdust, because the amount of mineral matter present in both the sawdust and the bigger wood blocks will be similar as no pre-treatment of the wood occurred. The reason for this is not altogether clear at this stage.

Another explanation for the two peaks may lie in the endothermic nature of the pyrolysis process. For a high heating rate the reaction rate is fast if the heat transfer to the particle is adequate. It is therefore possible that as the reaction rate increases, heat transfer limitations start hampering the reaction progress and the heat demand becomes greater than the heat supply. As the temperature is further increased, the amount of heat transfer by radiation increases significantly and the limitations are overcome.

Comparing dα/dT for the different heating rates, a trend very similar to the one observed for the sawdust particles is seen.

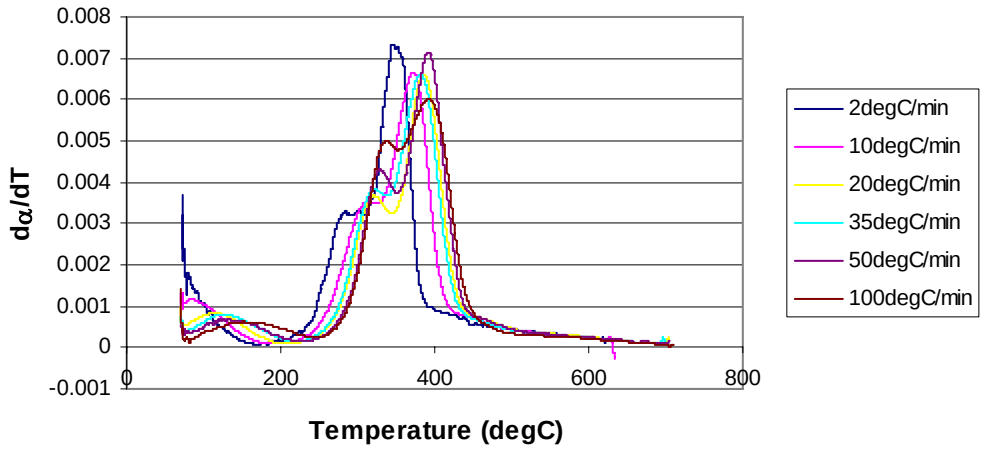

Figure 5.9 The change in conversion corresponding to a change temperature as a function of temperature for the 2 – 4 mm Rooikrans blocks.

Increasing the heating rate increases the thermal lag and the same change in conversion for a given increase in temperature is achieved at a higher temperature, hence the right-shift of the graphs for the higher heating rates. The dα/dT values are of the same order of magnitude as those for the sawdust particles, which suggests that an increase in particle size does not affect the rate of change of conversion with temperature. Figure 5.10 below is a comparison of dα/dT for the sawdust particles and the 2 – 4 mm blocks at a heating rate of 20 ˚C/min.

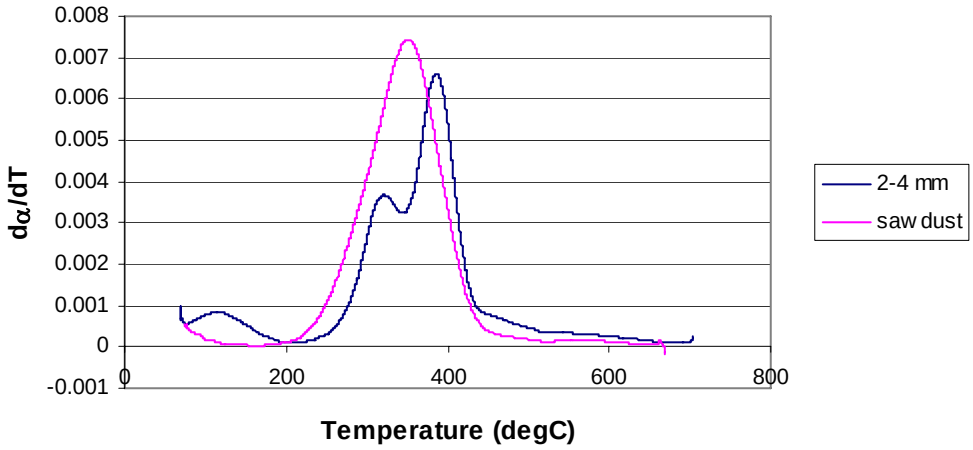

Figure 5.10 Comparison of dα/dT versus temperature for different particle sizes at a heating rate of 20 ˚C/min

The graph for the 2 – 4 mm blocks lies to the right of the graph for the sawdust. The reason for this is thermal lag. It takes longer for the larger particles to reach a given temperature because of the thermal limitations and temperature gradient inside these particles. The same dα/dT is thus reached at a higher temperature. As explained before, diffusion and heat transfer limitations or simply the different decomposition temperatures of the two most abundant chemical species in wood, cellulose and hemi-cellulose, are likely to be the reason for the "kink" observed in the graph for the 2 – 4 mm particles.

Figure 5.11 below compares the conversion versus temperature curves for the pyrolysis Rooikrans heartwood and sapwood particles. It can be seen that the conversion achieved is highest for the sapwood particles. The reason for this may be the fact that more volatiles are present in sapwood compared to the heartwood. In a commercial reactor, wood chips will of course not be separated into heartwood and softwood fractions and the conversion achieved will lie somewhere in between, depending on the relative amounts of each in the wood used as feedstock.

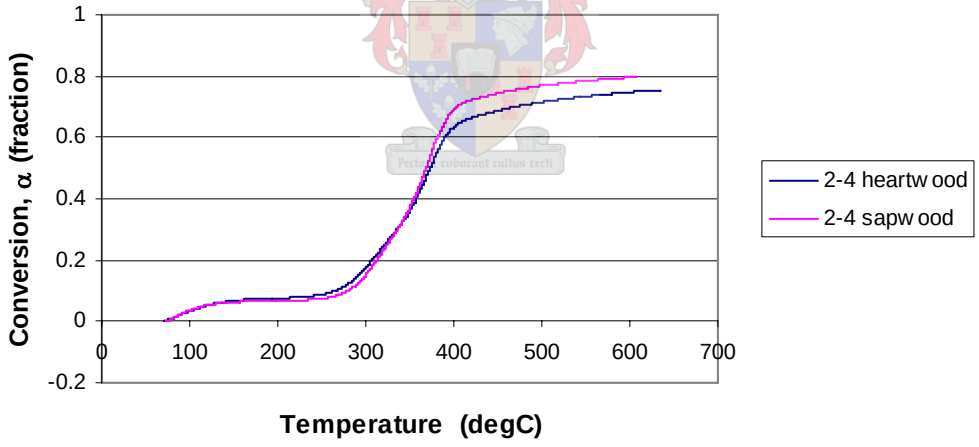

Figure 5.11 The effect of temperature on the conversion of heartwood and sapwood particles at a heating rate of 10 ˚C/min.

5.1.3 A comparison of the pyrolysis of Swarthaak wood sawdust with Rooikrans wood sawdust

A number of runs were also done with Swarthaak wood for comparative purposes. In the Figure below, the pyrolysis of Swarthaak wood sawdust is compared with that of Rooikrans wood sawdust at a heating rate of 10 ˚C/min.

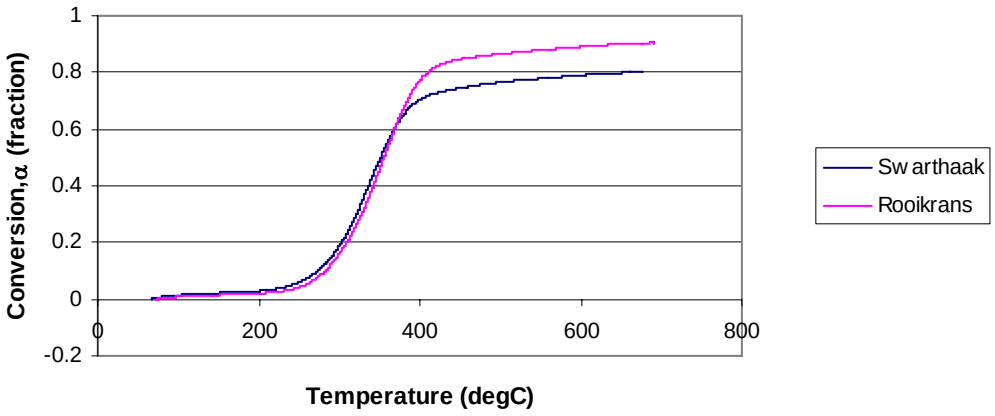

Figure 5.12 A comparison of the pyrolysis of Rooikrans and Swarthaak wood at a heating rate of 10 ˚C/min.

For both wood samples the pyrolysis reactions start at virtually the same temperature and proceed at almost the same rate. The conversion achieved by the Rooikrans wood is 10 % higher though. This is expected because the ash content of Swarthaak wood is 10 % higher than in Rooikrans wood, as seen in table 7.2 in chapter 7.

5.2 Isothermal results

Eight isothermal experiments at temperatures between 250 ˚C and 500 ˚C were carried out using the 2 – 4 mm Rooikrans blocks. Figure 5.13 below shows the conversion as a function of time for the pyrolysis of these blocks.

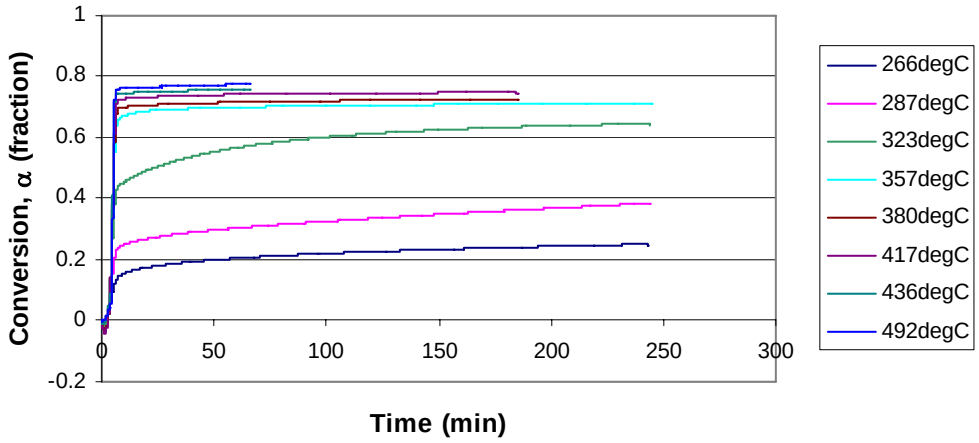

Figure 5.13 Isothermal experiments carried out with the 2 – 4 mm Rooikrans particles.

The sudden increase in conversion at the start of every experiment, evident in the above graph, took place during the heat-up period. A heating rate of 100 ˚C/min were used for all the experiments to minimise the heating-up period.

Table 5.1 Weight loss for isothermal experiments

T	α_{start} (%)	α_{final} (%)
266	15	25
287	24	38
323	15	64
357	67	71
380	70	72
417	72	74
436	74	75
492	76	77

For isothermal temperatures below 300 ˚C, the reaction rate is slow and the maximum conversion achieved after 4 hours is still below 40 %. At this point the conversion had not reached its maximum value and continued to increase at a very slow rate. According to **Ward and Braslaw (1985)** lignin does not start to decompose in measurable rates until temperatures exceed 280 ˚C, and the conversion achievable for lower temperatures will therefore necessarily be less. For isothermal temperatures above 380 ˚C the conversion increased by less than 5 %. The reason for this is simply because by the time the isothermal temperature was reached, most of the reactions had been completed. This is also clearly seen in Figure 5.1. As a result of this, the isothermal experiments performed at these temperatures were of little practical use.

The isothermal experiments could also not be used in the kinetic analysis, because the isoconversional method used required the activation energies to be determined at fixed conversions for different temperatures. As is evident from table 5.1, the conversions achieved during the isothermal stage rarely overlapped for the different temperatures.

5.3 The determination of the activation energies, pre-exponential factors and the rate of reaction

The modified Coats-Redfern method, as outlined in chapter 4, was used to determine the activation energies of Rooikrans wood sawdust at different levels of conversion.

Activation energies were not determined for the larger particle sizes, because heat transfer effects are not taken into account when using this method. Using the TGA data from the larger particles would have resulted in biased values for the activation energies. The values here determined are thus assumed to be the true activation energies for the pyrolysis of Rooikrans wood.

Figure 5.14 below is a plot of the left-hand side of equation 4.9 versus 1/T at conversions of 10, 20, 30, 40, 50, 60, 70 and 80 % for all six heating rates used in this study. Straight lines were fitted to the data for each level of conversion in order to determine the activation energy, E_a, and pre-exponential factor, A, from the slope and intercept of the straight line.

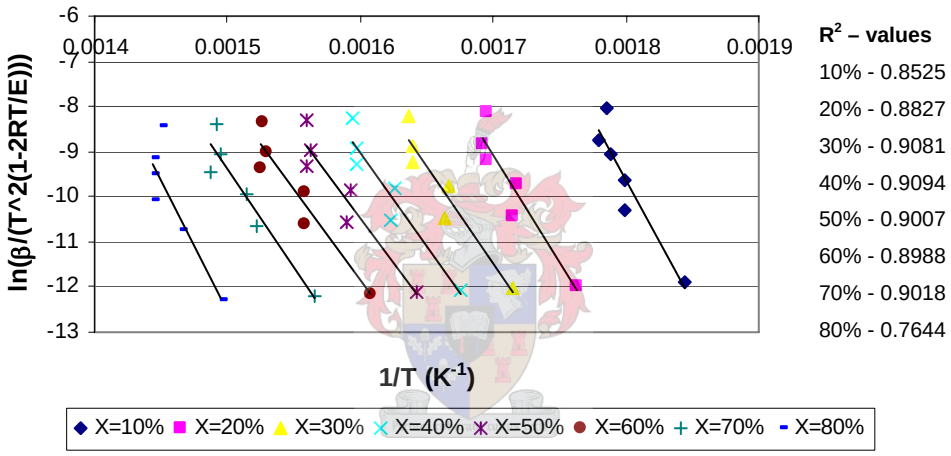

Figure 5.14 Determination of activation energies from a plot of equation 4.8.

Above a conversion of 80 %, the data did not exhibit straight-line behaviour at all. This may be attributed to the fact that the final conversions achieved for the different heating rates differed by as much as 5 %. This was discussed in section 5.1.1. It is, however, unlikely that conversions much above 80 % will be achieved in an industrial size commercial reactor, because of physical and economical constraints. Heat and diffusion limitations will play a much more significant role. The need for data above conversions of 80 % might therefore not be that severe. It can be seen that the data points, especially for the high conversions, for the high heating rates do not lie in line with the other data points, making the straight line fit worse. This is seen clearly from the R^2-value for a conversion of 80 %. Unfortunately there is some uncertainty about the reliability of the data obtained at these high heating rates.

Figure 5.15 below is a plot of the activation energies as a function of conversion.

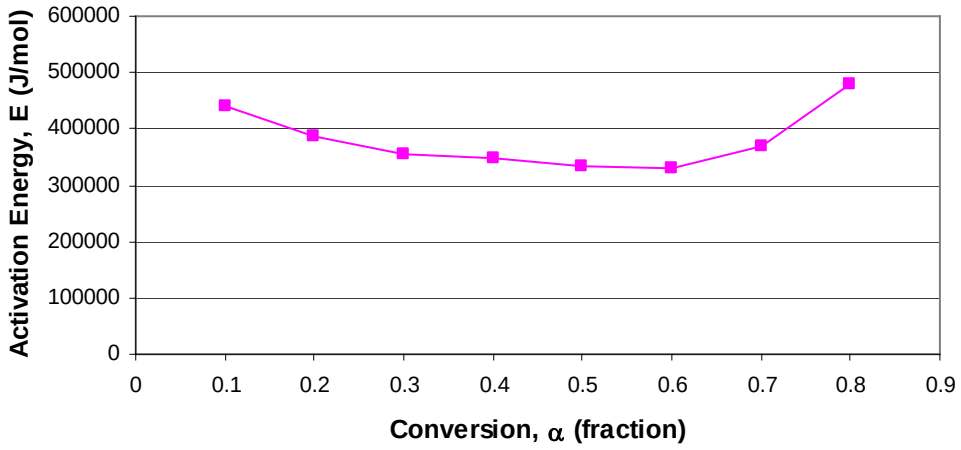

Figure 5.15 Calculated E_a values as a function of conversion for the pyrolysis of Rooikrans wood.

As explained in chapter 4, the A values are determined from the intercept of the straight-lines obtained in Figure 5.14. Linear interpolation and extrapolation was used to determine the E_a and A values for all the conversion levels not directly calculated from the above plot. Equation 4.12 through 4.15 can now be used to calculate the conversion as a function of temperature. Figure 5.16 below is a plot of conversion as a function of temperature assuming a 1st order reaction (equation 4.12).

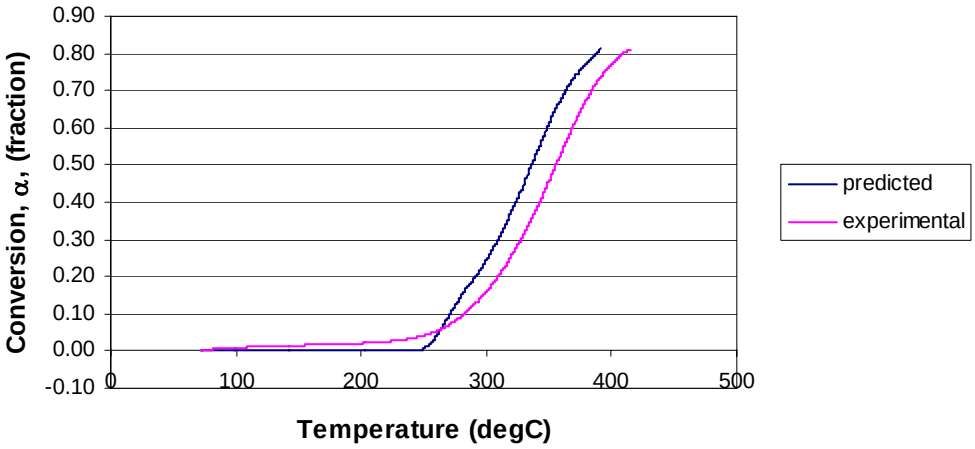

Figure 5.16 Comparison of model prediction of conversion versus temperature with experimental data.

It is evident from the above graph that the model prediction is an over-prediction of the real experimental data for temperatures above 260 ˚C. The conversion predicted

at a certain temperature is higher than the experimental value. Assuming different orders of reaction did not improve the prediction. The problem was solved by assuming that the E_a value calculated from equation 4.9 is the average E_a value for the interval $\alpha = 0$ to $\alpha = \alpha$. The actual E_a for each interval (0 – 10 %, 10 – 20 % and so forth) was calculated as follows

$$(E_{a(average),i} \times i) - \sum_{i=1}^{i-1} E_{a(actual)} \qquad (5.2)$$

where i is the interval. Eight intervals were used since eight values of E_a were calculated originally for the conversion intervals 0 – 10 %, 0 – 20 %, 0 – 30 %, 0 – 40 %, 0 – 50 %, 0 – 60 %, 0 – 70 % and 0 – 80 %. The new value of E_a was taken as the average value for each interval, and thus the actual value for the conversions 5 %, 15 %, 25 %, 35 %, 45 %, 55%, 65 % and 75 %. Linear interpolation and extrapolation were again used to calculate the values for every percentage of conversion (see appendix D). Using these values for E_a and the corresponding values for A, calculated from the intercept, the prediction of conversion versus temperature was still not very good. The problem seemed to lie with the calculation of A. It was decided to calculate A by linearising equation 4.7:

$$\ln\left(\frac{d\alpha}{dt}\right)_{\exp} = \ln A + \ln(1-\alpha) - \frac{E_a}{RT} \qquad (5.3)$$

Using the experimental values of α, $d\alpha/dt$ and the calculated values of E_a, lnA and thus A could be determined directly from equation 5.3. Figure 5.15 is a plot of conversion versus temperature using the new values for E_a and A for reactions orders of 1, 2, 2/3, ½.

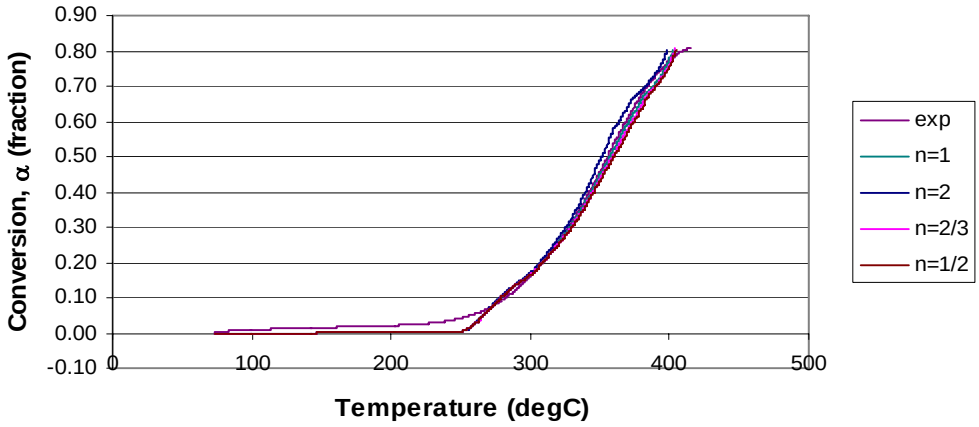

Figure 5.17 Kinetic model predictions of conversion versus temperature compared to experimental data.

The residual sum of squares (R^2) values for the different reaction orders are as follows:

Table 5.2 R^2 values for the kinetic model predictions of conversion versus temperature

Reaction order	R^2
1/2	0.997
2/3	0.997
1	0.997
2	0.997

A reasonably good fit is obtained for all the reaction orders, with the 1st order model yielding the best fit. Despite the complex nature of biomass and the complexity of the pyrolysis process, it seems possible thus, to model the overall pyrolysis process with a 1st order, single-step kinetic reaction model, provided the kinetic constants E_a and A are determined correctly. Even if, strictly speaking, this result is incorrect, its use may be justified for practical purposes. There would certainly not be much incentive to use more sophisticated kinetic models if the prediction obtained from a simple first order model is this good.

Figure 5.18 is a plot of the final calculated E_a values as a function of α.

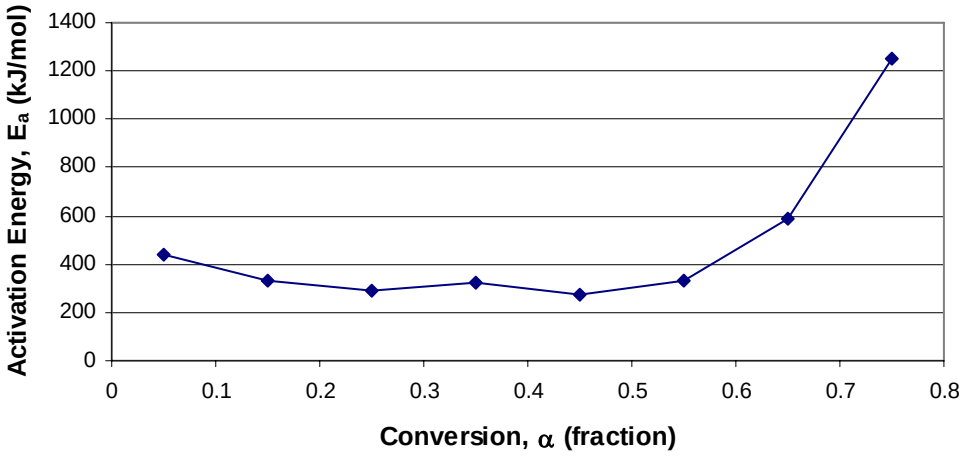

Figure 5.18 Final calculated activation energies as a function of conversion for the pyrolysis of Rooikrans wood.

It is clear from the above graph that apparent activation energy is not the same for all levels of conversion. This was expected as wood is a complex material. The trend observed in the above graph is not unlike the trend observed by **Reina et al. (1998)** using a more conventional method of kinetic analysis. It is possible to make sense of this trend by referring back to Figures 5.1 and 5.3. The first value for the activation energy, at the 5 % conversion mark, is higher than those following immediately after. The calculation of the apparent activation energy at this point is probably affected by the evaporation of water, which usually accounts for the first 5 % or so of conversion. For the sawdust however, a 5 % conversion is achieved only at a temperature of 250 ˚C. At this temperature one would have expected most of the moisture present in the sample to have evaporated, especially since the diffusion limitations in the sawdust would be almost negligible. It could therefore be the apparent activation energy necessary for the start of the release of more volatile components, extractives and possibly the decomposition of hemi-cellulose, which is known to start above 225 ˚C. The activation energy in the region 15 to 55 % conversion seems to be reasonably constant. It can be seen in Figure 5.1, for the 10 ˚C/min curve, that these conversions are reached at temperatures of roughly 295 - 360 ˚C. This is the steepest part of the curve with a roughly constant slope, and from Figure 5.3 it can be seen that this is the temperature range in which the reaction rate starts to increase rapidly at an almost constant rate and reach its maximum. It is fair to say that the main pyrolysis reactions

take place in this region. Cellulose is known to decompose between temperatures of 325 – 375 ˚C and lignin, most rapidly, between 310 – 420 ˚C.

As the temperature increases above 360 – 370 ˚C, the apparent activation energy starts to increase as well and the rate of the pyrolysis reactions starts to decrease. This can be seen in Figure 5.1 as the slope of the curve becomes less steep. Figure 5.3 shows this very clearly as the rate starts to decrease above this temperature. This increase in E_a may be the result of lignin decomposition. The differential mass loss curves (as in Figure 5.3) for the decomposition of lignin, obtained by **Várhegyi et al. (1997)**, showed a very wide and flat peak. Lignin is more resistant to thermal decomposition than cellulose and its decomposition is a slow process which continues throughout the temperature range.

Because the calculated E_a value represents the overall pyrolysis reaction, it is fair to say that the more predominant components will have a greater effect on this value. The fact that E_a stays relatively constant for conversions between 15 % and 55 % suggests that the pyrolysis reactions are probably dominated by the decomposition of cellulose, which is the main component in wood. As the decomposition of cellulose nears completion, the decomposition of lignin becomes more dominant. And because lignin is more resistant to thermal degradation, the apparent activation energy increases.

These results are very compatible with the two stage mechanism proposed by **Reina et al. (1998)**. The first stage is characterised by two distinct levels of activation energy. During this first stage the main components of wood are decomposed or depolymerised to form an intermediate of low molecular weight. There is an overlap of the decomposition of cellulose and lignin and an increase in the activation energy at the end of the first stage is caused by lignin, which is more resistant to thermal decomposition than cellulose. A high conversion is reached in during this first stage and large quantities of volatiles are released. The second stage, which starts at around 420 ˚C, is attributed to the cracking of residual organic components which decompose to produce gases and char. It can be seen from Figures 5.1 and 5.3 that the pyrolysis reactions are virtually complete at this stage. Unfortunately this study did not yield

activation energy values above a conversion of 80 %, but it is likely that the activation energy would decrease above this value as found by **Reina et al. (1998)**.

Figure 5.19 below is a semi-log plot of the pre-exponential factor as a function of conversion:

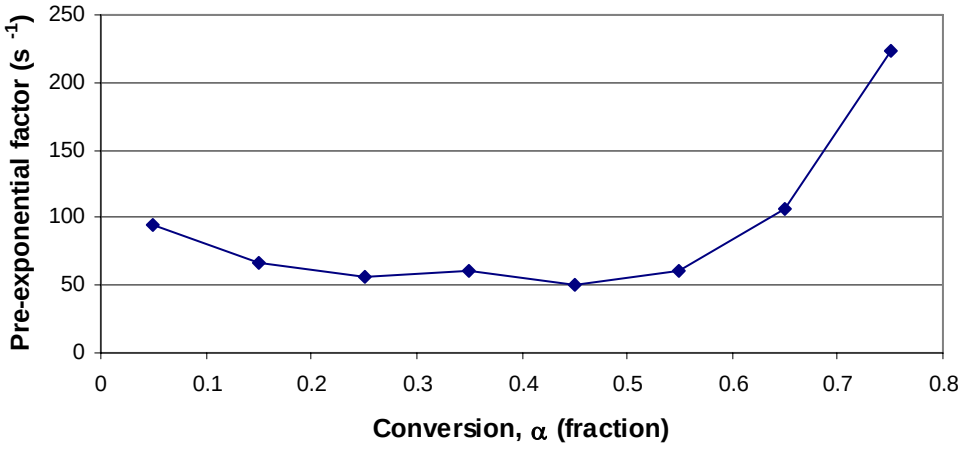

Figure 5.19 Calculated pre-exponential factors as a function of conversion for the pyrolysis of Rooikrans wood.

The pre-exponential factor as a function of conversion follows virtually the same trend as the activation energies. The physical meaning of the pre-exponential factor is, however, one for debate. According to **Maciejewski (2000)**, on the physical meaning of kinetic triplets, there are two options. The first one is that kinetic triplets have no physical meaning but can help in the prediction of rate of the process for conditions where the collection of experimental data is impossible. The second option is that kinetic parameters do have physical meaning and can be used to help understand solid-state reaction mechanisms. **Maciejewski** feels that the truth lies somewhere in between, but that the connection between the kinetic parameters and the reaction mechanism is usually very complex and it is therefore difficult to ascribe clear and simple physical meaning to effective kinetic values.

5.4 The prediction of the instantaneous pyrolysis rate

Figure 5.20 below is a plot of $d\alpha/dt$ versus temperature, calculated from equation 4.6.

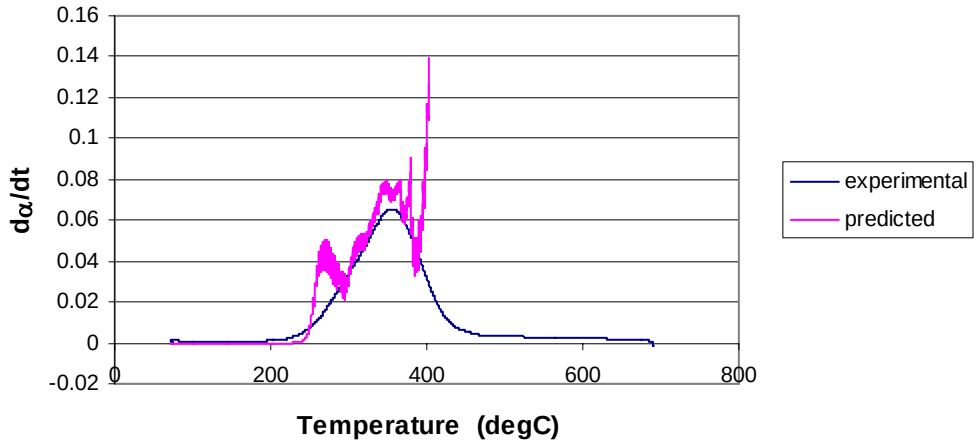

Figure 5.20 Comparison of instantaneous reaction rate predicted using equation 4.6 with the experimental data.

The results obtained from equation 4.7 were not good. It can be seen that the predicted curve is very "spiky" and that the final predicted values deviate significantly from the actual experimental values, although the general trend followed is the same. This was not entirely unexpected. Differentiating non-smooth data will increase the "spikyness" of the data. It can be seen from Figure 5.21 below that the predicted α versus T curve, given here only for the 1st order prediction, does not have a smooth

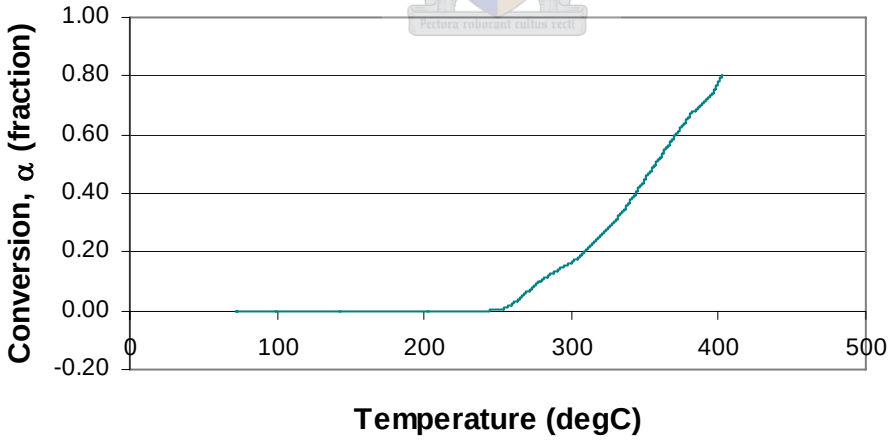

Figure 5.21 Predicted conversion versus temperature for a 1st order function

slope and the sharp increase in conversion towards the end is the reason for the tall "spike" at the end of the dα/dt curve. The smoothness of the curve can be improved by calculating the actual E_a values at every percent of conversion. This will of course minimise the errors introduced by interpolation.

5.5 The kinetic method of Koufopanos et al.

The method proposed by **Koufopanos et al. (1991)** (see chapter 2, section 2.10) was used to model the pyrolysis of Rooikrans and Swarthaak wood sawdust and Rooikrans wood 2 – 4 mm blocks. For the pyrolysis of the sawdust, the secondary reactions were neglected. Assuming that reactions 1 and 2 (see Figure 2.9) are both 1st order, the following E_a and A values were obtained from least-squares analysis for reactions 1 and 2.

Table 5.3 Best fit values for the kinetic parameters of the pyrolysis of Rooikrans and Swarthaak wood sawdust

Rooikrans	**E_a (kJ/mol)**	**A (min^{-1})**
Reaction 1	65	3.49E+04
Reaction 2	95	1.63E+06
Swarthaak		
Reaction 1	58	9.76E+03
Reaction 2	91	1.63E+06

Figures 5.22 and 5.23 below are plots of the predicted conversion as a function of temperature. R^2-values of 0.999 and 0.998 were obtained for the Rooikrans and Swarthaak samples respectively.

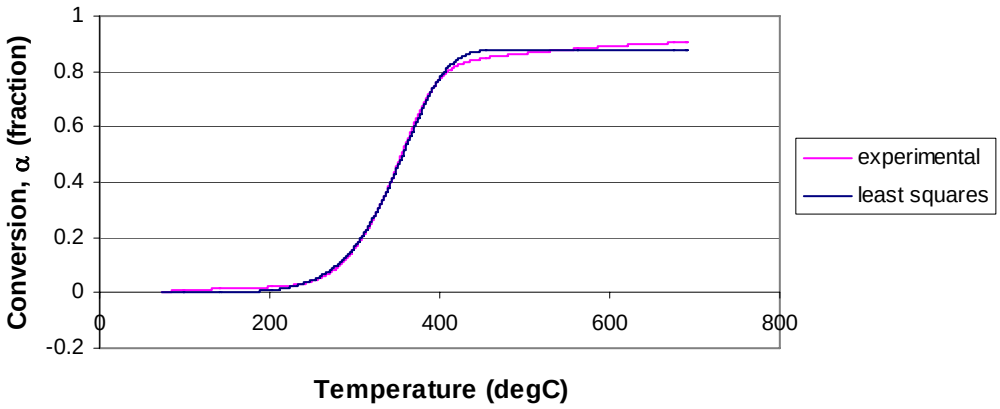

Figure 5.22 Predicted conversion as a function of temperature using the kinetic model by **Koufopanos et al.** for the Rooikrans sawdust.

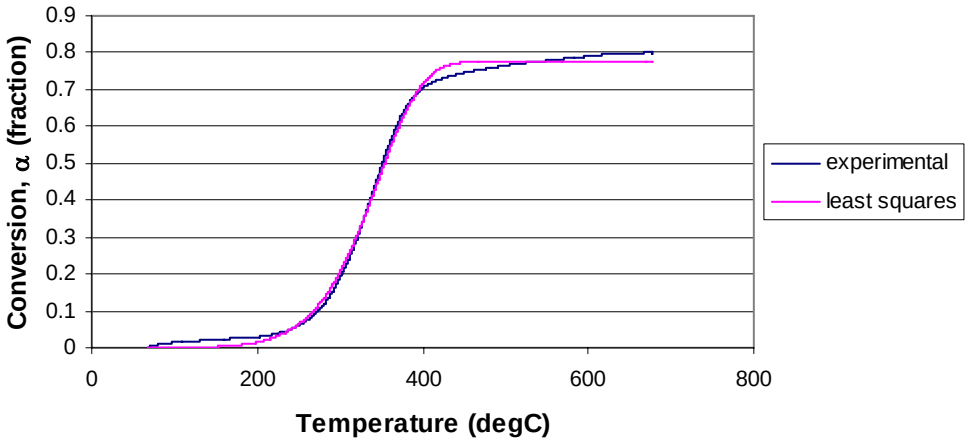

Figure 5.23 Predicted conversion as a function of temperature using the kinetic model by **Koufopanos et al.** for the Swarthaak sawdust.

It is difficult to make direct comparisons between the E_a and A values obtained from this method and the isoconversional method, because the E_a and A values from this method are for the individual reactions proposed in the kinetic scheme, while the E_a and A values from the isoconversional method are for the overall pyrolysis reactions. Nevertheless, some comparison may be possible.

The first products to be formed will be volatiles and gases. The activation energy of reaction 1 could therefore be compared to the initial activation energy obtained from the modified Coats-Redfern method. It is clear however, that these values differ significantly. The initial values from the modified Coats-Redfern method for Rooikrans are of the order of 300 to 400 kJ/mol, whereas the value obtained from this method is 65 kJ/mol. If an average of the activation energies for reactions 1 and 2 may be taken to represent the overall activation energy at the later stage of pyrolysis when reactions 1 and 2 occur simultaneously, it immediately becomes clear that this value is still significantly lower than the one obtained from the Coats-Redfern method. However, if reaction 2 becomes the more dominant reaction during the later stages of pyrolysis, then this method also predicts an increase in the activation energy, much like the Coats-Redfern method. The reason for the significant difference in magnitude of values obtained from the two methods is unclear. The values obtained from this method, however, depend on the accuracy of the proposed kinetic scheme and the values obtained from the model-free isoconversional method should therefore

be regarded as more accurate. Nevertheless, the prediction by this model is more accurate than that of the isoconversional method. It has to be noted at this stage that this method does, however, not incorporate multi-heating rate data, as is the case for the isoconversonal method. Figure 5.24 below is a plot of the experimental conversion as a function of temperature for Rooikrans wood sawdust with the predictions from the two models plotted on the same axes.

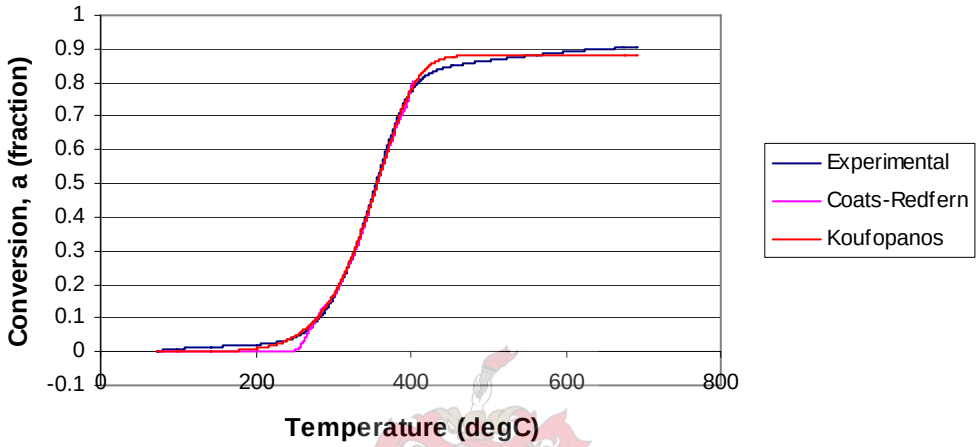

Figure 5.24 Comparison of predicted conversion versus temperature for **Koufopanos'** method and the Coats-Redfern method with the experimentally determined values for the fine Rooikrans sawdust at a heating rate of 10 ˚C.

As explained earlier, the method use by **Koufopanos et al (1991)** is dependent upon the reaction model chosen. For this reason the activation energies determined using this method cannot be trusted to the same degree as those obtained using the Modified Coats-Redfern isoconversional method. If, however, the actual values of the kinetic constants are not important and the main purpose is simply to predict accurately a conversion with temperature for a specific feedstock under specific conditions, the method used by **Koufopanos** may yield better results.

Figures 5.25 and 5.26 below are plots of the biomass decomposition and char generation predicted, using the method of **Koufopanos,** for the sawdust samples.

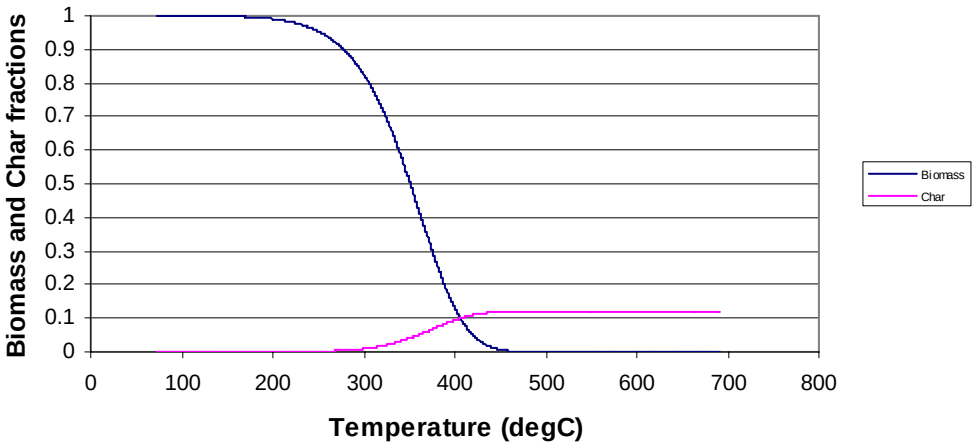

Figure 5.25 Predicted biomass and char fractions as a function of temperature for Rooikrans.

The final predicted char fraction is 0.12 or 12 %, which corresponds well to the experimental data where final conversions for the sawdust were between 85 and 89 %.

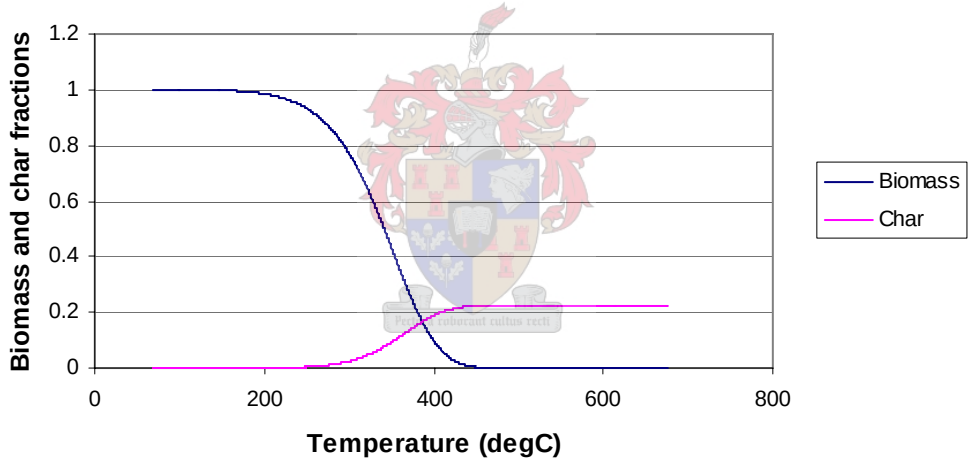

Figure 5.26 Predicted biomass and char fractions as a function of temperature for Swarthaak.

For Swarthaak wood the final char fraction is 22 % which corresponds to the experimentally obtained overall conversion of about 78 %.

Even though provision for larger particles are made by including reaction 3, heat transfer and diffusion limitations do affect the results enough for the prediction to be less accurate. Table 5.4 gives the best-fit values for the kinetic parameters for the pyrolysis of the 2 – 4 mm Rooikrans blocks.

Table 5.4 Best-fit values for the kinetic parameters of the pyrolysis of 2 – 4 mm Rooikrans wood blocks

	E_a (kJ/mol)	A (min^{-1})
Reaction 1	65.635	3.36E+04
Reaction 2	92.773	1.63E+06
Reaction 3	62.508	1.00E+05
δ		1.37

Fitting the model to the data for the larger particles still yielded E_a and A values for the first two reactions that are virtually similar to the ones obtained from fitting the model to the data for the pyrolysis of sawdust. This is correct as the activation energy for these pyrolysis reactions do not change. The activation energy for reaction 3 is again lower and may be compared to the decrease in activation energy found by **Reina et al. (1998)** for high conversions, which corresponds to the cracking of residual components. Figure 5.26 below is a plot of the predicted conversion as a function of temperature compared to the experimental data.

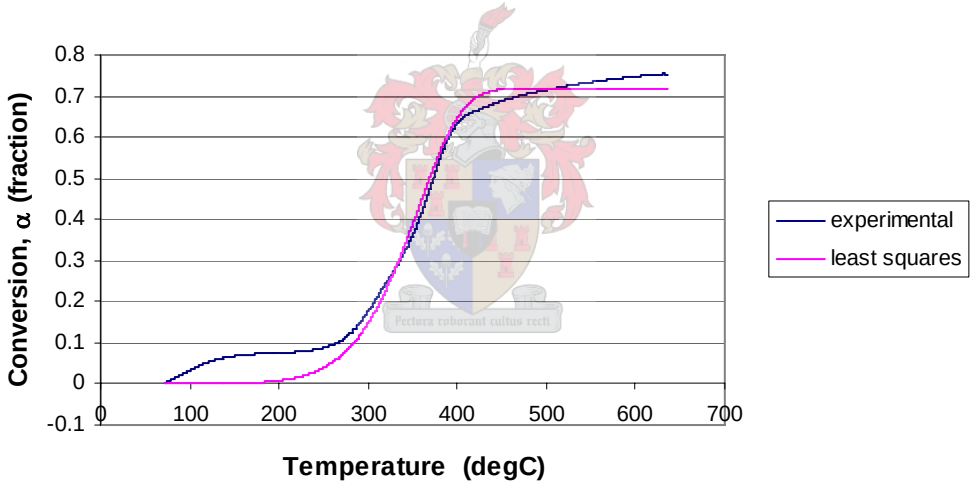

Figure 5.27 Predicted conversion as a function of temperature using the kinetic model by **Koufopanos et al.** for the 2 – 4 mm Rooikrans blocks.

An R^2 value of 0.993 was obtained.

It is noticeable that it is especially at lower temperatures, where mostly water evaporation takes place, where the model prediction is worst. The model may therefore still yield better results for drier wood. It is however unlikely that wood used in a commercial process will be completely dry and thus this will have to be taken into account when using this model for larger particles. Isoconversional

methods on the other hand will not yield better results either, unless more moisture is present in the sample used to determine the E_a and A values.

5.6 Reproducibility

Figure 5.27 below is a plot of four runs done in the TGA with Rooikrans wood sawdust at a heating rate of 20 ˚C/min, to test the reproducibility of the experiments. It is evident that the final conversion values deviate by as much as 6 %. For conversions below 80 % the graphs lie virtually on top of each other with the same slope. For instance, the temperature at which a conversion of 40 % is achieved, are 351, 355, 355 and 363 ˚C respectively. The deviation in final conversion, as also seen

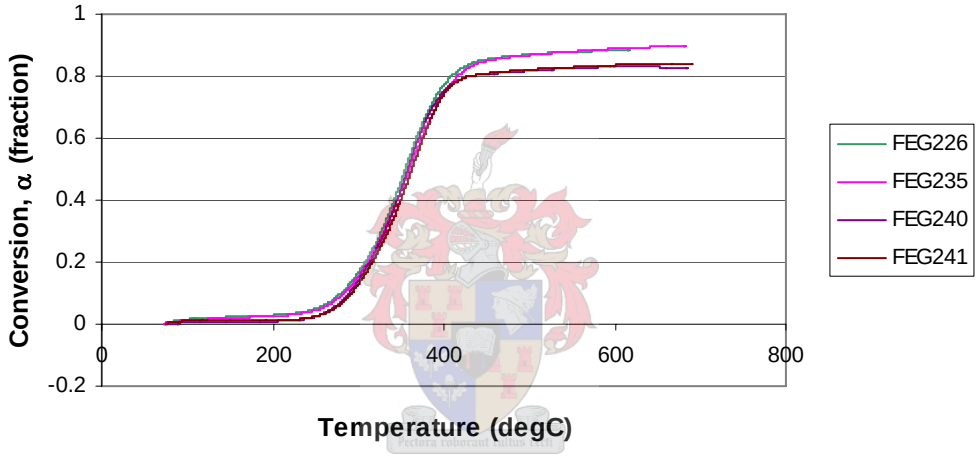

Figure 5.28 Six runs at a heating rate of 20 ˚C/min for Rooikrans wood sawdust.

in Figure 5.1 for the different heating rates, is attributed to differences in the samples used. The sawdust was created using a beltsander and was well-mixed, but creating a 100 % homogeneous sample and loading a 100 % representative sample every time is not possible with the naked eye. The experimental conditions may also have varied from run to run as the nitrogen flow rate and pressure in the TGA, were both set manually using a gas-flow meter and a manometer.

The mean conversion values as a function of temperature, as well as the standard deviations were calculated in Matlab using the Bootstrap method. A brief description of this method, found at, www.stat.wisc.edu/~larget/math496/bootstrap, is given: *The ideal way to estimate the standard deviation of the sample median is to take a very*

large number of samples from the original population, compute the sample median of each, and use the standard deviation of this large collection of simulated sample medians as an estimate of the true standard error. Unfortunately, we do not have the ability to sample repeatedly from the population. We can, however, sample repeatedly from our original sample, which is itself an estimate of the population. This is how the bootstrap works. Since only four runs of the same experiment were conducted, it was decided to use this method for calculating the uncertainty in the mean value for conversion at all temperatures.

Figure 5.29 below is a plot of the mean conversion value as a function of temperature, with the dotted and solid red lines above and below, two standard deviations from the mean. Thus, 95 % of conversion values at a specific temperature, for all experimental runs, will fall between these lines.

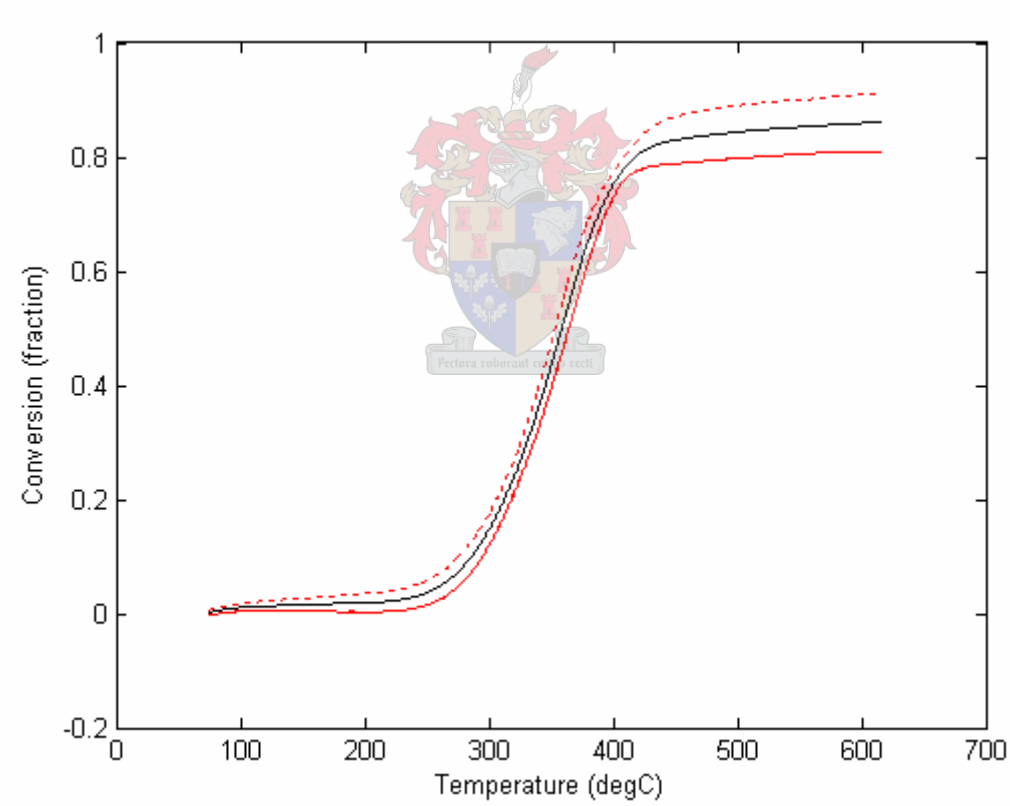

Figure 5.29 The mean and standard deviations of conversion as a function of temperature.

It is evident from the above graph that the standard deviation is relatively constant, at roughly 2.5 %, for the temperature range in which the majority of pyrolysis reactions take place, but for high temperatures, corresponding to conversions above 80 %, the uncertainty becomes greater, for the reasons given above. A maximum standard

deviation of 3.2 % is found for the highest temperature, which is 617 ˚C. This deviation from the mean made the calculation of the activation energies above a conversion of 80 % inaccurate.

6. Reactor Model Results

The results obtained from the mathematical model for vacuum pyrolysis in a rotary oven, developed in chapter 4, is presented in this chapter. The aim with the development of the model was, firstly, to simulate vacuum pyrolysis in a rotary oven, but also to provide a generic set of equations that may, at some stage, be used for scoping design calculations. It has to be noted at this point that accurate simulation of pyrolysis in a rotary oven is no easy task.

In a review of the modelling of particulate drying in theory and practice, **Kemp and Oakley (2002)** noted the great gulf between drying theory and industrial practice. Manufacturers have tended to rely on empirical data and rules based on pilot-plant testing and part of the reason for this is that much of the theory published on drying was not presented in a clear step-by-step design procedure and included little or no comparison with practical results. Another reason for the poor acceptance of academic theories for industrial users has been bad experiences when attempts were made to use published theory for practical design. Nevertheless, if an appropriate level of rigour is applied, theory can give good results. The reason for the difficulties though, is the complexity of the drying processes, which involves simultaneous heat, mass and momentum transfer. Many parameters, some of which depend highly on the solid structure and are difficult to measure, affect drying processes. In contrast to liquid and vapour-phase processes where the system is controlled by equilibrium thermodynamics and where all the necessary physical properties can be obtained from databanks, processes involving solids are much more difficult to model accurately.

The literature on drying is substantial and rotary ovens have been used for drying for many years. Vacuum pyrolysis on the other hand is a relatively new process. It is not known whether vacuum pyrolysis has been performed in a rotary oven, but certainly no model exists for this process in a rotary oven, and if it is true that the subject and modelling of drying is complex, then it is most certainly true for pyrolysis. It is with this in mind that the results from the model developed in chapter 4, are presented.

6.1 Base case simulation

Table 6.1 Selected parameter values used for the base case run

Design Parameters	
Furnace Diameter	0.7 m
Reactor diameter	0.5 m
Solids bed radius	0.083 m
Reactor wall emissivity	0.7
Operating parameters	
Gas flow rate	0.076 kg/s
Gas inlet temperature	1000 ^{o}C
Bed flow rate	100 kg/hr
Bed inlet temperature	25 ^{o}C
Gas and bed properties	
Gas heat capacity	1000 J/kgK
Gas viscosity	3.5e-05 Ns/m^2
Gas thermal conductivity	0.0407 W/mK
Bed heat capacity	2220 J/kgK
Bed density	170 kg/m^3
Bed emissivity	0.8
Heat of reaction	92000 J/kg

Pectora roborant cultus recti

The values of the chosen design parameters were for a pilot-scale rotary oven. A reactor diameter of 0.5 m was decided on as a first estimate. For the radiative heat transfer term, a bed diameter is needed. Since rotary ovens are typically filled to between 10 and 15 % by volume **(Perry, 1997)**, a bed radius of a third of the reactor radius was chosen. Such a bed radius corresponds to an 11 % filling. Reactor wall and bed emissivities (a measure of the ability of the bed to absorb or reflect radiated energy) were estimated from those used by **Roy et al. (1992)**. It was initially thought to build the pilot-scale reactor with a throughput of 100 kg/hr, so this Figure was used for the bed mass flow rate. The gas flow rate was estimated from **Boateng and Barr (1996)** who did some experiments in a pilot-scale reactor to validate their rotary kiln model. It is noted at this point that though the mass flow rate of the gas is rather low, the volumetric flow rate is in fact quite high. An inlet bed temperature of close to room temperature is reasonable as a first estimate and an inlet gas temperature of up

to a 1000 ˚C is realistic. The gas heat capacity, viscosity and thermal conductivity were taken to be that of air; the bed density was estimated from **Perry (1997)** and the bed heat capacity and heat of reaction were taken from **Roy (1987 and 1992)** who determined these values experimentally.

Figure 6.1 shows the results produced by the model (equations 4.1 to 4.3, 4.6 to 4.8 and 4.12 and 4.15) for the base case, using a first order kinetic model and a step size Δz of 0.05 m. It is a plot of the gas, wall and bed temperatures as a function of the axial position.

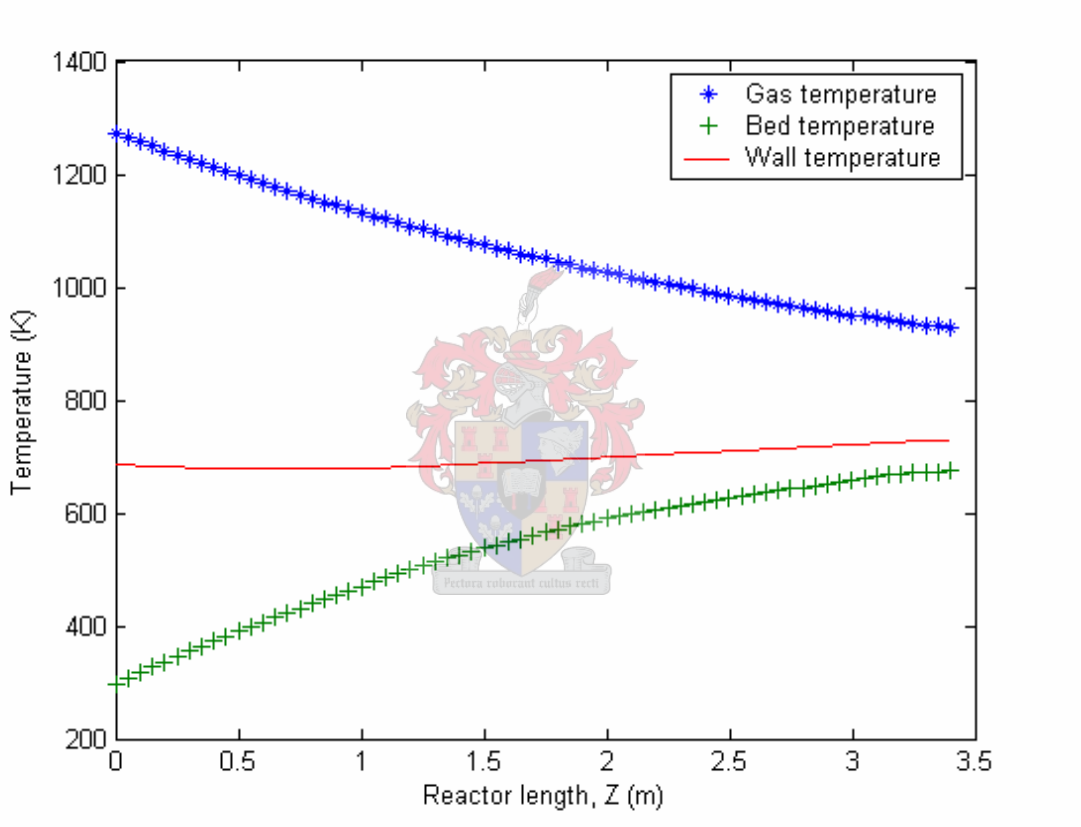

Figure 6.1 Gas, wall and bed temperatures as a function of axial position for the base case.

The above Figure should be read in conjunction with the curve for the reaction conversion as a function of axial position, given in Figure 6.2 below. It can be seen that the bed temperature increases to a value of about 674 K (400 ˚C) at a reactor length of 3.4 m before the simulation is stopped. This is because a conversion of 80% is reached. As explained earlier, the experimental kinetic results, used in the kinetic model, does not allow accurate determination of conversion above a value of 80 %. It is expected though that the conversion will not increase by much above this

temperature. This corresponds well to the experimental results obtained and presented in chapter 5.

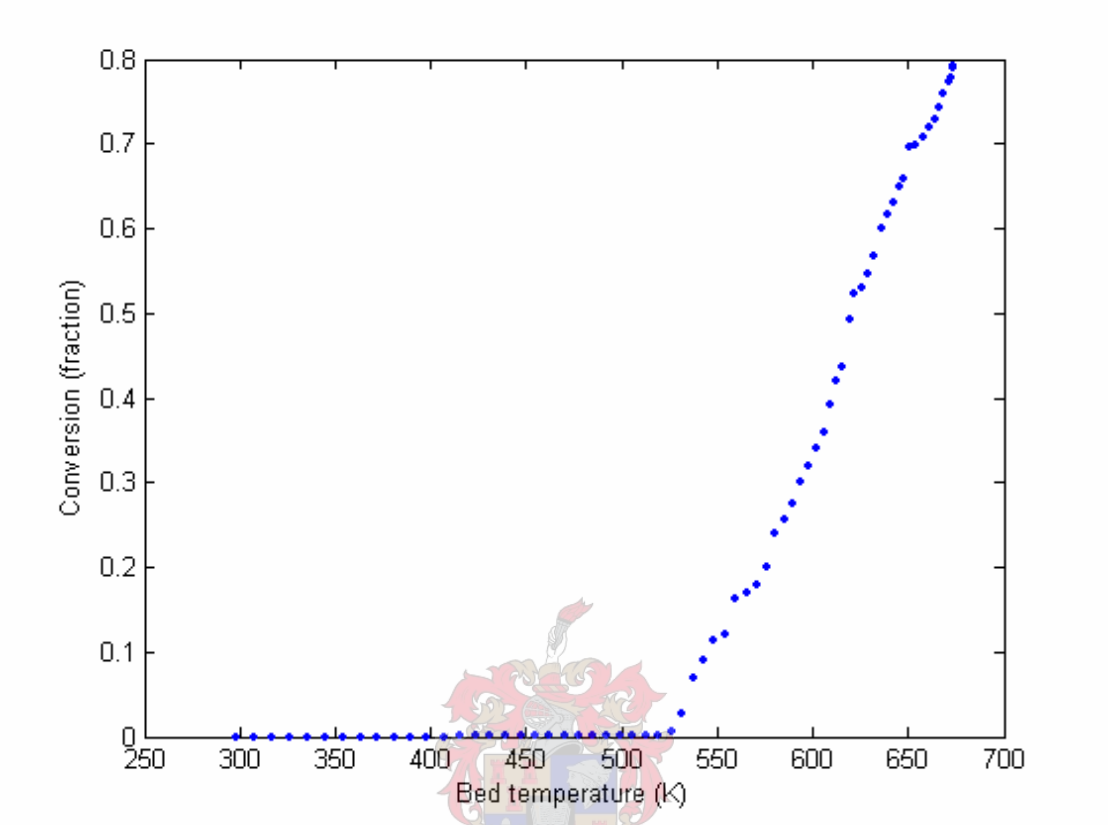

Figure 6.2 Conversion versus bed temperature in the rotary oven.

The above curve is exactly the same as the curve for a first order reaction shown in Figure 5.17, where the kinetic modelling was done in Excel. The pyrolysis reactions, and hence the conversion, start at a temperature of about 523 K (250 ˚C) and reach completion at a temperature of about 673 K (400 ˚C). This was confirmed by the experimental results which can be seen in Figure 5.1. Better experimental results will be needed on order to predict at higher conversions.

A calculated reactor length of 3.4 m, with a reactor diameter of 0.5 m, does not seem physically unrealistic. However, knowing the average residence time of the bed in the reactor would also indicate whether such a length will be plausible. The residence time of the particles in the bed can be defined as follows:

$$\tau = \frac{L}{Vs} \qquad (6.1)$$

In their paper on solid transport prediction in rotary cylinders, **Perron and Bui (1990)** present a formula which may be used for the calculation of the bed velocity:

$$V_s = KR\omega\nu^{\beta}\left[\left(\frac{R^2}{h^2\cos\varphi + 2h\sqrt{2hR - h^2\sin\varphi}}\right)\left(\frac{\Gamma + 2\tan\frac{\Gamma}{2}}{1-\cos\frac{\Gamma}{2}}\right)\right]^e \qquad (6.2)$$

Unfortunately the equation is empirical in nature and the two constants e and K must be determined from experimental data. A quick and simple calculation can however be done to get an idea of the velocity of the bed using the fact that the axial bed velocity is equal to the volumetric flow rate of the bed divided by the cross-sectional area of the bed:

$$Vs = \frac{Q}{A} \qquad (6.3)$$

Using the dimensions of the bed and the bed bulk density given, a velocity of about 27 m/h is calculated. This means, from equation 6.1, that the average residence time of the particles in the reactor will be 7.5 minutes if there is no volume reduction. This corresponds to a heating rate of 53 ˚C/min, since the bed is heated to 400 ˚C in 7.5 minutes. This is a very high heating rate and probably a bit unrealistic for a commercial scale rotary kiln or rotating oven. However, because there is an approximately 80% reduction in bed volume, the actual residence time will be considerably longer and could even be between 30 and 40 minutes. The calculation of the actual residence time is very complex and was not attempted. It has to be noted at this point that another shortcoming of the model is in the mass balance for the reactor bed. The value for $\dot{m}_b$ was taken as constant which is of course not correct. This will have to be corrected in future.

6.2 Model response to parameter changes

An easy way to gauge the reliability of a model is to check the model's response to changes in input parameters. In the case of a rotary oven the parameters most easily

changed are the operating parameters. These are, excluding speed of rotation, the gas flow rate, gas inlet temperature and the bed feed rate. These parameters were varied to see how the model would respond.

6.2.1 Changing the gas flow rate

Keeping all other variables constant while increasing the gas flow rate, one would expect to be able to achieve the same level of conversion with a shorter reactor. On the other hand, a longer reactor would be required if the gas flow rate were decreased. This was correctly predicted by the model. Changing the gas flow rate from 0.076 kg/s (base case) to 0.1 kg/s, decreased the reactor length needed to achieve a conversion of 80 % from 3.4 m to 2.35 m.

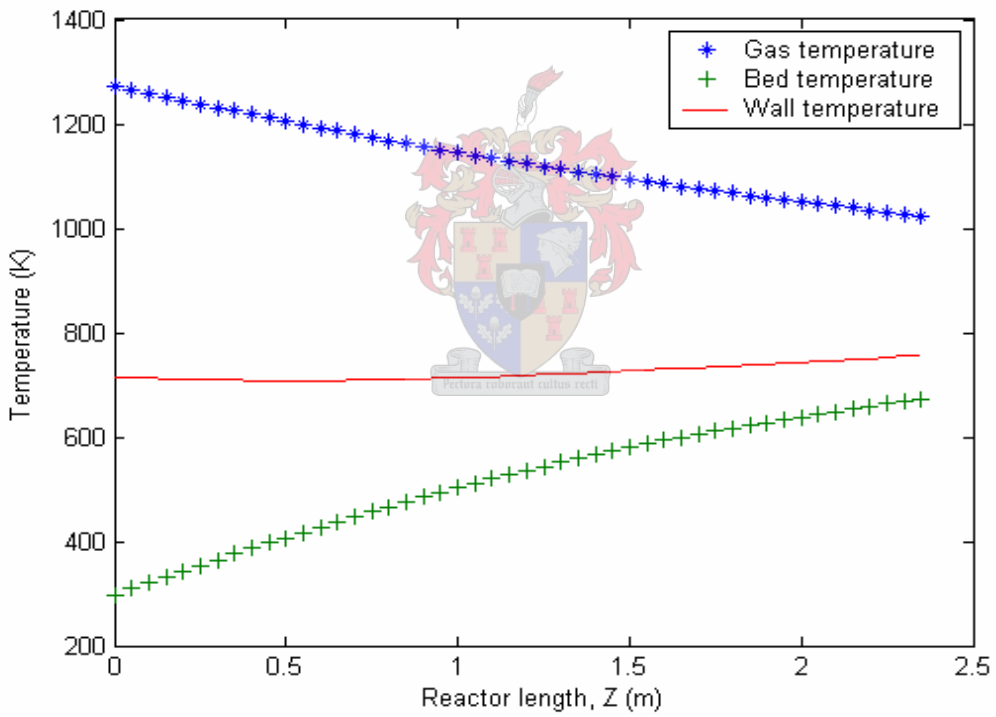

Figure 6.3 Gas, wall and bed temperatures as a function of axial position for a gas flow rate of 0.1 kg/s.

This is more clearly seen in Figure 6.4 below, which is a plot of the conversion as a function of reactor length. Decreasing the gas flow rate from 0.076 to 0.05 kg/s had the opposite effect. In this case however, the reactor conversion only reached a value of about 41 % at a reactor length of 4.6 m. At this point the bed temperature had levelled off at 612 K (339 ˚C) and started to go down, which probably means that the

energy consumed by the reactions is more than the energy supplied by the gas. Unfortunately the kinetic model cannot handle decreasing temperatures and the conversion then remains at the value achieved before the temperature started decreasing. Nonetheless, the model responded correctly to the decrease in gas flow rate. Even though the conversion would still have increased somewhat, it is quite probable that a conversion of less than 80 % would have been achieved. This is because the bed temperature reached a maximum value of only 339 ˚C, which is still 60 ˚C short of the 400 ˚C by which the reactions will have reached completion. Figure 6.5 below is the plot of the gas, wall and bed temperatures versus reactor length for the gas flow rate of 0.05 kg/s and Figure 6.6 is the plot of the conversion versus reactor length.

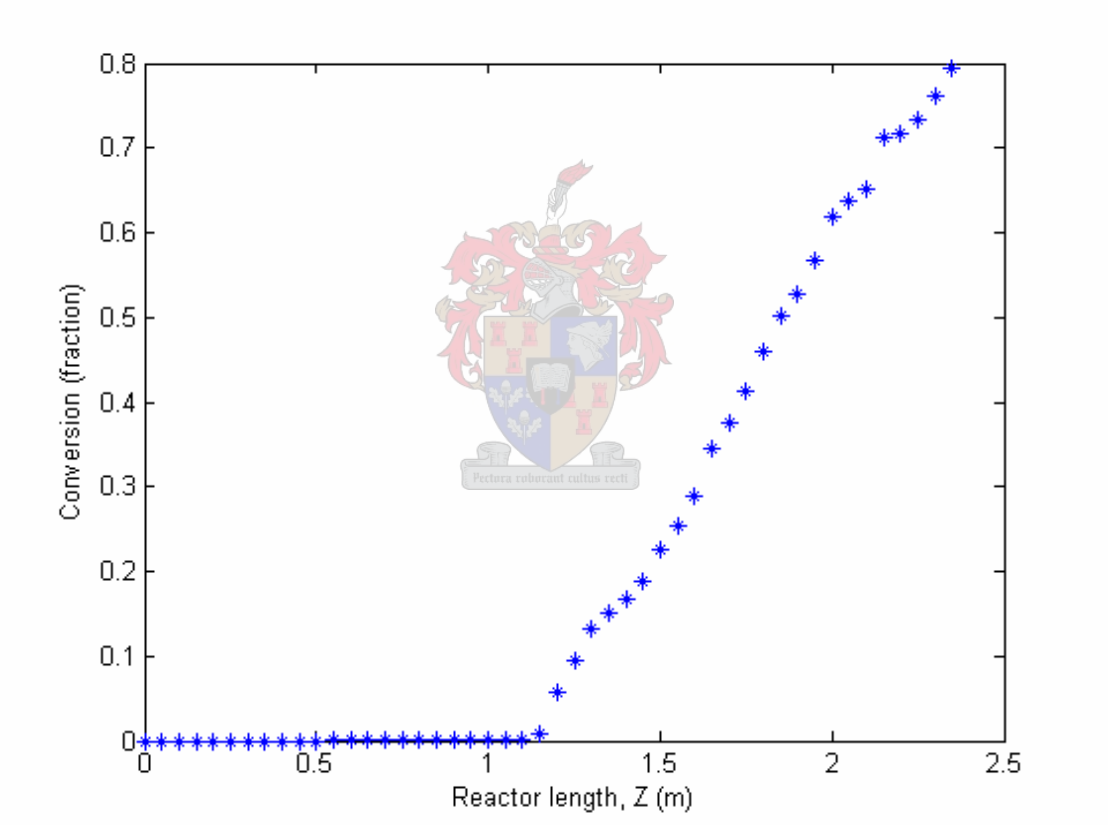

Figure 6.4 Conversion versus reactor length for a gas flow rate of 0.1 kg/s.

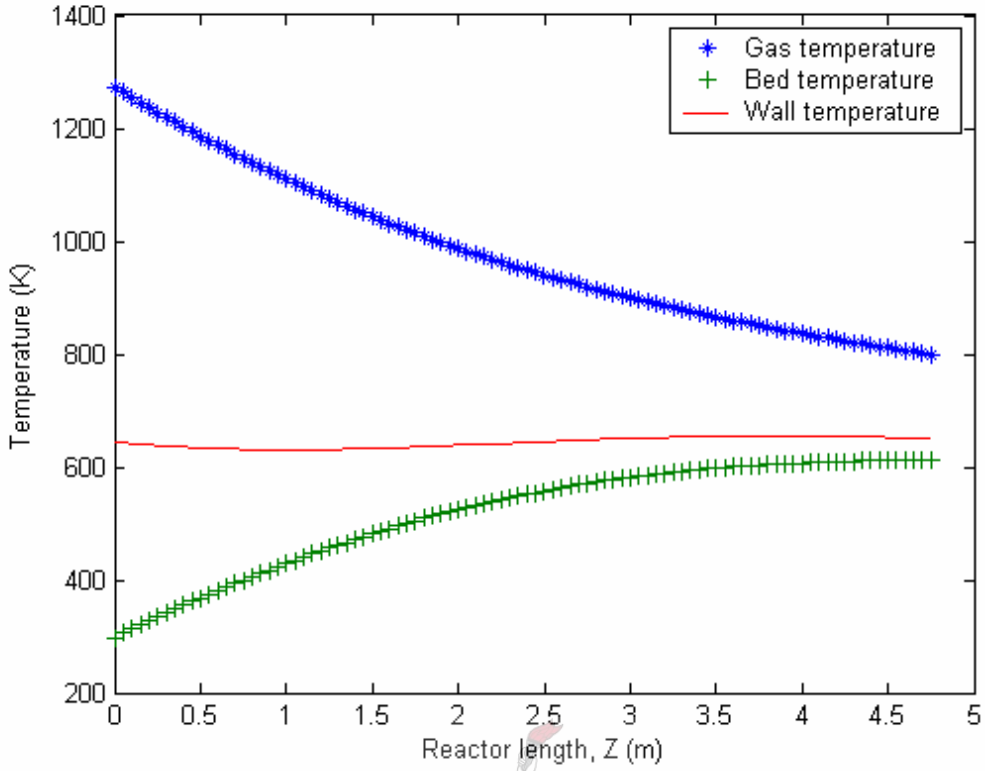

Figure 6.5 Gas, wall and bed temperatures versus reactor length for a gas flow rate of 0.05 kg/s.

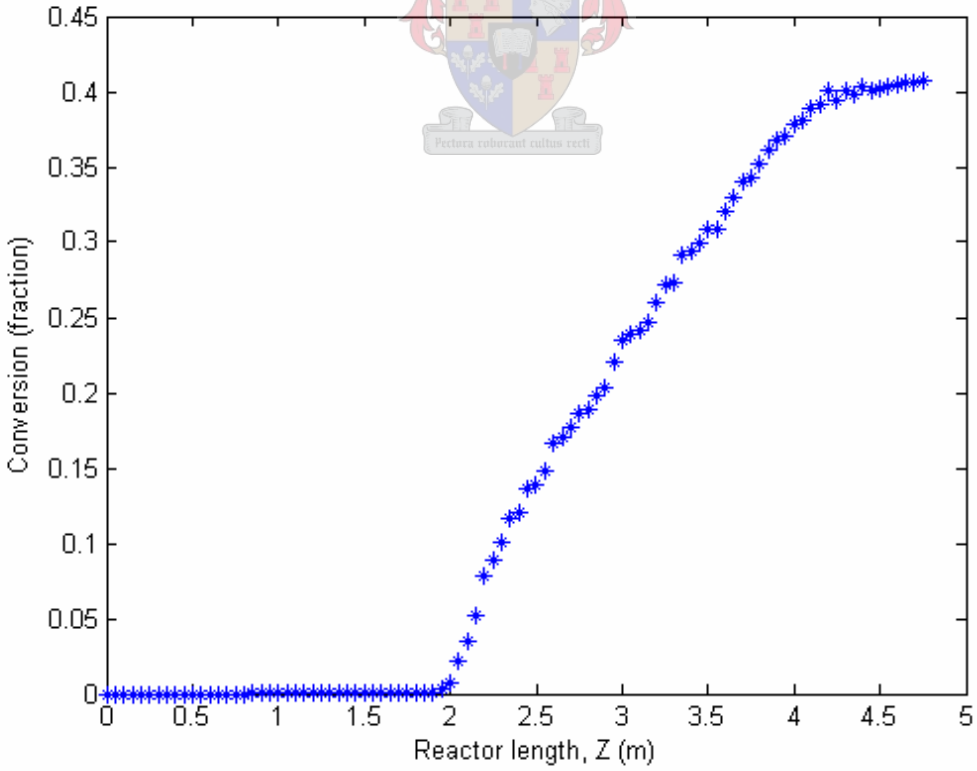

Figure 6.6 Conversion versus reactor length for a gas flow rate of 0.05 kg/s.

6.2.2 Changing the gas inlet temperature

Increasing the gas inlet temperature should have a very similar effect to increasing the gas flow rate, namely that a shorter reactor is needed to achieve the same level of conversion, and vice versa. Again, this was correctly predicted by the model. Increasing the gas inlet temperature to 1200 ˚C decreased the reactor length needed to 2.1 m. Decreasing the inlet temperature to 800 ˚C resulted in a similar situation to the one where the gas flow rate was decreased to 0.05 kg/s: the temperature levelled off at 614 K (341 ˚C) and a reactor length of 5 m before starting to decrease, with a final conversion of 43 %. Figures 6.7 and 6.8 below give the results for a gas inlet temperature of 800 ˚C, keeping all other variables constant at their base case values.

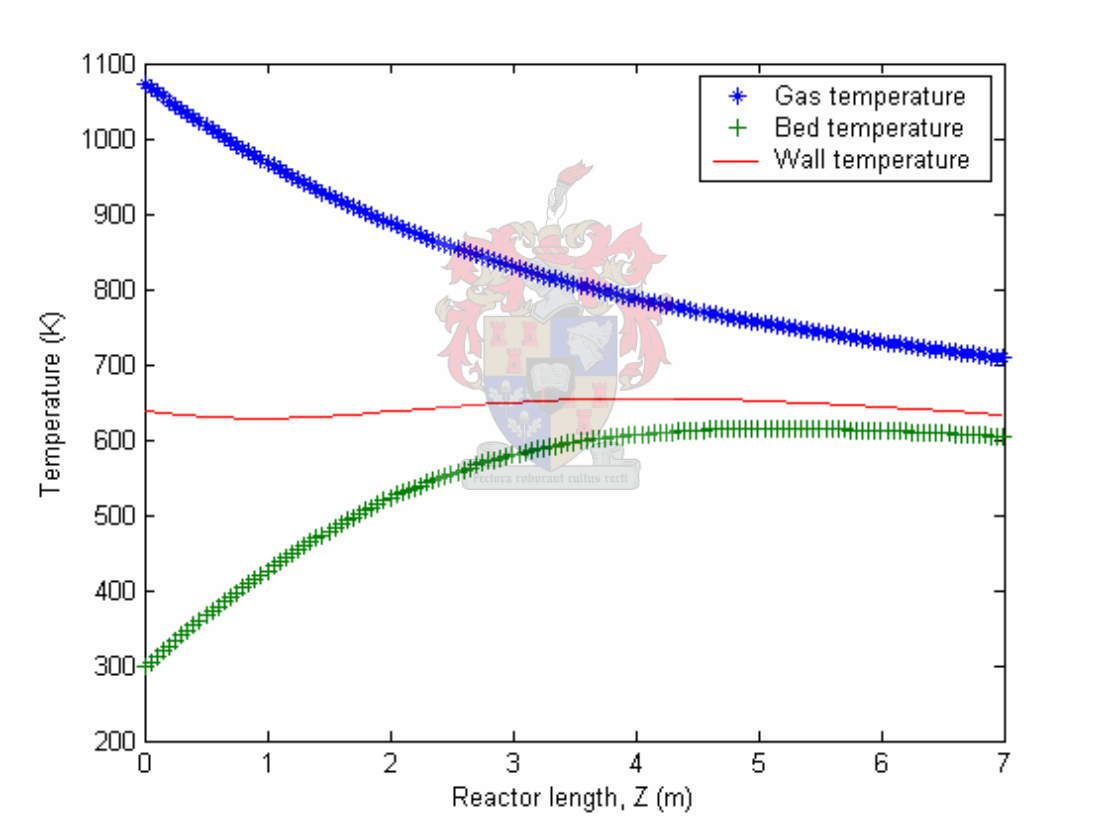

Figure 6.7 Gas, wall and bed temperatures versus reactor length for a gas inlet temperature of 800 ˚C.

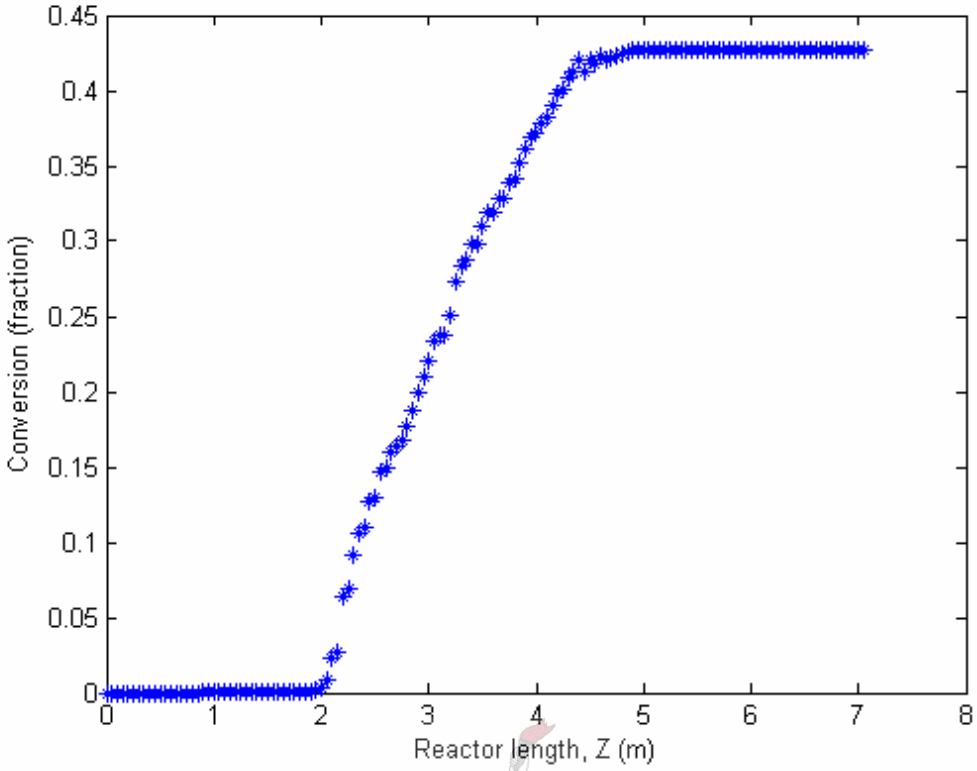

Figure 6.8 Conversion versus reactor length for a gas inlet temperature of 800 ˚C

As explained earlier, the kinetic model is unable to handle a decrease in bed temperature and it was programmed such that the conversion remained at a constant value when this happened. This explains the levelling off of the conversion in Figure 6.8.

6.2.3 Changing the bed feed rate

The last parameter varied to test the model response was the bed feed rate. If the bed feed rate is increased, a longer reactor will be necessary to achieve the same level of conversion, simply because there is more mass with the same heat input. Decreasing the bed feed rate should have the opposite effect, with a shorter reactor necessary to achieve the same result. This was clearly seen in the results from the model. Figure 6.9 below is a plot of the reactor temperatures as a function of reactor length for a bed feed rate of double the base case feed rate, namely 200 kg/h.

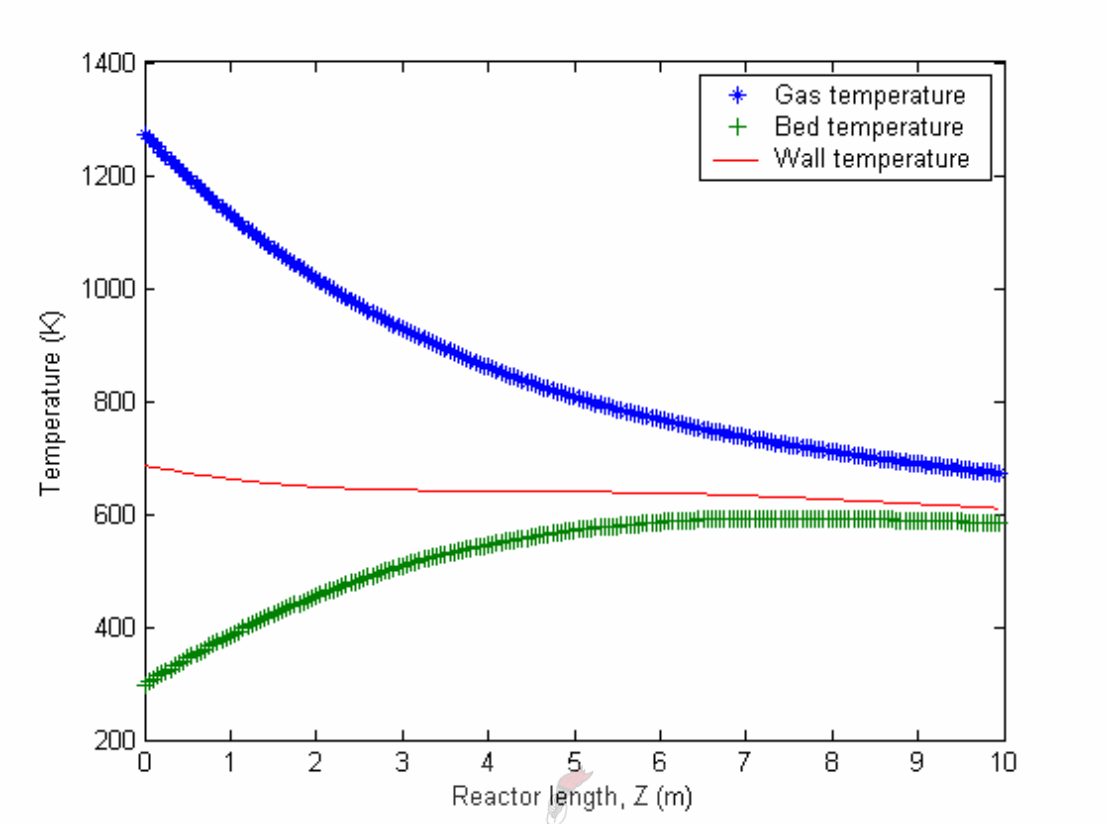

Figure 6.9 Gas, wall and bed temperatures versus reactor length for bed feed rate of 200 kg/h.

From the above Figure it can be seen that the gas flow rate was not high enough to increase the bed temperature to more than about 590 K (317 ˚C), before it started to decrease again after about 8 m. The conversion achieved for this condition was only 26 %. This is seen in Figure 6.10 below.

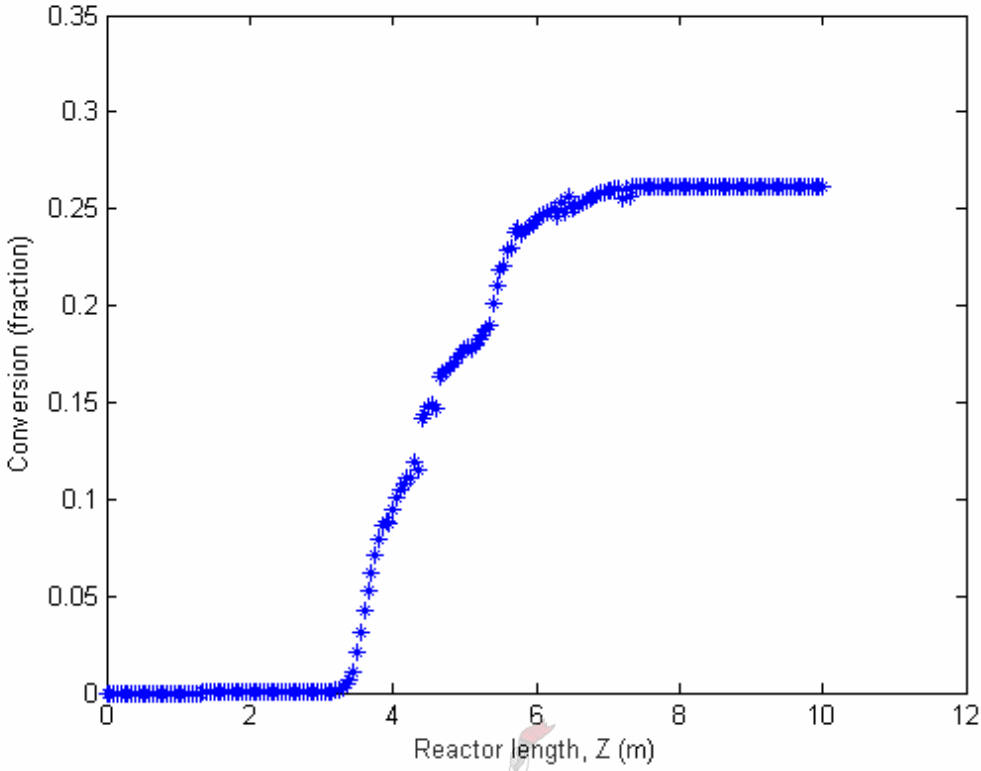

Figure 6.10 Conversion versus reactor length for a bed feed rate of 200 kg/h.

To achieve a conversion of 80 % for the bed feed rate of 200 kg/h, a higher gas flow rate or higher gas inlet temperature would be needed.

Changing the bed feed rate from 100 kg/h to 50 kg/h, the model predicted a reactor length of 1.25 m in order to achieve a conversion of 80 %.

6.3 Summary

From the results presented in this chapter it is clear that the reactor model gives reasonable results. Importantly, the model responded correctly to changes in the three operating parameters tested. For the base case a reactor length of 3.4 m was predicted.

The model used in this study is a simple, one-dimensional steady state model and as a first approximation it gives satisfactory results. The obvious flaw in the model is that it does not take radial temperature variations in the bed and particles into account.

The speed of rotation of the cylinder will not be very fast and the assumption of perfect mixing will therefore not hold. However, this non-uniformity in temperature may be accounted for to some degree by introducing the partial differential equation for the temperature profile inside a spherical particle and solving for an average bed temperature, as explained in Chapter 4. Unfortunately this was not implemented in the model due to time constraints. The results achieved with the present model do, however, provide a good first approximation.

7. Tube Furnace Results

The tube furnace used in this study was originally designed and built by **De Jongh (2001)** to study the basic principles of vacuum pyrolysis and investigate new applications for the vacuum pyrolysis process. **De Jongh** also investigated the possibility of using vacuum pyrolysis as a means of making intruder plant clearing projects profitable and used three different intruder plants, namely Asbos, Scholtzbos and Kraalbos, as feedstocks. It was found that vacuum pyrolysis could be used to produce economically valuable, high energy charcoal and oil products. The ash content of the wood used as feedstock did, however, significantly affect charcoal yields.

It was decided to do a number of runs with Rooikrans wood in the tube-furnace to compare the results with the conversion values obtained from the TGA experiments, and with the tube furnace results obtained by **De Jongh (2001)** for other intruder plant species.

Six experiments were done with Rooikrans wood (*Acacia cyclops)*. The samples were heated at a rate of 10 ˚C/min to a set isothermal temperature and pyrolysed for 60 minutes at this temperature. The following isothermal temperatures were used: 350, 450 and 520 ˚C. For the second experiment at 520 ˚C, the oven temperature was not set high enough and the temperature was isothermal at 500 ˚C.

7.1 Oil and charcoal yields

Figure 7.1 show the oil and charcoal yields on a water and ash-free basis. The first set of three experiments was conducted late in 2003, while the second set of three experiments was done in the early part of 2005 and the wood used did not come from the same batch.

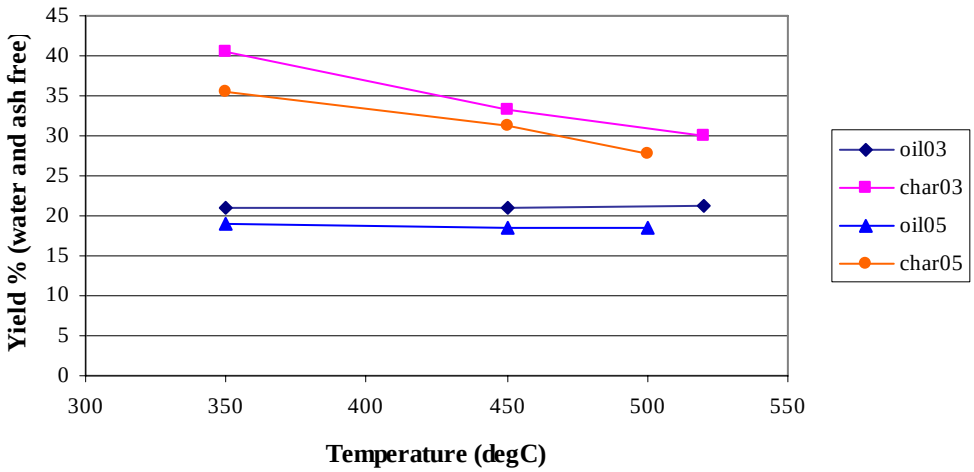

Figure 7.1 Oil and charcoal yields adjusted to a water and ash free basis for pyrolysis of Rooikrans wood at an absolute pressure of less than 5 kPa.

It can be seen from Figure 5.1 that the charcoal yield decreases as the temperature increases. This was expected, because more volatiles are removed from the charcoal at higher temperatures. The actual values for the charcoal yields compare very well to those obtained by **De Jongh (2001)**. At 350 ˚C, charcoal yields of the order of 37 to 40 % were achieved, which is similar to the 35 to 45 % yields **De Jongh (2001)** obtained for different types of wood. This Figure decreased to between 27 and 30 % for temperatures of 500 ˚C and above. Those obtained by **De Jongh (2001)** ranged from 25 to 35 %. The char yields obtained from the isothermal TGA experiments were slightly lower. For an isothermal temperature of 357 ˚C, a final char yield of 29 % was achieved. For isothermal temperatures of 436 ˚C and 492 ˚C, char yields of 25 % and 23 % were achieved respectively. The most probable reason for the lower char yields from the TGA experiments is the smaller size of the wood chips. The smaller the size of the wood chips, the less the diffusion effects and the more easily volatiles are removed from the wood. As explained in section 5.1.2, diffusion limitations will increase the residence time of volatiles in the solid, which result in secondary interactions with the char which will lead to higher char yields. Nevertheless, the trend observed is the same: as temperature increases the char yield decreases.

The reason for the consistently lower charcoal yields for the experiments conducted in early 2005, is not entirely clear. Firstly, as stated above, different batches of Rooikrans wood were used for the two different sets of experiments. Moisture

contents determined for both batches of Rooikrans wood were very close: 7.6 and 8.5 % respectively. It is therefore unlikely that this difference would have had any significant effect. Ash content is another factor which could affect charcoal and oil yields. The ash content of the different samples is given in table 7.1 below.

Table 7.1 Ash content of the different char samples of Rooikrans wood (values in %).

Temp/Year	2003	2005
350	6.0	2.7
450	4.9	3.1
520/500	6.2	1.7

The ash content of the samples pyrolysed in 2005 were between 4.5 and 1.8 % lower and since the oil and charcoal yields are given on an ash-free basis, one would have expected the 2005 yields to have been higher.

The age of the feedstock is known to affect oil and charcoal yields. This was investigated by **De Jongh (2001)** and it was found that aged wood gave lower charcoal and oil yields. Wood degrades with age and the degradation is accompanied by a loss of strength of the individual components. As a result, gases and vapours are released at lower temperatures because less energy is needed for the decomposition. Initial weight loss will therefore be lower, but as temperature increases, this difference will decrease. This decrease in difference is, however, not seen in the above results. It has to be added though that there is no certainty on the ages of the Rooikrans used in the experiments as different batches of wood were used. It is thus possible that the Rooikrans used in early 2005 was not older than that of 2003.

The reason for the difference remains unclear, but since the differences in the values are all within 5 % it falls within acceptable experimental limits.

Contrary to what was expected, the oil yield stayed virtually constant over the three temperatures tested. It is clear from **De Jongh's (2001)** results that the oil yield increased above 350 ˚C to a maximum before decreasing again. The maximum oil yield temperature was different for the different woods tested though, and ranged from 380 to 480 ˚C. Looking at the TGA conversion versus temperature curves for Rooikrans (Figures 5.1, 5.6, 5.7), it can be seen that at a heating rate of 10 ˚C/min,

most of the pyrolysis reactions were completed at a temperature of 400 ˚C. Above this temperature, only residual compounds still reacted. It is therefore very possible that the maximum oil yield temperature for Rooikrans would be closer to 400 ˚C. At a temperature of 350 ˚C the maximum conversion will not have been reached yet. From isothermal results, however, we see that for an isothermal temperature of 323 ˚C the conversion still increased by about 20 % to a final value of just above 60 %. Keeping the temperature constant at 350 ˚C for 60 minutes should therefore increase the conversion and oil yield substantially. It is still possible though that an even higher oil yield will result from an isothermal temperature of 400 ˚C. At 350 ˚C the char yield is also at its highest, which suggests that more compounds could still be released by increasing the temperature. It has to be noted at this point that maximum conversion, or mass loss, does not necessarily equal maximum oil yield. Non-condensable gases are also produced which do not condense out to yield pyrolysis oil. An isothermal temperature of 450 ˚C though, would probably be well above the maximum oil yield temperature, because most of the pyrolysis reactions in Rooikrans wood are completed at a temperature of 400 ˚C. As the oven heats up above 400 ˚C, the actual sample temperature will still be somewhat lower. As some of the longer chain compounds are released the higher oven temperature may crack these molecules into shorter chain compounds which do not condense out to form oil. As a result the oil yield will decrease. Increasing the temperature above 450 ˚C to 500 or 520 ˚C may not actually decrease the oil yield, because, unless the sample temperature lags far behind the oven temperature, most of the compounds that condense out to form oil will already have been released at this stage.

Figure 7.2 below is a plot of the measured temperatures as a function of time for the heating up period of the first experiment to 520 ˚C.

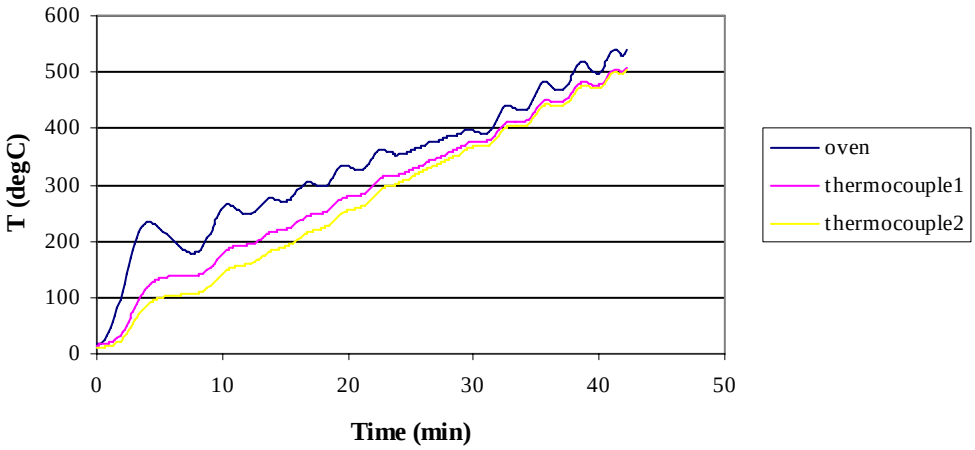

Figure 7.2 Measured temperatures in tube furnace as a function of time for the heating up period.

The lines in the above Figure labelled thermocouple 1 and 2 refer to the thermocouples placed inside the "bed" of wood chips placed in the tube furnace. It can be seen that the lag between the oven temperature, measured on the outside of the quartz tube, and the temperatures measured inside the bed, was not more than 35 ˚C at the end of the heating up period. It is thus fair to say that by the time the oven temperature reached 450 ˚C, the real sample temperature would probably have been very close to 400 ˚C, at which point most of the pyrolysis reactions would be complete. Of course some of the longer chained compounds might not yet have diffused out at this point, but keeping the oven temperature constant at 450 ˚C would only serve to increase the sample temperature further which might lead to cracking of those compounds that have not yet diffused out. This would lead to a lower oil yield.

One experiment was done with Swarthaak wood (*Acacia mellifera)* at 450 ˚C for comparative purposes. Table 7.2 below gives a summary of the main results compared to the corresponding values for Rooikrans wood.

Table 7.2 Comparison of results for Swarthaak and Rooikrans wood.

	Swarthaak	Rooikrans (03)	Rooikrans (05)
Ash content of charcoal (%)	13.6	4.9	3.1
Oil yield (%)	14.5	21.0	18.6
Char yield (%)	37.5	33.3	35.6

It is important to note that the ash content of the Swarthaak wood is about 10 % higher than for Rooikrans wood. It has been shown that some ash components catalyse decomposition reactions (**De Jongh, 2001)**. This would cause shorter chain non-condensable gases which would result in lower oil yields. It can be seen in the above table that the oil yield for the Swarthaak wood was between 4 and 7 % lower than that for Rooikrans wood. **De Jongh (2001)** also found that the oil yields for the wood with the highest ash content, was lower compared to woods with a lower ash content.

7.2 Oil Analysis

Oil analysis was done using GC/MS to identify some of the main components in the pyrolysis oil. The method used is described in chapter 3. Table 7.3 is a list of compounds identified with a certainty of more than 75 % in the three oil samples.

Table 7.3 Compounds identified in Rooikrans pyrolysis oil.

Compound	Certainty (%)
Acetic acid	91
1-hydroxy-2-Propanone	78
Propanol	78
1-hydroxy-2-Butanone	86
2-Furancarboxaldehyde	97
1-(acetyloxy)-2-Propanone	80
2-hydroxy-3-m-2-Cyclopenten-1-one	91
or	
Cyclooctane	90
2-methoxy-Phenol	95
or	
4-methoxy-Phenol	91
2-methoxy-4-methylphenol	95
2,6-dimethoxy-Phenol	91
4-ethyl-2-methoxy-Phenol	87
2,4-Dimethyl-3-(methoxycarbonanyl)-5	83
ethyl-Benzene	87
1-2-dimethyl-Benzene	97
or	

1-3-dimethyl-Benzene	95
or	
1-4-dimethyl-Benzene	95
2-Butenal	90
2-Furanmethanol	96
5-methyl-2-Furancarboxaldehyde	97

As expected, Acetic acid and phenols were positively identified. These components are known to be present in pyrolysis oil.

7.3 Energy values

The energy values of the different charcoal samples were also determined. Rooikrans wood char samples pyrolysed at 350, 450 and 500 ˚C yielded average energy values of 28, 30 and 31 MJ/kg respectively. The energy value for Swarthaak wood pyrolysed at 450 ˚C was only 27 MJ/kg. These values all compare very favourably with those of commercial products. The energy values for Ethosha brickets, Etosha charcoal and Charca brickets are 20, 27 and 25 MJ/kg respectively **(De Jongh, 2001)**. It is clear though that higher energy values are produced by chars with a lower ash content. As stated in chapter 3, the energy values for the pyrolysis oils could unfortunately not be determined, because the high water content of the oil prevented its ignition in the bomb calorimeter.

7.4 BET surface areas

The BET surface areas determined for Rooikrans char samples were much higher than those determined by **De Jongh (2001)** for Kraalbos, Scholtzbos and Asbos. This area could, however, not be determined for the sample pyrolysed at 350 ˚C, because the volatile content of this sample was too high and difficulties were experienced during degassing. Table 7.4 below gives the results obtained for the samples pyrolysed at 450 and 520 ˚C.

Table 7.4 BET surface area of Rooikrans wood samples pyrolysed at different temperatures.

Temperature (˚C)	BET surface area (m^2/g)
450	194
520	312

These values compare well to those found by **Darmstadt et al. (2000)**: for maple bark samples pyrolysed at 502 ˚C, surface areas ranging between 169 and 221 m^2/g were found, and for softwood, surface areas of 206 to 326 m^2/g were found. Because of these high surface areas, it is possible to use the charcoals produced by vacuum pyrolysis as feedstocks for the production of activated carbon.

7.5 Elemental composition of Rooikrans wood charcoal

The elemental composition of Rooikrans charcoal, pyrolysed at 450 ˚C, is given in Figure 7.3 below. Similar results to those of **De Jongh (2001)** were obtained. The main elements found were Ca, K, Na, Mg, P. None of these elements poses problems for the use of the charcoal as a fuel.

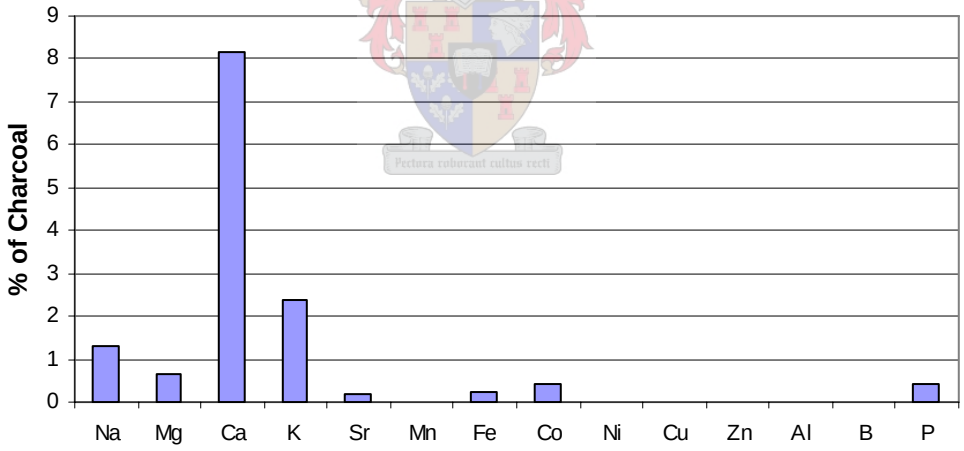

Figure 7.3 Elemental composition of Rooikrans charcoal pyrolysed at 450 ˚C.

8. Conclusions and Recommendations

8.1 Conclusions

8.1.1 TGA results

- The TGA experiments in this study were conducted under a pressure of 140 mm Hg. Unfortunately the effect of the low pressure was largely negated by the high nitrogen flow, necessary to prevent oxidation of the sample. The results did not differ much compared to results from experiments conducted under atmospheric conditions with the same high nitrogen flow rate. However, for the fine sawdust the reduced pressure would possibly not have had such a significant effect anyway. In larger particles the driving force for the gases to leave the particle will be greater under a reduced pressure than under atmospheric conditions. Where diffusion limitations start playing a role, as in larger particles, the effect of the vacuum should be much more noticeable.

- The different heating rates employed did not affect the rate of change of conversion with temperature of the pyrolysis reactions. The actual rate, $d\alpha/dt$ of the reactions does increase with an increase in the heating rate, simply because the same temperature and thus conversion is reached in a much shorter time. An increase in heating rate causes an increase in the thermal lag experienced by the particles. As a result, the same conversion is achieved at a slightly higher temperature, compared to a run under a lower heating rate.

- Heat and diffusion limitations start affecting the pyrolysis reactions as the particle size is increased. Lower conversions were achieved with larger Rooikrans blocks and a distinct “kink” in the rate curve was observed.

- The decomposition of the two main fractions of wood, namely the heartwood and sapwood, were compared. A higher conversion was achieved with the sapwood particles, and this is attributed to a difference in composition: More

volatile components reside in the sapwood and the mass loss for this fraction will thus be higher.

- Swarthaak wood was also pyrolysed in the TGA to compare the results with those obtained from pyrolysing Rooikrans wood. The conversion achieved for the Swarthaak wood was much lower. The most probable reason for this is the higher ash content of the Swarthaak wood.

- There are no published values for the activation energies of Rooikrans wood available for comparison with those obtained in this study. Using the E_a and A values, determined using the modified Coats-Redfern isoconversional method, a good prediction of the experimental results were made. Despite the fact that wood is a complex material with many different reactions taking place during its pyrolysis, a first order single step reaction model gave a very good prediction. Unfortunately, the irreproducibility of the experimental results at high temperatures prevented the determination of activation energies above a conversion of 80 %. Predictions above this conversion was, therefore, not possible.

- The results obtained from this study correspond reasonably well to the mechanistic model proposed by **Reina et al. (1998)**.

- The kinetic method of **Koufopanos et al. (1991)** was also used for comparative purposes. A direct comparison is, however, not possible because of the nature of the model, which is a parallel and serial reaction model where activation energies are determined for the individual reactions in the kinetic scheme. A good fit to the experimental data was achieved though. The obvious disadvantage of this method is that it is not model-free, like the isoconversional method, and the activation energies determined do not mean much unless the overall reactions proposed in the kinetic scheme are indeed correct. The effect of larger particles is accounted for in this model, even though it is only because the secondary reactions are neglected for very small particles.

8.1.2 Reactor model results

- The reactor model that was used in this study yielded reasonable results. The major simplifying assumption was that the bed was perfectly mixed and that the bed temperature was uniform in the radial direction. This of course reduces the accuracy of the model, but as a simple one-dimensional model it did succeed in providing a good first estimate. The reactor diameter was fixed at 0.5 m and for the base case a required reactor length of 3.4 m was predicted.

- The kinetic model was successfully integrated into the reactor model and correctly predicted the conversion along the length of the reactor. Unfortunately the kinetic parameters will have to be determined experimentally for every type of feedstock used.

- The model responded correctly to changes in the operating parameters, predicting longer or shorter reactor lengths.

8.1.3 Tube furnace results

- The results obtained for Rooikrans wood in the tube furnace are very similar to the results obtained by **De Jongh (2001)** for other wood types. Unfortunately a maximum oil yield temperature was not observed for Rooikrans wood, but only three different temperatures, 350, 450 and 500 ˚C were investigated. It is thus very possible that a maximum oil yield would have been observed at a temperature of 400 ˚C, for instance. The char yields obtained from Rooikrans wood showed the same tendencies and were of a similar order of magnitude to the woods tested by **De Jongh**.

- An average energy value of 29.7 MJ/kg was determined for Rooikrans wood. This is slightly higher than the values obtained for Scholzbos, Kraalbos and Asbos by **De Jongh**. This energy value is also higher than that of commercially available Charca Brikets, which has an energy value of 24.8 MJ/kg **(De Jongh, 2001)**. The ash content of Rooikrans wood charcoal, of the order of 10 %, compared well with that of commercial products. The BET surface area determined for the charcoal was also much higher than the surface

areas determined by **De Jongh.** The reason for this is not entirely clear. The surface areas determined in this study compare well with those determined by **Darmstadt et al. (2000),** and confirms the possibility of using the charcoal for the production of activated carbon.

- The percentage mass loss achieved in the tube furnace compared reasonably well with that achieved in the TGA for the larger particles. Much higher temperatures were used in the TGA though which resulted in slightly higher mass losses.

8.2 Recommendations

The TGA used in this study could not be sealed well enough for vacuum conditions to prevent the leakage of air. A high nitrogen flow rate was needed to prevent sample oxidation and this did affect the results. Doing the same experiments under vacuum, but with no or a very small nitrogen flow rate would serve to validate the results obtained in this study.

The exact mechanism of pyrolysis is still not understood. However, the kinetic modelling done in this study has shown that a first order kinetic model makes a good prediction of the conversion as a function of temperature. The results obtained in this study compares well to the mechanistic model, proposed by **Reina et al, 1998**, but further research is necessary to validate this. Experiments should be done on other biomass feedstocks to see whether the first order model predicts the reaction progress equally well.

Though the reactor model used in this study produced good results, the simplifying assumptions used do reduce the accuracy of the model. The first step forward should be to implement the model described in chapter 4 in Matlab, taking into account the temperature profile inside individual particles. Further improvement should include accounting for radial temperature variations in the bed and residence time in the reactor. However, the best way to obtain accurate information is to build a pilot scale reactor. This will allow the motion in the reactor to be carefully studied and residence

times, temperatures and conversions to be accurately measured. A possible shortcoming of the reactor model at the moment is that it does not depend directly on the reactor pressure. Incorporating the reactor pressure into the kinetic model would be ideal.

A rotary oven is good choice for a pilot scale reactor for vacuum pyrolysis of biomass and other feedstocks because of its simplicity, robustness and flexible nature. The sealing configuration would have to be carefully considered though. Bellows seals, capable of handling vacuum conditions and high temperatures have been patented, but will have to be tested for suitability in this application.

References

Antal, M.J. Jnr.; Várhegyi, G. (1995) Cellulose Pyrolysis Kinetics: The Current State of Knowledge. *Ind. Eng. Chem. Res.* 34 (1995) 703 – 717

Boateng, A.A.; Barr, P.V. (1996) A thermal model for the rotary kiln including heat transfer within the bed. *Int. J. Heat Mass Transfer*. 39 (10) (1996) 2131 – 2147

Brown, M.E.; Maciejewski, M.; Vyazovkin, S.; Nomen, R.; Sempere, J.; Burnham, A.; Opfermann, J.; Strey, R.; Anderson, H.L.; Kemmler, A.; Keuleers, R.; Janssens, J.; Desseyn, H.O.; Chao-Rui Li; Tang, Tong B.; Roduit, B.; Malek, J.; Mitsuhashi, T. (2000) Computational aspects of kinetic analysis. Part A: The ICTAC kinetics project-data, methods and results. *Thermochimica Acta* 355, 125 – 143

Burnham, A.K.; Braun, R.L. (1999) Global Kinetic Analysis of Complex Materials. *Energy & Fuels* 13, 1 – 22

Chaala, A.; Roy, C. (2003) Preliminary investigation of the vacuum pyrolysis of bituminous roofing waste materials. *Journal of Environmental and Engineering Science* 2, 119 – 126

Darmstadt, H.; Pantea, D.; Sümmchen, L.; Roland, U.; Kaliaguine, S.; Roy, C. (2000) Surface and bulk chemistry of charcoal obtained by vacuum pyrolysis of bark: influence of feedstock moisture content. *Journal of Analytical and Applied Pyrolysis* 53, 1 – 17

Darmstadt, H. www.gch.ulaval.ca/croy/process_e.html, (2002) (exact date unknown)

De Jongh, W.A. (2001) Possible applications for vacuum pyrolysis in the processing of waste materials. M.Sc. Thesis, Department of Process Engineering, Stellenbosch, South Africa.

Di Blasi, C. (1998) Comparison of semi-global mechanisms for the primary pyrolysis of lignocellulosic fuels. *Journal of Analytical and Applied Pyrolysis* 47, 43 – 64

Duke, J.A. (1983) Handbook of Energy Crops. unpublished, Website: [**http://www.hort.purdue.edu/newcrop/duke_energy/Acacia_cyclops.html**] (exact date unknown)

Gautschi, W.; Cahill, W.F. (1964) Exponential Integral and Related Functions. In: Handbook of Mathematical Functions, Abramowitz, M.; Stegun, I.A. (Eds.); Report AMS 55; National Bureau of Standards: Washington, DC, 228 – 231

Incropera, F.P.; DeWitt, D.P. (1996) Fundamentals of Heat and Mass Transfer, 4th edition , John Wiley & Sons, New York, chapter 7.

Jane, F.W. (1970) The structure of wood. 2nd edition, Adam and Charles Black, London.

Koufopanos, C.A., Papayannakos, N.; Lucchesi, A. (1989) Kinetic Modelling of the Pyrolysis Biomass and Biomass Components. *The Canadian Journal of Chemical Engineering* 67, 75 – 84

Koufopanos, C.A., Papayannakos, N. (1991) Modelling of the Pyrolysis of Biomass Particles. Studies on Kinetics, Thermal and Heat Transfer Effects. *The Canadian Journal of Chemical Engineering* 69, 907 – 915

Kemp, I.C.; Oakley, D.E. (2002) Modelling of particulate drying in theory and practice. *Drying Technology* 20 (9) 1699 – 1750

Kutaish, N.; Aggarwal, P.; Dollimore, D. (1997) Thermal analysis of calcium oxalate samples obtained by various routes. *Thermochimica Acta* 297, 131 – 137

Maciejewski, M. (2000) Computational aspects of kinetic analysis. Part B: The ICTAC Kinetics Project – the decomposition kinetics of calcium carbonate revisited, or some tips on survival in the kinetic minefield. *Thermochimica Acta* 355, 145 – 154

Meier, D.; Faix, O. (1999) State of the art of applied fast pyrolysis of lignocellulosic materials – a review. *Biosource Technology* 68, 71 – 77

Mujumdar, A.S. (ed) (1995) Handbook of Industrial Drying, 2nd ed, vol. 1. Marcel Dekker, Inc. New York, chapters 5 and 16.

Narayan, R.; Antal, Jr., M.J. (1996) Thermal Lag, Fusion, and the Compensation Effect during Biomass Pyrolysis. *Ind. Eng. Chem. Res.* 35, 1711 – 1721

Nonhebel, G.; Moss, A.A.H. (1971) Drying of Solids in the Chemical Industry. Butterworth & Co. (South Africa) (PTY) Ltd. Durban, chapters 8, 10 and 14.

Pakdel, H.; Couture, G.; Roy, C. (1994) Vacuum pyrolysis of bark residues and primary sludges. *Tappi Journal* vol. 77, no. 7, 205 – 211

Perron, J.; Bui, R.T. (1990) Rotary Cylinders: Solid Transport Prediction by Dimensional and Rheological Analysis. *The Canadian Journal of Chemical Engineering* 68, 61 – 68

Perry, R.H.; Green, D.W. (1997) Perry's Chemical Engineer's Handbook, 7th ed., McGraw-Hill book Co., New York, chapter 12.

Reina, J.; Velo, E.; Puigjaner, L. (1998) Kinetic Study of the Pyrolysis of Waste Wood. *Ind. Eng. Chem. Res.* 37, 4290 – 4295

Roy, C.; Lemieux, R.; De Caumia, B.; Blanchette, D. (1988) Processing of wood chips in a semi-continuous multiple-hearth vacuum –pyrolysis reactor. Chapter 3 *American Chemical Society.*

Roy, C.; Pakdel, H.; Brouillard, D. The role of extractives during vacuum pyrolysis of wood. *Journal of Applied Polymer Science* 41 (1990) 337 – 348

Roy, C.; Blanchette, D.; De Caumia, B.; Labrecque, B. (1992) Conceptual Design of a Biomass Pyrolysis Plant. *Advances in Thermochemical Biomass Conversion* , Interlaken, Switzerland, 1165 – 1186

Roy, C.; Yang, J.; Blanchette, D.; Korving, L. (1997) Development of a novel vacuum pyrolysis reactor with improved heat transfer potential. *Developments in Thermochemical Biomass Conversion* 1, Blackie Academic and Professional, Bridgwater, A.V., 351 – 367

Shafizadeh, F.; Chin, P.P.S. (1976) Thermal deterioration of wood. in: Wood Technology: Chemical Aspects, Goldstein, I.S. (editor) ACS Symposium series, American Chemical Society, August 31 – September 2, San Francisco, California

Thomas,R.J. (1976) Wood: Structure and Chemical Composition. in: Wood Technology: Chemical Aspects, Goldstein, I.S. (editor) ACS Symposium series, American Chemical Society, August 31 – September 2, San Francisco, California

Várhegyi, G.; Antal, M.J. Jnr.; Jakab, E.; Szabó, P. (1997) Kinetic modeling of biomass pyrolysis. *Journal of Analytical and Applied Pyrolysis* 42, 73 – 87

Vyazovkin, S. (1996) A Unified Approach to Kinetic Processing of Nonisothermal Data. *International Journal of Chemical Kinetics* 28, 95 – 101

Vyazovkin, S. (1997) Evaluation of Activation Energy of Thermally Stimulated Solid-State Reactions under Arbitrary Variation of Temperature. *Journal of Computational Chemistry* 18, 393 – 402

Vyazovkin, S. (2000) Computational aspects of kinetic analysis. Part C: The ICTAC Kinetics Project – the light at the end of the tunnel? *Thermochimica Acta* 355, 155 – 163

Ward, S.M.; Braslaw, J. (1985) Experimental Weight Loss Kinetics of Wood Pyrolysis under Vacuum. *Combustion and Flame* 61, 261 – 269

Traub, D.A. (2003) Rotary dryers. [http://www.process-heating.com/CDA/articleInformation/Drying_Files_item/0,3274,75846,00.html] (Exact date unknown)

www.pyne.co.uk, (2005) (March 1999 PyNe Guide 1) (Exact date unknown)

www.stat.wisc.edu/~larget/math496/bootstrap (2005) (Exact date unknown)

http://www.fibersource.com/f-tutor/cellulose.htm (2005) (Exact date unknown)

Bibliography

Anthony, D.B.; Howard, J.B. (1976) Coal Devolatilization and Hydrogasification. *AIChE Journal* 22, 625 - ??

Babu, B.V.; Chaurasia, A.S. (2003) Modeling, simulation and estimation of optimum parameters in pyrolysis of biomass. *Energy Conversion and Management* 44, 2135 – 2158

Babu, B.V.; Chaurasia, A.S. (2004) Parametric study of thermal and thermodynamic properties on pyrolysis of biomass in thermally thick regime. *Energy Conversion and Management* 45, 53 – 72

Babu, B.V.; Chaurasia, A.S. (2004) Pyrolysis of biomass: improved models for simultaneous kinetics and transport of heat, mass and momentum. *Energy Conversion and Management* 45, 1297 – 1327

Babu, B.V.; Chaurasia, A.S. (2004) Dominant design variables in the pyrolysis of biomass particles of different geometries in thermally thick regime. *Chemical Engineering Science* 59, 611 – 622

Babu, B.V.; Chaurasia, A.S. (2004) Heat transfer and kinetics in the pyrolysis of shrinking biomass particle. *Chemical Engineering Science* 59, 1999 – 2012

Bilbao, R.; Mastral, J.F.; Ceamos, J.; Aldea, M.E. (1996) Modelling of the pyrolysis of wet wood. *Journal of Analytical and Applied Pyrolysis* 36, 81 -97

Burnham, A.K.; Braun, R.L.; Gregg, H.R.; Samoun, A.M. (1987) Comparison of Methods for Measuring Kerogen Pyrolysis Rates and Fitting Kinetic Parameters. *Energy & Fuels* 1, 452 – 458

Bilbao, R.; Salvador, M.L.; Arauzo, J. (1994) Influence of the heating rate on the temperature profiles and on the conversion rate of powdery cellulose and pine sawdust. *Journal of Analytical and Applied Pyrolysis* 30, 145 – 159

Bilbao, R.; Salvador, M.L.; Arauzo, J. (1995) Kinetics and Modeling of Gas Formation in the Thermal Decomposition of Powdery Cellulose and Pine Sawdust. *Ind. Eng. Chem. Res.* 34, 786 – 793

Boateng, A.A.; Barr, P.V. (1996) Modelling of particle mixing and segragation in the transverse plane of a rotary kiln. *Chemical Engineering Science* 51(17), 4167 – 4181

Boucher, M.E.; Chaala, A.; Roy, C. (2000) Bio-oils obtained by vacuum pyrolysis of softwood bark as a liquid fuel for gas turbines. Part I: Properties of bio-oil and its blends with methanol and a pyrolytic aqueous phase. *Biomass and Bioenergy* 19, 337 - 350

Boucher, M.E.; Chaala, A.; Pakdel, H.; Roy, C. (2000) Bio-oils obtained by vacuum pyrolysis of softwood bark as a liquid fuel for gas turbines. Part II: Stability and ageing of bio-oil and its blends with methanol and a pyrolytic aqueous phase. *Biomass and Bioenergy* 19, 351 - 361

Burnham, A.K. (2000) Computational aspects of kinetic analysis. Part D: The ICTAC Kinetics Project – multi-thermal-history model-fitting methods and their relation to isoconversional methods, *Thermochimica Acta* 355, 165 – 170

Caballero, J.A.; Font, R.; Marcilla, A.; Conesa, J.A. (1995) New Kinetic Model for Thermal Decomposition of Heterogeneous Materials. Ind. Eng. Chem. Res. 34, 806 – 812

Cao, W.F.; Langrish, T.A.G. (1999) Comparison of residence time models for cascading rotary dryers. *Drying Technology* 17 (4 & 5), 825 – 836

Cao, W.F.; Langrish, T.A.G. (2000) The development and validation of a system model for a countercurrent cascading rotary dryer. Journal unknown, 99 – 115

Cao, N.; Darmstadt, H.; Roy, C.; Soutric, F. (2002) Thermogravimetric study on the steam activation of charcoals obtained by vacuum and atmospheric pyrolysis of softwood bark residues. *Carbon* 40, 471 – 479

Chan, W-C. R.; Kelbon, M.; Krieger-Brockett, B. (1988) Single-Particle Biomass Pyrolysis of Reaction Products with Process Conditions. *Ind. Eng. Chem. Res.* 27, 2261 – 2275

Das, P.; Ganesh, A. (2003) Bio-oil from pyrolysis of cashew nut shell – a near fuel. *Biomass and Bioenergy* 25, 113 – 117

Di Blasi, C. (1997) Influences of physical properties on the biomass devolatilization characteristics. *Fuel* 76(10), 957 – 964

Fan, L.T.; Fan, L-S.; Miyanami, K.; Chen, T.Y.; Walawender, W.P. (1977) A Mathematical Model for Pyrolysis of a Solid Particle. *The Canadian Journal of Chemical Engineering* 55, 47 – 53

Fan, L.T.; Fan, L-S.; Miyanami, K.; Walawender, W.P. (1977) A Mathematical Model for Pyrolysis of a Solid Particle: Effects of the Lewis Number. *The Canadian Journal of Chemical Engineering* 55, 317 – 325

Glikin, P.G. (1978) Transport of solids through flighted rotating drums. *Trans IChemE* 56, 120 – 126

Gray, M.R.; Corcoran W. H.; Gavalas G.R. (1985) Pyrolysis of wood-derived material. Effects of moisture and ash content. *Ind. Eng. Chem. Process Des. Dev.*, Vol. 24, No. 3, 646 – 651

Gupta, M.; Yang, J.; Métral, S.; Roy, C. (2004) Flow characterization of moving and stirred bed vacuum pyrolysis reactor from RTD studies. *Chemical Engineering Research and Design* 82 (A1), 34 – 42

Hatzilyberis, K.S.; Androutsopoulos, G.P. (1999) An RTD study for the flow of lignite particles through a pilot rotary dryer. *Drying Technology* 17 (4 & 5), 745 – 757

Hatzilyberis, K.S.; Androutsopoulos, G.P.; Salmas, C.E. (2000) Indirect thermal drying of lignite: Design aspects of a rotary dryer. *Drying Technology* 18(9), 2009 – 2049

Kelly, J.J.; O' Donnell, P. (1977) Residence time model for rotary drums. *Trans IChemE* 55, 243 – 252

Langrish, T.A.G.; Reay, D.; Bahu, R.E. (1988) An investigation into heat transfer in cascading rotary dryers. *J. Separ. Proc. Technol.* 9, 15 – 20

Lemieux, R.; Roy, C.; De Caumia, B.; Blanchette, D. (1987) Preliminary Engineering data for the scale up of a biomass vacuum pyrolysis reactor. *Preprints of Papers - American Chemical Society, Division of Fuel Chemistry* 32(2), 12 – 20

Lua, A.C.; Yang, T. (2004) Effects of vacuum pyrolysis conditions on the characteristics of activated carbons derived from pistachio-nut shells. *Journal of Colloid and Interface Science* 276, 364 - 372

Mastorakos, E.; Massias, A.; Tsakiroglou, C.D.; Goussis, D.A.; Burganos, V.N.; Payatakes, A.C. (1999) CFD predictions for cement kilns including flame modelling heat transfer and clinker chemistry. *Applied Mathematical Modelling* 23, 55 – 76

Matchett, A.J.; Baker, C.G.J. (1987) Particle Residence Times in Cascading Rotary Dryers. Part 1 – Deviation of a Two-Stream Model. *J. Separ. Proc. Technol.* 8, 11 – 17

Matchett, A.J.; Baker, C.G.J. (1988) Particle Residence Times in Cascading Rotary Dryers. Part 2 – Application of the Two-Stream Model to Experimental and Industrial Data. *J. Separ. Proc. Technol.* 9, 5 – 13

Matchett, A.J.; Sheikh, M.S. (1990) An Improved Model of Particle Motion in Cascading Rotary Dryers. *Trans IChemE* 68A, 139 – 148

Murwanashyaka, J.N.; Pakdel, H.; Roy, C. (2001) Step-wise and one-step vacuum pyrolysis of birch-derived biomass to monitor the evolution of phenols. *Journal of Analytical and Applied Pyrolysis* 60, 219 - 231

Migliavacca, G.; Parodi, E.; Bonfanti, L.; Faravelli, T.; Pierucci, S.; Ranzi, E. A (29/04/04) general mathematical model of solid fuels pyrolysis. JournalUnknown, (Article in press)

Milosavljevic, I.; Suuberg, E.M. (1995) Cellulose Thermal Decomposition Kinetics: Global Mass Loss Kinetics. *Ind. Eng. Chem. Res.* 34, 1081 – 1091

Pakdel, H.; Roy, C. (1987) Production and Characterization of Carboxylic Acids from Wood. Part I: Low Molecular Weight Carboxylic Acids. *Biomass* 13, 155 – 171

Pakdel, H.; Amen-Chen, C.; Roy, C. (1997) Phenolic compounds from vacuum pyrolysis of wood wastes. *The Canadian Journal of Chemical Engineering* 75, 121 – 126

Papadakis, S.E.; Langrish, T.A.G.; Kemp, I.C.; Bahu, R.E. (1992) A short-cut design method for cascading rotary dryers. *Drying '92: Proceedings of the 8th international drying symposium, Montreal, Quebec, Canada, August 2-5 1992* Elsevier, 1258 – 1267

Papadakis, S.E.; Langrish, T.A.G.; Kemp, I.C.; Bahu, R.E. (1994) Scale-up of cascading rotary dryers. *Drying Technology* 12 (1 & 2), 259 – 277

Patisson, F.; Lebas, E.; Hanrot, F.; Ablitzer, D.; Houzelot, J-L. (2000) Coal Pyrolysis in a Rotary Kiln: Part II. Overall Model of the Furnace. *Metallurgical and Materials Transactions B* 31B, 391 – 402

Pokol, G.; Gal, A.; Pungor, E. The Effect of Heat Transport within the Sample on the Shape of Thermoanalytical Curves. *Thermochimica Acta* 105 (1986) 313 – 331

Purcell, J.G. Practical Rotary Cascading Dryer Design. *The Chemical Engineer* July 1979

Reay, D. Theory in the Design of Dryers. *The Chemical Engineer* July 1979

Reina, J.; Velo, E.; Puigjaner, L. (1998) Thermogravimetric study of the pyrolysis of waste wood. *Thermochimica Acta* 320, 161 – 167

Renaud, M.; Grandmaison, J.L.; Roy, C.; Kaliaguine, S. (1988) Low-pressure upgrading of vacuum-pyrolysis oils from wood. Chapter 25 *American Chemical Society*

Renaud, M.; Thibault, J.; Trusiak, A. (2000) Solids transportation model of an industrial rotary dryer. *Drying Technology*18 (4 & 5), 843 – 865

Revol, D.; Briens, C.L.; Chabagno, J.M. (2001) The design of flights in rotary dryers. *Powder Technology* 121, 230 – 238

Roy, C.; De Caumia, B.; Plante, P.; Menard, H. (1983) Production of liquids from vacuum pyrolysis – Development of data base for continuous process. *Institute of Gas Technology: Energy from Biomass and Wastes VII.* Lake Buena Vista, Fa. Jan. 24-28, 1147 – 1170

Roy, C.; De Caumia, B.; Plante, P. (1990b) Performance study of a 30 kg/h vacuum pyrolysis process development unit. *Biomass for Energy and Industry* , New York, Elsevier Applied Science, 2.595 – 2.599

Roy, C.; Pakdel, H.; Zhang, H.G. (1994) Characterization and Catalytic Gasification of the Aqueous By-Product from Vacuum Pyrolysis of Biomass. *The Canadian Journal of Chemical Engineering* 72, 98 - 105

Roy, C.; Malendoma, C.; Yang, J. (2000) Determination of the overall heat transfer coeffocient in a vacuum pyrolysis moving and stirred bed reactor. *Trans IChemE* 78 (part A), 633 – 642

Shene, C.; Alvarez, P.I. (1994) Experimental study of residence time in a contact rotary dryer. *Drying Technology* 12(7), 1629 – 1651

Shene, C.; Bravo, S. (1998) Mathematical modelling of indirect contact rotary dryers. *Drying Technology* 16(8), 1567 – 1583

Sherrit, R.G.; Caple, R.; Behie, L.A.; Mehrotra, A.K. (1993) The Movement of Solids Through Flighted Rotating Drums. Part I: Model Formulation. *The Canadian Journal of Chemical Engineering* 71, 337 – 346

Sherrit, R.G.; Caple, R.; Behie, L.A.; Mehrotra, A.K. (1994) The Movement of Solids Through Flighted Rotating Drums. Part II: Solids-Gas Interaction and Model Validation. *The Canadian Journal of Chemical Engineering* 72, 240 – 248

Vamvuka, D.; Karakas, E.; Kastanaki, E.; Grammelis, P. (2003) Pyrolysis characteristics and kinetics of biomass residuals mixtures with lignite. *Fuel* 82, 1949 – 1960

Van Brakel, J. The Choice and Design of Dryers – a personal view. *The Chemical Engineer* July 1979

Varhegyi, G.; Till, F. (1999) Computer processing of the thermogravimetric-mass spectrometric and high pressure thermogravimetric data. Part 1. Smoothing and differentiation. *Thermochimica Acta* 329, 141 – 145

Várhegyi, G.; Szabó, P.; Jakab, E.; Till, F. (2001) Least squares criteria for the kinetic evaluation of thermoanalytical experiments. Examples from a char reactivity study. *Journal of Analytical and Applied Pyrolysis* 57, 203 – 222

Wang, F.Y.; Cameron, I.T.; Litster, J.D.; Rudolph, V. (1995) A fundamental study on particle transport through rotary dryers for flight design and system optimisation. *Drying Technology* 13 (5 -7), 1261 – 1278

Yang, J.; Miranda, R.; Roy, C. (2001) Using the DTG curve fitting method to determine the apparent kinetic parameters of thermal decomposition of polymers. *Polymer Degradation and Stability* 73, 455 – 461

Appendix A

TGA Experimental results

Experimental Results

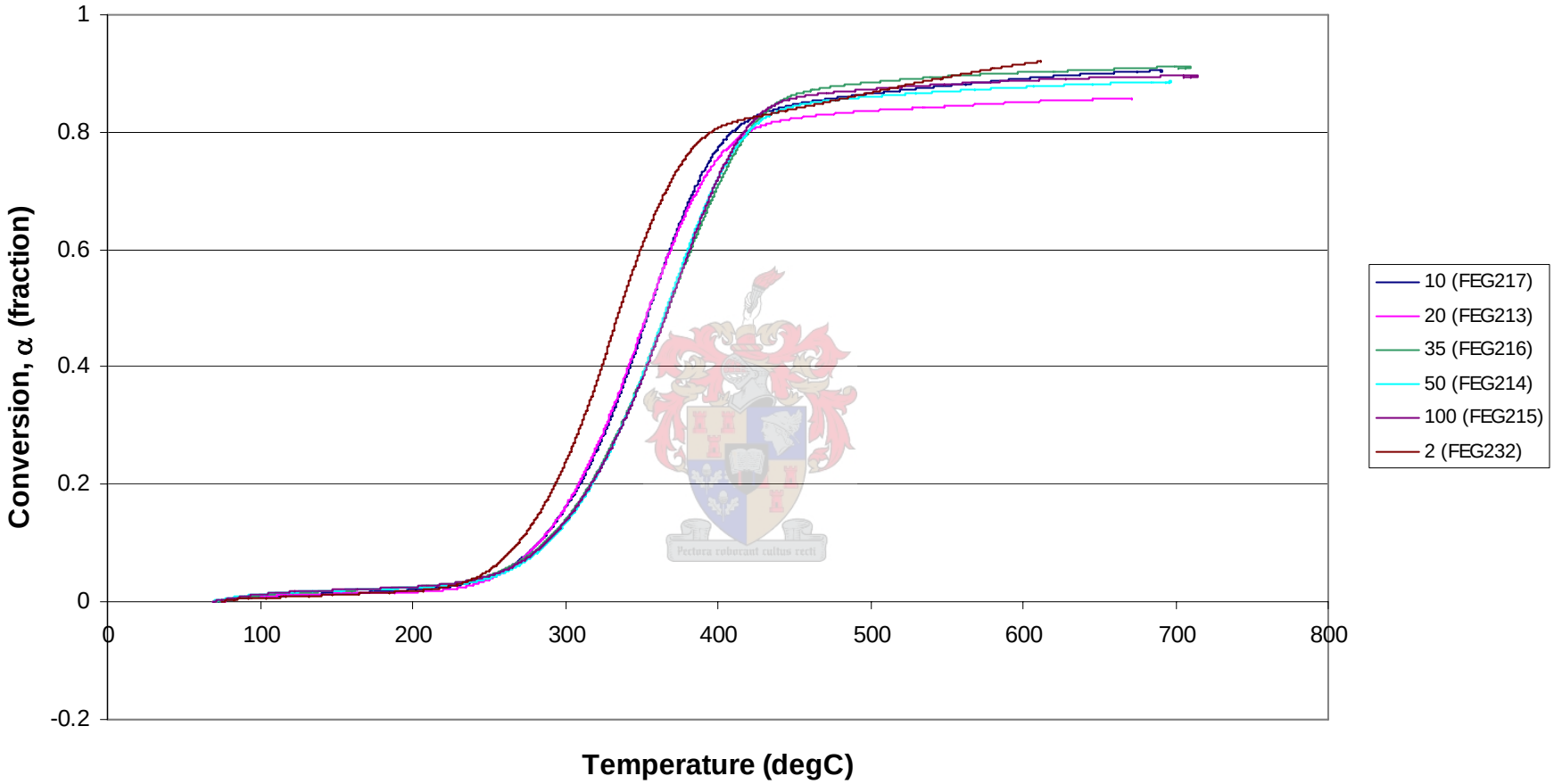

Figure A.1 Conversion versus temperature for different heating rates for Rooikrans sawdust.

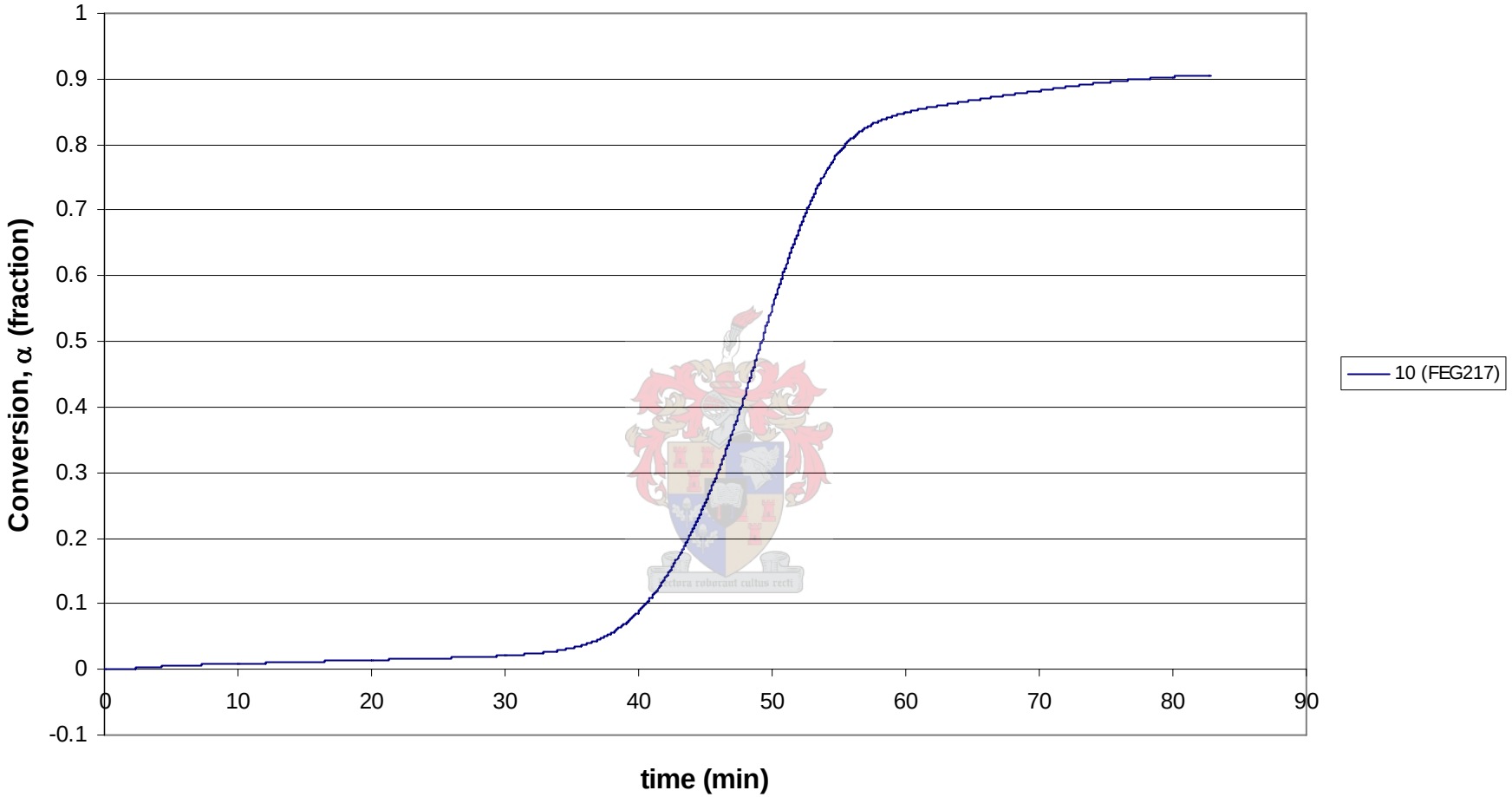

Figure A.2 Conversion versus time for a heating rate of 10 ˚C/min for Rooikrans sawdust.

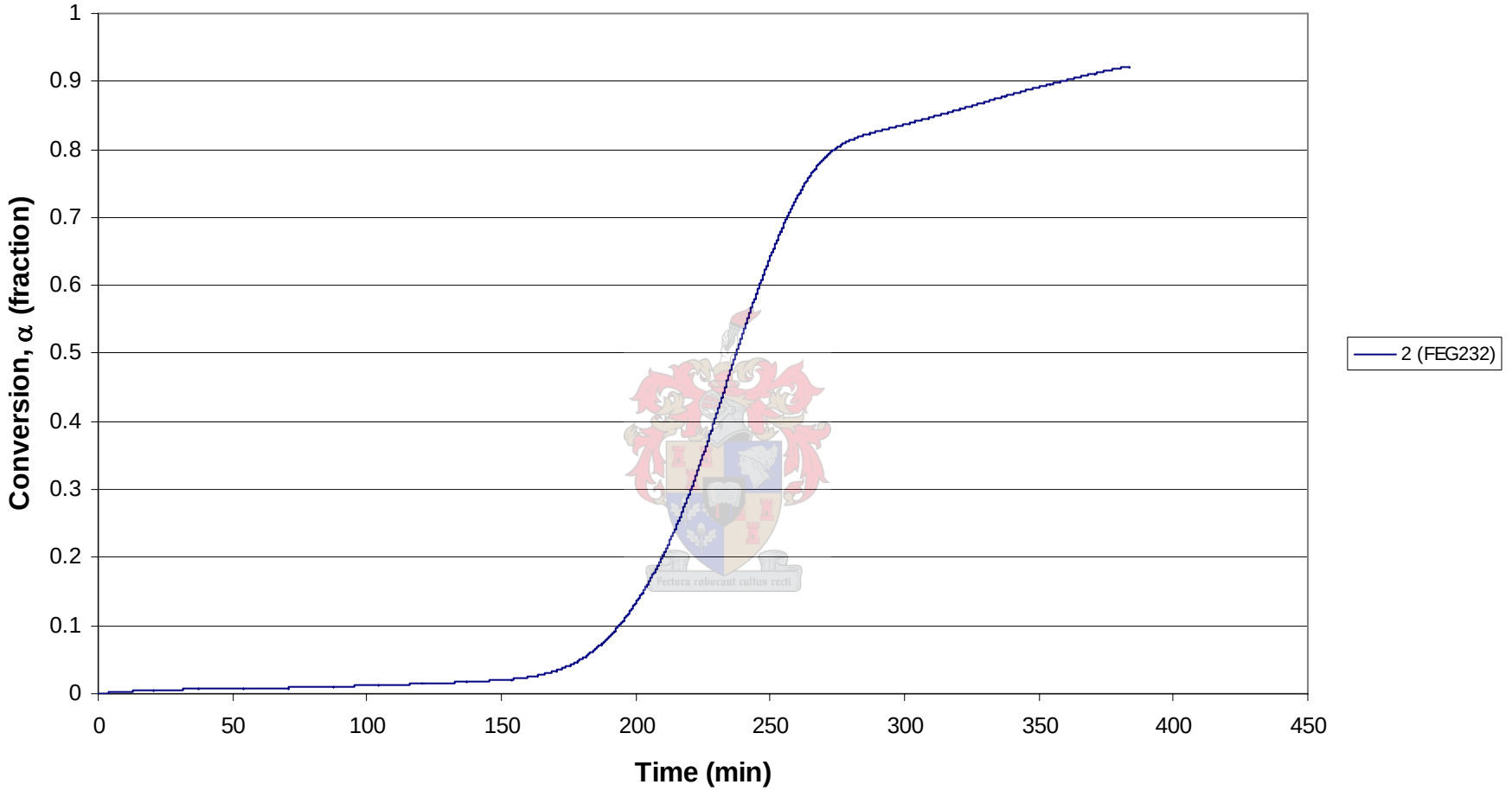

Figure A.3 Conversion versus time for a heating rate of 2 ˚C/min for Rooikrans sawdust.

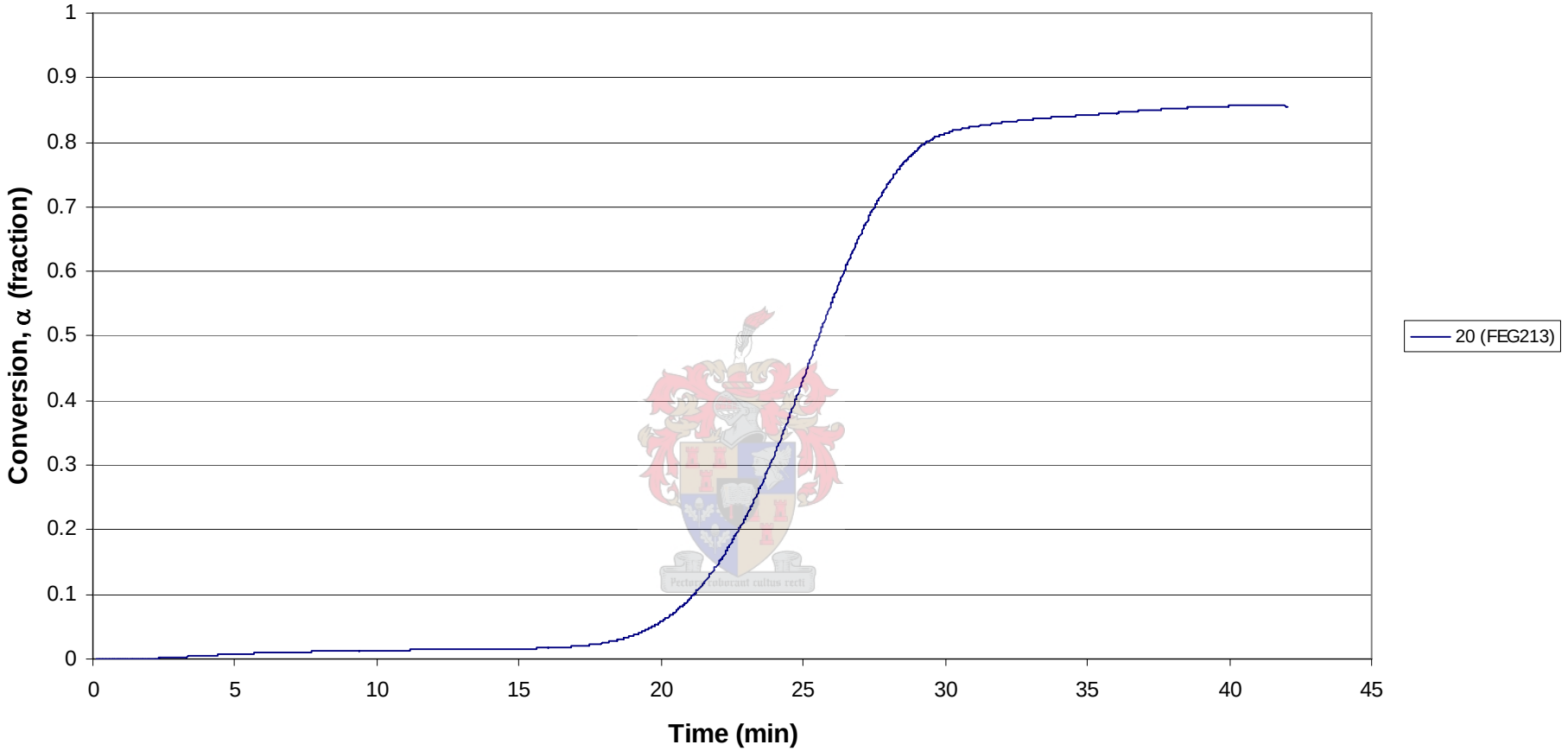

Figure A.4 Conversion versus time for a heating rate of 20 ˚C/min for Rooikrans sawdust.

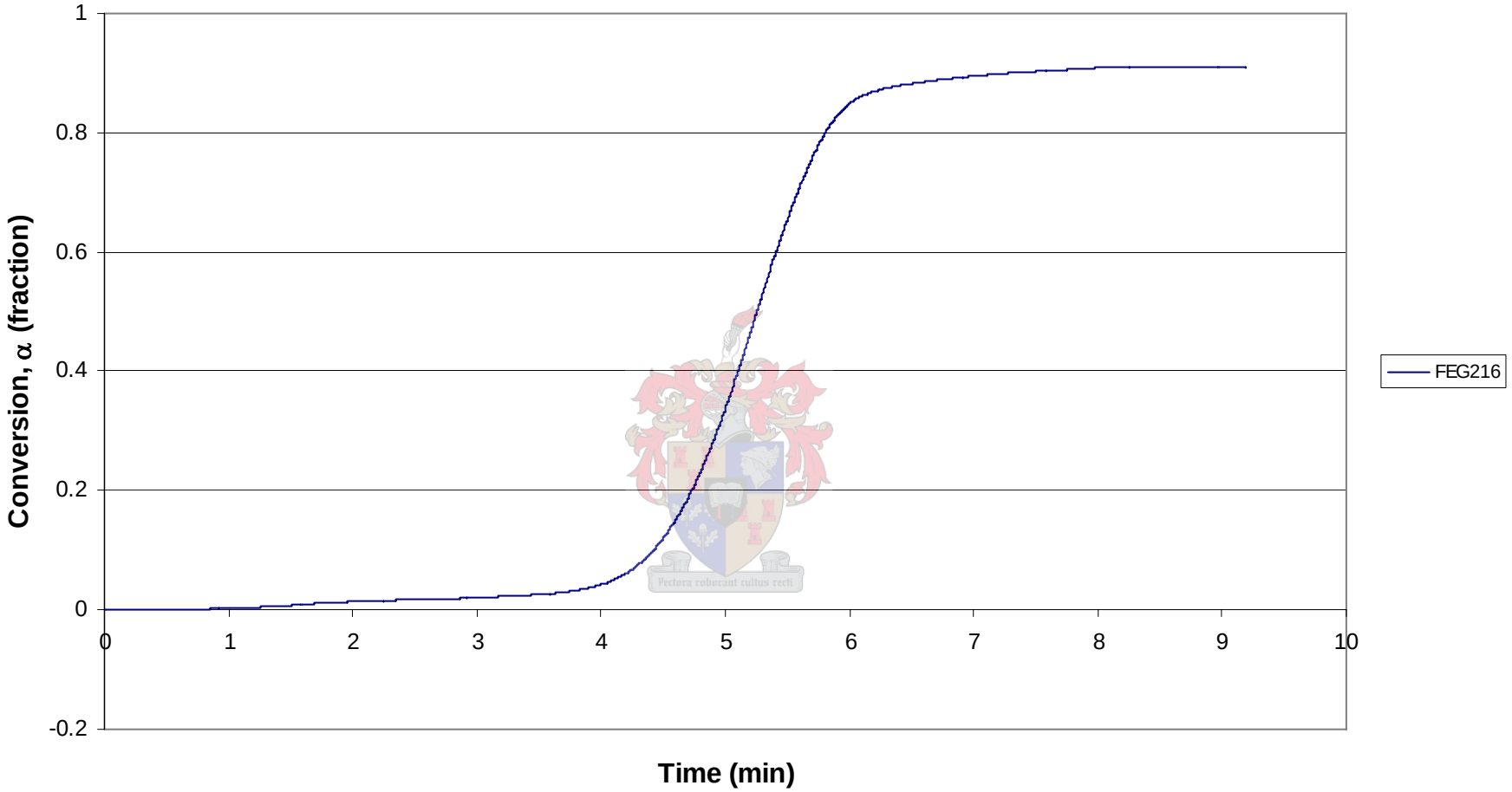

Figure A.5 Conversion versus time for a heating rate of 35 ˚C/min for Rooikrans sawdust. (An experimental occurred during this run and the heating rate of 35 ˚C/min was closer to 100 ˚C/min.)

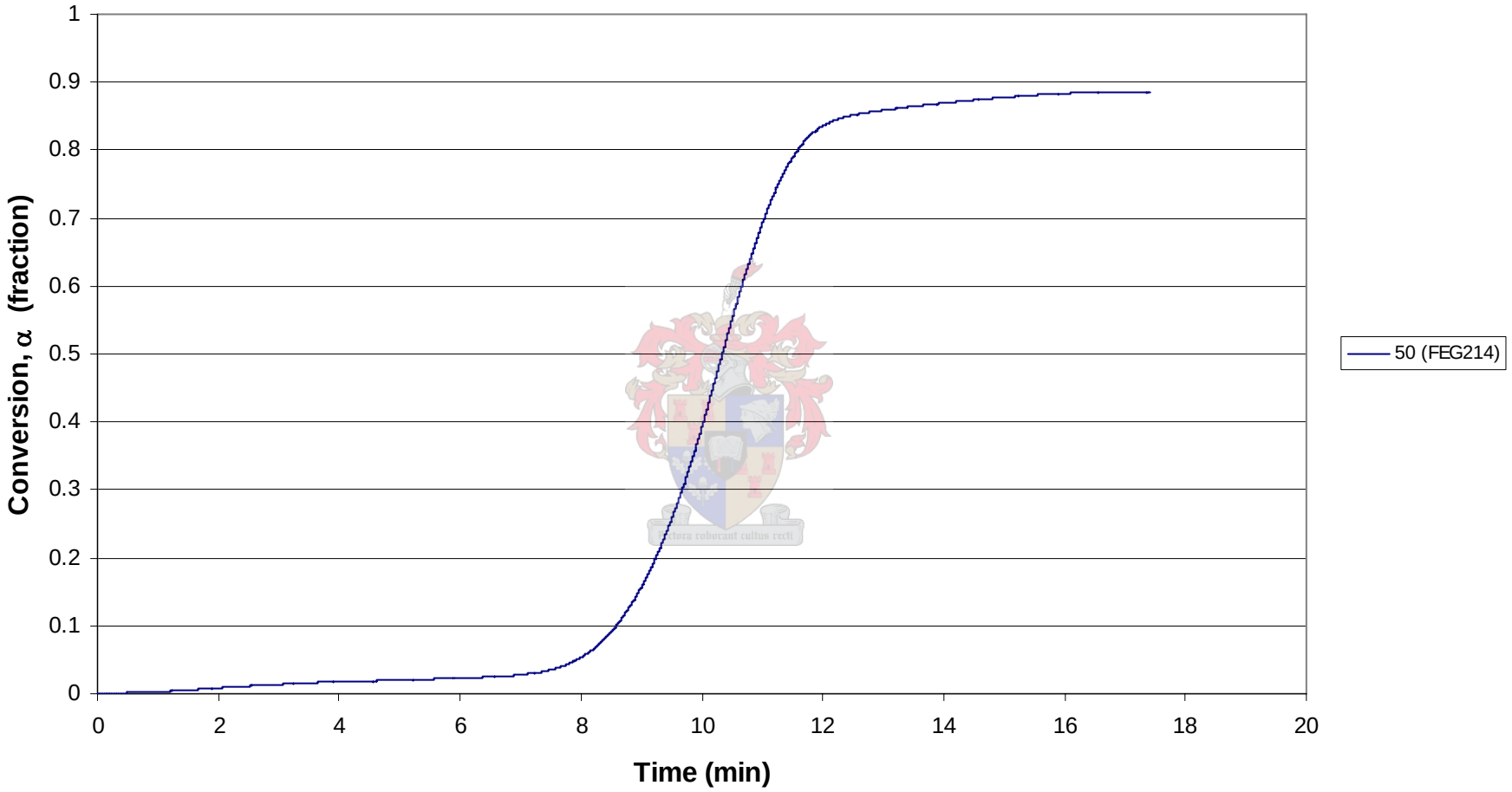

Figure A.6 Conversion versus time for a heating rate of 50 ˚C/min for Rooikrans sawdust.

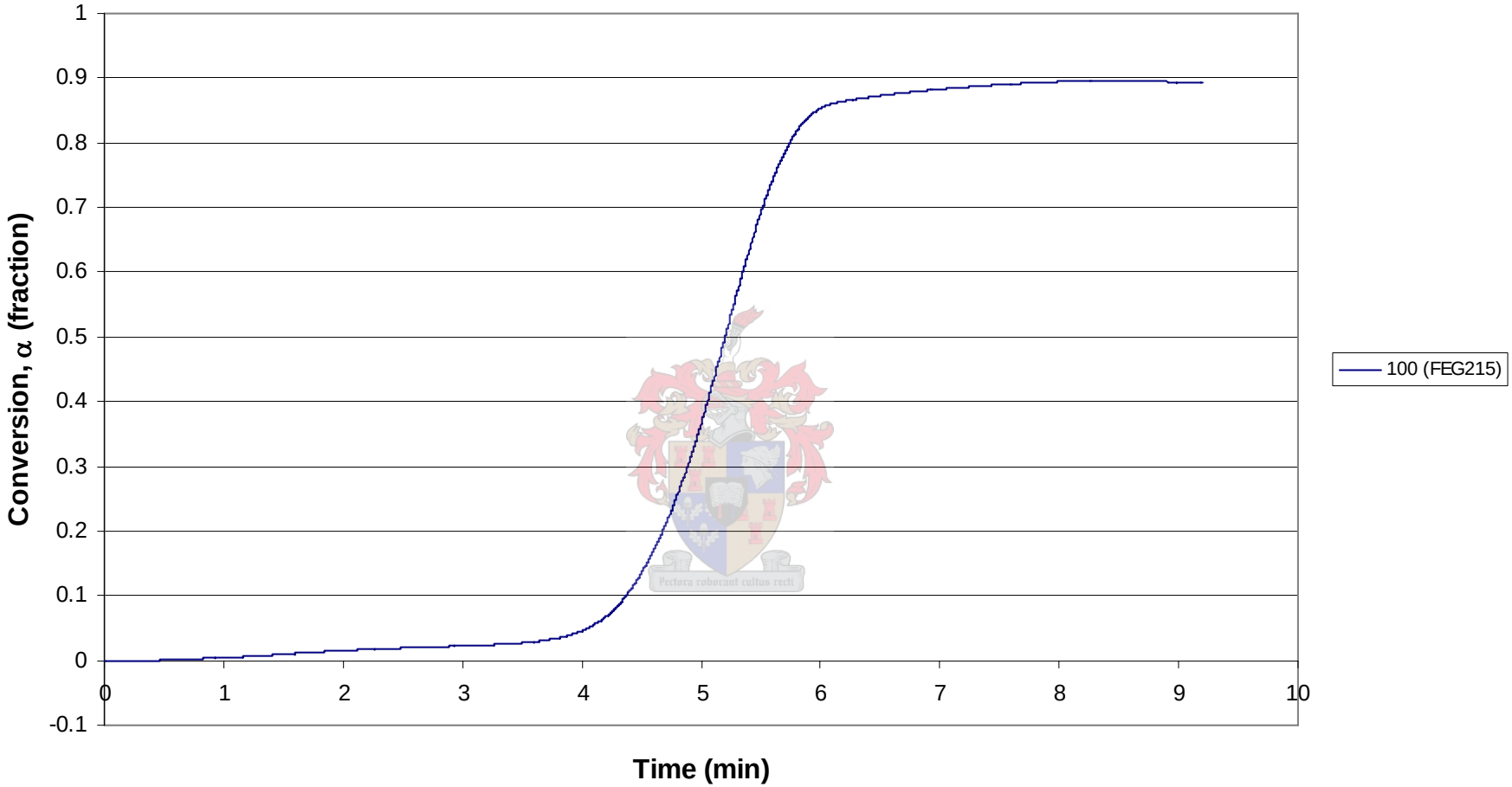

Figure A.7 Conversion versus time for a heating rate of 100 ˚C/min for Rooikrans sawdust.

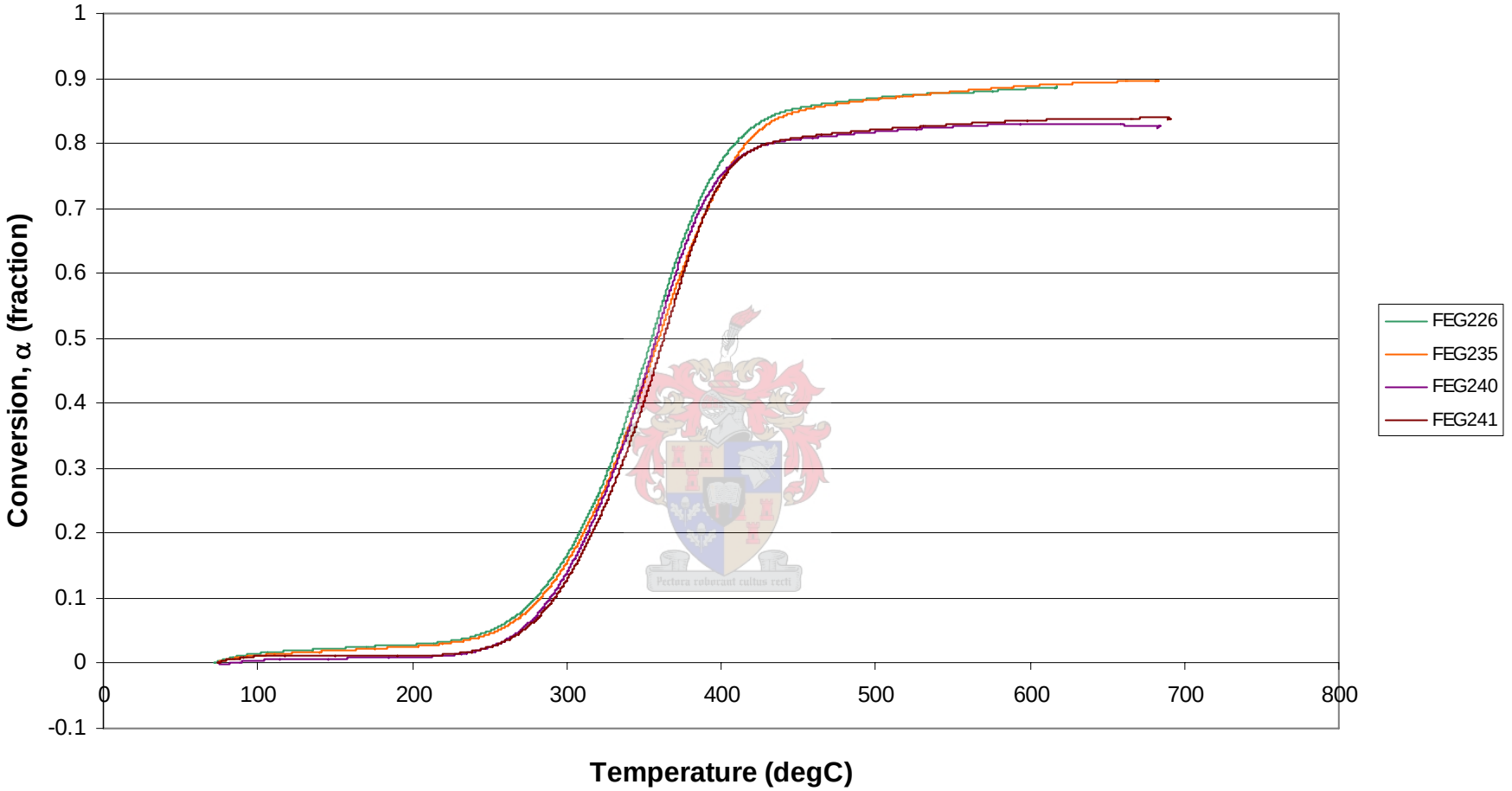

Figure A.8 Conversion versus temperature for 4 runs of 20 ˚C/min for Rooikrans sawdust.

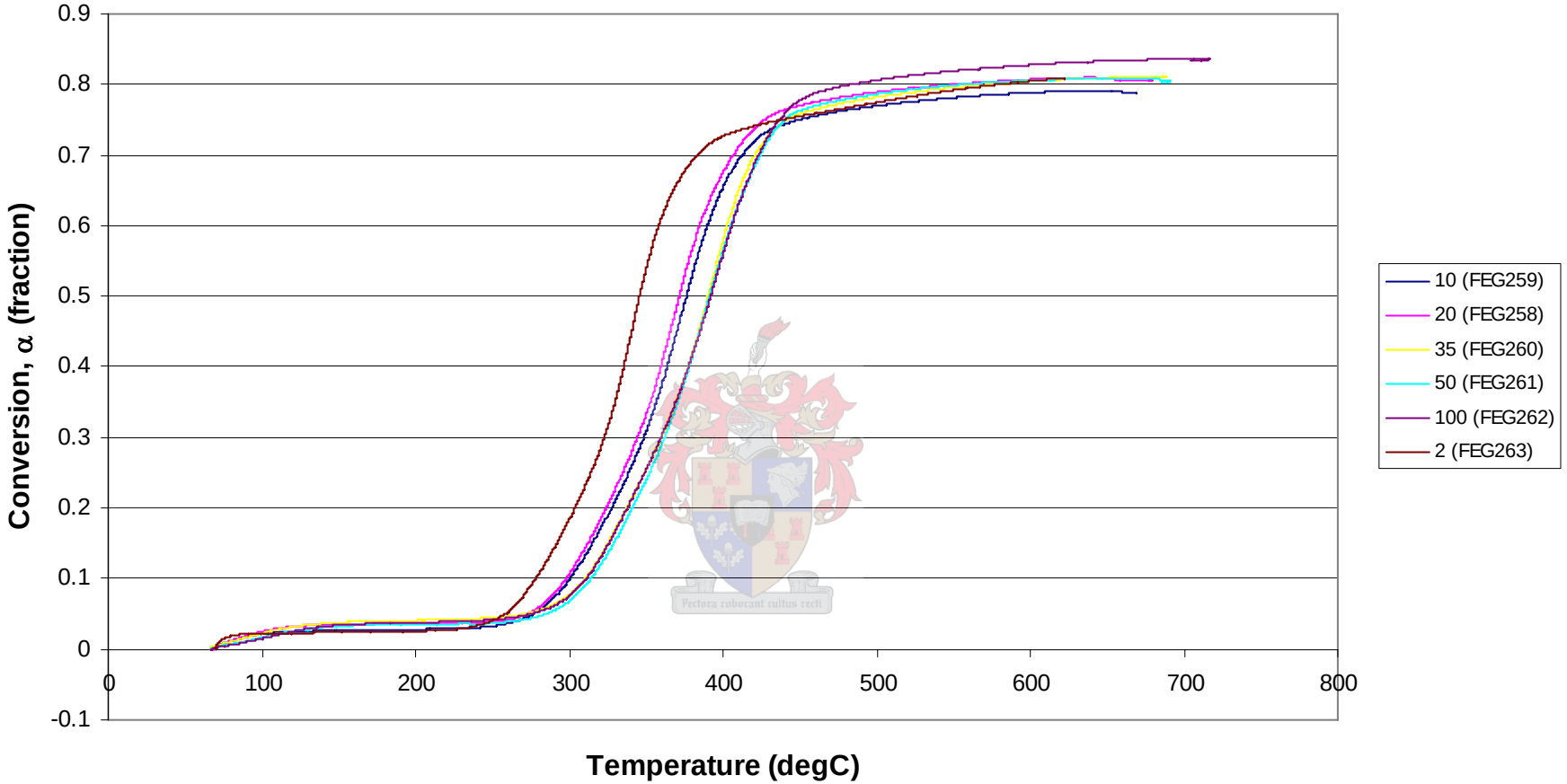

Figure A.9 Conversion versus temperature for different heating rates for the 1 – 2 mm sapwood Rooikrans blocks.

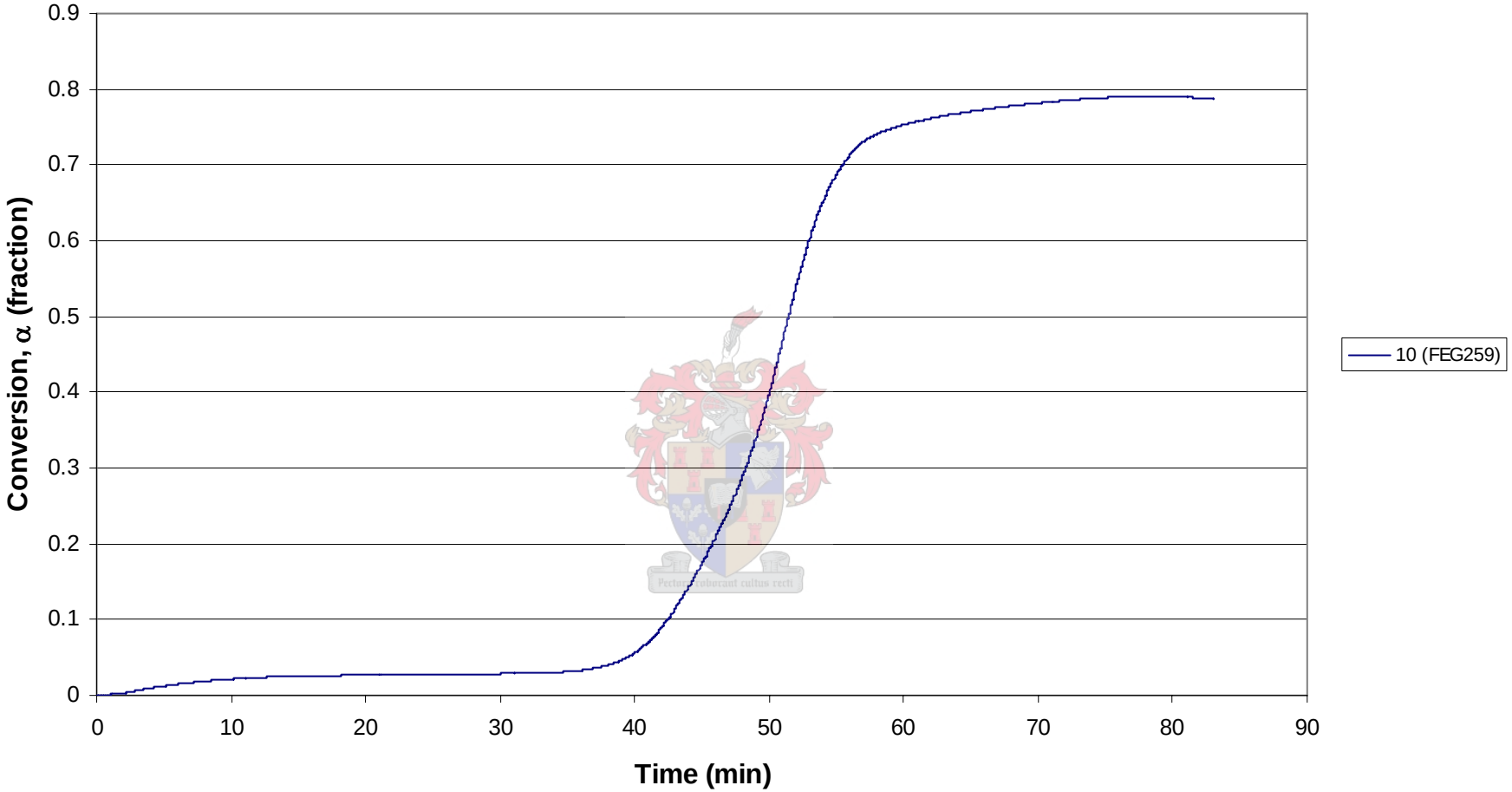

Figure A.10 Conversion versus time for a heating rate of 10 ˚C/min for the 1 – 2 mm sapwood Rooikrans blocks.

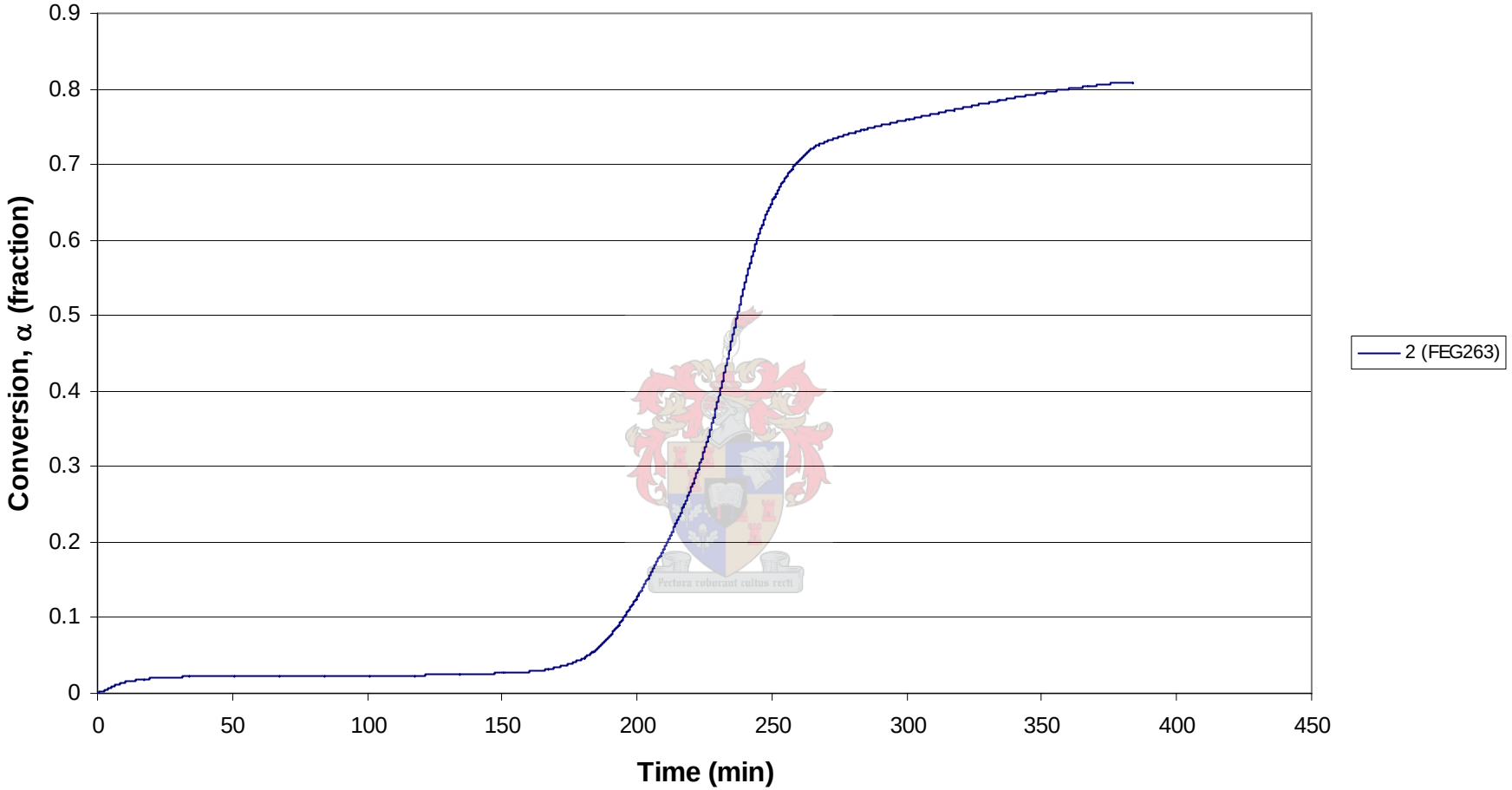

Figure A.11 Conversion versus time for a heating rate of 2 ˚C/min for the 1 – 2 mm sapwood Rooikrans blocks.

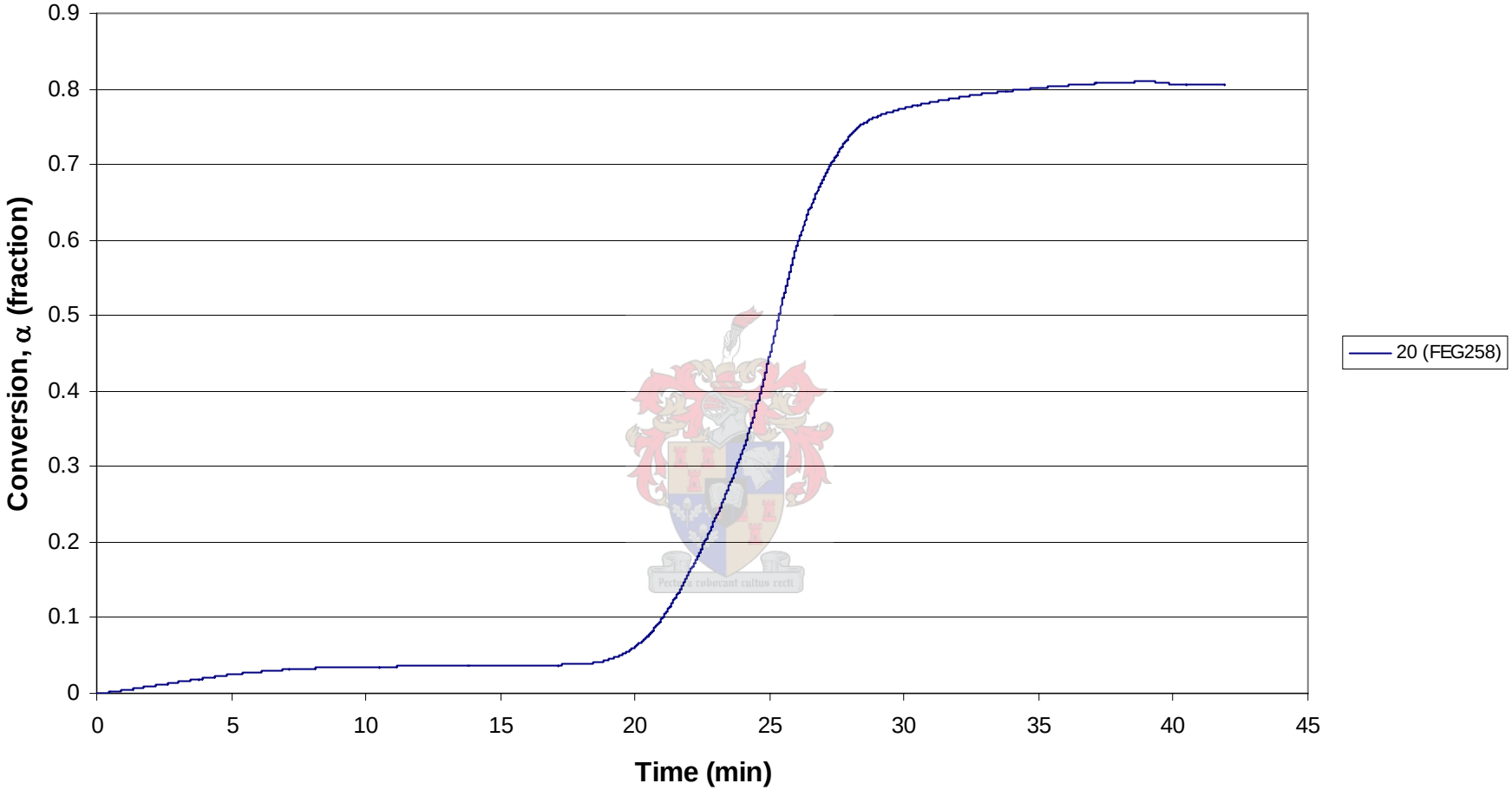

Figure A.12 Conversion versus time for a heating rate of 20 ˚C/min for the 1 – 2 mm sapwood Rooikrans blocks.

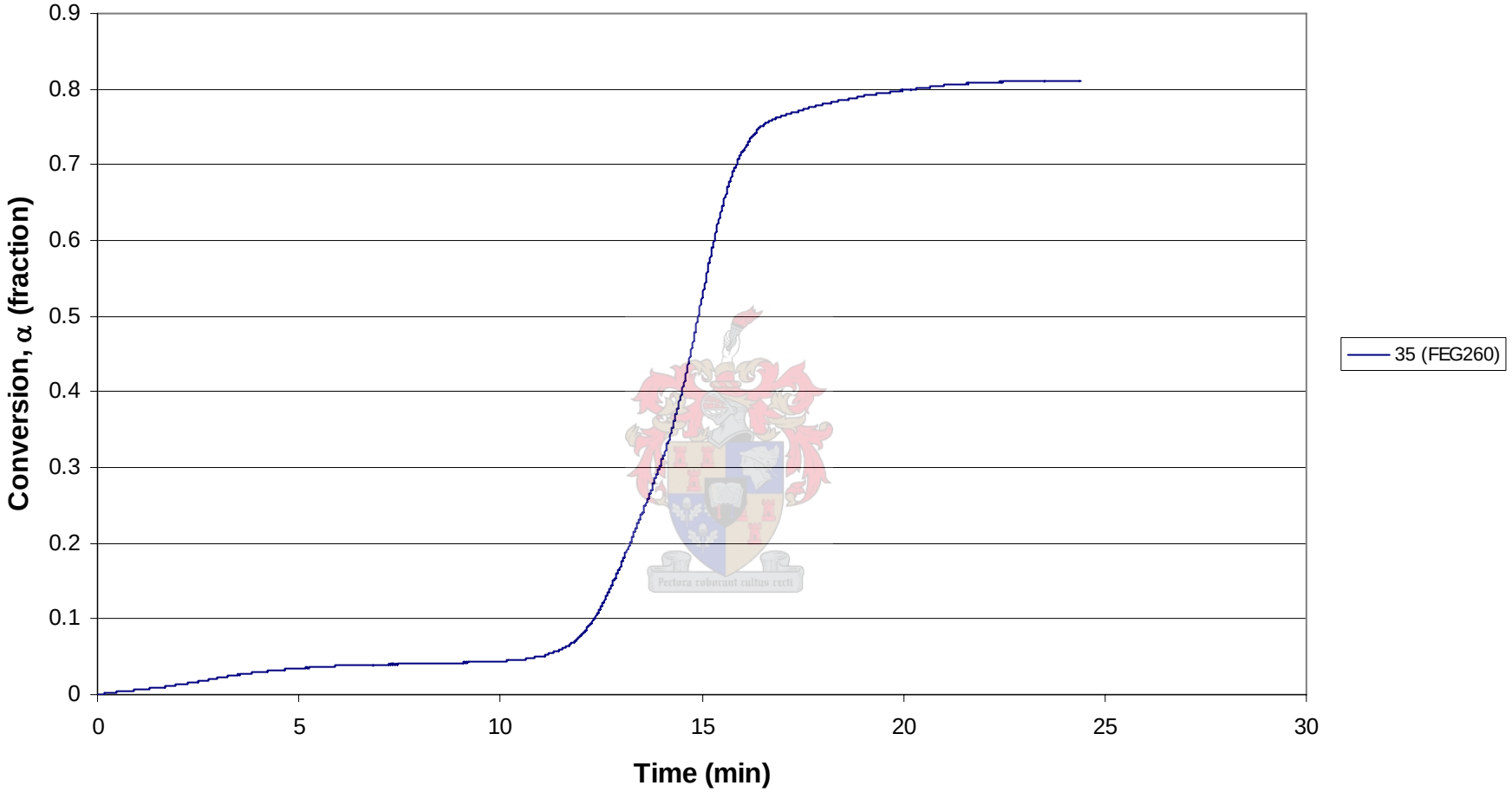

Figure A.13 Conversion versus time for a heating rate of 35 ˚C/min for the 1 – 2 mm sapwood Rooikrans blocks.

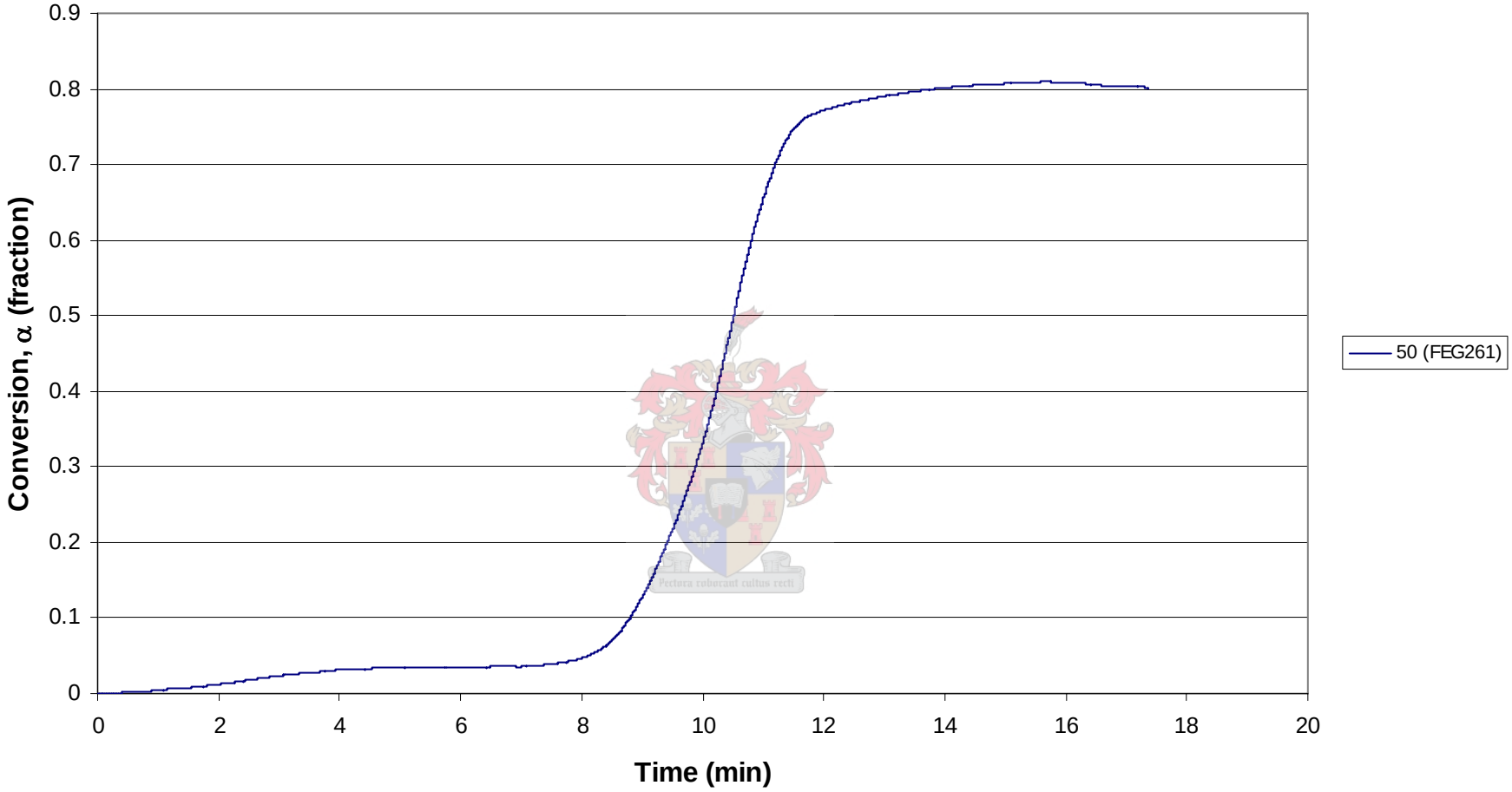

Figure A.14 Conversion versus time for a heating rate of 50 ˚C/min for the 1 – 2 mm sapwood Rooikrans blocks.

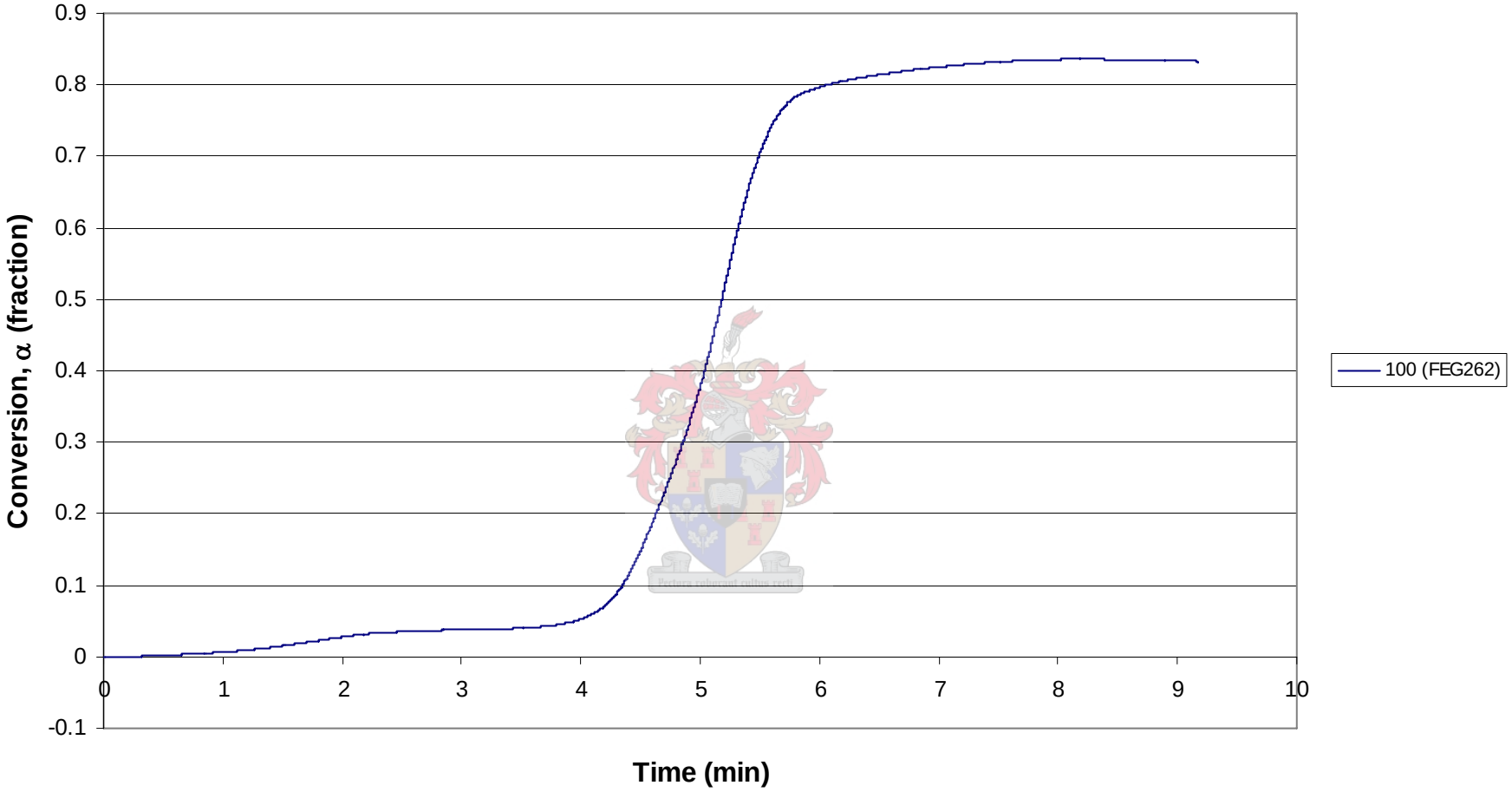

Figure A.15 Conversion versus time for a heating rate of 100 ˚C/min for the 1 – 2 mm sapwood Rooikrans blocks.

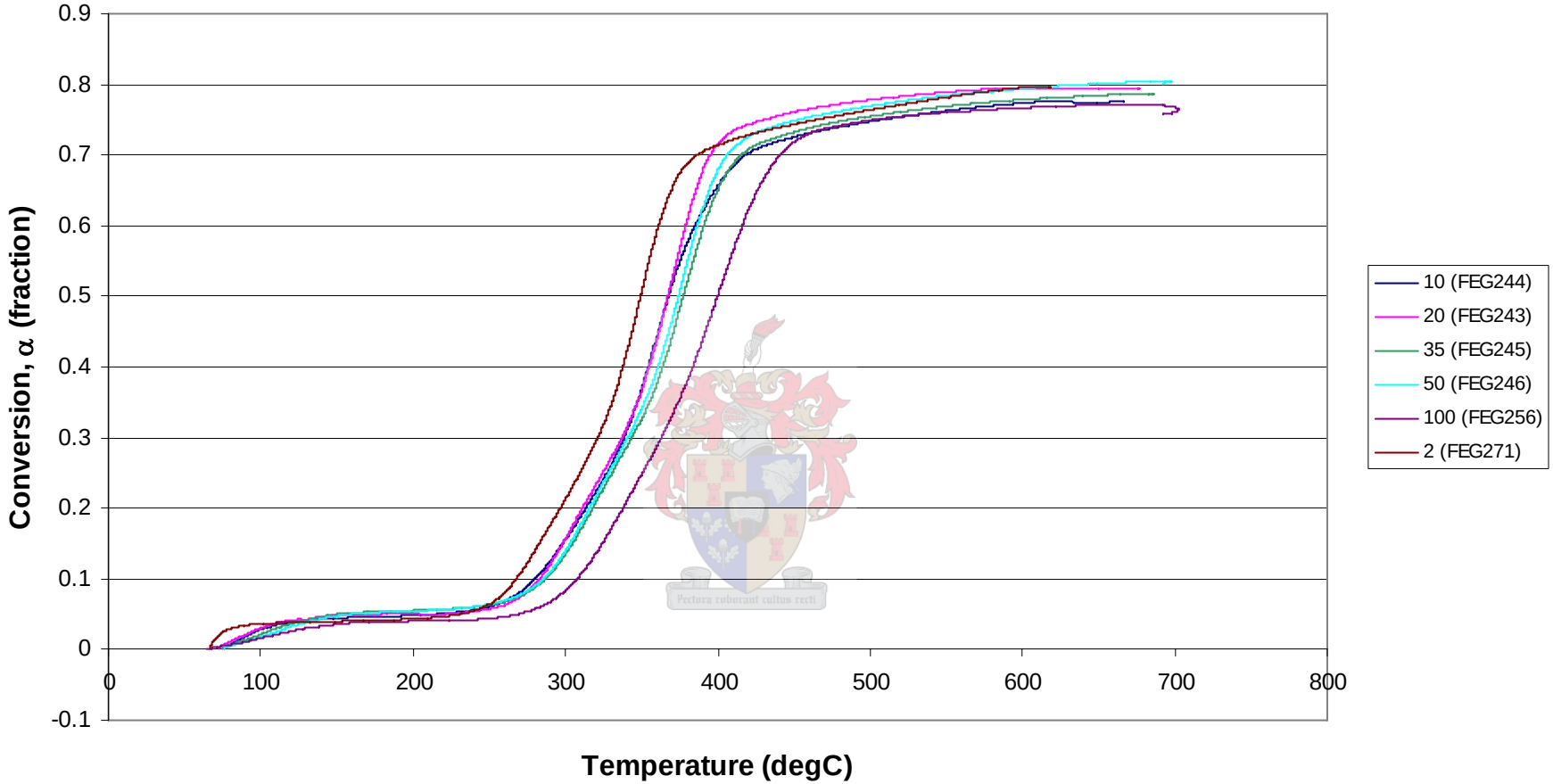

Figure A.16 Conversion versus temperature for different heating rates for the 1 – 2 mm heartwood Rooikrans blocks.

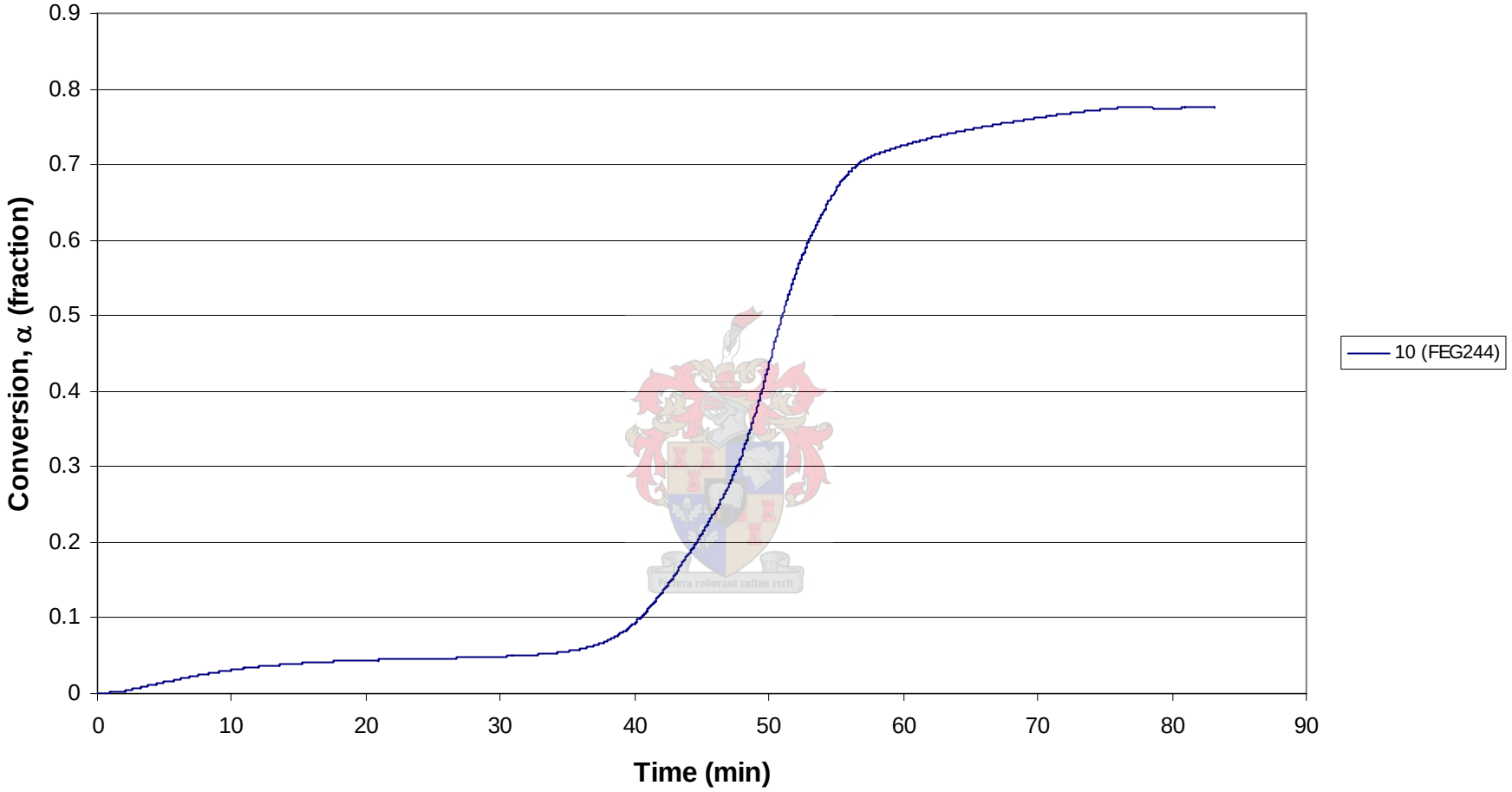

Figure A.17 Conversion versus time for a heating rate of 10 ˚C/min for the 1 – 2 mm heartwood Rooikrans blocks.

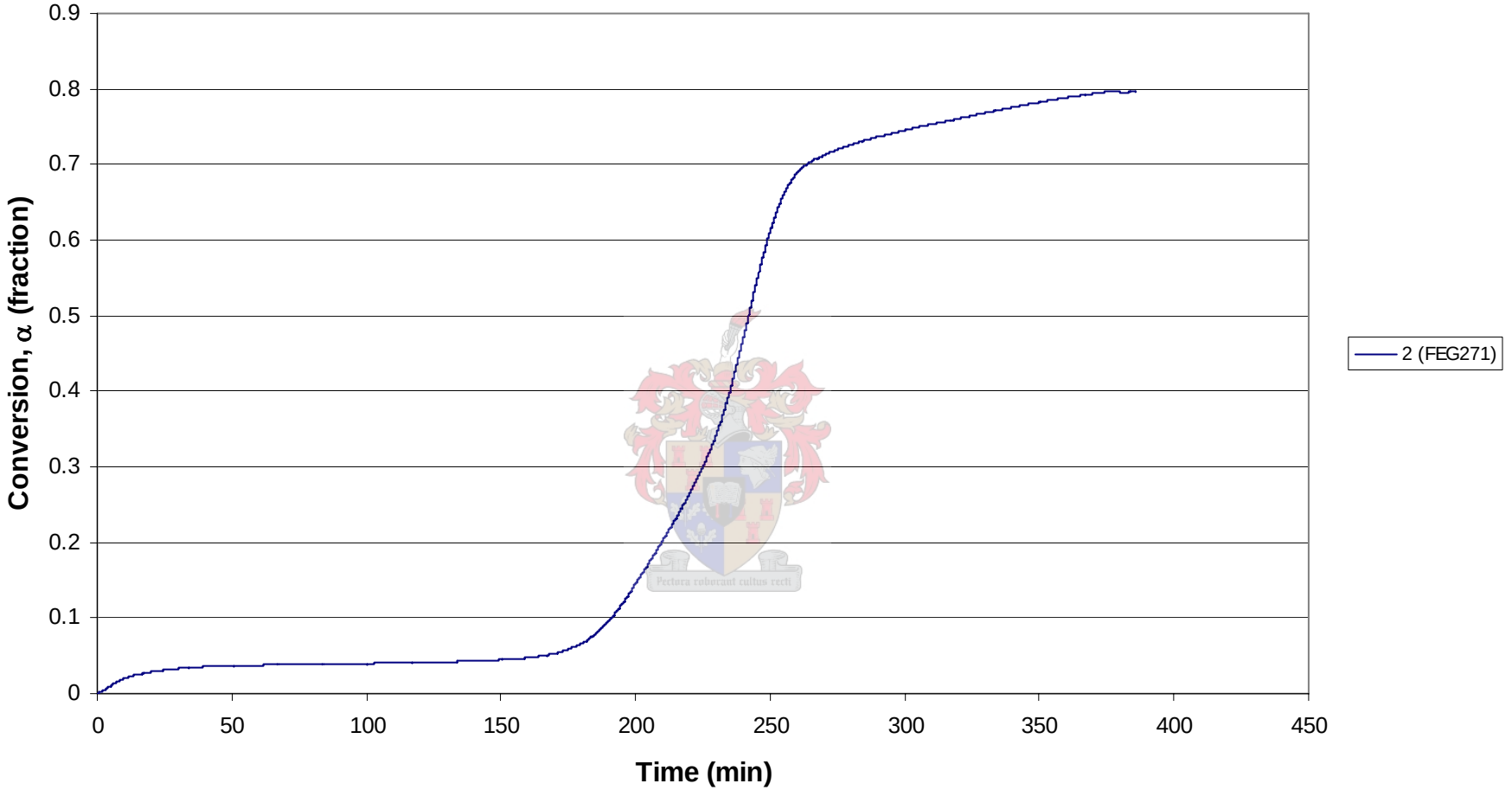

Figure A.18 Conversion versus time for a heating rate of 2 ˚C/min for the 1 – 2 mm heartwood Rooikrans blocks.

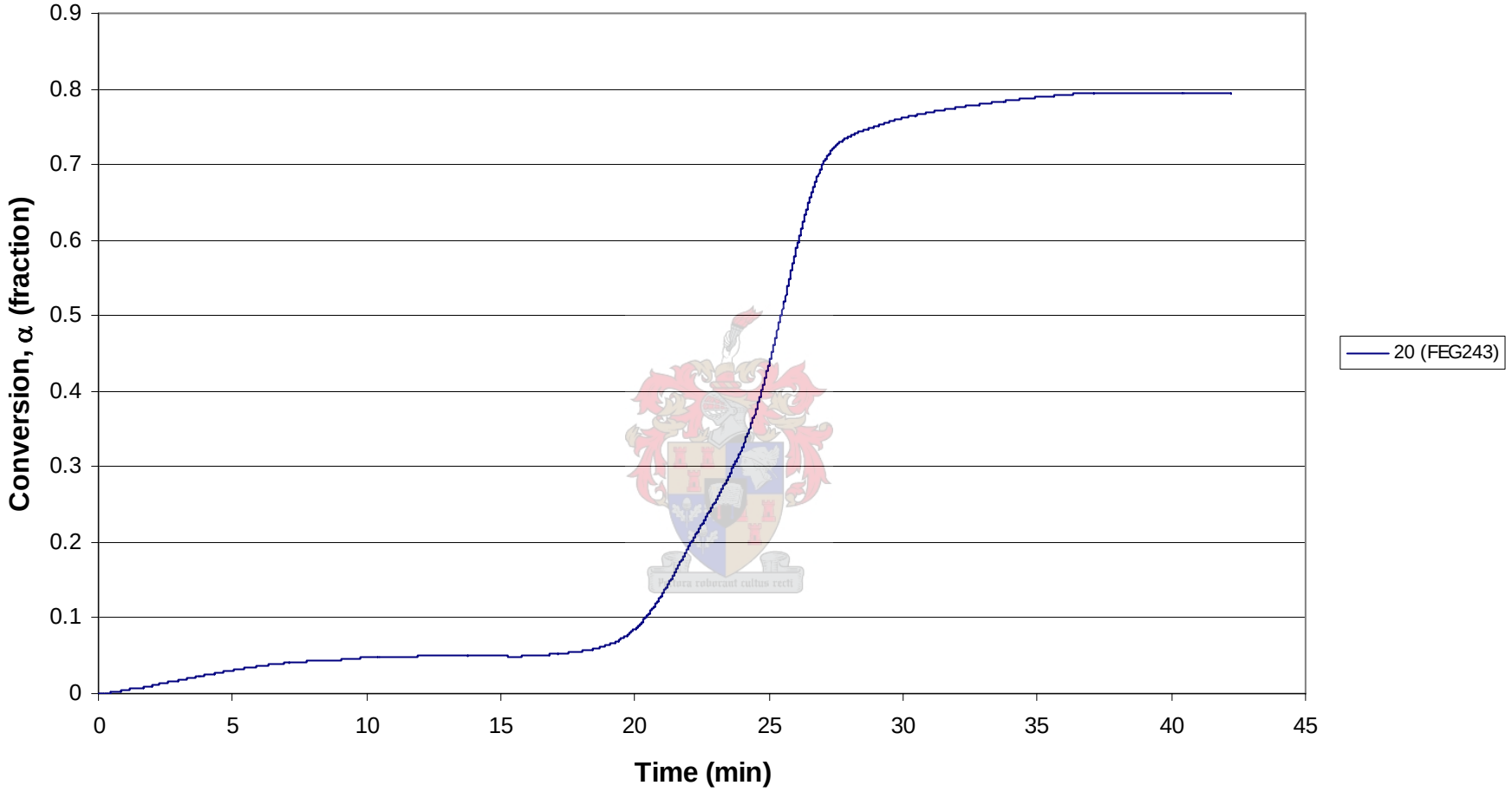

Figure A.19 Conversion versus time for a heating rate of 20 ˚C/min for the 1 – 2 mm heartwood Rooikrans blocks.

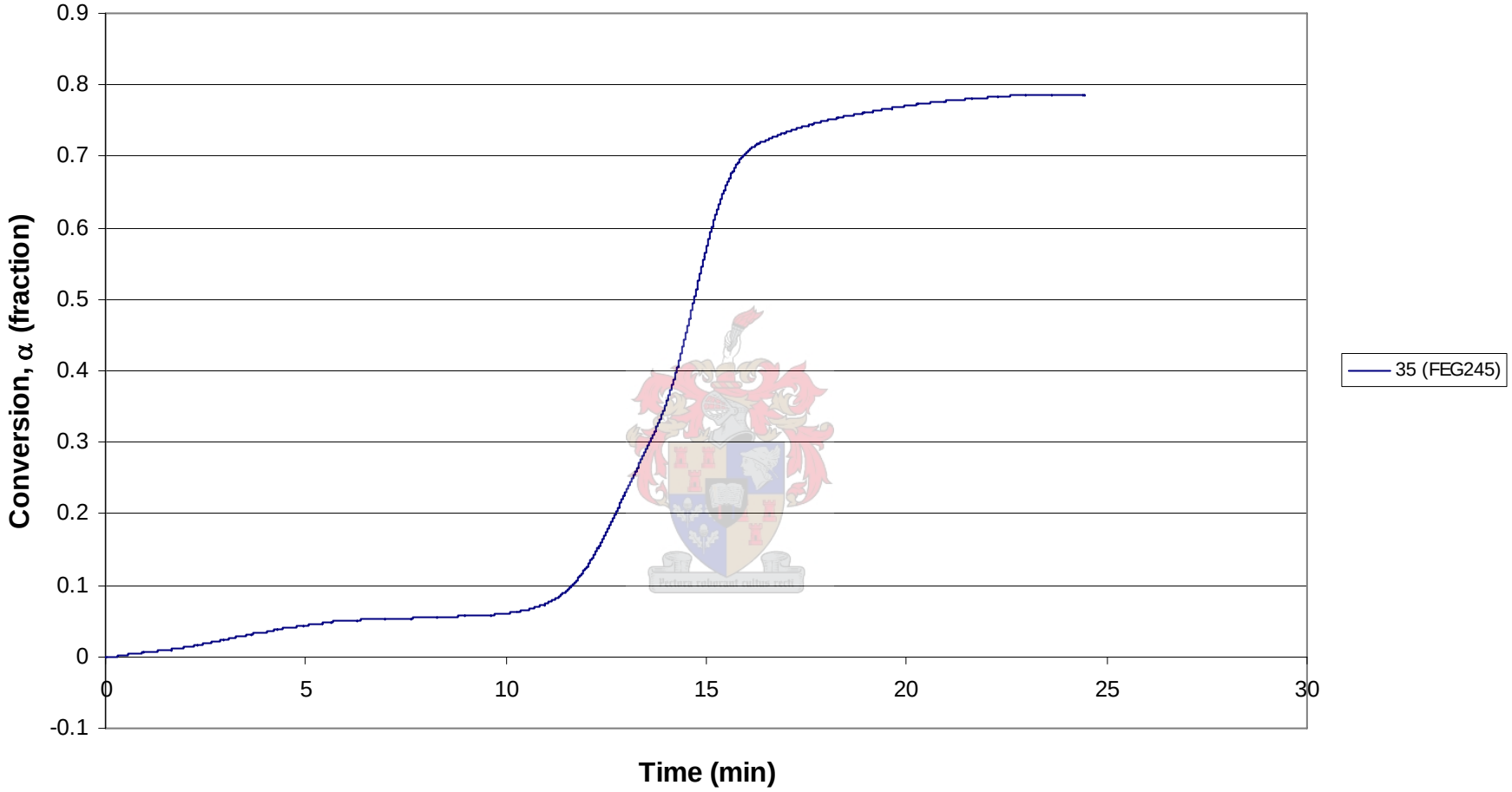

Figure A.20 Conversion versus time for a heating rate of 35 ˚C/min for the 1 – 2 mm heartwood Rooikrans blocks.

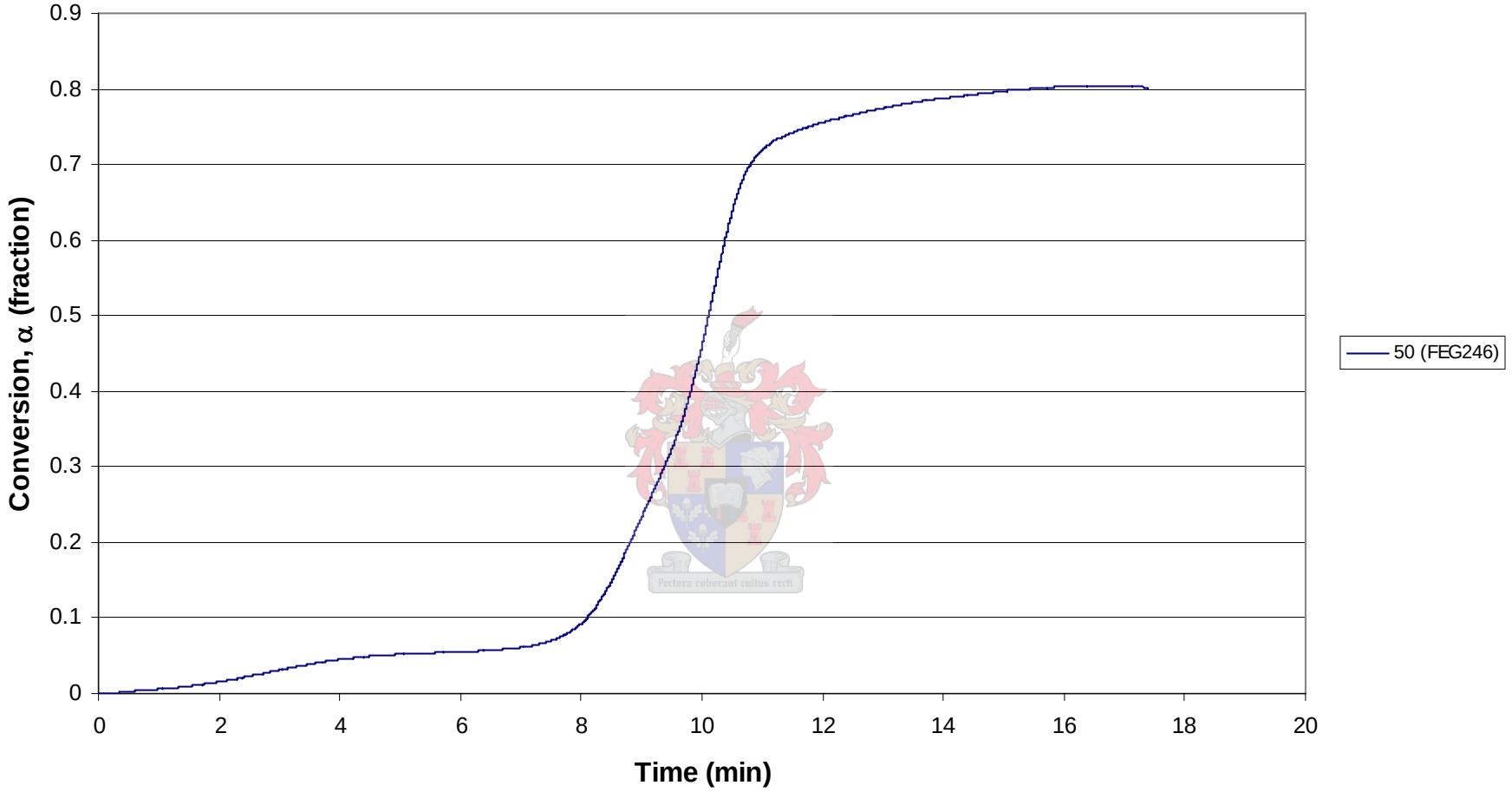

Figure A.21 Conversion versus time for a heating rate of 50 ˚C/min for the 1 – 2 mm heartwood Rooikrans blocks.

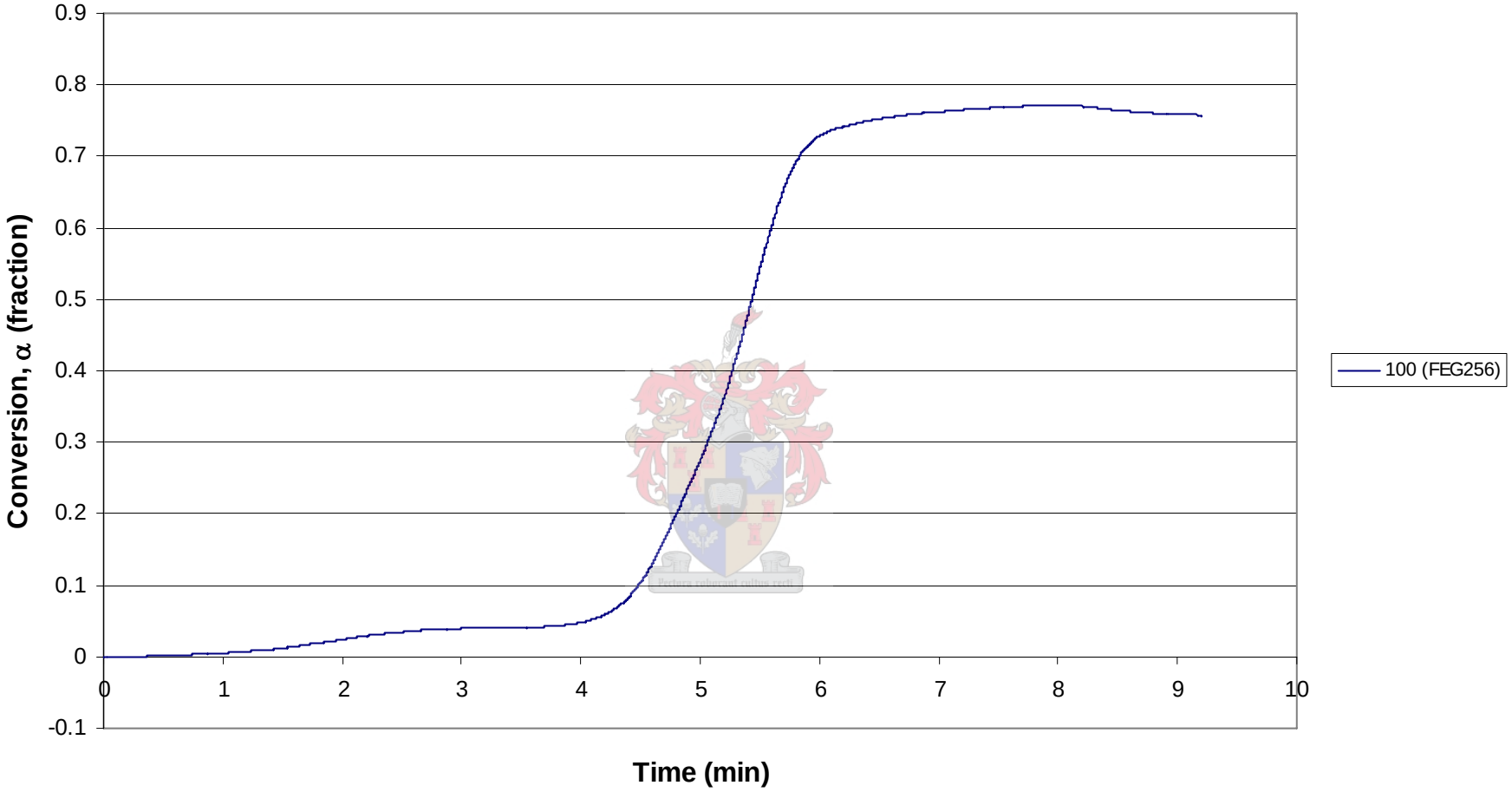

Figure A.22 Conversion versus time for a heating rate of 100 ˚C/min for the 1 – 2 mm heartwood Rooikrans blocks.

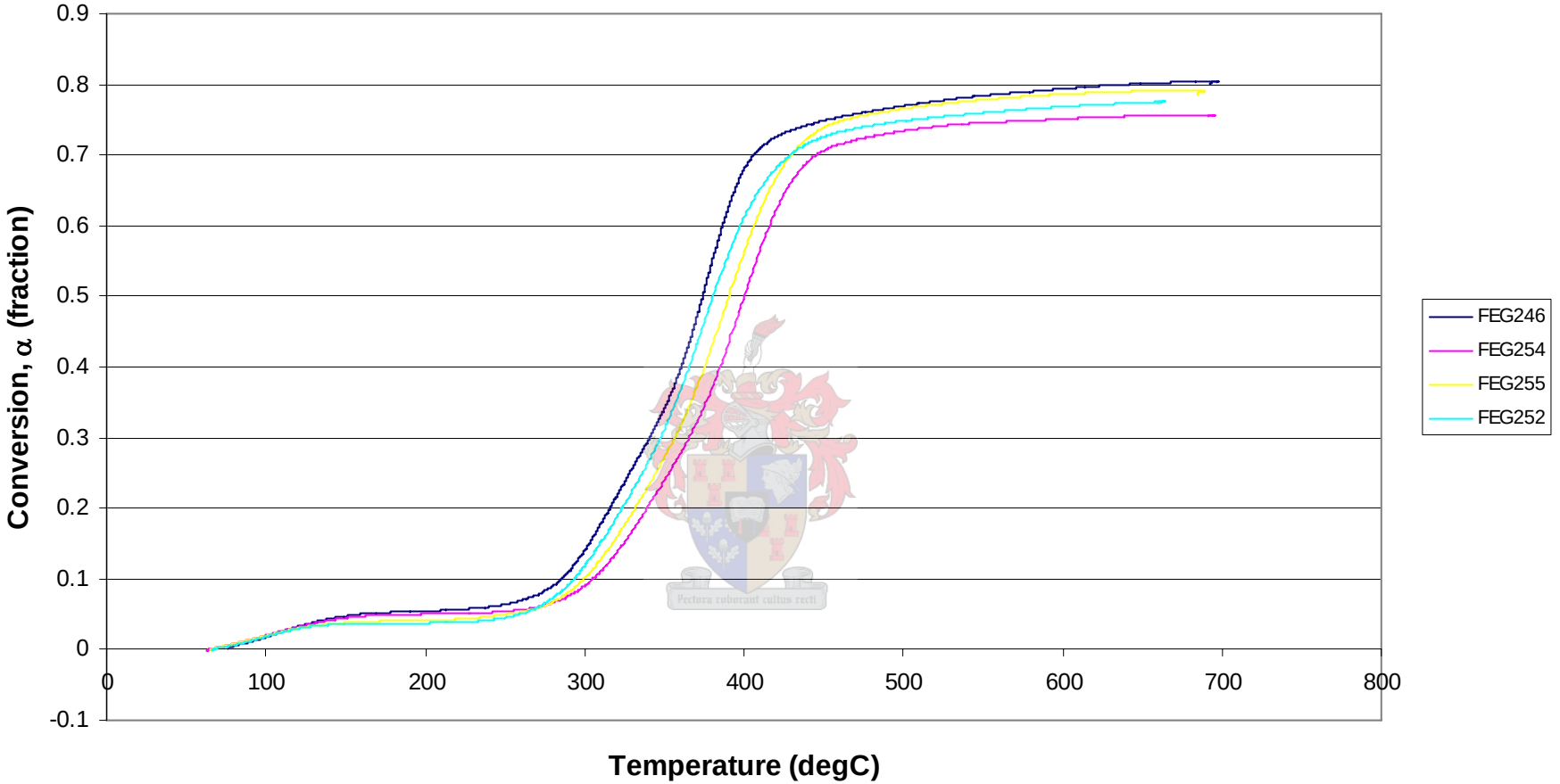

Figure A.23 Conversion versus temperature for 4 runs of 50 ˚C/min for 1 – 2 mm heartwood Rooikrans blocks.

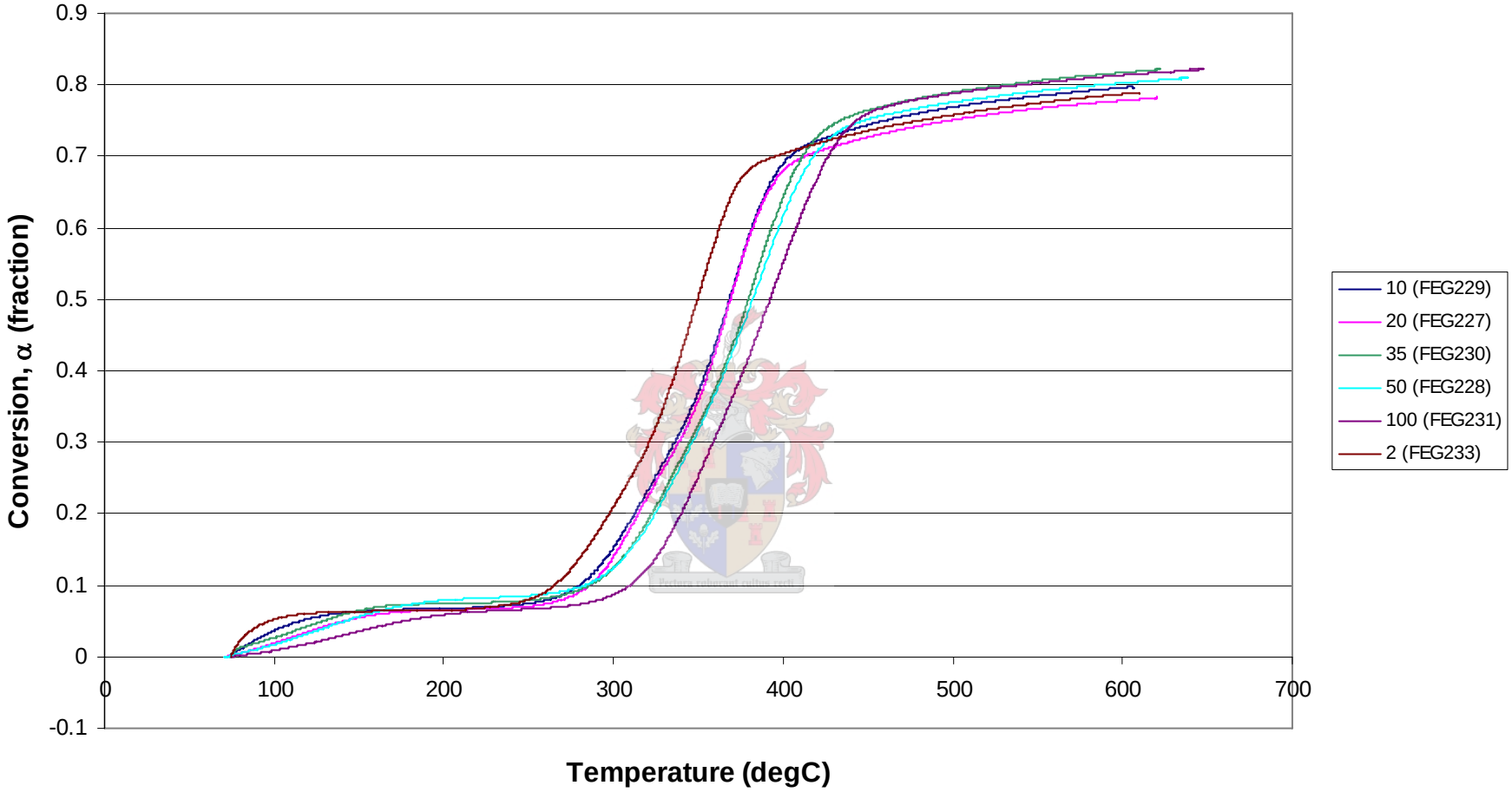

Figure A.24 Conversion versus temperature for different heating rates for the 2 – 4 mm sapwood Rooikrans blocks.

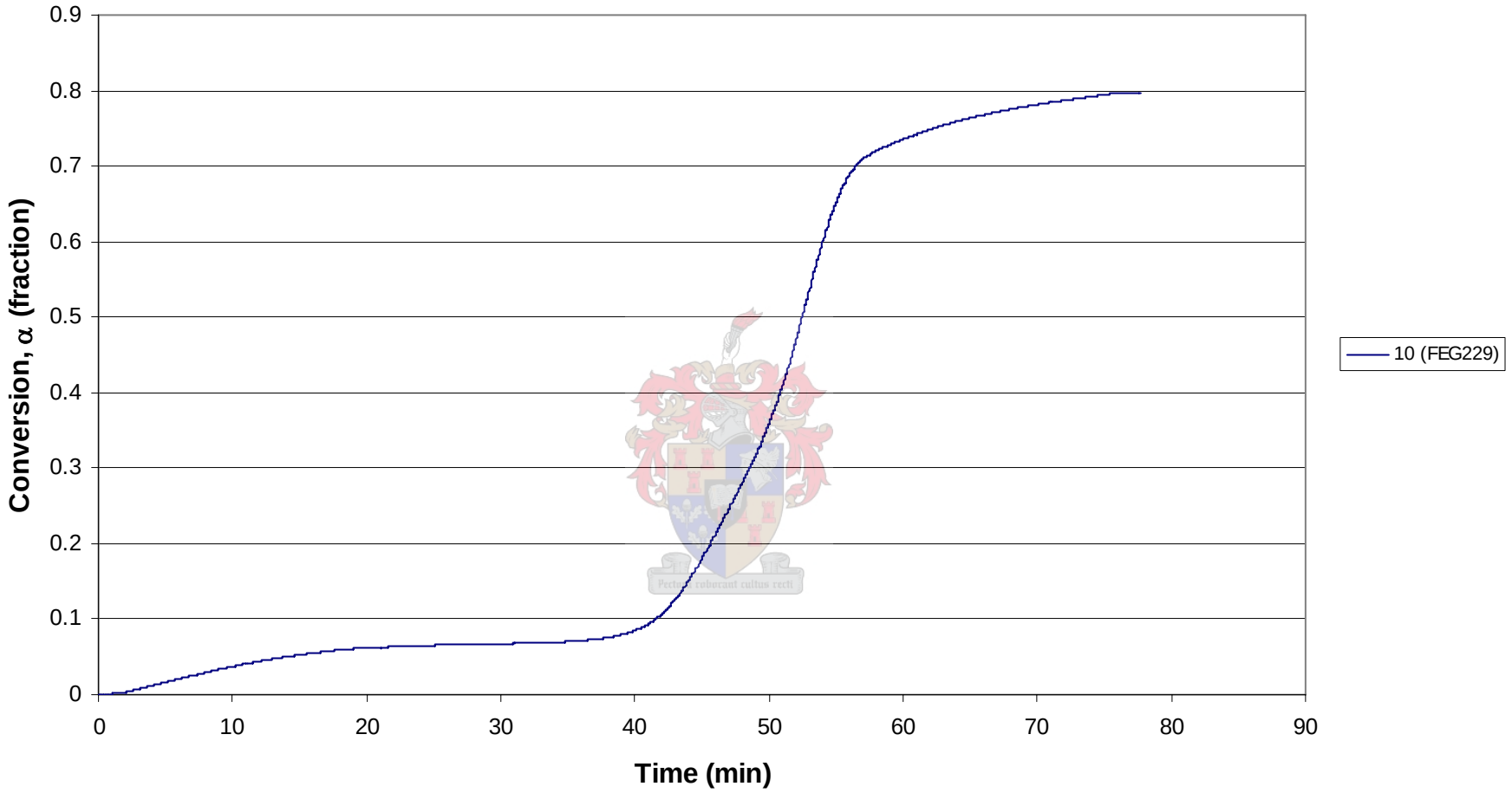

Figure A.25 Conversion versus time for a heating rate of 10 ˚C/min for the 2 – 4 mm sapwood Rooikrans blocks.

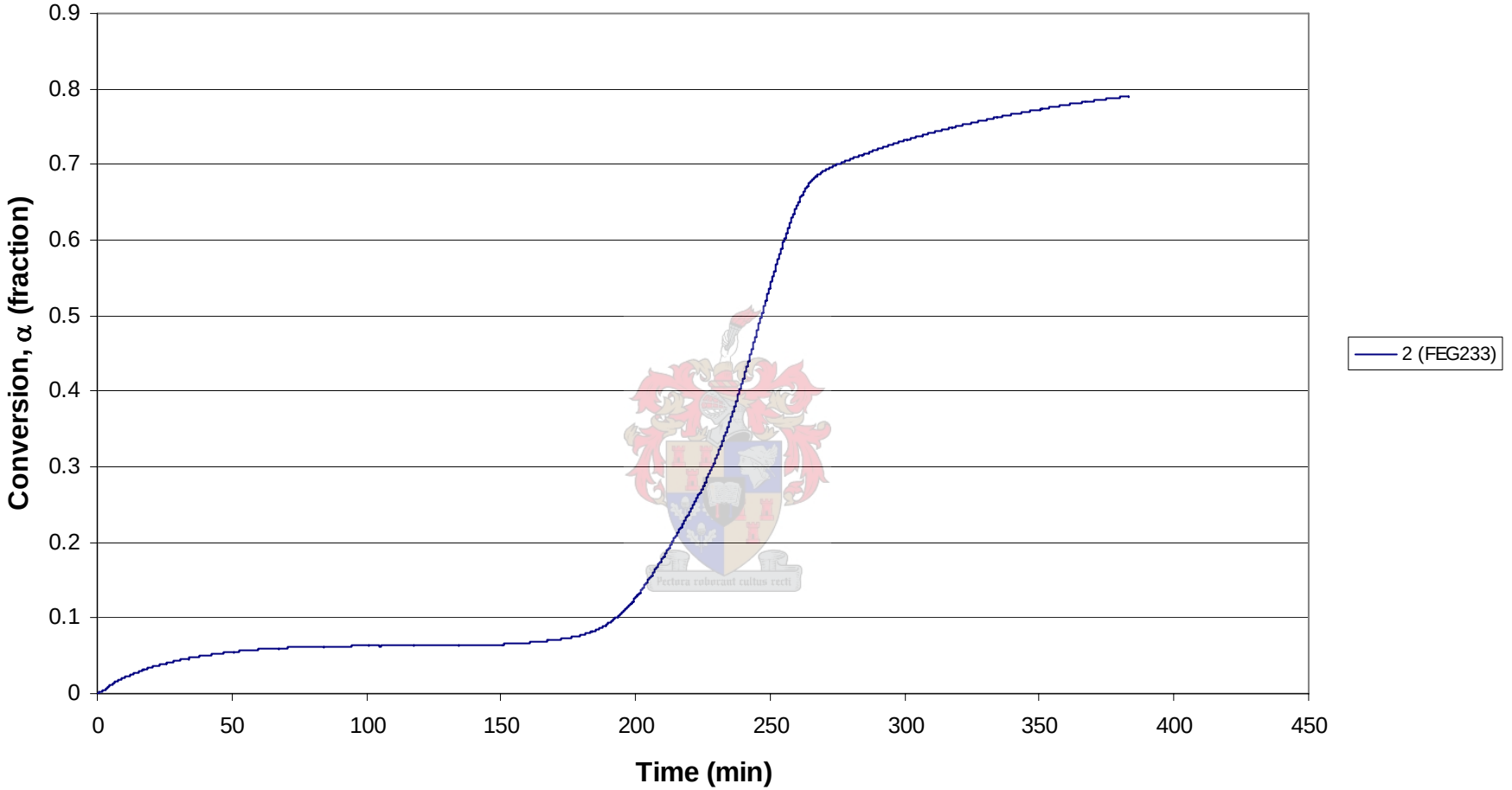

Figure A.26 Conversion versus time for a heating rate of 2 ˚C/min for the 2 – 4 mm sapwood Rooikrans blocks.

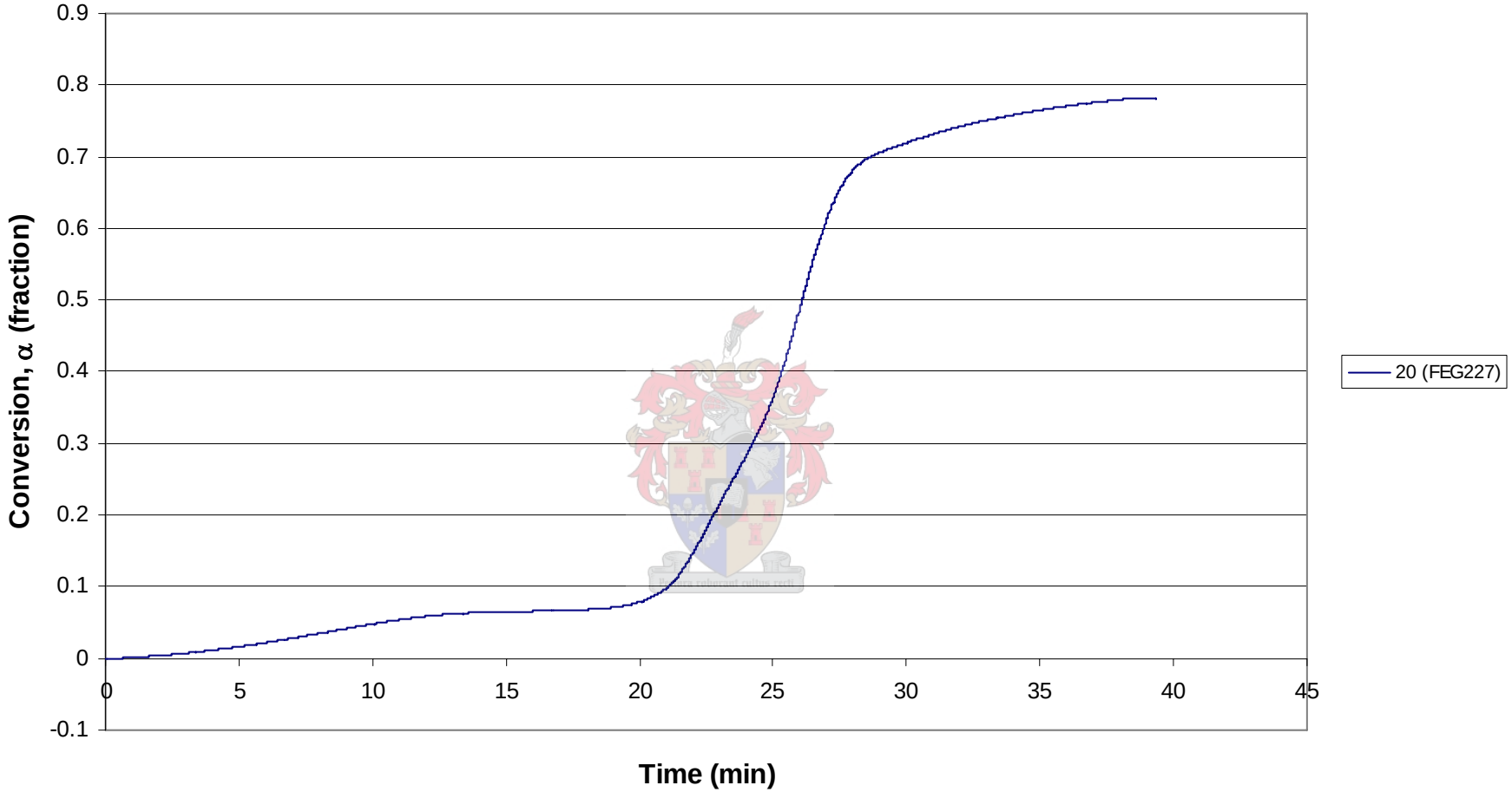

Figure A.27 Conversion versus time for a heating rate of 20 ˚C/min for the 2 – 4 mm sapwood Rooikrans blocks.

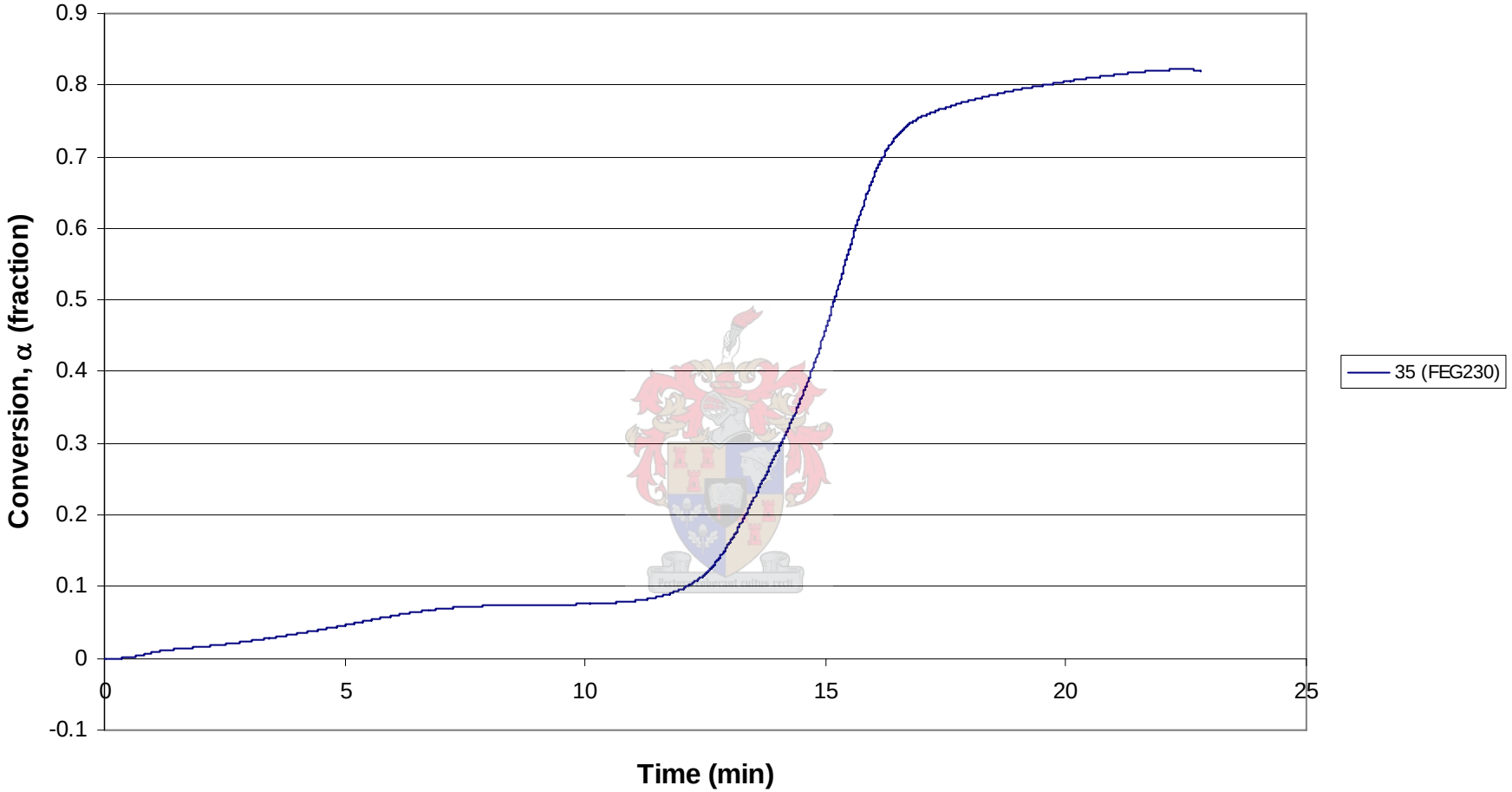

Figure A.28 Conversion versus time for a heating rate of 35 ˚C/min for the 2 – 4 mm sapwood Rooikrans blocks.

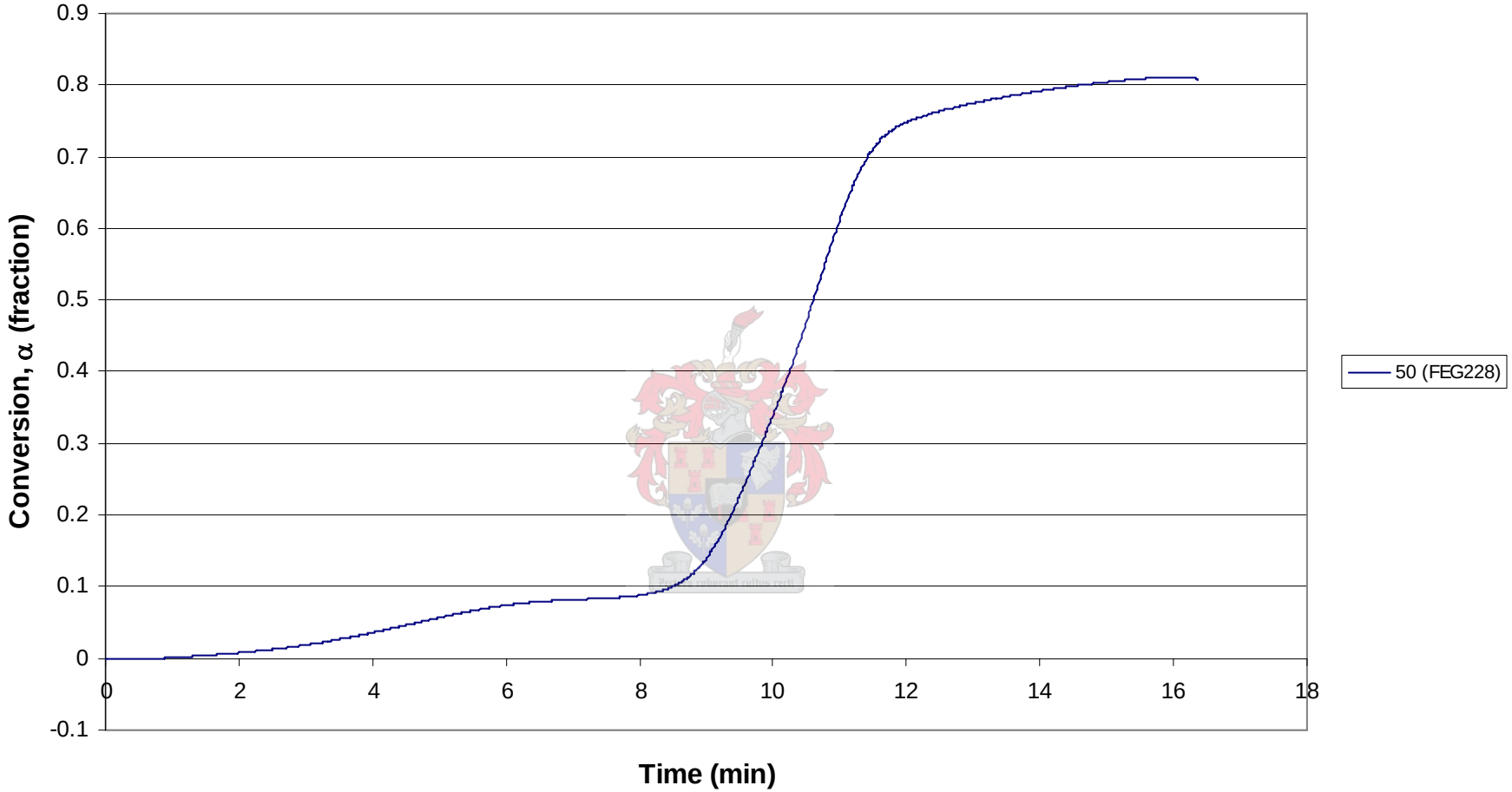

Figure A.29 Conversion versus time for a heating rate of 50 ˚C/min for the 2 – 4 mm sapwood Rooikrans blocks.

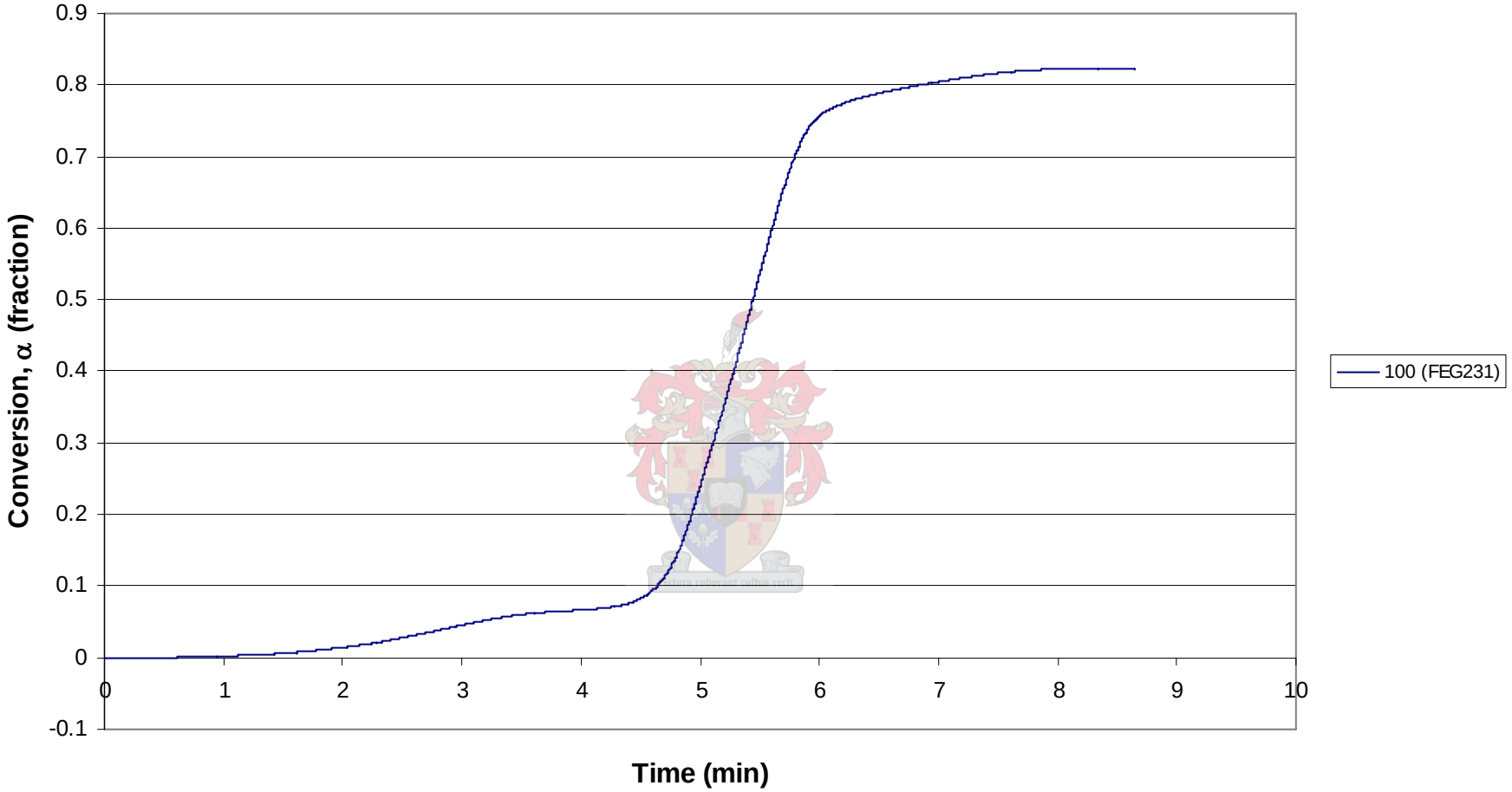

Figure A.30 Conversion versus time for a heating rate of 100 ˚C/min for the 2 – 4 mm sapwood Rooikrans blocks.

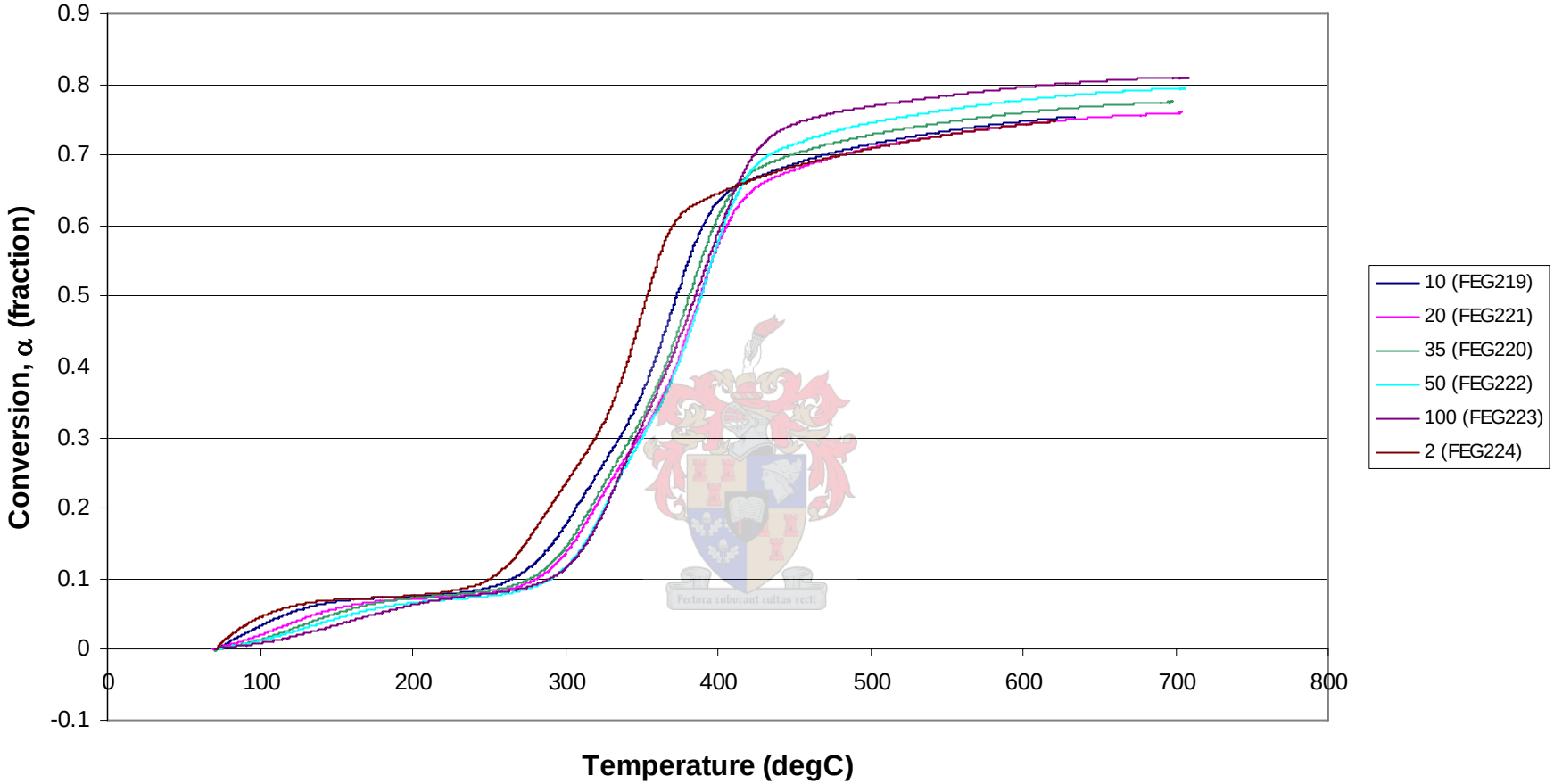

Figure A.31 Conversion versus temperature for different heating rates for the 2 – 4 mm heartwood Rooikrans blocks.

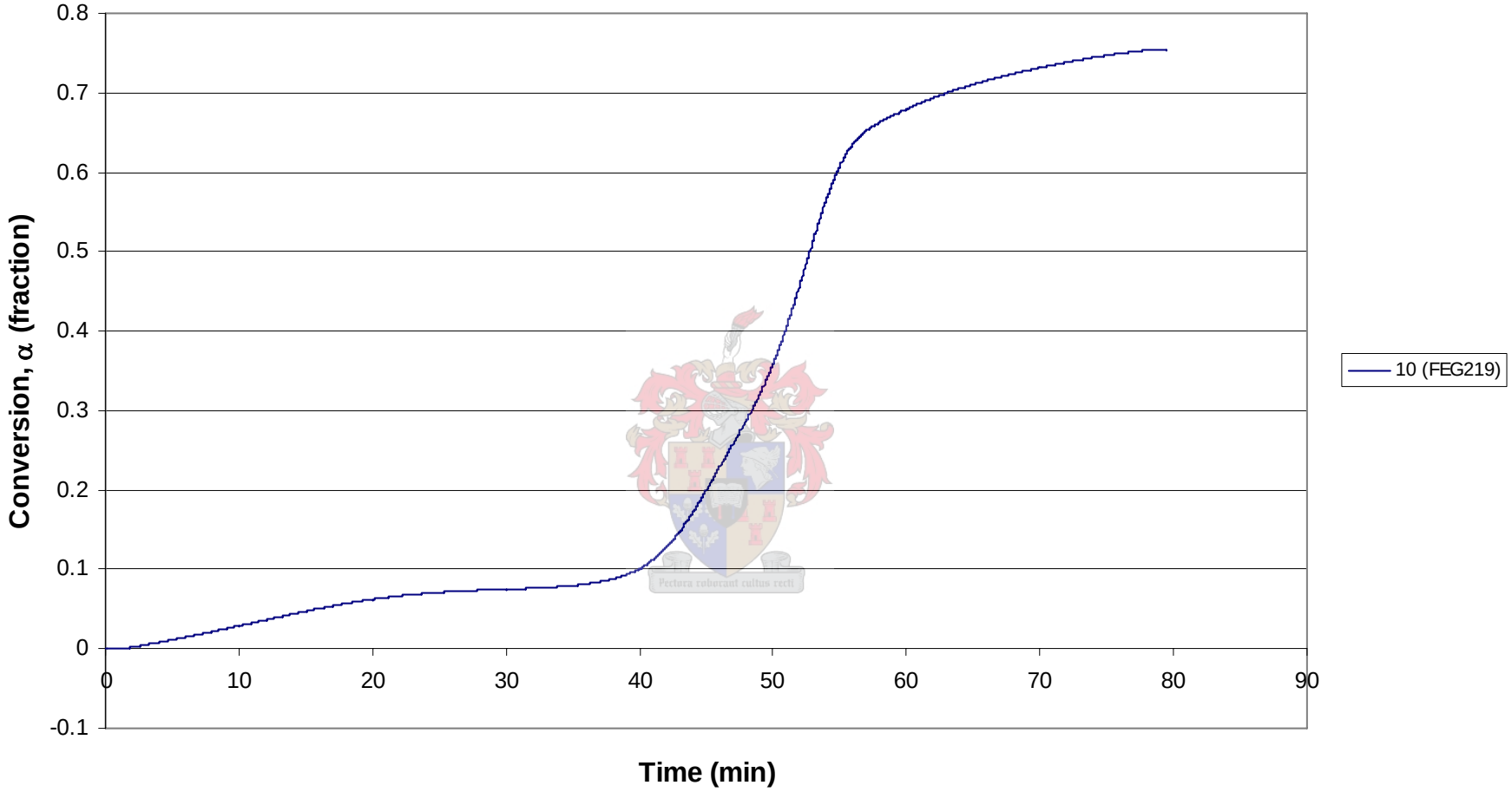

Figure A.32 Conversion versus time for a heating rate of 10 ˚C/min for the 2 – 4 mm heartwood Rooikrans blocks.

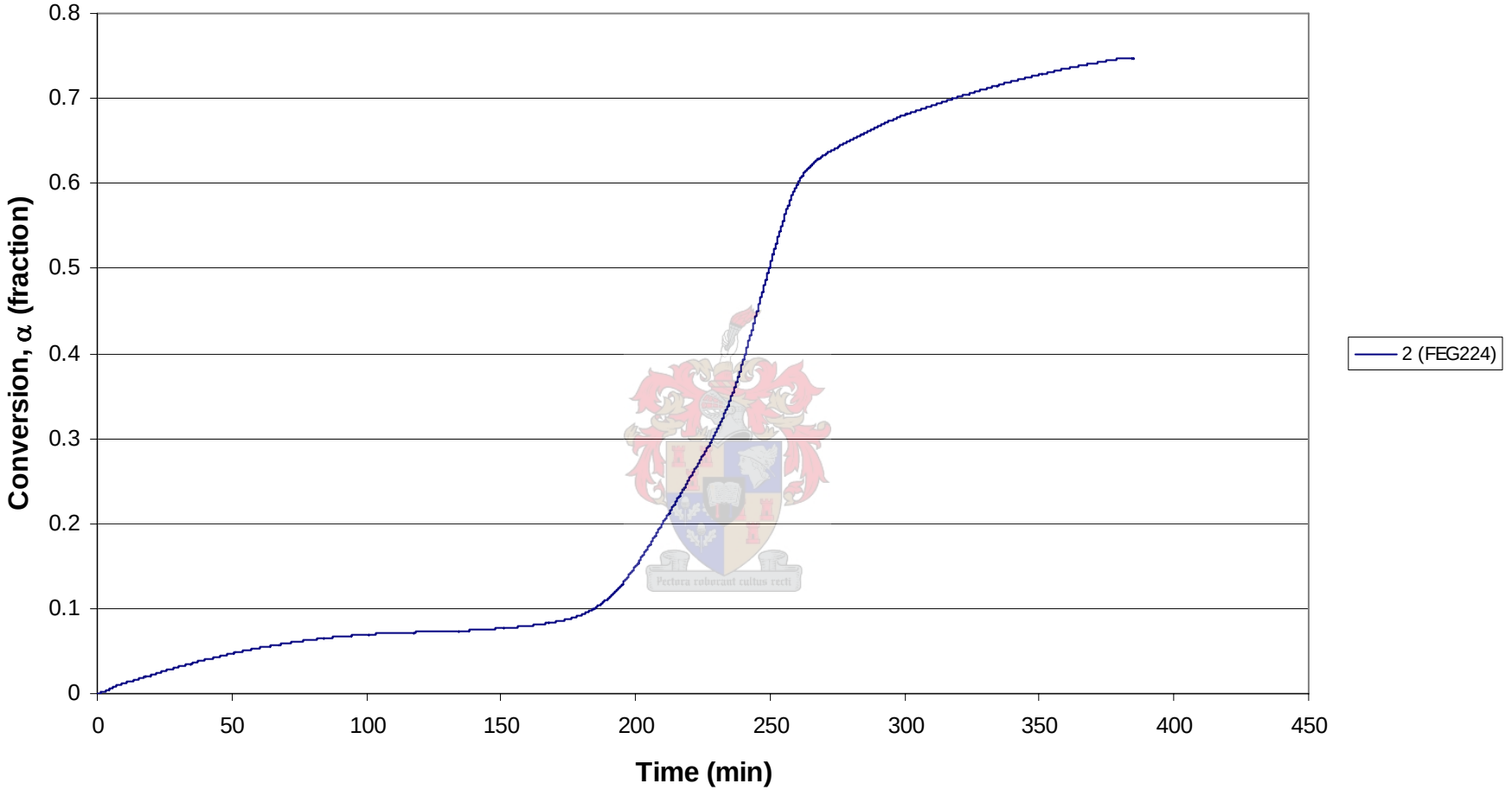

Figure A.33 Conversion versus time for a heating rate of 2 ˚C/min for the 2 – 4 mm heartwood Rooikrans blocks.

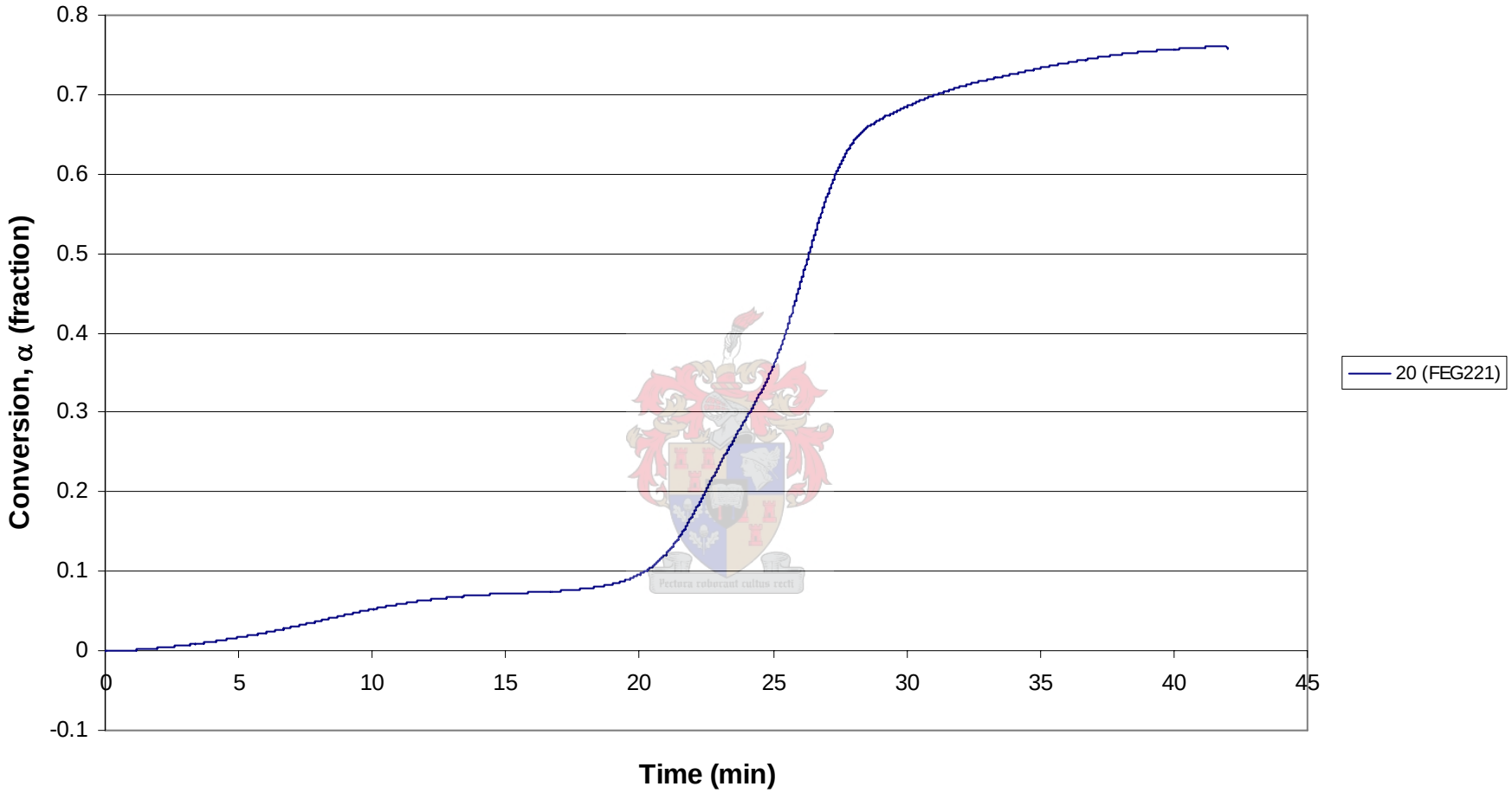

Figure A.34 Conversion versus time for a heating rate of 20 ˚C/min for the 2 – 4 mm heartwood Rooikrans blocks.

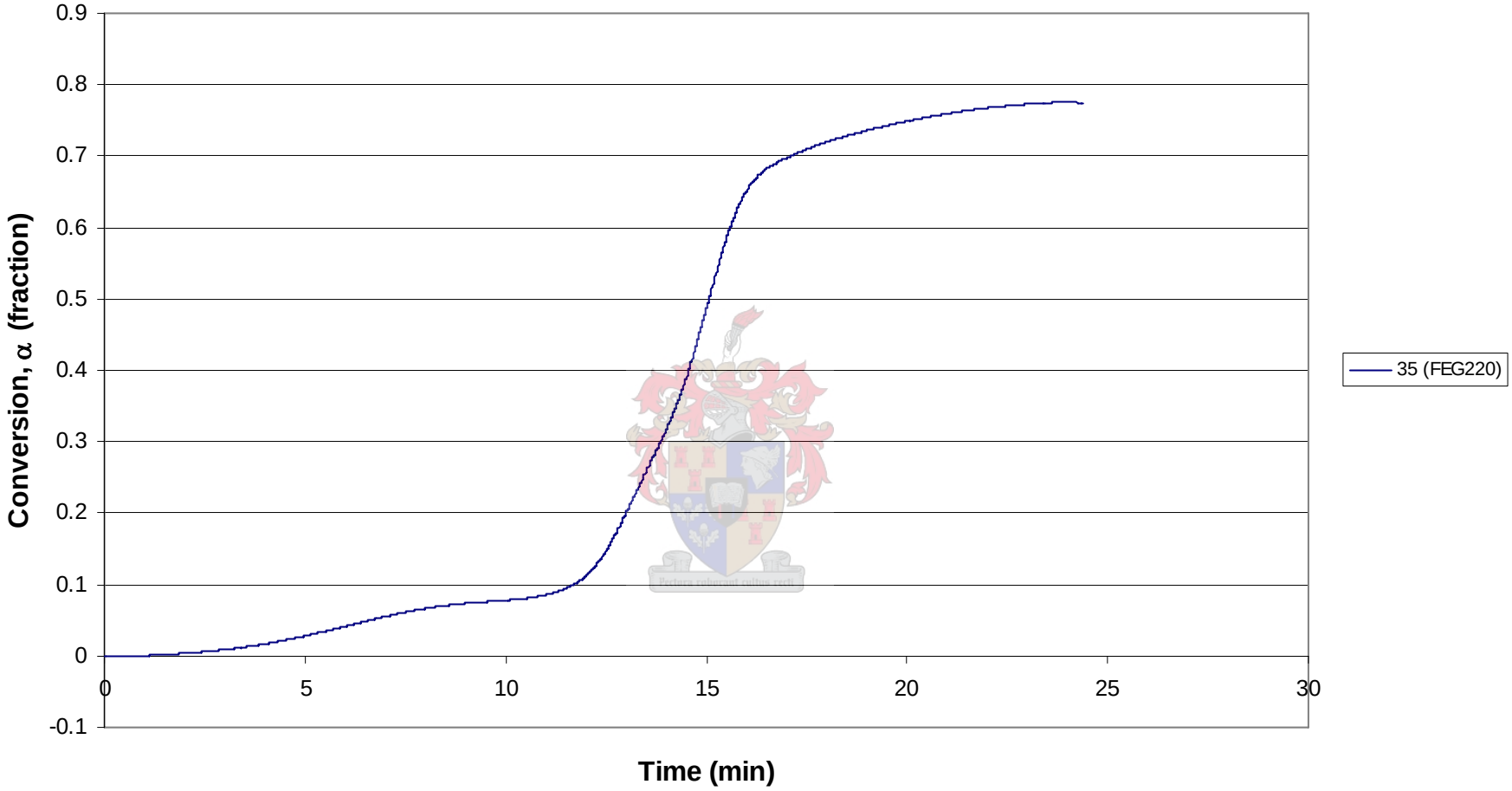

Figure A.35 Conversion versus time for a heating rate of 35 ˚C/min for the 2 – 4 mm heartwood Rooikrans blocks.

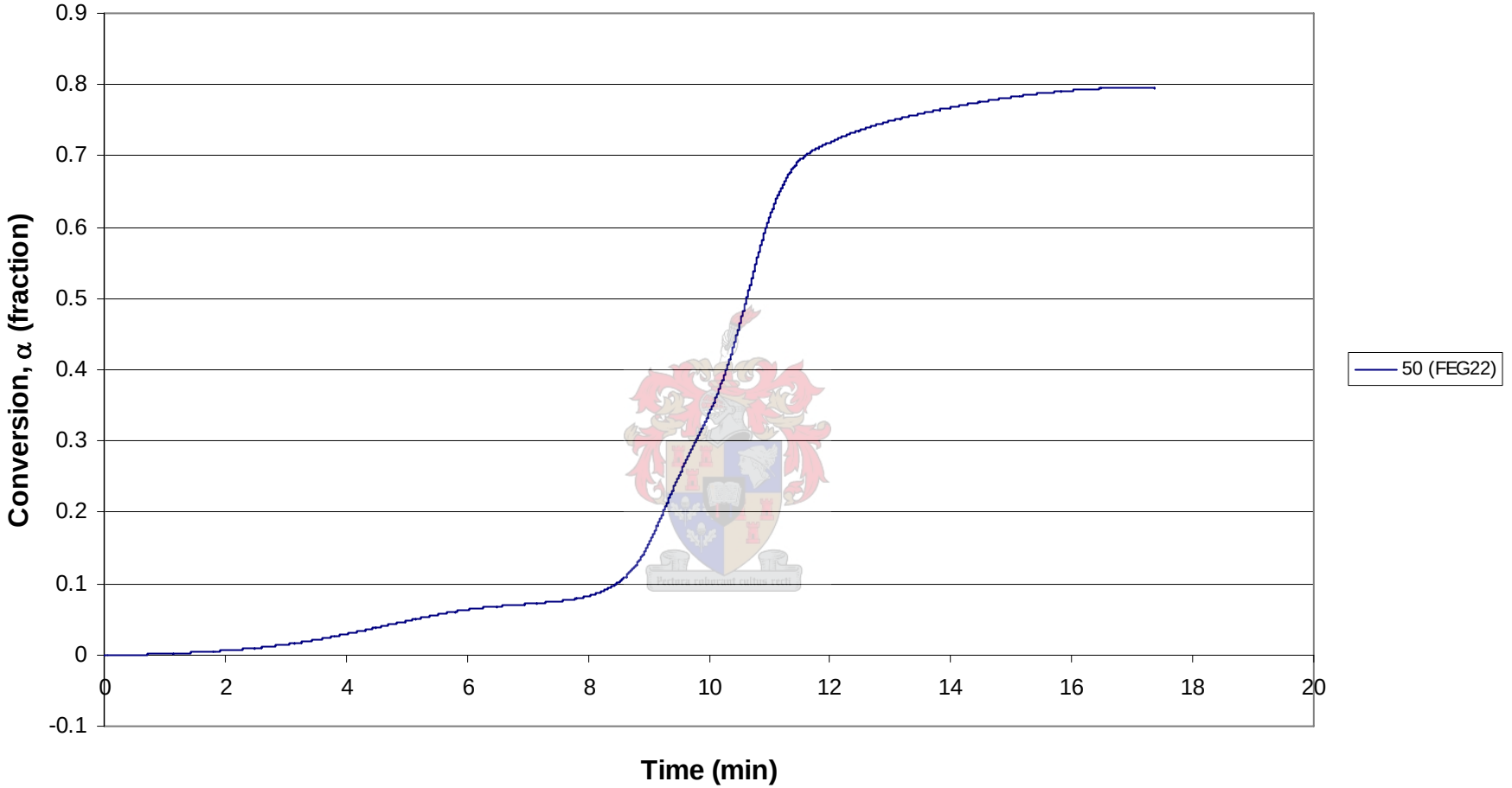

Figure A.36 Conversion versus time for a heating rate of 50 ˚C/min for the 2 – 4 mm heartwood Rooikrans blocks.

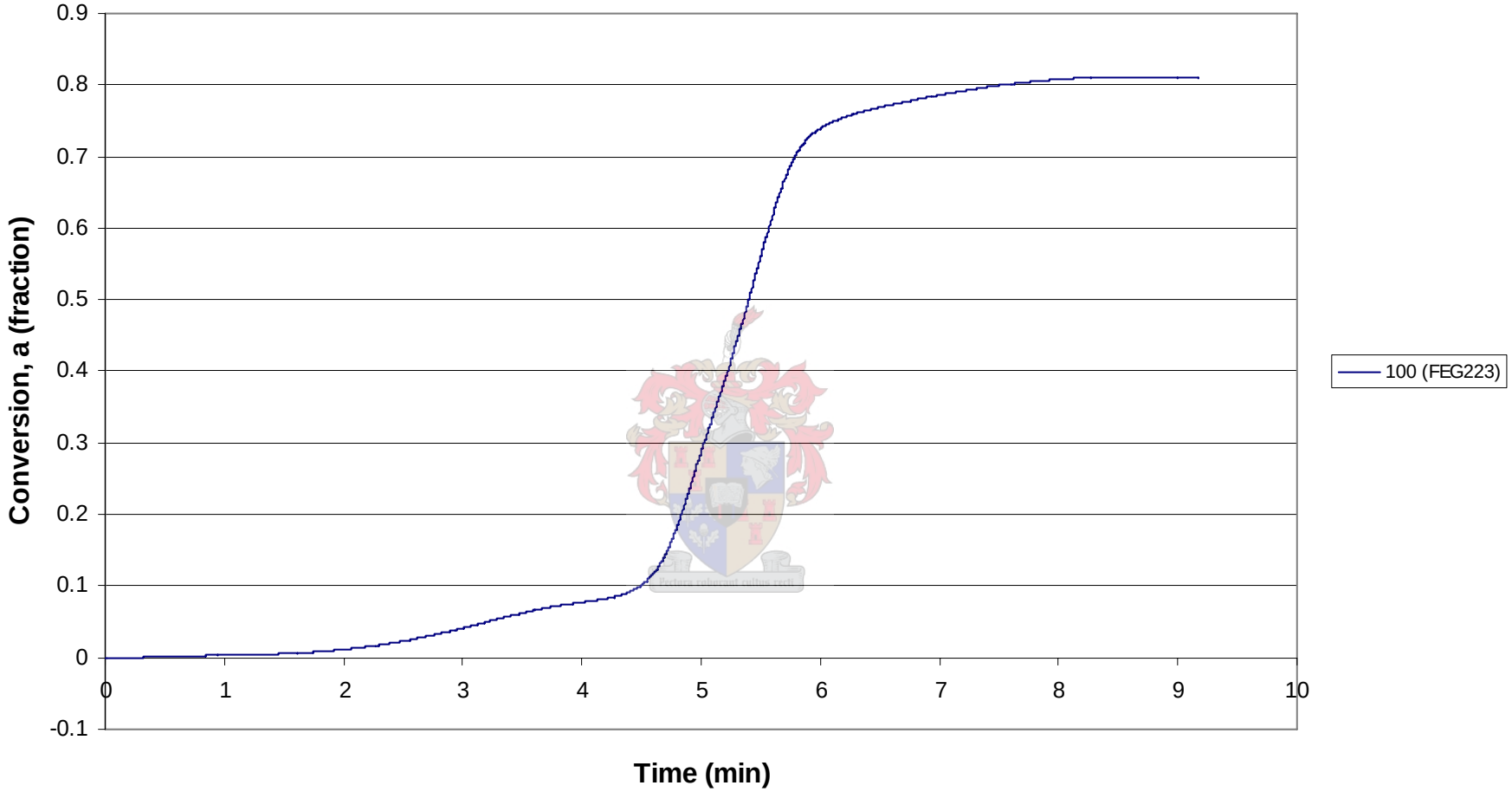

Figure A.37 Conversion versus time for a heating rate of 100 ˚C/min for the 2 – 4 mm heartwood Rooikrans blocks.

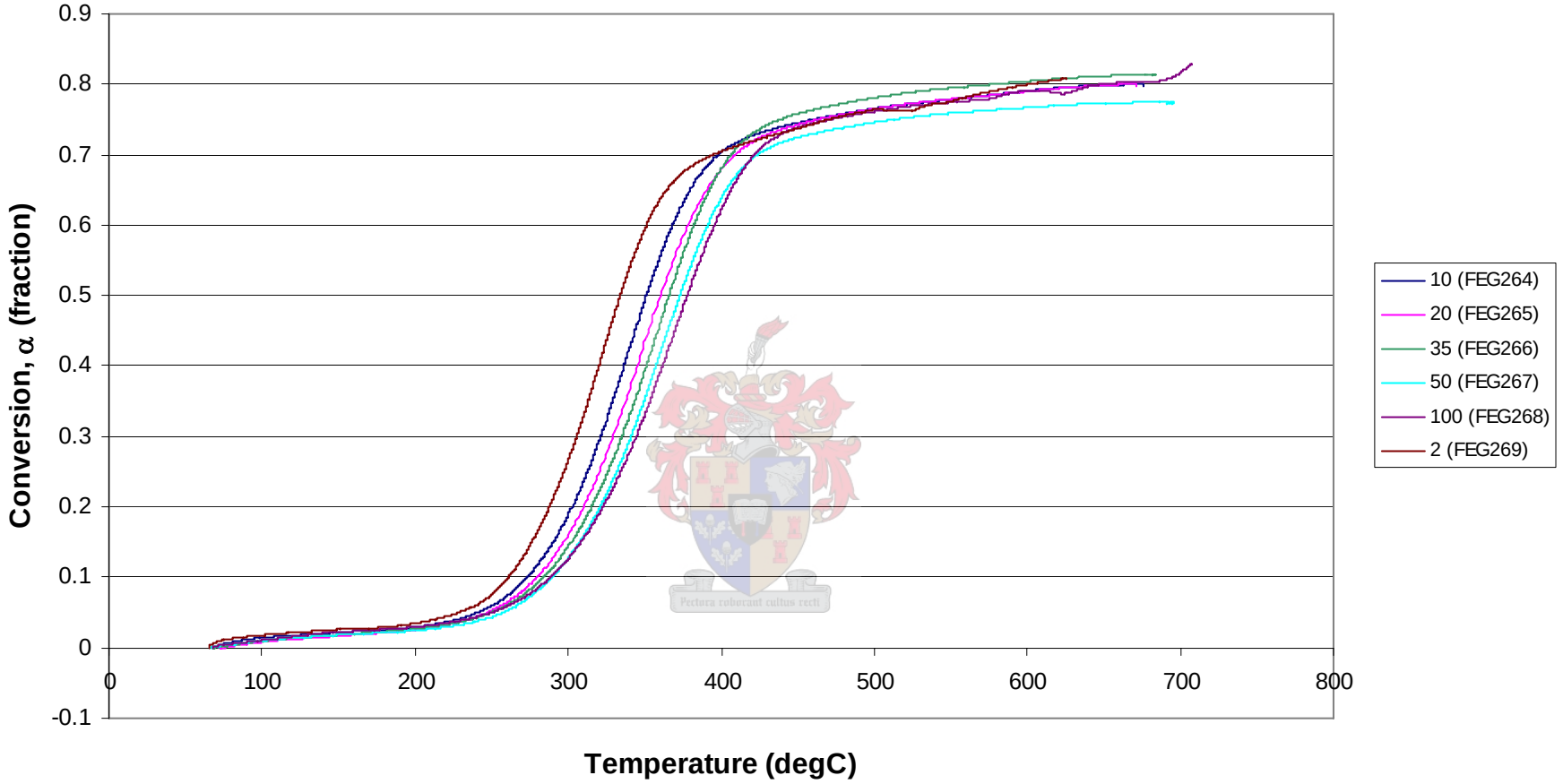

Figure A.38 Conversion versus temperature for different heating rates for the Swarthaak wood sawdust.

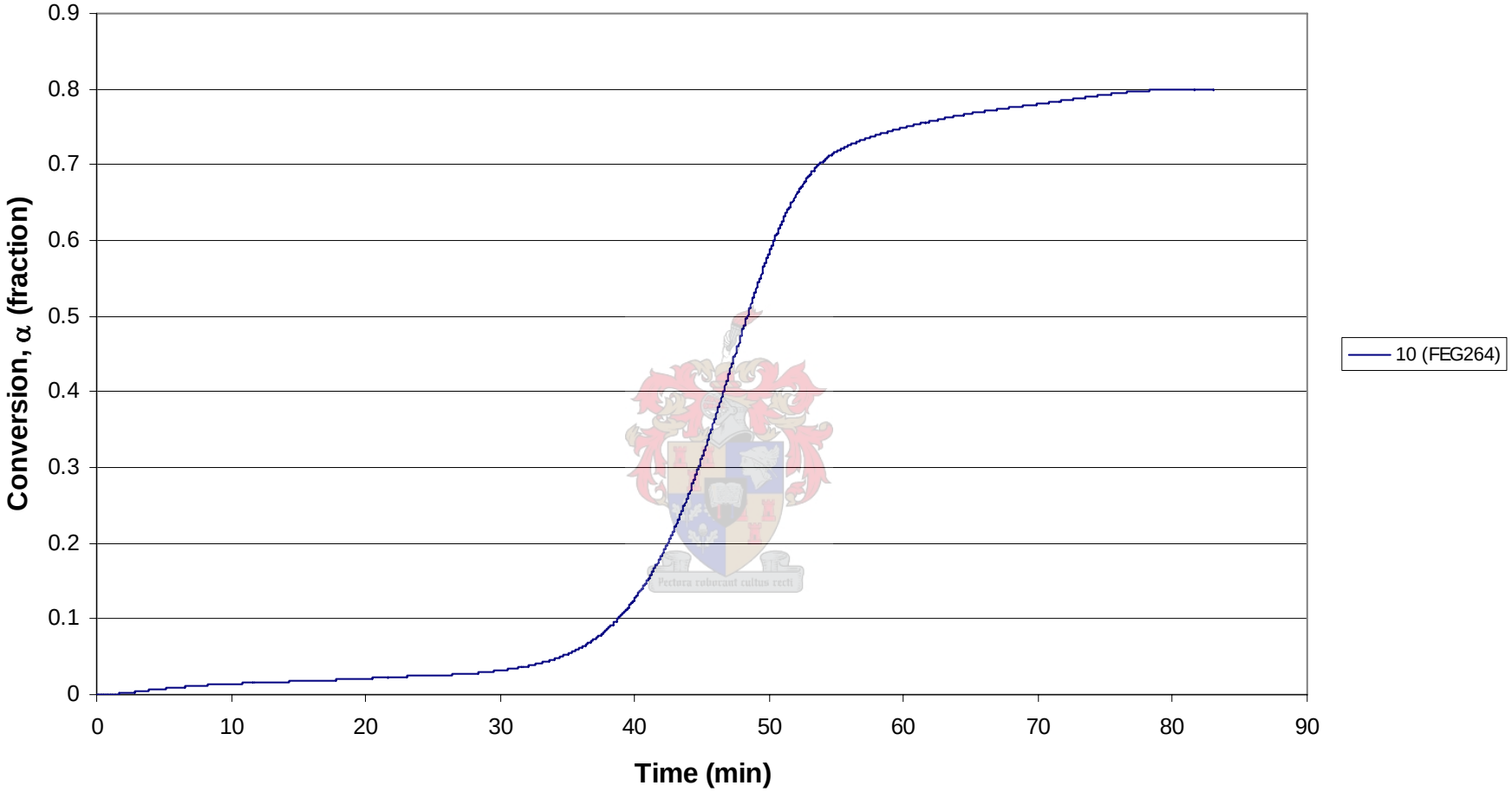

Figure A.39 Conversion versus time for a heating rate of 10 ˚C/min for Swarthaak wood sawdust.

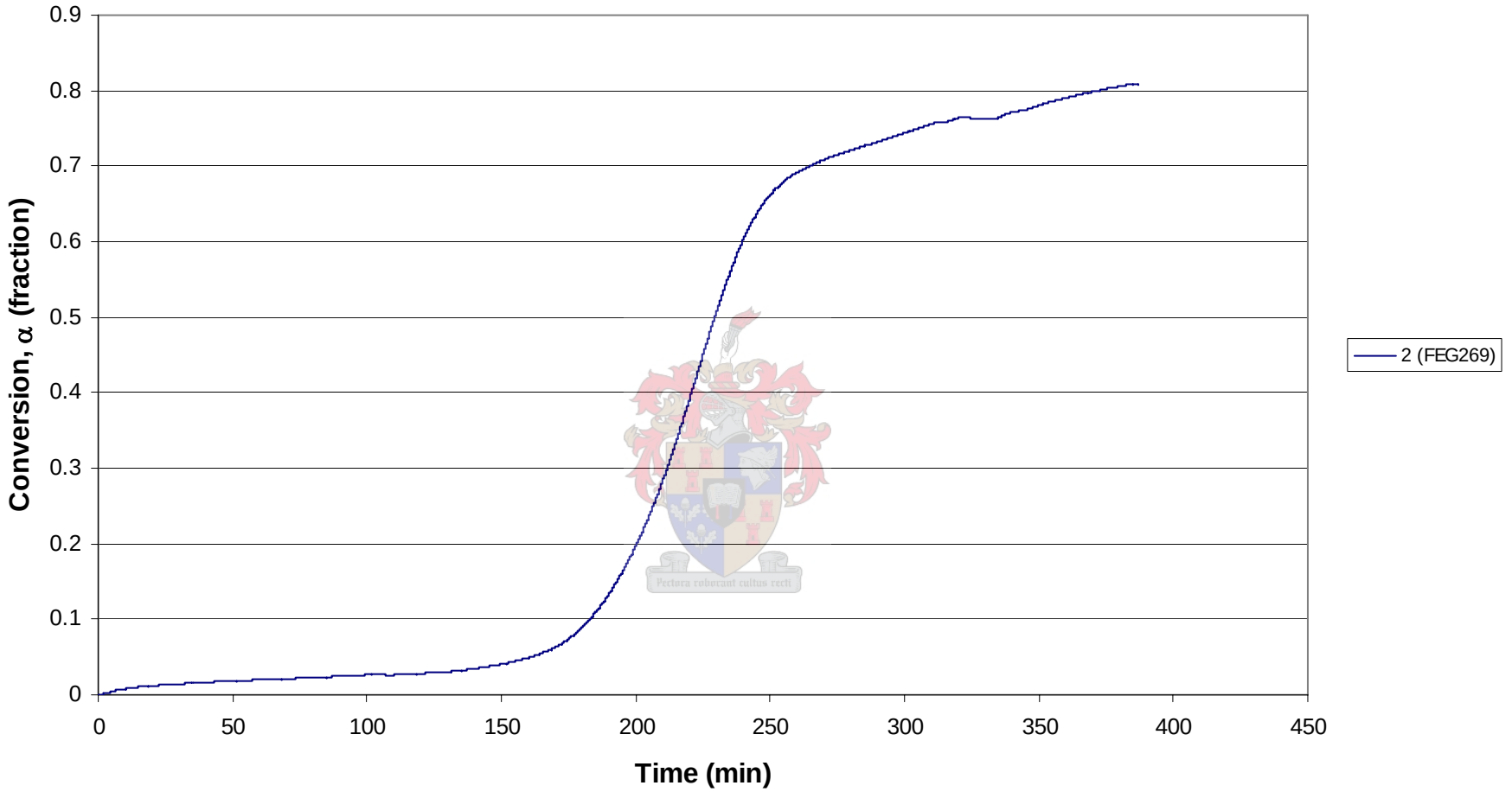

Figure A.40 Conversion versus time for a heating rate of 2 ˚C/min for Swarthaak wood sawdust.

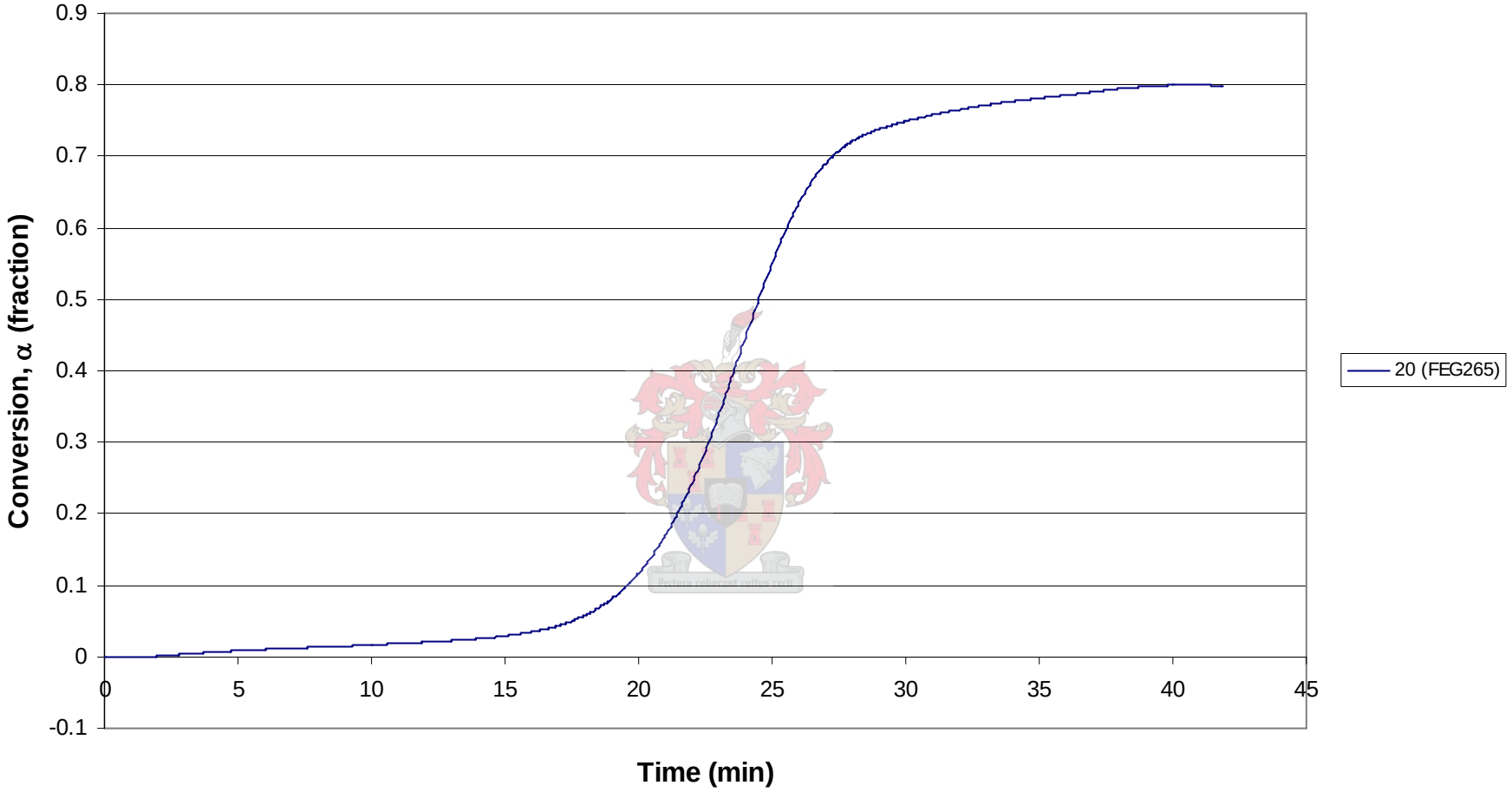

Figure A.41 Conversion versus time for a heating rate of 20 ˚C/min for Swarthaak wood sawdust.

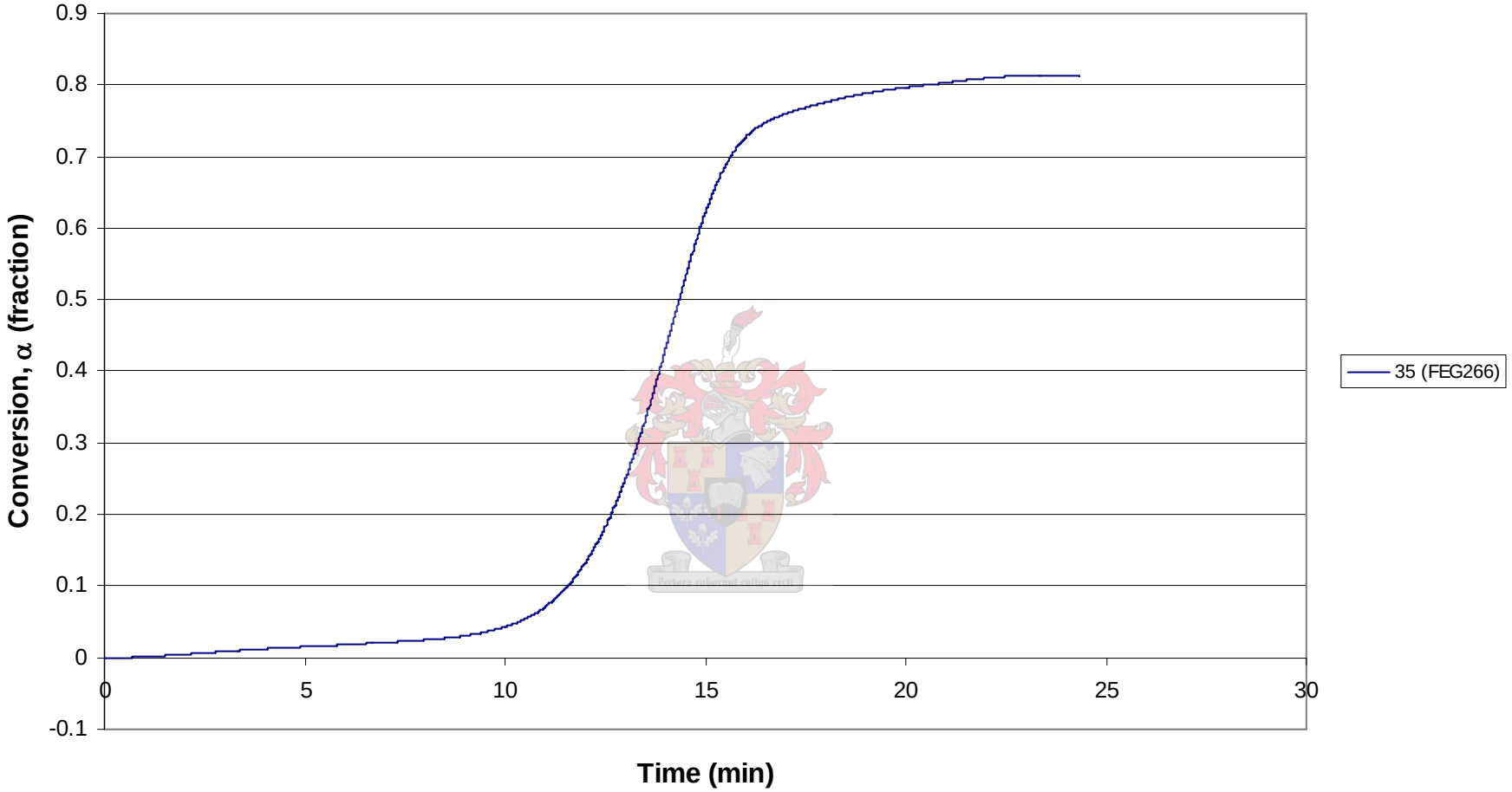

Figure A.42 Conversion versus time for a heating rate of 35 ˚C/min for Swarthaak wood sawdust.

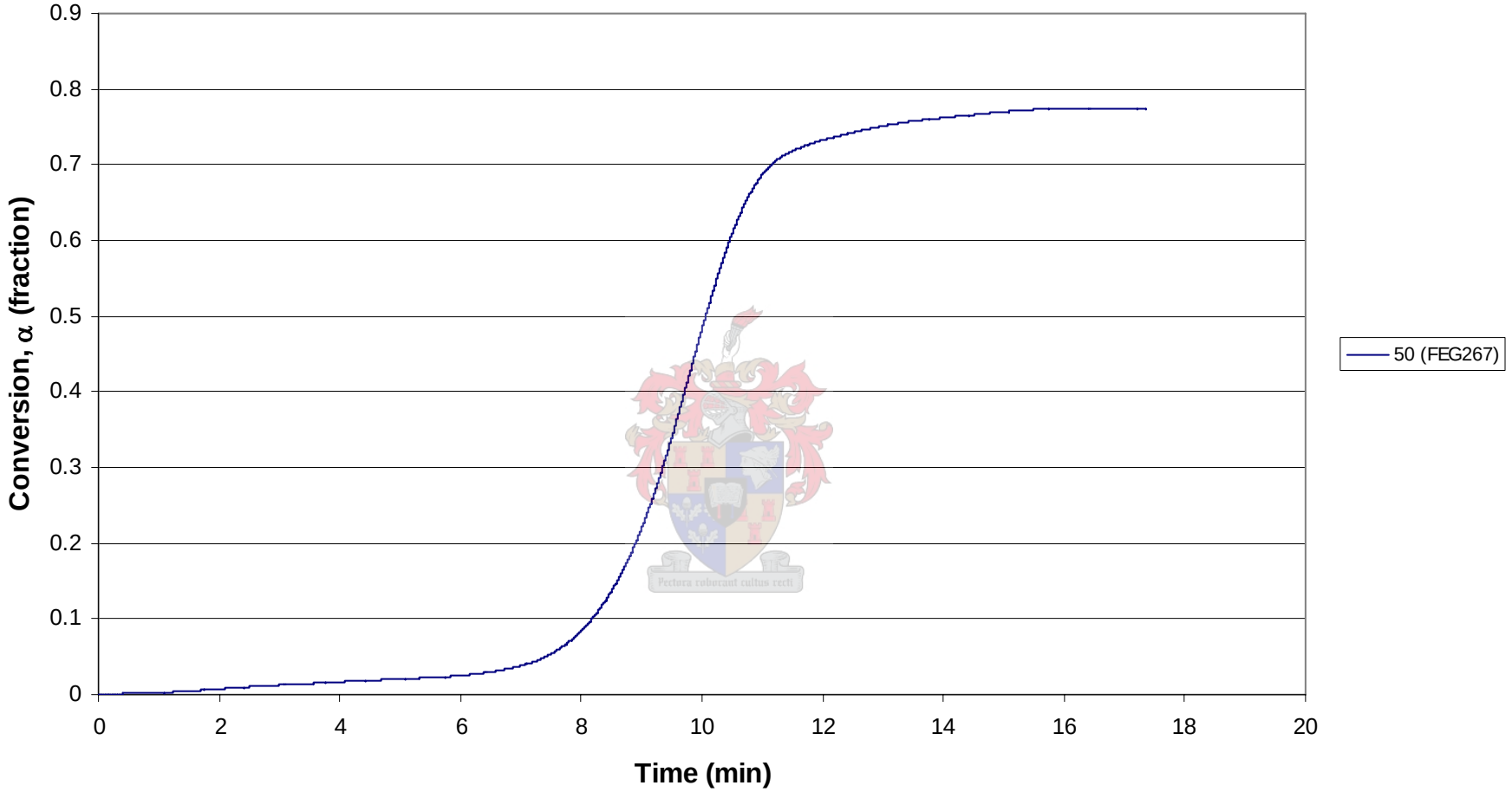

Figure A.43 Conversion versus time for a heating rate of 50 ˚C/min for Swarthaak wood sawdust.

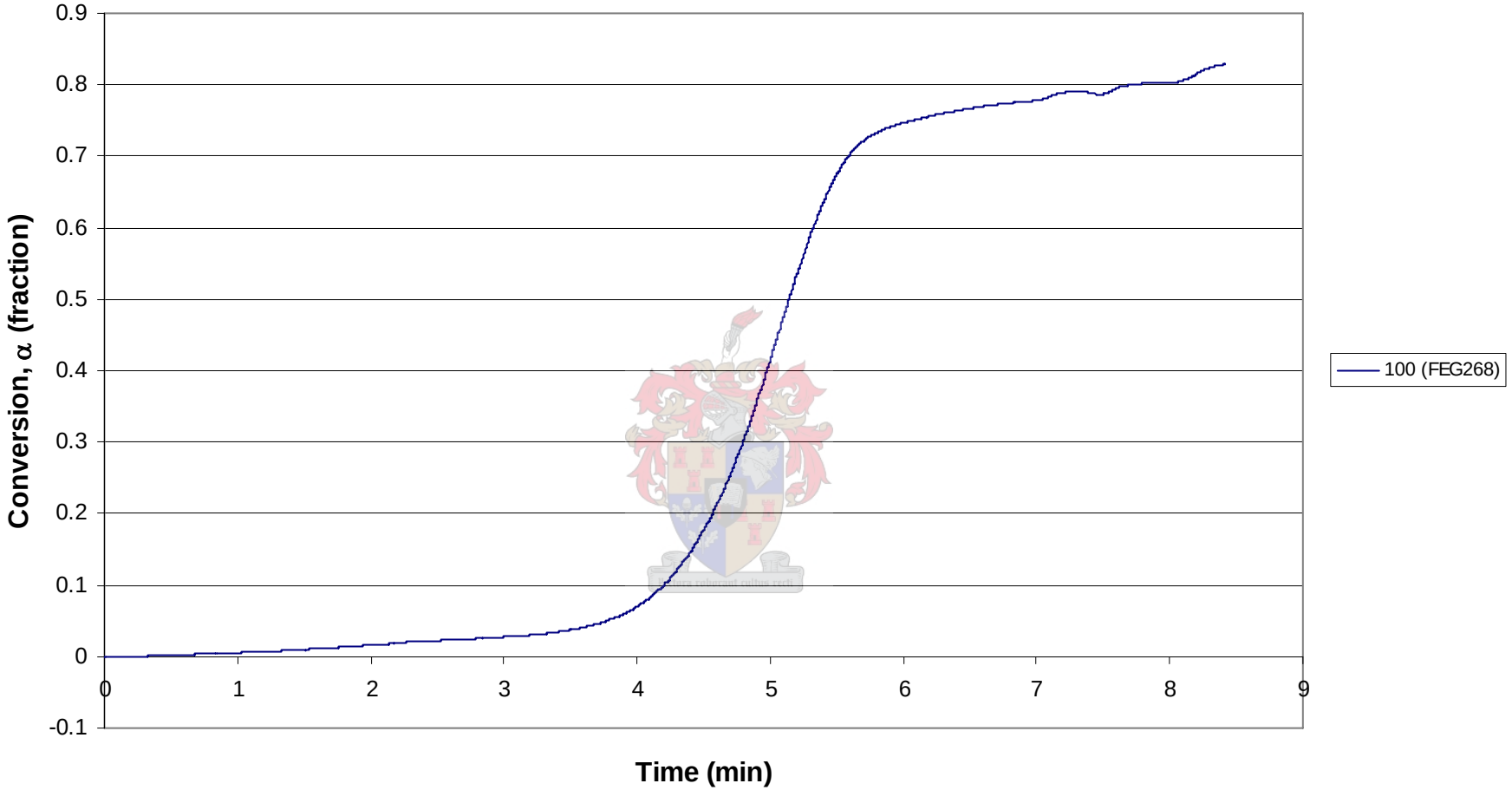

Figure A.44 Conversion versus time for a heating rate of 100 ˚C/min for Swarthaak wood sawdust.

Appendix B

TGA calibration and data smoothing

TGA calibration and data smoothing

TG analysers are often calibrated using magnetic transition standards. Known standards are placed in the crucible and heated under normal operating conditions to a temperature above its Curie point under the presence of a magnetic field. At the Curie point temperature the material loses its magnetism and a mass change is observed. This temperature is used to calibrate the TGA. A full description of this method can be found in the Annual Book of ASTM Standards, volume 14.02.

Unfortunately the Curie point method for calibration could not be made to work in the TGA used in this study. The nickel standard kept on falling off the crucible and a clear temperature reading could not be made. As a result it was decided to use Calcium Oxalate (CaC_2O_4) as a standard instead.

Data for commercial $CaC_2O_4.H_2O$ from Fischer Scientific was obtained from a paper by **Kutaish et al. (1997)**. The temperatures of the peaks in the DTG curve (derivative curve of the mass loss curve) were taken as standard temperatures and compared to those achieved in the TGA used for this study. The following formula, obtained from the ASTM standard, was used to adjust the temperatures:

$$T = (T_0 \times S) + I \qquad \text{(B.1)}$$

where S and I are the slope and intercept respectively, T_0 is the observed temperature and T is the actual temperature.

Figure B.1 below is a plot of the conversion versus temperature for a run with calcium oxalate performed in this TGA, and Figure B.2 is a plot of $d\alpha/dT$ versus temperature, to show the peaks obtained.

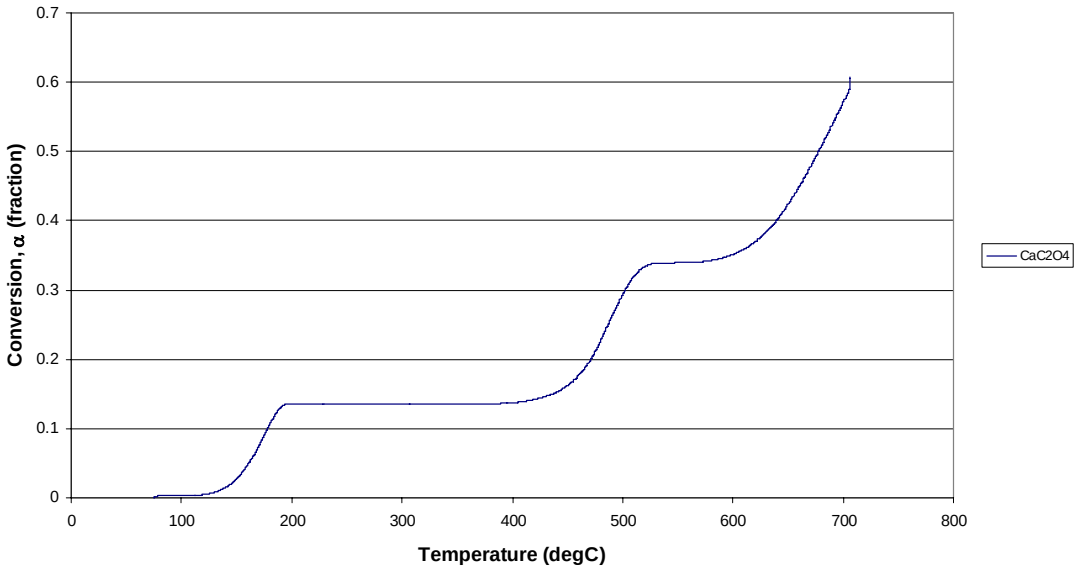

Figure B.1 Conversion versus temperature for calcium oxalate.

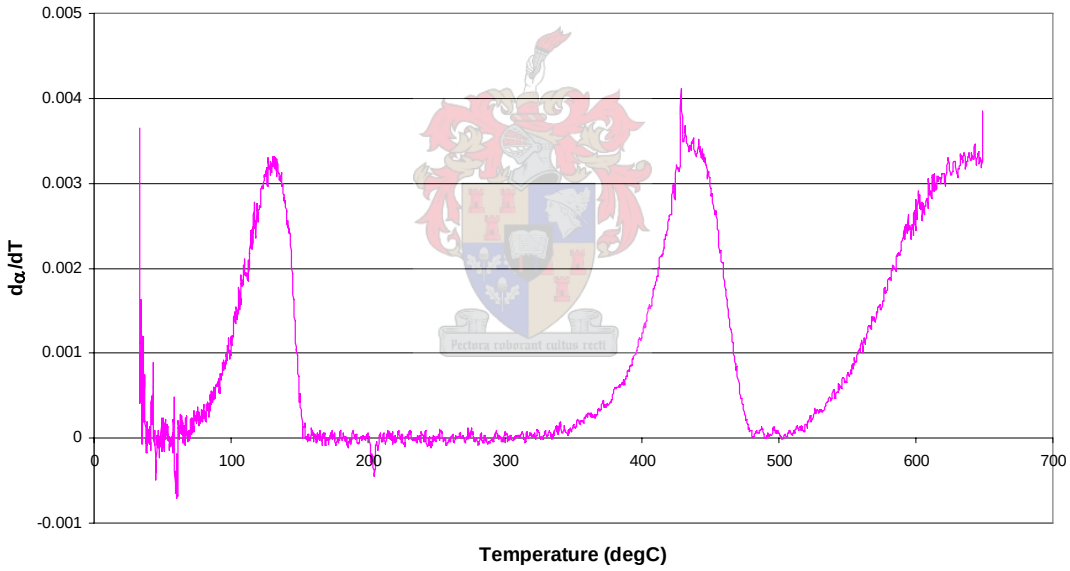

Figure B.2 DTG plot for calcium oxalate.

Data smoothing were done for all the raw data obtained from the TGA. Single Spectrum Analysis (SSA) was used for this purpose. Every dataset was exported to Matlab where the smoothing was done before the data was imported back into Excel.

Appendix C

Derivation of the Modified Coats-Redfern kinetic equation

Derivation of the Modified Coats-Redfern Kinetic Equation

The derivation for equation 4.9, as used by **Burnham and Braun (1999)**, and also in this study, is given in this section. Details can be found in **Burnham and Braun (1999)**.

The equation for the rate of conversion of biomass during thermal decomposition usually has the following form for an n^{th} order reaction:

$$\frac{d\alpha}{dt} = k(T)x^n \qquad \text{(C-1)}$$

where x denotes the unreacted fraction, so $x = 1- \alpha$. This is the notation used by **Burnham and Braun (1999)**. The Arrhenius constant, k, is given by

$$k = Ae^{\frac{-Ea}{RT}} \qquad \text{(C-2)}$$

Integrating equation C-1 yields

$$x = \left[1-(1-n)\int_0^t k(T)dt\right]^{1/(1-n)} \qquad \text{(C-3)}$$

For a constant heating rate the kinetic integral may be approximated as follows:

$$\int_0^t k(T)dt = \left(\frac{ART^2}{H_r E}\right)\left(\frac{1-2RT}{E}\right)e^{\frac{-E}{RT}} \qquad \text{(C-4)}$$

This equation is substituted into equation C-3 to give

$$x = \left[1 - (1-n)\left(\frac{ART^2}{H_R E}\right)\left(\frac{1-2RT}{E}\right)e^{\frac{-E}{RT}}\right]^{\frac{1}{1-n}} \qquad \text{(C-5)}$$

The conventional way of analysing a 1st order reaction is to linearise equation C-1 and determine the rate constant at each temperature from the slope of ln(-dx/dt) vs time. The activation energy and frequency factor is then determined from a fit of ln(k) vs 1/T to a straight line. More general methods, like Friedman's method and the Coats-Redfern method **(Burnham and Braun, 1999)** can be used and are valid for any thermal history. The method used in this study is the modified Coats-Redfern method, developed by **Burnham and Braun (1999)**. Equation C-5 is linearised to yield equation 4.9 which can then be plotted to determine the kinetic parameters. This is done as follows:

Raise both sides of equation C-5 to the power of 1/(1-n) and rearrange:

$$x^{(1-n)} = 1 - \left(\frac{AR(1-n)}{R}\right)\left(\frac{T^2(1-\frac{2RT}{E}}{H_r}\right)e^{\frac{-E}{RT}} \qquad \text{(C-6)}$$

Make exp(-E/RT) the subject of the formula and rearrange:

$$e^{\frac{-E}{RT}} = \frac{\left(\frac{H_r}{T^2(1-\frac{2RT}{E}}\right)}{\left(\frac{AR(1-n)}{E(1-x^{(1-n)}}\right)} \qquad \text{(C-7)}$$

Taking natural logs on both sides and rearranging yields equation 4.9:

$$\ln\left[\frac{\beta}{T^2(1-2RT/E_a)}\right] = -\frac{E_a}{RT} + \ln\left(-\frac{AR}{E_a \ln(1-\alpha)}\right) \qquad \text{(C-8)}$$

Appendix D

Calculation of the activation energy for all levels of conversion

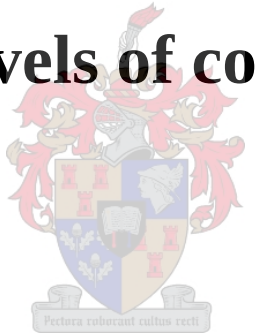

Calculation of the activation energy for all levels of conversion

Shown below is a sample calculation for the activation energy, E_a, as calculated for all conversions.

From equation 4.9 the average activation energies for the conversion intervals 0 – 10 %, 0 - 20 % and 0 -30 % are determined: X = 0 - 10 %, E_a = 441 440 kJ/mol

X = 0 - 20 %, E_a = 388 305 kJ/mol

X = 0 - 30 %, E_a = 355 115 kJ/mol

Using equation 5.2, the actual activation energies for the conversions 5, 15 and 25 % are determined:

For X = 5 %: E_a = 441 440 × 1 – 0 = 441 440 kJ/mol

For X = 15 %: E_a = 388 305 × 2 – 441 440 = 335 170 kJ/mol

For X = 25 %: E_a = 355 115 × 3 – 335 170 – 441 440 = 288 735 kJ/mol

Linear interpolation is now used to calculate the activation energy for every level of conversion:

eg. For X = 6 %, E_a = 441 440 + (6 – 5)/(15 – 5) × (335 170 – 441 440) = 430 813 kJ/mol

Appendix E

Calculation of the surface-to-particle contact heat transfer coefficient for conduction

Calculation of the surface-to-particle contact heat transfer coefficient for conduction

Schlünder's model can be used to calculate the surface-to-particle contact heat transfer coefficient for spherical particles in contact with a heated surface. A slightly more detailed discussion of this model is found in **Roy et al (1997)**. A sample calculation is done below to show that radiation is more dominant than conduction in the rotary oven.

Three modes of heat transfer take place from the heated surface to the bottom layer of particles: (1) thermal conduction through the gas layer between the particles and the heating surface, α_{wp}, (2) thermal conduction through the void space between the particles, α_{wg}, (3) heat transfer by radiation, α_r. The contact heat transfer coefficient can therefore be expressed as follows:

$$\alpha_{ws} = \alpha_{wp} + \alpha_{wg} + \alpha_r \qquad \text{(E-1)}$$

where

$$\alpha_{wp} = \phi_A \frac{4\lambda_g}{d_p}\left[\left\{\frac{2(\sigma + S_r)}{d_p} + 1\right\}\ln\left\{\frac{d_p}{2(\alpha + S_r)}\right\} - 1\right] \qquad \text{(E-2)}$$

with

ϕ_A = area fraction of contact points

λ = thermal conductivity of the particle bed (W/mK)

d_p = diameter of the particle (m)

σ = modified mean free path of the gas molecules (m)

S_r = sum of the particle and surface roughness

and

$$\alpha_{wg} = (1 - \phi_A)\frac{2\lambda_g / d_p}{\sqrt{2} + (2\sigma + 2S_r)/d_p} \qquad \text{(E-3)}$$

with

λ_g = thermal conductivity of the gas

and

$$\alpha_r = \frac{0.2268}{\frac{2}{\varepsilon} - 0.264}\left(\frac{T}{100}\right)^3 \qquad \text{(E-4)}$$

with

T = Temperature of the surface

Calculating α_{wp} and α_{wg} requires σ, S_r and ϕ_A to be known. However, these two terms together represent the heat transfer coeficient for conduction from the surface to the particle and can thus be calculated if α_r and α_{ws} are known. **Roy et al (1997)** experimentally measured α_{ws} at 250 W/mK for gravel as feedstock in their agitated bed reactor. Assuming a temperature of 1000 ˚C for the reactor wall and a thermal emmisivity of 0.9 for the feedstock and inserting this into equation E-4 yields a value of 238 W/mK for α_r. Therefore, by equation E-1, the sum of α_{wp} and α_{wg} must equal 12 W/mK, which is significantly less than the heat transfer coefficient for radiation from the wall to the bed.

Appendix F

Matlab code for reactor model

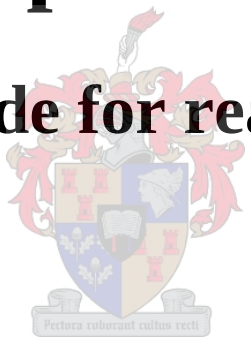

Code for reactor model

```
%Reactor Design
clear all;
clc;

global s;
global Dreactor;
global Rreactor;
global Rbed;
global Aw;
global Tg_current Tb_current
global E1;
global E2;
global hw;

Dreactor = 0.5;                 % [m] first estimate
Rreactor = Dreactor/2;
Rbed = 1/3*Rreactor;            % [m] Corresponds to 11% filling
Doutside = 0.7;                 % [m] Guess/estimate
XSAoutside = pi*(Doutside^2)/4;
XSAreactor = pi*(Dreactor^2)/4;
XSAgasflow = XSAoutside - XSAreactor;
DIFF = 1e-3;

k0 = 4.06562E-40;
X0 = 0;

mg = 0.076;                     % [kg/s] Estimate from Boateng and Barr, table 2, pg 2139
Tg0 = 1273;

    Cpg = 1000;                 % [J/kgK] Air @ STP
    Aw = pi*Dreactor;           % [m] Effective heat transfer area per unit kiln length

    Gt = mg/XSAgasflow;          % [kg/m2s] Gas flow velocity
    de = 4*XSAgasflow/Dreactor;   % 4* XSA for flow/wetted perimeter

    viscair = 3.5e-5;           % [Ns/m2] Taken from Thomson at bulk fluid T = (550+450)/2
    kf =0.0407;                 % [W/mK] Fluid thermal conductivity - from Thomson, appendix E, air @ 500degC

    Re = Gt*de/viscair;         % Reynolds Number
    Pr = Cpg*viscair/(kf/1000); % Prandtl Number

    Nu = 0.021*Re^0.8*Pr^0.33;  % Nusselt Number: 0.021 for gases - See Coulson and Richardson vol 6, pg 663.
Neglect (viscosity/viscosity of air)^0.14...
    hw = Nu*kf/de;              % [W/m2K] Heat transfer coefficient for gas on outside of reactor from Nu =
hw*de/kf

    mb = 0.0278;                % [kg/s] Corresponds to 100kg/h feedrate of woodchips to reactor
    Cpb = 2220;                 % [J/kgK] Taken from C.Roy et al - Conceptual Design and Evaluation... pg. 1178
```

```
s = 5.67e-8;                    % [W/m2K4] sigma = Stefan-Boltzman constant
E1 = 0.8;                       % Emissivity for metallic surface - from C.Roy, Conceptual Design...
E2 = 0.9;                       % Emissivity for biomass - from C.Roy, Conceptual Design...
deltaHrb = 92000;               % [J/kg] Heat of Reaction - from C.Roy, Preliminary Engineering Data...

dz = 0.05;

Tb0 = 298;                      % [K] = 25 degC
Tw0 = 700;                      % [K] = initial guess


Tg = zeros(1);
Tb = zeros(1);
Tw = zeros(1);
Tg(1) = Tg0;
Tb(1) = Tb0;
Tg_current = Tg(1);
Tb_current = Tb(1);

k(1) = k0;
X(1) = X0;

lambda0 = 4.06562E-40;
lambda(1) = lambda0;

i = 0;
z = 0;
Z(1) = z;


while (1),
   i = i+1;

   last_Tg_current = Tg_current; last_Tb_current = Tb_current;   % store last values of Tg and Tb


   %First solve for Tw from the "balance equation" using Newton's Method
   steps = 0;
   e = 1e-8;
   Maxstep = 40;
   flag1 = 0; flag2 = 0;

   while all([flag1,flag2])~=1,

      Tw0 = Tw0 - f(Tw0)/df(Tw0);
      steps = steps + 1;
      if abs(f(Tw0)) < e,
         flag1 = 1;
      else
         flag1 = 0;
```

```
        end

        if steps > Maxstep,
            flag2 = 1;
        else
            flag2 = 0;
        end

    end

    Tw(i)= Tw0;


    %Solve for Tg using Runge-Kutta order 4

    K1g = dz*(hw*Aw*(Tg(i) - Tw(i)))/(mg*Cpg);
    K2g = dz*(hw*Aw*((Tg(i)+K1g/2) - Tw(i)))/(mg*Cpg);
    K3g = dz*(hw*Aw*((Tg(i)+K2g/2) - Tw(i)))/(mg*Cpg);
    K4g = dz*(hw*Aw*((Tg(i)+K3g) - Tw(i)))/(mg*Cpg);

    Tg(i+1) = Tg(i) - (K1g + 2*K2g + 2*K3g + K4g)/6;
    Tg_current = Tg(i+1);



    K1b = dz*((s*Aw*(Tw(i)^4-Tb(i)^4))/(1/E1 + (1-E2)/E2*(Rreactor/Rbed)) -
lambda(i)*(pi*Rreactor^2)*deltaHrb)/(mb*Cpb);
    K2b = dz*((s*Aw*(Tw(i)^4-(Tb(i)+K1b/2)^4))/(1/E1 + (1-E2)/E2*(Rreactor/Rbed)) -
lambda(i)*(pi*Rreactor^2)*deltaHrb)/(mb*Cpb);
    K3b = dz*((s*Aw*(Tw(i)^4-(Tb(i)+K2b/2)^4))/(1/E1 + (1-E2)/E2*(Rreactor/Rbed)) -
lambda(i)*(pi*Rreactor^2)*deltaHrb)/(mb*Cpb);
    K4b = dz*((s*Aw*(Tw(i)^4-(Tb(i)+K3b)^4))/(1/E1 + (1-E2)/E2*(Rreactor/Rbed)) -
lambda(i)*(pi*Rreactor^2)*deltaHrb)/(mb*Cpb);



    Tb(i+1) = Tb(i) + (K1b + 2*K2b + 2*K3b + K4b)/6;
    Tb_current = Tb(i+1);


    [XEnd,kEnd] = kinetics( Tb(i), Tb_current, k(i), X(i) );

    X(i+1) = XEnd;
    k(i+1) = kEnd;


    lambda(i+1) = (k(i+1)*(1-X(i+1))*150)/60;
   % 150 = density of bed
    if lambda(i+1) > 7
```

```
            lambda(i+1) = 7;
        end

        fprintf(1,'iteration: %d \t Tb_current=%4.2f \t Tg_current=%4.2f \t next_z=%4.2f k =%.2f lambda = %.2f X =
%.2f\n',...
        i,Tb_current,Tg_current,z, k(i+1), lambda(i+1), X(i+1));



        z = z + dz;
        Z(i+1) = z;


        FLAG = ( z > 4 );

        if FLAG,
            %ZZ = [Z' Tg' Tb'];
            %save(filename,'ZZ','-ASCII');
            %clear Z Tg Tb;
            break;
        end
    end


    plot(Z,Tg,'*',Z,Tb,'+');
    %plot(Z(1,1:200),Tg(1,1:200),'*',Z(1,1:200),Tb(1,1:200),'+',Z(1:1:200),T
    %w(1,1:200)'.');
    %plot(Z,lambda,'*');
    %plot(Z,X,'*');
    %plot(Tb,X,'.');
    %plot( Z, k, '*' );
```

Appendix F

Code for kinetics

```
%Give the kinetics a go!

function[XEnd,kEnd] = kinetics(T0,TEnd,k0,X0)

% Calculating the fraction remaining
%   Xp=exp[-SUM_p(delta_Up)];

XEnd = X0;
kEnd = k0;

M = load('richardt.txt');

R = 8.314;
Hr = 10;
a1 = 2.334733;
a2 = 0.250621;
b1 = 3.330657;
b2 = 1.681534;

c = T0;
d = TEnd;
dT = 0.5;
n = (d-c)/dT;                    % Temperature interval: From 298K - 623K

T0 = c;
Xp0 = 1-X0;

%T = zeros(1,floor(n+1));
%k = zeros(1,n+1);
%Xp = zeros(1,n+1);
%X = zeros(1,n+1);
%Up = zeros(1,n);
X = [];
k = [];
Up = [];
Xp = [];

T(1) = T0;
k(1) = k0;
Xp(1) = Xp0;
X(1) = X0;
Up(1) = 0;

i = floor(X(1)*100)+1;
if i > size(M,1)
        i = size(M,1);
end
if i < 1
        i = 1;
```

```
end

for j = 1:floor(n+1)
   T(j+1) = T(j)+dT;
   k(j+1) = M(i,3)*exp(-M(i,2)/(R*T(j+1)));

                        LT = M(i,2)/(R*T(j+1));
                        FirstTerm = 1.0 - ( (LT^2 + a1*LT + a2)/(LT^2 + b1*LT + b2)  );

                        LT = M(i,2)/(R*T(j));
                        SecondTerm = 1.0 - ( (LT^2 + a1*LT + a2)/(LT^2 + b1*LT + b2)  );

                        Up(j+1) = (1/Hr)*( T(j+1)*k(j+1)*FirstTerm-T(j)*k(j)*SecondTerm );

                        if Up(j) < 0
                                Up(j) = (Up(j-1)+Up(j+1))/2;
                        end

                        Xp(j+1) = Xp0*exp(-sum(Up(1:j+1)));
                        X(j+1) = 1-Xp(j+1);

                        i = floor(X(j+1)*100)+1;
                        if i > size(M,1)
                                i = size(M,1);
                        end
                        if i < 1
                                i = 1;
                        end

end

if TEnd-T0 > 0
        XEnd = X(j+1);
        kEnd = k(j+1);
else
        disp('Warning TEnd-T0 <= 0 in kinetics()');
end
```